

**A mathematical model for studying the impact of
climate variability on malaria epidemics in South Africa**

Gbenga Jacob Abiodun

A Thesis submitted in partial fulfillment of the requirements for the degree of
Doctor of Philosophy in the Department of Mathematics and Applied Mathematics
at the Faculty of Natural Sciences, University of the Western Cape

Supervisors: Prof. Peter Witbooi and Prof. Kazeem Okosun

October 2016

Keywords

Mosquito

Malaria

Anopheles

Temperature

Rainfall

Climate

Basic reproduction number

Disease-free equilibrium

Endemic equilibrium

Infectious diseases

Stability analysis

Sensitivity analysis

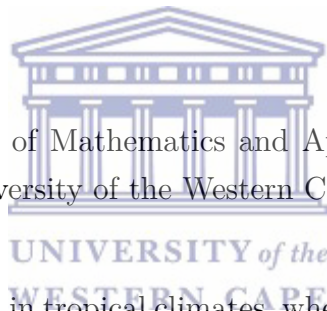


Abstract

A mathematical model for studying the impact of climate variability on malaria epidemics in South Africa

Gbenga Jacob Abiodun

PhD thesis, Department of Mathematics and Applied Mathematics, Faculty of Natural Sciences, University of the Western Cape



Malaria is most prevalent in tropical climates, where there are sufficient rainfall for mosquitoes to breed and conducive temperatures for both the mosquito and protozoa to live. A slight change in temperature can drastically affect the lifespan and patterns of mosquitoes, and moreover, the protozoan itself can only survive in a certain temperature range. With higher temperatures, mosquitoes can mature faster, and thus have more time to spread the disease. The malaria parasite also matures more quickly at warmer temperatures. However, if temperatures become too high, neither mosquitoes nor the malaria pathogen can survive. In addition, stagnant water is also a major contributor to the spread of malaria, since most mosquito species breed in small pools of water. The correct amount and distribution of rainfall increases the possible breeding sites for mosquito larvae, which eventually results in more vectors to spread the disease. With little rainfall, there are few places for the mosquitoes to breed. For these reasons, and in order to control mosquito population, it is important to

examine the weather parameters such as temperature and rainfall which are imperative in determining the disease epidemics. Accurate seasonal climate forecasts of these variables, together with malaria models should be able to drive an early warning system in endemic regions. These models can also be used to evaluate the possible change in regions under climate change scenarios, and the spread of malaria to new regions.

In this study, we develop and analyse a mosquito model to study the population dynamics of mosquitoes. Ignoring the impact of climate, the model is further developed by introducing human compartments into the model. We perform both analytical and numerical analyses on the two models and verify that both models are epidemiological and mathematical well-posed. Using the next generation matrix method, the basic reproduction number of each system is calculated. Results from both analyses confirm that mosquito- and disease-free equilibria are locally asymptotically stable whenever $\mathcal{R}_0 < 1$ and unstable whenever $\mathcal{R}_0 > 1$. We further establish the global stability of the mosquito-free equilibrium using a Lyapunov function. In order to examine the effectiveness of control measures, we calculate the sensitivity coefficients of the reproductive number of the mosquito-human malaria model and highlight the importance of mosquito biting rate on malaria transmission. In addition, we introduce climate dependent parameters of *Anopheles gambiae* and climate data of Limpopo province into the malaria model to study malaria transmission over the province.

Climate variables and puddle dynamics are further incorporated into the mosquito model to study the dynamics of *Anopheles arabiensis*. The climate-dependent functions are derived from the laboratory experiments in the study of Maharaj [114], and we further verify the sensitivity of the model to parameters through sensitivity analysis. Running the climate data of Dondothena village in Kwazulu-Natal province over the mosquito model, it is used to simulate the impact of climate variables on the population dynamics of *Anopheles arabiensis* over the village. Furthermore, we incorporate human compartments into the climate-based mosquito model to explore the impact of climate variability

on malaria incidence over KwaZulu-Natal province over the period 1970-2005. The outputs of the climate-based mosquito-human malaria model are further analysed with Principal Component Analysis (PCA), Wavelet Power Spectrum (WPS) and Wavelet Cross-coherence Analysis (WCA) to investigate the relationship between the climate variables and malaria transmission over the province.

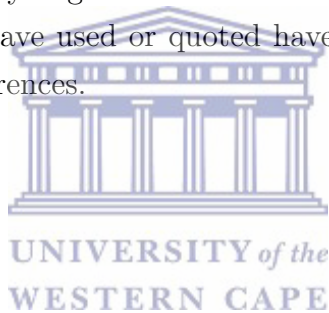
The results from the mosquito model fairly accurately quantify the seasonality of the population of *Anopheles arabiensis* over the study region and also demonstrate the influence of climatic factors on the vector population dynamics. The model simulates the population dynamics of both immature and adult *Anopheles arabiensis* and increases our understanding on the importance of mosquito biology in malaria models. Also, the simulated larval density produces a curve which is similar to observed data obtained from another study.

In addition, the mosquito-malaria models produce reasonable fits with the observed data over Limpopo and KwaZulu Natal provinces. In particular, they capture all the spikes in malaria prevalence. Our results further highlight the importance of climate factors on malaria transmission and show the seasonality of malaria epidemics over the provinces. The results of the PCA on the model outputs suggest that there are two major process in the model simulation. One of the processes indicate high loadings on the population of Susceptible, Exposed and Infected humans, while the other is more correlated with Susceptible and Recovered humans. However, both processes reveal the inverse correlation between Susceptible-Infected and Susceptible-Recovered humans respectively. Through spectrum analysis, we notice a strong annual cycle of malaria incidence over the province and ascertain a dominant periodicity of one year. Consequently, our findings indicate that an average of 0 to 120-day lag is generally noted over the study period, but the 120-day lag is more associated with temperature than rainfall. The findings of this study would be useful in an early warning system or forecasting of malaria transmission over the study areas.

October 2016

Declaration

I declare that *A mathematical model for studying the impact of climate variability on malaria epidemics in South Africa* is my work, that it has not been submitted before for any degree or examination in any other university, and that all the sources I have used or quoted have been indicated and acknowledged by complete references.



Gbenga Jacob Abiodun

October 2016

Signed.....

Acknowledgments

My praise and gratitude to Almighty God, the Alpha and Omega of this work.

First and foremost I would like to thank my advisor Professor Peter Witbooi and co-supervisor, Professor Kazeem Okosun for their tremendous support and guidance towards my Ph.D. Their contagious joy and enthusiasm for research was a motivation for me during the study. I appreciate their time, ideas, and constant encouragement to make my Ph.D. experience productive and stimulating.

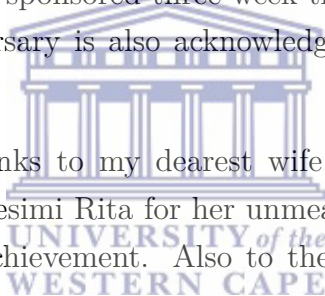
I would like to express my special appreciation to Professor R. Maharaj (South African Medical Research Council) for his advice and for sharing his, up to then unpublished, experimental data with this project. I also thank the review research team of the Climate System Analysis Group (CSAG) at University of Cape Town (UCT) for their suggestions and ideas towards the success of this work. I further thank my host supervisor at International Institute for Applied Systems Analysis (IIASA), Dr R. Mazzucco for advice and mentoring during my 3-month visit to Austria. In addition, the entire staff members and colleagues at IIASA are appreciated for the wonderful summer period.

Many thanks to all staff members and colleagues at the Department of Mathematics and Applied Mathematics, University of the Western Cape for companionship and for making my stay in the department pleasant and memorable.

The South African Weather Service (SAWS) and South African Department of Health are respectively thanked for the climate and malaria data used for this study.

I also appreciate and acknowledge that this research was carried out for the iDEWS (infectious Diseases Early-Warning System) project supported by SATREPS (Science and Technology Research Partnership for Sustainable Development) Program of JICA (JAPAN International Cooperation Agency)/AMED (Japan Agency for Medical Research and Development) in Japan and the ACCESS (Applied Centre for Climate and Earth Systems Science) program of NRF (National Research Foundation) and DST (Department of Science and Technology in South Africa). In addition, the financial support from iDEWS on this project and the sponsored three-week training in Japan is greatly appreciated. Merseta bursary is also acknowledged towards the completion of this thesis.

Finally, special thanks to my dearest wife, an icon of love and beauty, Mrs Abiodun Oluwanifesimi Rita for her unmeasurable support and ceaseless prayers towards this achievement. Also to the Abioduns, in-laws, and dear friends, I love you all!



Dedication

This thesis is dedicated to the **Abioduns** and in honour of my late father, **Pa Solomon Ola Abiodun**.



Contents

Keywords		i
Abstract		ii
Declaration		v
Acknowledgement		vi
Dedication		viii
List of Tables		xvi
List of Figures		xxiii
Publications		xxiv
1 Introduction		1
1.1 Malaria background		2
1.2 Mosquito bionomics		2
1.3 Malaria biology		4



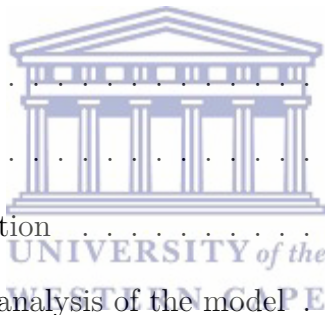
1.3.1	The parasite cycle	5
1.3.2	Age and immunity	7
1.4	Factors affecting malaria	8
1.4.1	Climatic factors	8
1.4.2	Other factors	9
1.5	Malaria distribution over Africa	10
1.6	Malaria models	12
1.7	Stability for ordinary differential equations	16
1.7.1	Lyapunov functions and stability	18
1.7.2	Routh-Hurwitz criteria	22
1.7.3	Hartman-Grobman theorem	23
1.7.4	Bendixson-Dulac theorem	24
1.7.5	Bifurcation analysis	25
1.8	Some statistical analyses	26
1.8.1	Principal Component Analysis (PCA)	26
1.8.2	Wavelet Power Spectrum (WPS)	26
1.8.3	Wavelet Cross-coherence Analysis (WCA)	27
1.9	Objectives	27
1.10	Outline of the thesis	28
2	Basic malaria model and analysis	30
2.1	Introduction	30

2.2	Model description	31
2.3	Invariant region	37
2.4	Positivity of solutions	38
2.5	Existence of the disease-free equilibrium	42
2.5.1	Reproduction number	43
2.5.2	Local stability of the disease-free equilibrium point	49
2.5.3	The endemic equilibrium point E_1	53
2.6	Summary	56
3	Modelling the impact of climatic variables on malaria transmission	57
3.1	Abstract	57
3.2	Introduction	58
3.3	Methodology	60
3.3.1	Model formulation	60
3.3.2	Model analysis without climate parameters	62
3.3.2.1	Existence and stability of equilibria	64
3.3.2.2	Existence of endemic equilibria	65
3.3.3	Model analysis with climate-dependent parameters	68
3.3.3.1	Study case and data	68
3.3.3.2	Parameter estimates	71
3.4	Results and discussion	73
3.4.1	Effects of temperature-dependent parameters	73



3.4.2	Spatial distribution of malaria reproduction number over Limpopo	76
3.5	Conclusion	77
4	Analysis of mosquito model without climate variables	81
4.1	Model formulation	81
4.2	Existence and stability of equilibria	84
4.2.1	Existence of equilibrium points	84
4.2.2	Stability of the equilibrium points	86
4.2.3	Global stability of mosquito-free equilibrium	89
4.3	Numerical analysis of the model	90
5	Modelling the influence of temperature and rainfall on the population dynamics of <i>Anopheles arabiensis</i>	96
5.1	Abstract	97
5.2	Introduction	97
5.3	Methods	100
5.3.1	Study area	100
5.3.2	Entomological data	100
5.3.3	Climate data	101
5.3.4	Model formulation	102
5.3.4.1	Puddle dynamics	106
5.3.4.2	Parameters and functions of the model	108

5.4	Results and discussion	108
5.4.1	Model validation	108
5.4.2	Sensitivity analysis	110
5.4.2.1	Model sensitivity to parameters	110
5.4.2.2	Model sensitivity to temperature	113
5.5	Conclusion	120
6	Mathematical modelling and analysis of mosquito-human malaria model	123
6.1	Abstract	124
6.2	Introduction	124
6.3	Model formulation	126
6.4	Mathematical analysis of the model	130
6.4.1	Invariant region	130
6.4.2	Positivity of solutions	133
6.4.3	Disease-free equilibrium and stability analysis	134
6.4.4	Local stability of the disease-free equilibrium	135
6.4.5	Endemic equilibria and stability analysis	139
6.4.6	Local stability of the endemic equilibrium	140
6.5	Sensitivity analysis of model parameters	150
6.6	Results and discussion	151
6.7	Conclusion	152



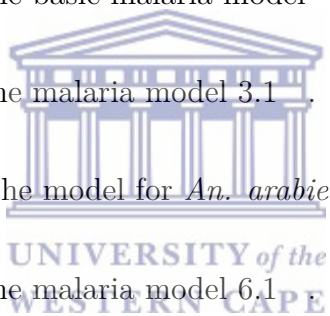
7	Exploring the impact of climate variability on malaria transmission using a dynamic mosquito-human malaria model	157
7.1	Abstract	158
7.2	Introduction	159
7.3	Material and methods	160
7.3.1	Study area	160
7.3.2	Climate and malaria data	161
7.3.3	Mosquito-malaria model formulation	162
7.3.4	Analysis of the model outputs	165
7.3.4.1	Principal Component Analysis (PCA)	165
7.3.4.2	Wavelet Power Spectrum (WPS)	166
7.3.4.3	Wavelet Cross-coherence Analysis (WCA)	167
7.4	Results and discussion	168
7.4.1	Model validation	168
7.4.2	Time series of human population dynamics	169
7.4.3	Malaria and climate variability	169
7.4.3.1	Correlation between climate variables and model outputs	169
7.4.3.2	Wavelet time series analysis of climate variables and malaria	171
7.4.3.3	The lag and cross-correlation of climate variability and malaria	172
7.5	Conclusion	178

8	Concluding remarks and scope for future research	183
8.1	Concluding remarks	183
8.2	Scope for future research	186
	Appendices	187



List of Tables

2.1	State variables of the basic malaria model	35
2.2	Parameters of the basic malaria model	36
3.1	Parameters of the malaria model 3.1	79
5.1	Parameters of the model for <i>An. arabiensis</i>	122
6.1	Parameters of the malaria model 6.1	156
7.1	The Principal Component Analyses (with varimax normalized loadings) showing the possible correlation between the model outputs.	171
7.2	Parameters of the mosquito-malaria model	182



List of Figures

1.1	The image of (a) <i>An. gambiae</i> , (b) <i>An. arabiensis</i> and (c) <i>An. funestus</i> . Source: Centers for Disease Control and Prevention (CDC).	4
1.2	Images of five malaria species. Source: Centers for Disease Control and Prevention (CDC).	6
1.3	Cycle of the malaria parasite in the human and mosquito host (after [55, 66]).	7
1.4	(a) Distribution of endemic malaria, (b) length, (c) onset month, and (d) end month of the malaria transmission season in Africa (for more details cp. [41, 55, 184]. Source: MARA, http://www.mara.org.za). In the regions with two seasons each year, the maps in (c) and (d) refer to the first season in the year.	11
1.5	Malaria risk map for South Africa (released by National Department of Health; after [128]).	13
2.1	Flow diagram of the basic malaria transmission model	34
3.1	Flow diagram for malaria transmission model	61
3.2	Map of South Africa showing (in red) Limpopo province.	69

3.3 (a) Daily mean temperature and (b) rainfall of Limpopo province between January 2002 - December 2004. 70

3.4 Simulation of (a) mosquito death rate, (b) mosquito biting rate, (c) progression rate of mosquitoes, and (d) \mathcal{R}_0 versus temperature. 75

3.5 The reported cases and modelled cases for Limpopo province, South Africa 2002 - 2004. 76

3.6 Simulation of basic reproduction number when δ_v is low ($\delta_v = 0.2$). 77

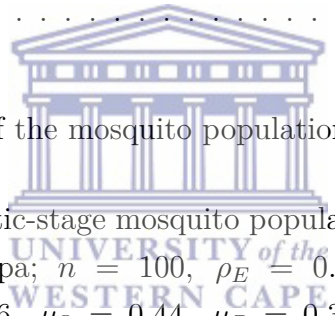
3.7 Simulation of basic reproduction number when δ_v is high ($\delta_v = 0.9$). 78

4.1 Flow diagram of the mosquito population model 83

4.2 Simulated aquatic-stage mosquito population with low progression rate of pupa; $n = 100$, $\rho_E = 0.5$, $\rho_L = 0.14$, $\rho_P = 0.04$, $\mu_E = 0.56$, $\mu_L = 0.44$, $\mu_P = 0.37$, $\rho_{Ah} = 0.46$, $\rho_{Ar} = 0.43$, $\rho_{Ao} = 0.5$, $\mu_{Ah} = 0.18$, $\mu_{Ar} = 0.0043$, $\mu_{Ao} = 0.41$, $\mu_r = 0.043$, $\mathcal{R}_0 = 0.55$ 92

4.3 Simulated adult-stage mosquito population with low progression rate of pupa; $n = 100$, $\rho_E = 0.5$, $\rho_L = 0.14$, $\rho_P = 0.04$, $\mu_E = 0.56$, $\mu_L = 0.44$, $\mu_P = 0.37$, $\rho_{Ah} = 0.46$, $\rho_{Ar} = 0.43$, $\rho_{Ao} = 0.5$, $\mu_{Ah} = 0.18$, $\mu_{Ar} = 0.0043$, $\mu_{Ao} = 0.41$, $\mu_r = 0.043$, $\mathcal{R}_0 = 0.55$ 93

4.4 Simulated aquatic-stage mosquito population with high progression rate of pupa; $n = 100$, $\rho_E = 0.5$, $\rho_L = 0.14$, $\rho_P = 0.08$, $\mu_E = 0.56$, $\mu_L = 0.44$, $\mu_P = 0.37$, $\rho_{Ah} = 0.46$, $\rho_{Ar} = 0.43$, $\rho_{Ao} = 0.5$, $\mu_{Ah} = 0.18$, $\mu_{Ar} = 0.0043$, $\mu_{Ao} = 0.41$, $\mu_r = 0.043$, $\mathcal{R}_0 = 1.01$ 94



- 4.5 Simulated adult-stage mosquito population with high progression rate of pupa; $n = 100$, $\rho_E = 0.5$, $\rho_L = 0.14$, $\rho_P = 0.08$, $\mu_E = 0.56$, $\mu_L = 0.44$, $\mu_P = 0.37$, $\rho_{Ah} = 0.46$, $\rho_{Ar} = 0.43$, $\rho_{Ao} = 0.5$, $\mu_{Ah} = 0.18$, $\mu_{Ar} = 0.0043$, $\mu_{Ao} = 0.41$, $\mu_r = 0.043$, $\mathcal{R}_0 = 1.01$ 95
- 5.1 Map showing the location of Dondotha in KwaZulu-Natal province. 101
- 5.2 Daily rainfall over calibration period showing the daily rainfall of the study area; Dondotha village in KwaZulu-Natal province, South Africa between January 2002 and December 2004. 102
- 5.3 Daily mean temperature over calibration period showing the daily mean temperature of the study area; Dondotha village in KwaZulu-Natal province, South Africa between January 2002 and December 2004. 103
- 5.4 Flow diagram of the mosquito population model 105
- 5.5 Parameter estimates and curves fit for (a) larvae development rate, (b) larvae mortality rate of *An. arabiensis*. See additional files in Appendices for other parameters. 109
- 5.6 Model validation and climate monthly data of New Halfa town, eastern Sudan. (a) Monthly rainfall, (b) mean monthly temperature, and (c) showing the simulated and observed collected larvae over the study area and period. 111
- 5.7 Model sensitivity to parameters. This highlights the sensitivity of the model to parameters. See main text for details. 112
- 5.8 Sensitivity of aquatic-stage mosquito population dynamics to temperature. Effect of constant temperature on (a) eggs, (b) larvae, and (c) pupa *An. arabiensis*. 114

5.9	Sensitivity of adult mosquito population dynamics to temperature. Effect of constant temperature on adult <i>An. arabiensis</i> (a) searching for host, (b) resting, and (c) searching for oviposition site.	115
5.10	Simulated population of immature <i>An. arabiensis</i> . Simulations of (a) eggs, (b) larvae, and (c) pupae population dynamics with climate variables.	117
5.11	Simulated population of adult <i>An. arabiensis</i> . Simulations of adult mosquitoes (a) searching for mating, (b) searching for host, (c) resting, and (d) searching for oviposition site with climate variables.	118
5.12	Spatial distribution of temperature and oviposition rate over South Africa. This highlights the spatial distribution of (a) observed temperature, and (b) simulated oviposition rate over South Africa.	119
6.1	Flow diagram for malaria transmission model	128
6.2	Bifurcation diagram for model 6.1 showing the endemic equilibrium values for the proportion of infectious, using parameters in Table 6.1	152
6.3	Sensitivity index of \mathcal{R}_0 to parameters evaluated at the baseline parameter values given in Table 6.1	153
6.4	Simulations of human and mosquito population with low biting rate, $\epsilon = 0.2$, $\mathcal{R}_0 = 0.3$	154
6.5	Simulations of human and mosquito population with high biting rate, $\epsilon = 0.5$, $\mathcal{R}_0 = 1.1$	155
7.1	The map of KwaZulu-Natal province, South Africa. Source: GIS unit of the Medical Research Council of South Africa. . . .	161

- 7.2 The flow diagram of the mosquito-human malaria model 164
- 7.3 The modelled and reported cases of malaria over KwaZulu-Natal province, South Africa for 2002-2004. 168
- 7.4 Time series of (a) daily mean temperature, (b) rainfall and simulated (c) Susceptible human, (d) Exposed human, (e) Infected human and (f) Recovered human over KwaZulu-Natal province from 1970 - 2005. 170
- 7.5 The wavelet analysis of the climate variables of KwaZulu-Natal province from 1970-2005. The time series of average monthly (a) rainfall and (d) temperature. The WPS of (b) rainfall and (e) temperature time series. The cross-hatched region is the cone of influence, where zero padding has reduced the variance and only pattern above the region are considered reliable. The colour code values from blue (low values) to red (high values). The power has been scaled by the global wavelet spectrum (at right). The global WPS of (c) rainfall and (f) temperature. The black contour line corresponds to 10% significance level, using the global wavelet as the background spectrum. . . . 173
- 7.6 The wavelet analysis of simulated human population dynamics of KwaZulu-Natal province from 1970-2005. The time series of monthly (a) Susceptible, (d) Exposed, (g) Infected and (j) Recovered human. The WPS of (b) Susceptible, (e) Exposed, (h) Infected and (k) Recovered human monthly time series. The cross-hatched region is the cone of influence, where zero padding has reduced the variance and only pattern above the region are considered reliable. The colour code values from blue (low values) to red (high values). The power has been scaled by the global wavelet spectrum (at right). The global WPS of (c) Susceptible, (f) Exposed, (i) Infected and (l) Recovered human. The black contour line corresponds to 10% significance level, using the global wavelet as the background spectrum. . . . 174

- 7.7 The wavelet analysis of the principal components connecting the simulated human population from 1970-2005. The time series of average monthly (a) Factor 1 and (d) Factor 2. The WPS of (b) Factor 1 and (e) Factor 2 time series. The cross-hatched region is the cone of influence, where zero padding has reduced the variance and only pattern above the region are considered reliable. The colour code values from blue (low values) to red (high values). The power has been scaled by the global wavelet spectrum (at right). The global WPS of (c) Factor 1 and (f) Factor 2. The black contour line corresponds to 10% significance level, using the global wavelet as the background spectrum. 175
- 7.8 Cross-correlation coefficients of time series of daily climate variables and simulated (a) Susceptible human, (b) Exposed human, and (c) Infected human at several lags. 176
- 7.9 Cross-correlation coefficients of time series of daily climate variables and simulated (a) Recovered human, (b) Factor 1, and (c) Factor 2 at several lags. 177
- 7.10 Wavelet coherence of rainfall and simulated (a) Susceptible human, (b) Exposed human, (c) Infected human, (d) Recovered human, (e) Factor 1 and (f) Factor 2 over KwaZulu-Natal province between 1970-2005. The arrows indicate the relative phasing of the variables, while the faded regions represent the cone of influence and are not considered for the analyses 179
- 7.11 Wavelet coherence of temperature and simulated (a) Susceptible human, (b) Exposed human, (c) Infected human, (d) Recovered human, (e) Factor 1 and (f) Factor 2 over KwaZulu-Natal between 1970-2005. The arrows indicate the relative phasing of the variables, while the faded regions represent the cone of influence and are not considered for the analyses. 180
- 1 Additional File 1: Curves fit for gonotrophic rate, development and mortality rate of immature *An. arabiensis*. 189

2	Additional File 2: Simulated biting rate of <i>An. arabiensis</i> for 2002.	190
3	Additional File 3: Simulated larvae development rate of <i>An. arabiensis</i> for 2002.	190
4	Maple code for endemic equilibrium	191



List of Publications

Part of this thesis has been either submitted for publication or published in the form of the following research papers in international journals.

1. Abiodun, G.J., Maharaj, R., Witbooi, P. and Okosun, K.O., 2016. Modelling the influence of temperature and rainfall on the population dynamics of *Anopheles arabiensis*. *Malaria Journal*, 15(1), p.1.
2. Abiodun, G.J., Witbooi, P. and Okosun, K.O. Modelling and analysing the impact of temperature and rainfall on mosquito population dynamics over KwaZulu-Natal, South Africa. Accepted for publication in *International Journal of Biomathematics*.
DOI: <http://dx.doi.org/10.1142/S1793524517500553>
3. Abiodun, G.J., Witbooi, P. and Okosun, K.O. Modelling the impact of climatic variables on malaria transmission. Accepted for publication in *Hacettepe Journal of Mathematics and Statistics*.
4. Abiodun, G.J., Witbooi, P., Okosun, K.O. and Maharaj, R. Exploring the impact of climate variability on malaria transmission using a dynamic mosquito-human malaria model. Submitted for publication.
5. Abiodun, G.J., Witbooi, P. and Okosun, K.O. Mathematical modelling and analysis of mosquito-human malaria model. Submitted for publication.

Chapter 1

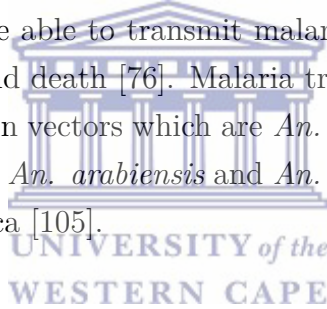
Introduction

Malaria remains one of the most dangerous infectious and prevalent diseases found in tropical and subtropical regions. Globally, every year the mosquito-borne disease causes about 273 million clinical cases and more than one million deaths [192]. It is estimated that more than 40% of the total world population, are exposed to the deadly disease as Sub-Saharan Africa carries an extremely high share of the global burden [203]. Malaria afflicts mostly children under the age of 5 years and pregnant woman who tend to dwell in malaria-prone rural areas [195]. In children, it causes neurological injury, advanced coma, pulmonary edema and kidney problems as a result of damaged vascular system [40]. The impact on pregnant woman leads to an increase of infant low birth weight and infant mortality [122, 180]. Malaria has also been linked to poverty; people suffering from malaria often struggle to earn a living [55]. It is noted that endemic malaria countries have lower rates of economic growth than non-malaria countries [66, 134, 169].

1.1 Malaria background

The origin of the word malaria is from the Italian phrase, (Mal aria) meaning bad air. It was initially thought that the disease came from fetid marshes. Laveren (1880) later discovered that the real cause of malaria is *Plasmodium*. This malaria pathogen can only be transmitted to humans when they are bitten by an infected female *Anopheles* mosquito.

Anopheles (*An.*) is a genus of mosquito from the family of *Culicidae* which comprises several species. Female *Anopheles* require proteins for egg production. Some of these species prefer to feed on human blood (*anthropophily*), while others prefer to feed on animals (*zoophily*). Also, out of these species, only about 40 species are able to transmit malaria well enough to cause substantial human illness and death [76]. Malaria transmission in tropical Africa is sustained by three main vectors which are *An. gambiae*, *An. arabiensis* and *An. funestus* [162], while *An. arabiensis* and *An. funestus* are the main causes of malaria in South Africa [105].



1.2 Mosquito bionomics

The term *bionomics* is used to describe both the ecology of a mosquito species (e.g. larval habitats) and its behaviour (e.g. host biting preferences). Below are some *bionomics* of the three main vectors of malaria transmission with their images in Fig. 1.1

- *An. gambiae* - It is known to be one of the most efficient vectors of malaria in the world and has been studied extensively [38]. It is considered to be highly *anthropophilic*, it prefers to feed on human (e.g., [64]). It is a relatively long-lived species (although not as long as *An. funestus*), with a short larval development period [143]. The larvae are able to develop very quickly (approximately 6 days from egg to adult under

optimal conditions and temperatures). For this reason, it is often found in generally small and temporary fresh water associated with human activity such as pools, puddles, water in hoof prints, wheel ruts or areas of rice cultivation [53, 123]. *An. gambiae* typically feed late at night, a characteristic shared with *An. funestus* that may increase their ability to effectively transmit malaria parasites (e.g., [32]).

- *An. arabiensis* - When compared to *An. gambiae*, *An. arabiensis* is described as *exophagic* (feeds outdoor) and *exophilic* (rests outside) [201]. It is also known to have a wide range of feeding and resting patterns, depending on geographical location (e.g., [61]). There is great variation in the feeding preference depending on the local variation in host availability and composition of the local genotypes of the vector (e.g., [201]). *An. arabiensis* is commonly found in dry, savannah environments and sparse woodland (e.g., [62]), also in forested areas. Its larval habitats are similar to those of *An. gambiae*: generally small, temporary, sunlit, clear and shallow fresh water pools [63], although *An. arabiensis* is able to utilize a greater variety of locations than *An. gambiae*, including slow flowing, partially shaded streams (e.g., [1]) and a variety of large and small natural and man-made habitats. Blood feeding times also vary in frequency but biting generally occurs during the night. Peak evening biting times can begin in the early evening (19:00) or early morning (03:00) (e.g., [189]). This species does, however, demonstrate a predisposition to *exophilic* (or partial *exophilic*) behaviour regardless of where it blood feeds or the source of its meal (e.g., [57]). This behavioural trait, to a greater or lesser extent, is considered to be related to polymorphic chromosomal inversions depending on location (e.g., [39]).
- *An. funestus* - A typical *An. funestus* larval habitat is a large, permanent or semi-permanent body of fresh water with emergent vegetation, such as swamps, large ponds and lake edges [178]. Larvae have been found in both shaded and sunlit environments and it is concluded that *An. funestus* uses emergent vegetation as refuge against predation while



Figure 1.1: The image of (a) *An. gambiae*, (b) *An. arabiensis* and (c) *An. funestus*. Source: Centers for Disease Control and Prevention (CDC).

the shading it casts, or the presence of shade from overhanging plants, is of lesser importance [61]. *An. funestus* is considered to be highly *anthropophilic* and bites late night around 22:00 (e.g., [32]). Its populations from 12 countries have been divided into three geographical locations; eastern Africa, western and central Africa, and southern Africa [58].

1.3 Malaria biology



Malaria is caused by protozoan parasites of the genus *Plasmodium*. There are over 120 species of the parasite genus *Plasmodium* [54], though only five of them cause malaria (see Fig. 1.2 for images): These are:

- *P. falciparum* - It is the most dangerous and commonly found in Africa (e.g., [176]). It can cause severe infection because it multiplies rapidly in the blood, and can thus cause severe blood loss (i.e. *anemia*). Also, the parasites can clog small blood vessels. When this occurs in the brain, cerebral malaria results, a complication that can be fatal. Its incubation period is 9 - 14 days [199]. It is also resistant to most of the drugs used in the prevention and treatment of malaria [141].
- *P. vivax* - It is more common in temperate areas, such as Asia, Latin America and some parts of Africa. Because of the population densities especially in Asia it is probably the most prevalent human malaria parasite. *P. vivax* (as well as *P. ovale*) has dormant liver stages *hypnozoites*

that can activate and invade the blood *relapse* several months or years after the infecting mosquito bite. The incubation period in the human body is approximately 12 - 17 days for the symptoms of the disease to become apparent [199].

- *P. ovale* - It is found mostly in Africa (especially West Africa) and the islands of the western Pacific. It is biologically and morphologically very similar to *P. vivax*. However, unlike *P. vivax*, it can infect individuals who are negative for the duffy blood group, which is the case for many residents of sub-Saharan Africa. This explains the greater prevalence of *P. ovale* (rather than *P. vivax*) in most of Africa. It has an incubation period of 8-17 days in an infected person. Like *P. vivax*, it can hide in the liver of partially treated people to reemerge later on [116].
- *P. malariae* - It is found worldwide and it is the only human malaria parasite species that has a three-day cycle. The other three species discussed above are known to have a two-day cycle. If not treated, *P. malariae* can cause a long-lasting, chronic infection that in some cases can last a lifetime. In some chronically infected patients it can cause serious complications such as the *nephrotic* syndrome. Its incubation period is 2-4 weeks in an infected person.
- *P. knowlesi* - is found throughout Southeast Asia as a natural pathogen of long-tailed and pig-tailed macaques. It has recently been shown to be a significant cause of *zoonotic* malaria in that region, particularly in Malaysia. It has a 24-hour replication cycle and so can rapidly progress from an uncomplicated to a severe infection; fatal cases have been reported.

1.3.1 The parasite cycle

A female *Anopheles* mosquito carrying malaria-causing parasites feeds on a human and injects the parasites in the form of *sporozoites* into the bloodstream.

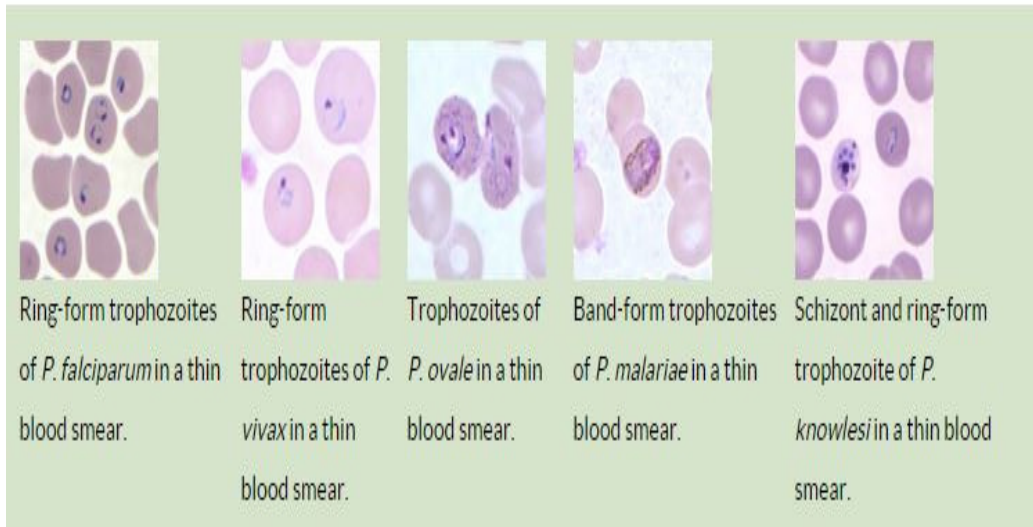


Figure 1.2: Images of five malaria species. Source: Centers for Disease Control and Prevention (CDC).

The *sporozoites* travel to the liver and invade liver cells (see Fig. 1.3). Over 5-16 days (depending on the malaria parasite species), the *sporozoites* grow, divide, and produce tens of thousands of haploid forms, called *merozoites*, per liver cell. The *merozoites* exit the liver cells and re-enter the bloodstream, beginning a cycle of invasion of red blood cells, asexual replication, and release of newly formed *merozoites* from the red blood cells repeatedly over 1-3 days. This multiplication can result in thousands of parasite-infected cells in the host bloodstream, leading to illness and complications of malaria that can last for months if not treated. Some of the *merozoite*-infected blood cells leave the cycle of asexual multiplication. Instead of replicating, the *merozoites* in these cells develop into sexual forms of the parasite, called male and female *gametocytes*, that circulate in the bloodstream. When a mosquito bites an infected human, it ingests the *gametocytes*. In the mosquito gut, the infected human blood cells burst, releasing the *gametocytes*, which develop further into mature sex cells called gametes. Male and female gametes fuse to form diploid zygotes, which develop into actively moving *ookinetes* that burrow into the mosquito midgut wall and form *oocysts*. Growth and division of each *oocyst* produces thousands of active haploid forms called *sporozoites*. After 8-15 days,

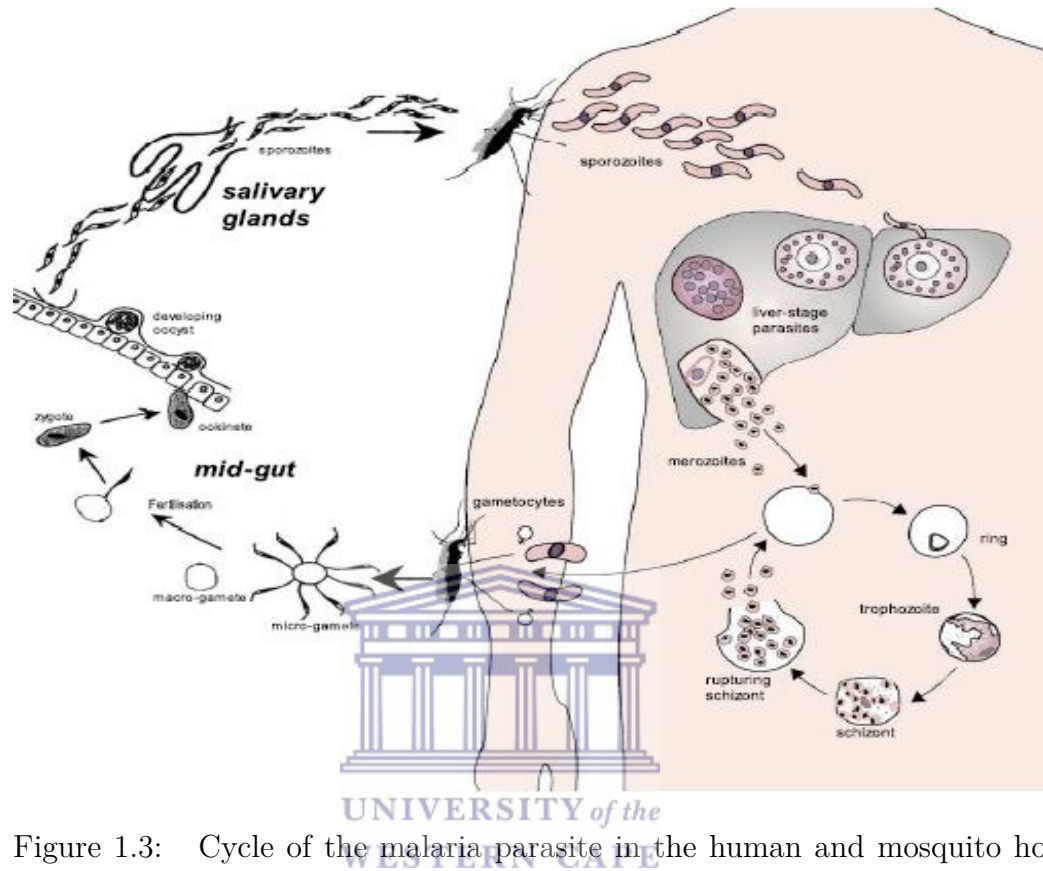


Figure 1.3: Cycle of the malaria parasite in the human and mosquito host (after [55, 66]).

the *oocyst* bursts, releasing *sporozoites* into the body cavity of the mosquito, from which they travel to and invade the mosquito salivary glands. The cycle of human infection re-starts when the mosquito takes a blood meal, injecting the *sporozoites* from its salivary glands into the human bloodstream.

1.3.2 Age and immunity

In biology, immunity is the balanced state of having adequate biological defenses to fight infection, disease, or other unwanted biological invasion. Various biological processes influence the transmission of the malaria parasite and the malaria prevalence [55]. At birth, children are temporarily protected from infection due to the transfer of antibodies from mother [200]. They lose this

immunity after a few months and become susceptible to any disease. However, when the immunity is lost, they quickly develop protection against non-severe disease [70].

1.4 Factors affecting malaria

1.4.1 Climatic factors

Major climatic factors influencing malaria transmission are temperature and rainfall [131, 190]. Temperature affects malaria through various biological processes. The first is the *gonotrophic cycle*, which is the egg production. It is established that egg production only occurs when temperature exceeds 10°C and that the rate of egg development is highly influenced by temperature (e.g., [46]). The second is the *sporogonic cycle*, which is the development of malaria parasite within vectors. It takes temperature of above 16°C to complete the *sporogonic cycle* (e.g., [46]). Thirdly, the ambient air temperature affects the mosquitoes mortality rate. For instance, temperature below 10°C is noted to reduce the duration of survival (e.g., [85]). Fourthly, larval development of mosquitoes depends on water temperatures. For example, *An. gambiae s.s.* emerge as adults only between water temperatures of 18 and 34°C and most larvae develop between 22 and 26°C [8]. The second major climatic factor affecting the spread of malaria is precipitation. Rainfall influences the abundance of aquatic habitats (eggs, larvae and pupae) available to mosquitoes for oviposition [55]. Mosquitoes deposit their eggs in ponds, puddles, or even hoof prints (e.g., [56]). However, excessive rainfall can negatively influence mosquito breeding. Immoderate rainfall can lead to flushing of breeding sites and high losses of aquatic habitats (e.g., [145]). This can paradoxically lead to decrease in malaria transmission [51]. Provided that appropriate breeding places persist, mosquito populations rapidly increase short after the beginning of the rainy season [100, 144]. The population can drop during a following dry season to such low levels that malaria transmission cannot be sustained [117].

For this reason, malaria is mostly seasonal in Africa (e.g., [55]).

Several studies have examined the influence of climate variability on year-to-year variation of seasonal malaria epidemic over the African highlands [152]. For example, Thomson *et al* [188] found that both daily rainfall and annual malaria anomalies are significantly related to the sea surface temperature (SSTs). Hay *et al* [75] confirmed the existence of cycles of disease periodicity of more than one-year long. Using the time-series modelling approach, Zhou *et al* [212] recently ascertained that rainfall and temperature play a significant role in the inter-annual variability of malaria across multiple East African highlands. Their results in contrast to [75] suggested that malaria epidemics in the highlands are initiated by climate variables. More recently, Pascual *et al* [152] combined both a time-series epidemiological model and a statistical approach to analyse monthly cases of malaria from 1970 to 2003 over a highland in Western Kenya. The findings from their study revealed the existence of multiyear cycles of malaria incidence over the study period. Their findings also highlighted the impact of rainfall over malaria resurgence in 1990. It is concluded in line with the study of Zhou *et al* [212] that climate variables play significant roles at different temporal scales and should be considered when building predictive models.

1.4.2 Other factors

Human activities also play a crucial role in transmission and prevention of malaria across Africa [55]. Activities such as deforestation and cultivation of natural swamps increase local temperatures by several degrees (e.g., [65]). It is also established that land cover affects the duration of larval development through its effects on water temperature [133]. Crop irrigation is another important factor affecting the spread of malaria. It has a strong influence on mosquito breeding by increasing the surface water availability [71]. For instance in Africa, irrigated rice cultivation is associated with higher densities of main vectors of malaria and with an extension of the breeding season (e.g.,

[22]).

1.5 Malaria distribution over Africa

Studies [41, 55, 190] have shown that the transmission and distribution of malaria is highly influence by environmental and meteorological conditions. For instance, in Sub-Sahara Africa, the transmission of malaria is highly seasonal (e.g., [41]). Climate variables such as temperature, rainfall and humidity influence biological parameters of malaria [185]. These factors also play significant roles in the availability of mosquitoes which are the vectors of the disease (e.g., [7, 145]). Hence, climate changes are expected to affect transmission of malaria transmission [68]. Malaria is highly centered in the tropics, reaching into subtropical regions on five continents (see Fig. 1.4). Warm and moist conditions in the tropics lead to a stable transmission of the malaria parasite. The malaria belt in Africa is bounded by the dry Sahara as well as the colder temperate zone of South Africa. In West Africa, transmission of malaria is mainly influenced by rainfall. Also in most regions, suitable mosquito breeding sites are only sustained during the rainy season and therefore annual transmission follows seasonal rains [90].

Malaria incidence and control in South Africa

Malaria was first recognized among the early settlers and travelers in Southern Africa [16]. In the mid-19th century, the early pioneers leaving the non-malarious Cape province soon experienced the menace of malaria in the northern Transvaal [59]. Over 20 000 deaths were recorded prior to the implementation of malaria control in the 1930s. During this period, indoor feeding habitat of malaria vectors were recognised and indoor spraying was introduced [59]. Further efforts to eradicate malaria continued through 1960s which led to eradication of *An. funestus* [59].

As a result of the constant efforts to meet the national elimination target by 2018, South Africa has achieved 85% decrease in reported cases from 2000

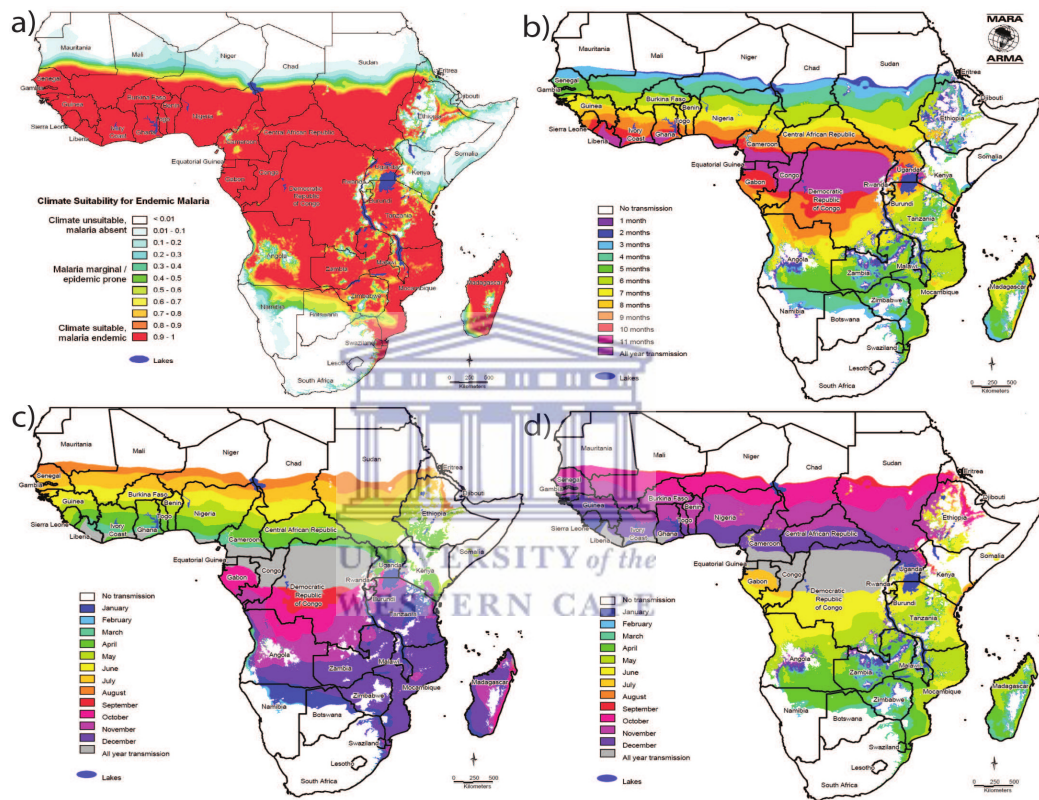


Figure 1.4: (a) Distribution of endemic malaria, (b) length, (c) onset month, and (d) end month of the malaria transmission season in Africa (for more details cp. [41, 55, 184]. Source: MARA, <http://www.mara.org.za>). In the regions with two seasons each year, the maps in (c) and (d) refer to the first season in the year.

to 2011 [206]. A noticeable decrease of 64,624 malaria cases to 9,866 cases were recorded during this period as 424 deaths were reduced to 54 deaths. In addition to these persistence controls, transmission has also been limited to three provinces in the north and northeastern parts (as shown in Fig. 1.5) of the country KwaZulu-Natal, Limpopo, and Mpumalanga [16, 41, 127]. It is endemic along the border with Mozambique and Zimbabwe. Although, despite this enormous decline in malaria transmission, approximately 10% of the country's 50 million populations remain at risk of malaria infection [115, 206]. More importantly, malaria transmission is also noted to be seasonal in the three provinces, with transmission limited to the warm and rainy summer months (September to May). Hence malaria is unstable and epidemic-prone [41].

1.6 Malaria models

In early 20th century, Ross [165] developed the first mathematical model of malaria transmission. He formulated two ordinary differential equations to examine malaria transmission from mosquito vectors to human hosts and vice versa. The model was also used to determine the transmission rate between the host-compartments. In 1928, Ross concluded that there is a possibility of malaria eradication provided numbers of *Anopheles* are reduced below a certain number [55, 166].

Several mathematical malaria models have been developed after the Ross' work (e.g., [141]). For instance, in the 1950s, Macdonald refined the basic model of Ross (e.g., [113]). More factors such as proportion of infective bites is being considered in his model [111], although the model was criticised for ignoring immunity factor [55]. Numerous studies thereafter have considered this factor in their models. Struchiner *et al* [181] further modified the Garki model, considering the fact that immune individuals can lose their immunity. Parasitological data from Senegal is used to refine the work of Cancré *et al* [25] by means of a Bayesian calibration. Their results indicated that in the Ndiop region, about 60% of the immune lose their immunity during the dry season.

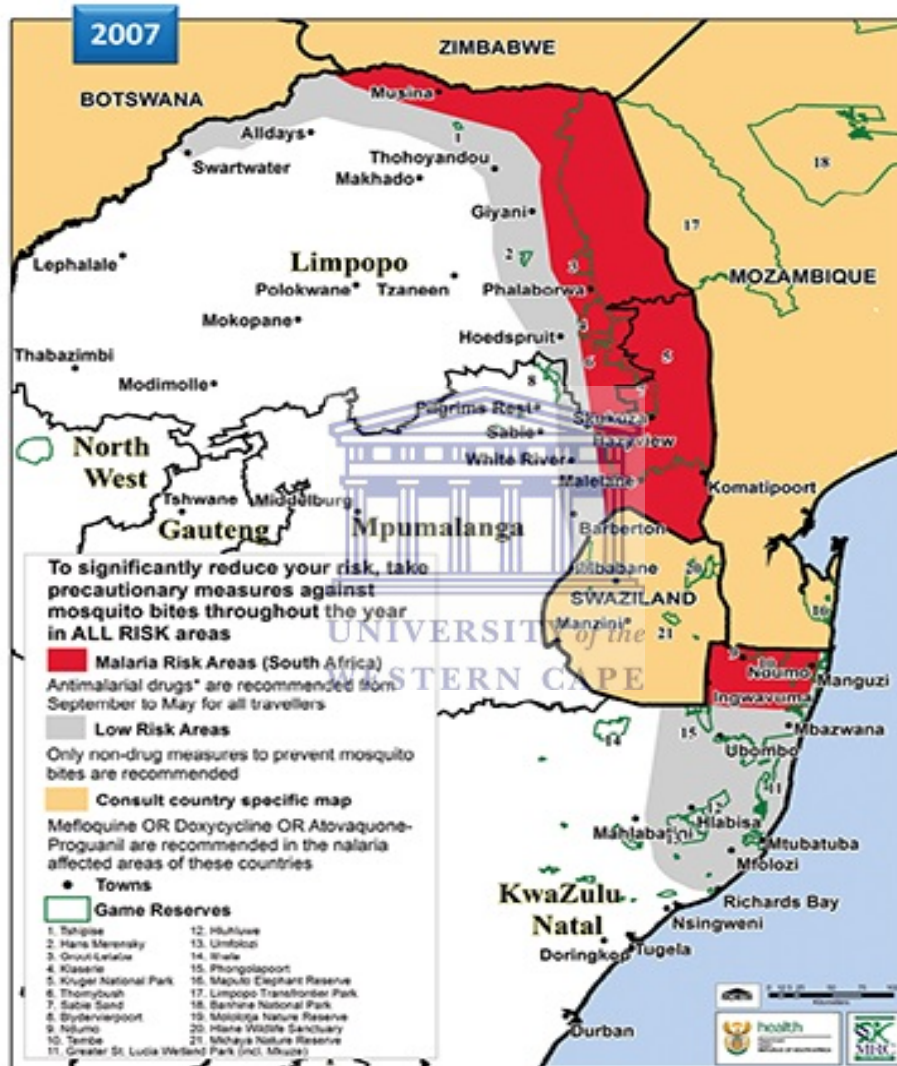


Figure 1.5: Malaria risk map for South Africa (released by National Department of Health; after [128]).

Also, Okosun and Makinde [142] derived and analysed a deterministic model for the transmission of malaria disease with drug resistance in the infective individuals. In their studies, it is established that some individuals can be drug resistant, but with effective control of these individuals, the spread of malaria can be reduced.

The major set-back of classic differential-equation malaria models is the uncertain assumption of quasi-static vector numbers and constant parasite development rates [80]. These mathematical systems were established without any dynamical equations for the number of mosquitoes [136]. Most parameter values pertaining to the development of malaria were also uncertain. In addition, studies are yet to identify a persuasive functional relation for the mosquito survival probability [55]. More importantly, most of these studies also ignored the impact of climate on mosquito population dynamics and the impact on parasite development were also neglected.

However, several studies have considered the distribution of mosquito vectors and malaria with environmental and meteorological variables. These variables (generally including temperature, rainfall, and humidity data) can possibly be used to predict malaria distributions, as they also influence many biological processes [55]. For instance, in the Malaria Atlas Project, a large set of nationally reported case-incidence data and biological temperature- and rainfall-dependent rules of transmission exclusion was used to generate a global spatial distribution of *P. falciparum* malaria [69]. Hay *et al* [74] and Thomson *et al* [186] determined the relationship between malaria incidence and precipitation to predict the epidemic region. Logistic regression and a geo-statistical approach based on environmental factors were also used to examine the distribution of parasite ratios in Mali [87] and over West Africa [88]. Hence, climate- or weather-driven malaria models provide a better understanding of dynamics of malaria transmission.

Numerous climate-based malaria models have also been developed. In the previous studies of Martens *et al* [107, 109, 110], Jetten *et al* [82], and Lindsay and Martens [101], climate data were used to simulate the relation-

ship between climate variables and the basic reproduction rate \mathcal{R}_0 of malaria. *The Mapping Malaria Risk in Africa* (MARA) project [117] presents a simple climate-based distribution model of malaria transmission (hereafter referred to as MDM: MARA Distribution Model) for sub-Saharan Africa [41]. The MDM was based on rainfall and temperature determinants of the parasite development and mosquito survival. Depinay *et al* [45] also developed a comprehensive model to simulate the population dynamics and the development of African *Anopheles* using local environmental data. Using daily temperature and rainfall data, Pascual *et al* [151] introduced a mosquito population model to analyse the development and mortality of larvae as well as mosquito survival. Furthermore, Hoshen and Morse [80] presented the so-called Liverpool Malaria Model (LMM), a weather-driven, mathematical-biological model to simulate the dynamics of malaria parasites. The model also simulates the size and behaviour of the total mosquito population and malaria prevalence within human hosts. Morse *et al* [130] further described the integration of the LMM into a probabilistic multi-model seasonal forecast system [149, 187], which was used in the national malaria control programme in Botswana and surrounding countries [84]. Alonso *et al* [4] developed a mosquito-human malaria model to examine the impact of warmer temperature on malaria incidence in a highland region of East Africa. Their findings suggest that climate change plays an important role in escalating malaria incidence in the region. Also, the recent study of Tompkins *et al* [190] introduced a new dynamical community malaria model (VECToR borne disease model of the International Centre for Theoretical Physics: VECTRI) that accounts for the temperature and rainfall influences on the parasite and vector life cycles. The model put into consideration a simple surface hydrology and accounts for the population density in the calculation of daily mosquito biting rates.

However, these models in the previous studies are difficult to quantify because of many uncertainties [100]. For this reason and limitations, some of the models are not able to give accurate descriptions of the current situation of global malaria, so they have a limited value for assessing the impact of long-term climate change [159, 163]. Also, most studies miss a realistic

linkage between environmental conditions and the survival in aquatic stages [55]. Hydrological changes are also likely to significantly contribute to rates and efficiency with which mosquito populations grow and transmit pathogens [173]. Hence, mosquito breeding must be adequately simulated in relation to hydrological processes instead of precipitation [183].

1.7 Stability for ordinary differential equations

In this section, we present results which will be used to prove the local stability for systems of ordinary differential equations. Hence the following definitions and theorems will be used to determine the local stability of the disease free equilibrium of a system of ordinary differential equations.

Definition 1.7.1 ([141], **The basic reproductive number**).

The basic reproductive number is used to measure the ability of the disease to reproduce, and is denoted by R_0 . This is defined as the expected number of secondary cases reproduced by one infected individual in his/her entire infectious period. When $R_0 < 1$, each infected individual can produce an average of less than one new infected individual during his entire period of infectiousness. In this case the disease will not persist in the population and may be eradicated. But in a situation where $R_0 > 1$ implies that each infected individuals during the entire period of infectiousness can produce more than one new infected individual. This is a strong indication that the disease can persist and invade the population.

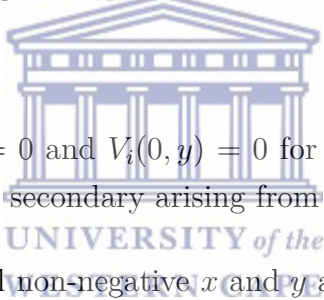
Definition 1.7.2 ([141], **The next generation method**).

The so-called next generation method introduced by van den Driessche et al. [196] and Diekmann et al. [47] is a general method for deriving R_0 in cases where one or more classes of infectives are involved. Suppose we have n disease compartments and m non-disease compartments, and let $x \in \mathbb{R}^n$ and $y \in \mathbb{R}^m$ be the sizes of these compartments. Also, denote the rate of secondary

infection increase of the i^{th} disease compartments by F_i . However V_i is the rate of disease progression, death and recovery decrease the i^{th} compartment, the compartmental model can then be written in the form:

$$\begin{aligned}\frac{dx_i}{dt} &= F_i(x, y) - V_i(x, y), \quad i = 1, \dots, n, \\ \frac{dy_j}{dt} &= g_j(x, y), \quad j = 1, \dots, m.\end{aligned}\tag{1.1}$$

The calculation of the basic reproduction number is based on the linearization of the ordinary differential equations (ODE) model about a disease-free equilibrium, while the following assumptions ensure the existence and well-posedness of a model.

- 
1. Assume $F_i(0, y) = 0$ and $V_i(0, y) = 0$ for all $y \geq 0$ and $i = 1, \dots, n$. All new infections are secondary arising from infected hosts.
 2. $F_i(0, y) \geq 0$ for all non-negative x and y and $i = 1, \dots, n$. Then function F represent new infections and cannot be negative.
 3. $V_i(0, y) \leq 0$ whenever $x_i = 0, i = 1, \dots, n$. Each component, V_i represents a net outflow from compartment i and must be negative (inflow only) whenever the compartment is non- empty.
 4. Assume $\sum_{i=1}^n V_i(x, y) \geq 0$ for all non-negative x and y . The sum represents the total outflow from all infected compartments. Terms in the model leading to increases in $\sum_{i=1}^n x_i$ are assumed to represent secondary infections and therefore belong in F .
 5. Assume the disease-free system $\frac{dy}{dt} = g(0, y)$ has a unique equilibrium that is asymptotically stable. That is, all solutions with initial conditions of the form $(0, y)$ approach a point $(0, y_0)$ as $t \rightarrow \infty$. This point is referred to as the disease-free equilibrium.

Assuming that F_i and V_i meet above conditions, we can form the next generation matrix (operator) FV^{-1} from matrices of partial derivatives of F_i and V_i particularly

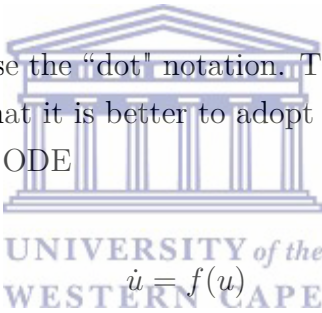
$$F = \left[\frac{\partial F_i(x_0)}{\partial x_j} \right] \quad \text{and} \quad V = \left[\frac{\partial V_i(x_0)}{\partial x_j} \right] \quad (1.2)$$

where $i, j = 1, \dots, m$ and where x_0 is the disease-free equilibrium. The R_0 is given by the spectral radius (dominant eigenvalue) of the matrix FV^{-1} .

1.7.1 Lyapunov functions and stability

In this Section, we (ab)use the "dot" notation. The reason for this is that this abuse is so widespread that it is better to adopt it.

Suppose we are given an ODE



$\dot{u} = f(u)$ (1.3)

and differentiable function

$$V : N \rightarrow \mathbb{R}, \quad x \mapsto V(x) \quad (1.4)$$

where $N \subseteq \mathbb{R}^n$. Denoting by $t \mapsto u(t)$ a solution of (3.11) and using the chain rule we obtain

$$\frac{d}{dt}V(u(t)) = \sum_{k=1}^n \partial_k V(u(t)) \frac{du_k(t)}{dt} = \nabla V(u(t)) \cdot f(u(t)), \quad (1.5)$$

where

$$\partial_k V(x) := \frac{\partial V(x_1, \dots, x_n)}{\partial x_k} \quad (1.6)$$

$$\nabla V(x) := (\partial_1 V(x), \dots, \partial_n V(x))^T \quad (1.7)$$

for $x = (x_1, \dots, x_n)^T \in \mathbb{R}^n$.

Due to the above calculation, the following notation is often used

$$\dot{V}(x) = \nabla V(x) \cdot f(x), \quad (1.8)$$

despite V not being a function of time and the “dotted” V not being exactly a time derivative. This notation comes from the fact that we are “dotting” the composite of V with u , $V(u(t))$, with respect to time and the rigorous notation should be $V(u)$ or $V \circ u$. Since this is a bit more cumbersome, we stick to “dot” notation \dot{V} .

Hence the following technical result, summarises the idea behind Lyapunov functions.

Lemma 1.7.3 ([68], **Lyapunov barrier**).

Let $V : N \rightarrow \mathbb{R}$, be continuously differentiable, where $N \subseteq \mathbb{R}^m$, is a non-empty open and bounded set, with $\dot{V}(x) \leq 0$ for all $x \in N$, and let $m = \min_{x \in \partial N} V(x)$. Then, for any $u_0 \in N$ such that $V(u_0) < m$, the set $C(u_0) = \{u \in N : V(u) \leq V(u_0)\}$ has the property that $\Gamma^+(u_0) \subseteq C \subseteq N$.

Proof. Choose $u_0 \in N$ such that $V(u_0) < m$. Since $u(t)$ is continuous, be either $u_0 \in N$ for all $t \geq 0$ or there exist $t_1 > 0$ such that $u_0 \in N$ for $0 \leq t < t_1$ and $u(t_1) \in \partial N$. However in the latter case, as $\dot{V} \leq 0$ for all $u \in N$,

$$V(u(t_1)) = V(u_0) + \int_0^{t_1} \dot{V}(u(t)) dt \leq V(u_0) < m, \quad (1.9)$$

which contradicts $u(t_1) \in \partial N$, since $m = \min_{u \in \partial N} V(u)$. Therefore $u(t) \in C$ for all $t \geq 0$, i.e., $\Gamma^+(u_0) \subseteq C(u_0)$. \square

Definition 1.7.4 ([68], **(Sign) definite functions**).

A function $F : N \rightarrow \mathbb{R}$ is *positive definite* at $u^* \in N$ if

- (i) $F(u^*) = 0$
- (ii) $F(u) > 0$ for all $u \in N$ with $u \neq u^*$

F is *negative definite* if $-F$ is positive definite.

Definition 1.7.5 ([68], **Lyapunov functions**).

A continuous differentiable function $V : N \rightarrow \mathbb{R}$, where $N \subseteq \mathbb{R}^m$, is a *Lyapunov function* for $\dot{u} = f(u)$ at $u^* \in N$ if

- (i) $V(u)$ is positive definite at u^* , and
- (ii) $\dot{V}(u) \leq 0$ for all $u \in N$.

If in addition, $\dot{V}(u)$ is negative definite at u^* , then V is a *strict Lyapunov function*.

Theorem 1.7.6 ([68], **Lyapunov's first stability theorem (Lyapunov stability condition)**).

Suppose that u^* is a fixed point of $\dot{u} = f(x)$. Suppose that for some open set $N \subseteq \mathbb{R}^m$, containing u^* there exists $V : N \rightarrow \mathbb{R}$, such that V is Lyapunov at u^* . Then u^* is Lyapunov-stable.

Proof. Let $B(u^*, \epsilon)$ be the (closed) ball of radius ϵ centered at u^* ,

$$B(u^*, \epsilon) := \{u : \|u - u^*\| \leq \epsilon\},$$

and choose $\epsilon > 0$ sufficiently small that $B(u^*, \epsilon) \subseteq N$. To prove Lyapunov stability we need to find $\delta > 0$ such that if $u_0 \in B(u^*, \delta)$ then $\Gamma^+(u_0) \subset B(u^*, \epsilon)$.

Note that as V is a Lyapunov function at u^* defined on N and $B(u^*, \epsilon) \subseteq N$ it follows that V is a Lyapunov function at u^* defined on $B(u^*, \epsilon)$. Let

$$m = \min_{u \in \partial B(u^*, \epsilon)} V(u),$$

where $\partial B(u^*, \epsilon)$ is the boundary of $B(u^*, \epsilon)$. Since a continuous function on a compact (closed and bounded) set achieves its infimum, there exists

$y \in \partial B(u^*, \epsilon)$ such that $V(y) = m$. Moreover, since $V(u) > 0$ throughout $B(u^*, \epsilon) \setminus \{u^*\}$, it follows that $m > 0$.

As V is continuous and $V(u^*) = 0$ there exists $\delta > 0$ such that $V(u) < m$ for all $u \in B(u^*, \delta)$.

Applying Lyapunov Barrier Lemma above to the set $N := B(u^*, \epsilon)$ and any point $u_0 \in B(u^*, \delta)$. It gives $\Gamma^+(u_0) \subseteq B(u^*, \epsilon)$ as required. \square

Theorem 1.7.7 ([68], **Lyapunov's second stability theorem (Lyapunov asymptotic stability condition)**).

Suppose there exist a Lyapunov function and let u^ be a fixed point of $\dot{u} = f(u)$ and suppose that for some open set $N \subset \mathbb{R}^m$, containing u^* , there exists $V : N \rightarrow \mathbb{R}$, such that V is strict Lyapunov at u^* . Then u^* is asymptotically stable.*

Proof. Since a strict Lyapunov function is a Lyapunov function, Lyapunov's first stability theorem implies that u^* is Lyapunov-stable and it remains only to prove quasi-asymptotic stability (q.a.s.).

Define ϵ and δ as in the proof of Lyapunov's first stability theorem. Thus if $u_0 \in B(u^*, \delta)$ then $\Gamma^+(u_0) \subseteq B(u^*, \epsilon)$. Pick any such $u_0 \in B(u^*, \delta)$.

Since $\dot{V}(u(t)) \leq 0$ it follows that $V(u(t))$ is non-increasing in t and as V is bounded below by 0 it follows that $\lim_{t \rightarrow \infty} V(u(t)) = c \geq 0$ exists. We shall show that $c = 0$.

As $\Gamma^+(u_0)$ is bounded, $\omega(u_0)$ is non-empty. Consider any $x \in \omega(u_0)$. Then since there exist $t_k \rightarrow \infty$ such that $S(t_k)u_0 \rightarrow x$ as $k \rightarrow \infty$, by continuity of V ,

$$V(x) = \lim_{k \rightarrow \infty} V(S(t_k)u_0) = c.$$

But since $\omega(u_0)$ is forward invariant, if $x \in \omega(u_0)$ then $S(t)x \in \omega(u_0)$ for all $t \geq 0$, and so

$$V(S(t)x) = c \quad \forall t \geq 0.$$

Thus $\dot{V}(x) = 0$ for all $x \in \omega(u_0)$. But $\dot{V}(u) \neq 0$ for $u \neq u^*$, and thus $x = u^*$. So $\omega(u_0) = \{u^*\}$. As V is positive-definite at u^* , $V(u^*) = 0$, i.e. $c = 0$. Therefore $u(t) \rightarrow u^*$ as $t \rightarrow \infty$, showing that u^* is q.a.s. \square

1.7.2 Routh-Hurwitz criteria

The Routh-Hurwitz stability criterion is a necessary and sufficient condition to establish the stability of a single-input, single-output (SISO), linear time invariant (LTI) control system. The criterion establishes a systematic way to show that the linearized equations of motion of a system have only stable solutions. Consider the characteristic equation

$$\Omega^n + a_1\Omega^{n-1} + a_2\Omega^{n-2} + \dots + a_{n-1}\Omega + a_n = 0, \quad (1.10)$$

determining the n eigenvalues Ω of a real $n \times n$ square matrix A . Then the eigenvalues Ω all have negative real parts if

$$H_1 > 0, H_2 > 0, H_3 > 0, \dots, H_n > 0,$$

where H_n are the following determinants:

$$H_1 = |a_1|,$$

$$H_2 = \begin{vmatrix} a_1 & 1 \\ a_3 & a_2 \end{vmatrix},$$

$$H_2 = \begin{vmatrix} a_1 & 1 & 0 \\ a_3 & a_2 & a_1 \\ a_5 & a_4 & a_3 \end{vmatrix},$$

$$H_n = \begin{vmatrix} a_1 & 1 & \dots & 0 \\ a_3 & a_2 & \dots & 0 \\ \vdots & \vdots & \ddots & \vdots \\ a_{2n-1} & a_{2n-2} & \dots & a_n \end{vmatrix}.$$

The steady state is stable (that is, $\text{Re}(\Omega) < 0$) for all λ if and only if $H_j \geq 0$ for all $j = 1, 2, 3, \dots, n$.

The criterion can be performed using either polynomial divisions or determinant calculus.



1.7.3 Hartman-Grobman theorem

Definition 1.7.8 ([13], **Hyperbolic Fixed Point**).

A hyperbolic fixed point for a system of differential equation is a point at which the eigenvalues of the Jacobian for the system evaluated at that point all have nonzero real parts.

Theorem 1.7.9 ([141], **Hartman-Grobman theorem**).

Let $f : \mathbb{R}^n \rightarrow \mathbb{R}^n$ be a smooth map with a hyperbolic fixed point p . Let A denote the linearization of f at point p . Then there exists a neighbourhood U of p and a homeomorphism

$$h : U \rightarrow \mathbb{R}^n$$

such that

$$f_U = h^{-1} \circ A \circ h$$

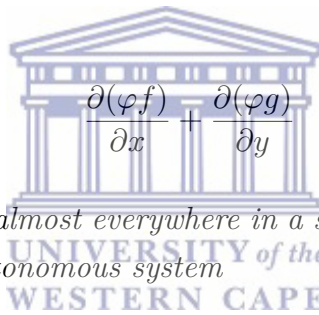
that is, in the neighbourhood U of p , f is topologically conjugate to its linearization.

The theorem explains the local behaviour of dynamical systems in the neighbourhood of a hyperbolic equilibrium point.

1.7.4 Bendixson–Dulac theorem

Theorem 1.7.10 ([23], **Bendixson–Dulac theorem**).

If there exists a C^1 function $\varphi(x, y)$ (called the Dulac function) such that the expression



$$\frac{\partial(\varphi f)}{\partial x} + \frac{\partial(\varphi g)}{\partial y}$$

has the same sign ($\neq 0$) almost everywhere in a simply connected region of the plane, then the plane autonomous system

$$\frac{dx}{dt} = f(x, y),$$

$$\frac{dy}{dt} = g(x, y),$$

has no periodic solutions lying entirely within the region.

Proof. Without loss of generality, let there exist a function $\varphi(x, y)$ such that

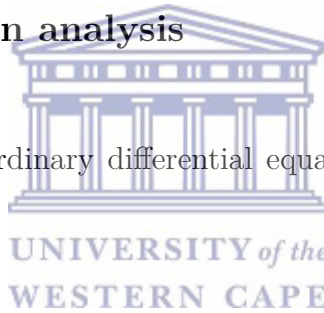
$$\frac{\partial(\varphi f)}{\partial x} + \frac{\partial(\varphi g)}{\partial y} > 0$$

in simply connected region \mathbf{R} . Let C be a closed trajectory of the plane autonomous system in \mathbf{R} . Let D be the interior of C . Then by Green's Theorem,

$$\iint_D \left(\frac{\partial(\varphi f)}{\partial x} + \frac{\partial(\varphi g)}{\partial y} \right) dx dy = \oint_C (-\varphi g dx + \varphi f dy) = \oint_C (-y dx + x dy).$$

But on C , $dx = \dot{x}dt$ and $dy = \dot{y}dt$, so the integral evaluates to 0. This is a contradiction, so there can be no such closed trajectory C . \square

1.7.5 Bifurcation analysis



Consider a family of ordinary differential equations that depend on one parameter ϱ

$$x' = f(x, \varrho), \tag{1.11}$$

where $f : \mathbb{R}^{n+1} \rightarrow \mathbb{R}^n$ is analytic for $\varrho \in \mathcal{I} \subset \mathbb{R}$, $x \in \mathcal{X} \subset \mathbb{R}^n$. Let $x = x_0(\varrho)$ be a family of equilibrium points of Equation 1.11, that is, $f(x_0(\varrho), \varrho) = 0$. Now let

$$z = x - x_0(\varrho).$$

Then

$$z' = A(\varrho)z + O(|z|^2),$$

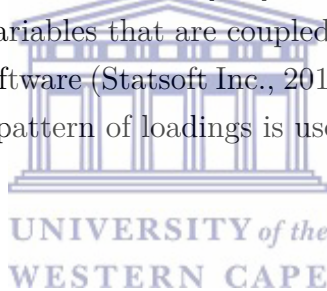
where $A(\varrho) = \frac{\partial f}{\partial x}(x_0(\varrho), \varrho)$.

Let $\varrho_1, \varrho_2, \dots, \varrho_n(\varrho)$ be the eigenvalues of $A(\varrho)$. If, for some i , $\text{Re} \varrho_i(\varrho)$ changes sign at $\varrho = \varrho_0$, we say that ϱ_0 is a bifurcation point of Equation 1.11.

1.8 Some statistical analyses

1.8.1 Principal Component Analysis (PCA)

Principal Component Analysis (PCA) is used to analyse the data generated from the model. PCA is useful in identifying common modes of variability between variables [83, 139, 161], and can reduce numerous number of inter-related variables to a few principal components that capture much of the variance of the original dataset [139]. PCA has been widely and successfully used to help understand, interpret, and reconstruct large, multivariate datasets, both with spatial extent [197] and at single sites [160]. Here, PCA is applied to identify the meteorological variables that are coupled with the model outputs. To achieve this, Statistica software (Statsoft Inc., 2013) using the varimax rotation option to obtain a clear pattern of loadings is used for the analysis.



1.8.2 Wavelet Power Spectrum (WPS)

Wavelet analysis is a method of decomposing a time series into time-frequency space. This view offers interesting insights into the dominant modes of a time series and how those modes vary over time. In contrast to Fourier analysis, wavelet analysis highlights the study of signals whose spectra change with time. In addition, the time-frequency analysis reveals further characteristics such as the periodic components with time progression [29, 152, 191]. The wavelet power spectrum also calculates the distribution of variance between frequency f and different time locations τ . In order to compare the wavelet power spectrum with classical spectral methods, the global wavelet spectrum is computed as the time average of the wavelet power spectrum for each frequency component [152]. For a better understanding of this method and analysis, see [30].

1.8.3 Wavelet Cross-coherence Analysis (WCA)

Time-series analyses have been used to examine the dynamics of several disease epidemics, as it seemed to be the only substitute [28, 77], they are more useful in short-term analyses [11, 50]. They are typically noisy and complex [30]. For these reasons, wavelet cross-coherence is often considered as a substitute. It is a method for analyzing the coherence and phase lag between two time series as a function of both time and frequency [31]. As given in Fourier analysis, the univariate wavelet power spectrum can be extended to quantify statistical relationships between two time series $x(t)$ and $y(t)$ by computing the wavelet coherence

$$R_{x,y}(f, \tau) = \frac{|\langle W_{x,y}(f, \tau) \rangle|}{|\langle W_x(f, \tau) \rangle|^{1/2} \cdot |\langle W_y(f, \tau) \rangle|^{1/2}},$$

where $\langle \rangle$ indicates smoothing in both time and frequency; $W_x(f, \tau)$ represents the wavelet transform of series $x(t)$; $W_y(f, \tau)$ is the wavelet transform of series $y(t)$; and $W_{x,y}(f, \tau) = W_x(f, \tau) \cdot W_y^*(f, \tau)$ is the cross wavelet power spectrum. The wavelet coherence provides local information about the extent to which two non-stationary signals $x(t)$ and $y(t)$, are linearly correlated at a particular frequency (or period). $R_{x,y}(f, \tau)$ is equal to 1 when there is a perfect linear relationship at a particular time and frequency between the two signals [30].

1.9 Objectives

Since malaria transmission and distribution of *Anopheles* are climate- and weather-dependent, the objectives of this thesis are as follow:

- To develop a detailed mosquito model that includes both aquatic and adults stages to under-study the impact of temperature and rainfall on the population dynamics of *Anopheles* mosquitoes.

- To develop and validate mosquito-human malaria model over epidemic regions in South Africa.
- To apply the mosquito-human malaria model to study the effect of climate variability on malaria epidemics over South Africa.

1.10 Outline of the thesis

The thesis is organized as follows:

Chapter 1 offers the biological background of malaria, literature review on malaria models, as well as the objectives of this study. In Chapter 2 of this thesis, we present and analyse a basic malaria model without climate-dependent variables or any intervention strategies. In Chapter 3, we further extend the model and introduce climate-dependent parameters of *Anopheles gambiae* to study malaria transmission dynamics over Limpopo province. Ignoring climate variables, a detailed mosquito model is presented and analysed in Chapter 4. The mosquito model is developed further in Chapter 5 by incorporating climate-dependent parameters into the model. In the same chapter, the model is validated and used to simulate mosquito population dynamics of a village in KwaZulu-Natal province.

Chapter 6 further extends the mosquito model in Chapter 4 by incorporating exposed and infected mosquitoes with human compartments into the model. The detailed mosquito-human malaria model is both analytically and numerically analysed with simulated results.

In Chapter 7 of this thesis, we introduce climate-dependent parameters into the mosquito-human malaria model in Chapter 6 to study the dynamics of human population in KwaZulu-Natal province. The impact of climate variability on malaria transmission over the province is investigated by performing some statistical analyses on the model outputs.

Before we move on to the rest of the thesis, it is important to mention

that simulation results presented in this work are performed using MATLAB, FORTRAN and Ferret.



Chapter 2

Basic malaria model and analysis

2.1 Introduction



Mathematical models for transmission dynamics of malaria are useful in providing a better knowledge of the disease, to plan for the future and to carry out the suitable and appropriate control measures [92]. Several studies (e.g., [37, 92, 138, 165, 194]) have considered used mathematical models to investigate the development of epidemiological disease. The study of malaria using mathematical modeling was originated from the work of Ross [165]. In the study, it was suggested that, if mosquito population can be reduced to below a certain threshold then malaria can be eradicated [165]. His model was modified by MacDonald by including super-infection and concluded that reducing the number of mosquitoes have little effect on epidemiology of malaria in areas of intense transmission [92, 111]. The works of Ross and Macdonald were further extended by Ngwa *et al* [138] with the popular generalized malaria model, which includes both the human and mosquito interactions. Ignoring immunity to disease, Tumwiine *et al* [194] used an SIS and SI model in the human hosts and mosquito vectors respectively, for the study of malaria

epidemic that lasts for a short period. It was concluded in their study that the system is in equilibrium only at the point of extinction. More important results highlighted numerically. Also, in the study of Chiyaka *et al*, mathematical model was used to investigate the malaria treatment and spread of drug resistance in an endemic population. Analysis from the study showed that if the treated humans become immediately uninfected to mosquitoes then treatment will always reduce the number of sensitive infections. Also, their results revealed that the spread of drug resistance with treatment as a control strategy depends on the ratio of the infectious periods of treated and untreated humans and on the transmission rates from infectious humans with resistant and sensitive infections.

In this chapter, we present a basic deterministic model of malaria transmission dynamics. An SEIRS submodel for the mosquito-to-human malaria transmission dynamics and an SEI submodel for the human-to-mosquito malaria transmission dynamics (hereafter, $S_h E_h I_h R_h + S_v E_v I_v$) are also analysed. The primary aim of this chapter is neither to present any new results nor part of the major work from this thesis, but to offer a basic and general background of the model, and some mathematical analyses of the model without climate-dependent variables or any intervention strategies.

2.2 Model description

We consider a basic deterministic $S_h E_h I_h R_h + S_v E_v I_v$ malaria model with the assumption about the nature and time rate of transfer from one compartment to another. We also consider the framework of the model to describe a disease with temporary immunity on recovery from infection. The model indicates that the passage of individuals is from the susceptible class, S_h , to the exposed class, E_h , then to infective class, I_h , and finally to the recovery class, R_h . $S_h(t)$ represents the number of individuals not yet infected with the malaria parasite at time t , or those susceptible to the disease. Malaria as one from many diseases has a latent or exposed phase, $E_h(t)$, during which an individual is said to be

infected but not infectious. Whereas, $I_h(t)$ denotes the number of individuals who have been infected with malaria and are capable of spreading the disease to those in the susceptible class. This is done through infecting the susceptible mosquitoes. Let $R_h(t)$ be the compartment for individuals who have recovered from the disease. We assume these humans have no plasmodium parasites in their bodies and hence can not transmit the infection to mosquitoes. We denote the total human population by $N_h(t)$ such that

$$N_h(t) = S_h(t) + E_h(t) + I_h(t) + R_h(t).$$

It is explained in the study of Killeen *et al* [86] that a susceptible human bitten by an infectious anopheles mosquito may become infected with a finite probability that depends on the abundance of infectious mosquitoes and human hosts. We also assume a horizontal standard incidence with homogeneous mixing meaning that susceptible individuals get infected through contact with infected mosquitoes. The susceptible human population is increased by recruitment (birth and immigration) at a constant rate, Φ_h . In this study, infected immigrants are excluded from the recruitment process because we assume that most individuals who are sick will not travel, also that there is a strict and constant screening exercise to reject infected individuals into the population under study. When susceptible human gets bitten by an infectious female anopheles mosquito, there is a finite probability, β that the parasite (in the form of sporozoites) will be passed on to the human. After this successive bite, the parasite then moves to the liver where it develops into its next life stage. At this stage, the infected human will move to the exposed class. After a while, the parasite, now in form of merozoites enters the blood stream. Hence, the exposed individuals become infectious and progress to infected state at a constant rate η_h . We further assume that the individuals do not recover by natural immunity and exclude the direct infectious-to-susceptible recovery. This is a realistic simplifying assumption because most people have some period of immunity before becoming susceptible again. Individuals who have experienced infection may after some time recover with natural immunity at a constant rate α and move to the recovered class. Since disease-induced immunity due

to malaria is temporary, individuals leave the recovered state to the susceptible state at a fraction q . Humans leave the population through natural death at constant rate μ_h and the infected humans have an additional disease-related death rate constant γ . The mosquito population, $N_v(t)$ is divided into three classes: susceptible, $S_v(t)$; exposed, $E_v(t)$; and infectious, $I_v(t)$ such that

$$N_v(t) = S_v(t) + E_v(t) + I_v(t)$$

In this study, only female anopheles mosquitoes considered as the transmission vector since only female mosquito bites human for blood meals. The female mosquitoes enter the susceptible class through birth at a rate Γ_v . They become infected by biting infectious humans at a rate ϵ . The parasites (in the form of gametocytes) enter the mosquito with probability ξ , when the mosquito bites an infectious human, and the mosquito moves from the susceptible to the exposed class. Depending on the ambient temperature and humidity, after some period of time, the parasite develops into sporozoites and enters the mosquito's salivary glands, and the mosquito progresses at a rate η_v , from the exposed class to the infectious class. We assume that the infective period of the vector ends with its death, and therefore the vector does not recover from being infective [6]. We assume the disease does not kill the infected mosquitoes while the susceptible ones leave the population through natural death, μ_v . The rate of infection of susceptible individual is β_h , and the rate of infecting a susceptible mosquito is ξ_v and κ is the contact rate per human per unit time.

We illustrate the model flow diagram in Figure 2.1, which translates to equation 2.1

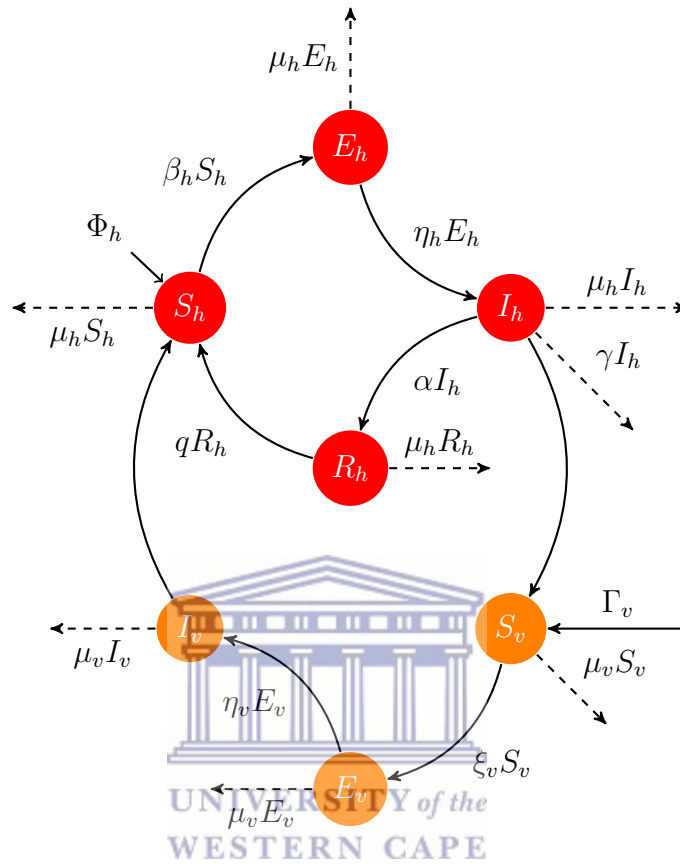
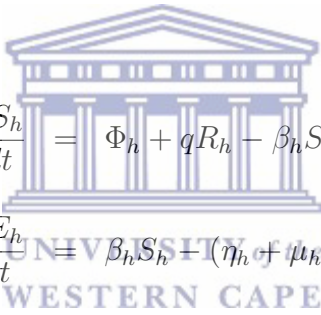


Figure 2.1: Flow diagram of the basic malaria transmission model

The summary of the state variables and parameters satisfying equation 2.1 are presented in Table 2.1 and Table 2.2 respectively. It is assumed that all state variables and parameters of the basic model for both human and mosquito populations are positive for all $t \geq 0$ as will be analysed in a suitable region.

Table 2.1: State variables of the basic malaria model

Symbol	Description
S_h	Number of susceptible humans at time t
E_h	Number of exposed humans at time t
I_h	Number of infectious humans at time t
R_h	Number of recovered humans at time t
S_v	Number of susceptible mosquitoes at time t
E_v	Number of exposed mosquitoes at time t
I_v	Number of infectious mosquitoes at time t
N_h	Total human population at time t
N_v	Total mosquito population at time t



$$\begin{aligned}
\frac{dS_h}{dt} &= \Phi_h + qR_h - \beta_h S_h - \mu_h S_h \\
\frac{dE_h}{dt} &= \beta_h S_h (\eta_h + \mu_h) E_h \\
\frac{dI_h}{dt} &= \eta_h E_h - (\alpha + \gamma + \mu_h) I_h \\
\frac{dR_h}{dt} &= \alpha I_h - (q + \mu_h) R_h \\
\frac{dS_v}{dt} &= \Gamma_v - \xi_v S_v - \mu_v S_v \\
\frac{dE_v}{dt} &= \xi_v S_v - (\eta_v + \mu_v) E_v \\
\frac{dI_v}{dt} &= \eta_v E_v - \mu_v I_v
\end{aligned} \tag{2.1}$$

where $\beta_h = \frac{\beta \epsilon \kappa I_v}{N_h}$ and $\xi_v = \frac{\xi \epsilon \kappa I_h}{N_h}$.

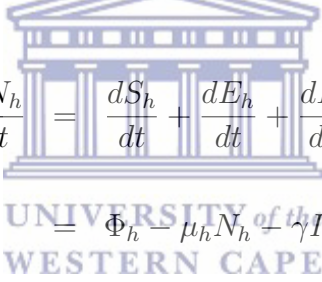
Table 2.2: Parameters of the basic malaria model

Symbol	Description
Φ_h	Recruitment rate of humans
μ_h	Per capita natural death rate for humans
η_h	Progression rate of humans from the exposed state to the infectious state
γ	Per capita disease-induced death rate for humans
q	Per capita rate of loss of immunity
α	Recovery rate for humans from the infected state to the recovered state with natural immunity
β_h	Force of infection for susceptible humans to exposed individuals
β	Probability that a bite results in transmission of infection to the human
Γ_v	Birth rate of mosquitoes
μ_v	Per capita natural death rate for mosquitoes
η_v	Progression rate of exposed mosquitoes to infected mosquitoes
ϵ	Biting rate of mosquito
κ	Contact rate
ξ_v	Force of infection for susceptible mosquitoes to exposed mosquitoes
ξ	Probability that a bite results in transmission of the parasite from an infectious human to the susceptible mosquito

From the study of Tumwiine *et al* [194], the term $\frac{\beta\epsilon\kappa S_h I_v}{N_h}$ is denoted as the rate at which the human hosts S_h get infected by infected mosquitoes I_v and $\frac{\beta\epsilon\kappa S_v I_h}{N_h}$ refers to the rate at which the susceptible mosquitoes S_v are infected by the infected human hosts I_h . This implies that the rate of infection of susceptible human S_h by infected mosquito I_v is dependent on the total number of humans N_h available per vector.

2.3 Invariant region

The total population sizes N_h and N_v can be determined by the differential equations



$$\begin{aligned} \frac{dN_h}{dt} &= \frac{dS_h}{dt} + \frac{dE_h}{dt} + \frac{dI_h}{dt} + \frac{dR_h}{dt} \\ &= \Phi_h - \mu_h N_h - \gamma I_h, \end{aligned} \quad (2.2)$$

It is noted that in the absence of the disease ($\gamma = 0$), we have

$$\begin{aligned} \frac{dN_h}{dt} &= \frac{dS_h}{dt} + \frac{dE_h}{dt} + \frac{dI_h}{dt} + \frac{dR_h}{dt} \\ &= \Phi_h - \mu_h N_h, \end{aligned} \quad (2.3)$$

and

$$\begin{aligned} \frac{dN_v}{dt} &= \frac{dS_v}{dt} + \frac{dE_v}{dt} + \frac{dI_v}{dt} \\ &= \Gamma_v - \mu_v N_v \end{aligned} \quad (2.4)$$

Lemma 2.3.1. *The model system (2.1) has solutions which are contained in the feasible region $\Omega = \Omega_h + \Omega_v$.*

Proof: Let $(S_h, E_h, I_h, R_h, S_v, E_v, I_v) \in \mathbb{R}_+^7$ be any solution of the system with non-negative initial conditions. Since

$$\frac{dN_h}{dt} \leq \Phi_h - \mu_h N_h, \quad (2.5)$$

and using Birkhoff and Rota Theorem on differential inequality [13], we have $0 \leq N_h \leq \frac{\Phi_h}{\mu_h}$, hence

$$\Phi_h - \mu_h N_h \geq K e^{-\mu_h t} \quad (2.6)$$

where K is constant. Therefore, all feasible solutions of the human population only of the system (2.1) are in the region

$$\Omega_h = \left\{ (S_h, E_h, I_h, R_h) \in \mathbb{R}_+^4 : S_h + E_h + I_h + R_h \leq \frac{\Phi_h}{\mu_h} \right\} \quad (2.7)$$

Similarly, the feasible solutions of the mosquito population only are in the region

$$\Omega_v = \left\{ (S_v, E_v, I_v) \in \mathbb{R}_+^3 : S_v + E_v + I_v \leq \frac{\Gamma_v}{\mu_v} \right\} \quad (2.8)$$

Thus, the feasible set for model system (2.1) is given by

$$\Omega = \left\{ (S_h, E_h, I_h, R_h, S_v, E_v, I_v) \in \mathbb{R}_+^7 : S_h, E_h, I_h, R_h, S_v, E_v, I_v \geq 0; N_h \leq \frac{\Phi_h}{\mu_h}; N_v \leq \frac{\Gamma_v}{\mu_v} \right\},$$

which is a positively invariant set under the flow induced by the model (2.1). Hence the system is epidemiologically meaningful and mathematically well-posed in the domain Ω . Also in this domain it is sufficient to consider the dynamics of the flow generated by the model (2.1). Moreover, the usual existence, uniqueness and continuation of results hold for the system. \square

2.4 Positivity of solutions

In this section, we show that the solutions of the system 2.1 are positive.

Lemma 2.4.1. *Let the initial condition be*

$$\{(S_h(0), S_v(0)) > 0, (E_h(0), I_h(0), R_h(0), E_v(0), I_v(0)) \geq 0\} \in \Omega.$$

Then the solution set $\{(S_h, E_h, I_h, R_h, S_v, E_v, I_v)\}(t)$ of the model system (2.1) is positive for all $t > 0$.

Proof: From the first equation of system (2.1), we have

$$\begin{aligned} \frac{dS_h}{dt} &= \Phi_h + qR_h - \beta_h S_h - \mu_h S_h \geq -\beta_h S_h - \mu_h S_h \\ &\geq -(\beta_h + \mu_h)S_h \end{aligned}$$

$$\begin{aligned} \int \frac{1}{S_h} dS_h &\geq -\int (\beta_h + \mu_h) dt \\ S_h(t) &\geq S_h(0) e^{-\int (\beta_h + \mu_h) dt} \geq 0. \end{aligned}$$

From the second equation of system (2.1) we have

$$\begin{aligned} \frac{dE_h}{dt} &= \beta_h S_h - (\eta_h + \mu_h)E_h \geq -(\eta_h + \mu_h)E_h \\ \int \frac{1}{E_h} dE_h &\geq -\int (\eta_h + \mu_h) dt \\ E_h(t) &\geq E_h(0) e^{-(\eta_h + \mu_h)t} \geq 0. \end{aligned}$$

Also from the third equation of system (2.1)

$$\begin{aligned} \frac{dI_h}{dt} &= \eta_h E_h - (\alpha + \gamma + \mu_h)I_h \\ \int \frac{1}{I_h} dI_h &\geq -\int (\alpha + \gamma + \mu_h) dt \\ I_h(t) &\geq I_h(0) e^{-(\alpha + \gamma + \mu_h)t} \geq 0. \end{aligned}$$

The fourth equation of system (2.1) gives

$$\begin{aligned}\frac{dR_h}{dt} &= \alpha I_h - (q + \mu_h)R_h \\ \int \frac{1}{R_h} dR_h &\geq - \int (q + \mu_h) dt \\ R_h(t) &\geq R_h(0)e^{-(q+\mu_h)t} \geq 0.\end{aligned}$$

Considering the fifth equation of system (2.1), we solve for $S_v(t)$

$$\begin{aligned}\frac{dS_v}{dt} &= \Gamma_v - \xi_v S_v - \mu_v S_v \\ &\geq -(\Gamma_v + \mu_v)S_v \\ \int \frac{1}{S_v} dS_v &\geq - \int (\Gamma_v + \mu_v) dt \\ S_v(t) &\geq S_v(0)e^{-(\int \Gamma_v dt + \mu_v t)} \geq 0.\end{aligned}$$

The sixth equation of system (2.1) gives

$$\begin{aligned}\frac{dE_v}{dt} &= \xi_v S_v - (\eta_v + \mu_v)E_v \\ \int \frac{1}{E_v} dE_v &\geq - \int (\eta_v + \mu_v) dt \\ E_v(t) &\geq E_v(0)e^{-(\eta_v + \mu_v)t} \geq 0.\end{aligned}$$

From the seventh equation of system (2.1), we have

$$\begin{aligned}\frac{dI_v}{dt} &= \eta_v E_v - \mu_v I_v \\ \int \frac{1}{I_v} dI_v &\geq - \int \mu_v dt \\ I_v(t) &\geq I_v(0)e^{-\mu_v t} \geq 0.\end{aligned}$$

Furthermore, it is important to show that the region Ω is positively invariant. The right hand sides of equations (2.2) and (2.4) are both bounded by $\Phi_h - \mu_h N_h$ and $\Gamma_v - \mu_v N_v$, respectively. It thus follows that

$$\begin{aligned}\frac{dN_h}{dt} &< 0 \quad \text{if} \quad N_h(t) > \frac{\Phi_h}{\mu_h} \\ \frac{dN_v}{dt} &< 0 \quad \text{if} \quad N_v(t) > \frac{\Gamma_v}{\mu_v}\end{aligned}$$

and

Using a standard comparison theorem [211], it has been shown above that

$$N_h(t) \leq \frac{\Phi_h}{\mu_h}(1 - e^{-\mu_h t}) + N_h(0)e^{-\mu_h t},$$

and

$$N_v(t) \leq \frac{\Gamma_v}{\mu_v}(1 - e^{-\mu_v t}) + N_v(0)e^{-\mu_v t}.$$

Moreover, if $N_h(0) < \frac{\Phi_h}{\mu_h}$ then $N_h(t) \leq \frac{\Phi_h}{\mu_h}$ and if $N_v(0) < \frac{\Gamma_v}{\mu_v}$ then $N_v(t) \leq \frac{\Gamma_v}{\mu_v}$. Therefore Ω is positively invariant. If $N_h(0) > \frac{\Phi_h}{\mu_h}$ and $N_v(0) > \frac{\Gamma_v}{\mu_v}$, then either the solution enters Ω in finite time, or $N_v(t)$ approaches $\frac{\Gamma_v}{\mu_v}$ and $N_h(t)$ approaches $\frac{\Phi_h}{\mu_h}$ asymptotically, and the infected state variables E_h, I_h, E_v and I_v approaches zero as $t \rightarrow \infty$. \square

2.5 Existence of the disease-free equilibrium

In this section, we analysed system (2.1) in order to obtain the equilibrium points of the system and its stability. Let $E = (S_h^*, E_h^*, I_h^*, R_h^*, S_v^*, E_v^*, I_v^*)$ be the steady-state of system (2.1). Then, the equilibrium points are obtained by setting the right hand sides of system (2.1) to zero, that is;

$$\begin{aligned}
 \Phi_h + qR_h - \beta_h S_h - \mu_h S_h &= 0 \\
 \beta_h S_h - (\eta_h + \mu_h)E_h &= 0 \\
 \eta_h E_h - (\alpha + \gamma + \mu_h)I_h &= 0 \\
 \alpha I_h - (q + \mu_h)R_h &= 0 \\
 \Gamma_v - \xi_v S_v - \mu_v S_v &= 0 \\
 \xi_v S_v - (\eta_v + \mu_v)E_v &= 0 \\
 \eta_v E_v - \mu_v I_v &= 0
 \end{aligned} \tag{2.9}$$

The population will never be extinct as long as the human recruitment term Φ_h and the mosquito birth term Γ_v are not zero. This implies that there is no trivial equilibrium point, thus $(S_h^*, E_h^*, I_h^*, R_h^*, S_v^*, E_v^*, I_v^*) \neq (0, 0, 0, 0, 0, 0, 0)$. The model system (2.1) has a steady state in the absence of malaria diseases, that is, $E_h = I_h = E_v = I_v = 0$. Hence, the disease-free equilibrium (DFE) denoted as E_0 , of the model system (2.1) is given by

$$\begin{aligned}
E_0 &= (S_h^*, E_h^*, I_h^*, R_h^*, S_v^*, E_v^*, I_v^*) \\
&= \left(\frac{\Phi_h}{\mu_h}, 0, 0, 0, \frac{\Gamma_v}{\mu_v}, 0, 0 \right)
\end{aligned} \tag{2.10}$$

2.5.1 Reproduction number

The basic reproduction number (sometimes called basic reproductive rate, basic reproductive ratio) denoted by \mathcal{R}_0 , of an infection is the number of cases one case generates on average over the course of its infectious period, in an otherwise uninfected population. In other words, it is the number of secondary infections that one infectious individual would create over the duration of the infectious period, provided that everyone else is susceptible. It is useful as it helps determine whether or not an infectious disease can spread through a population. When $\mathcal{R}_0 < 1$, it implies that each individual produces, on average, less than one new infected individual and hence the disease dies out with time. On the other hand, when $\mathcal{R}_0 > 1$, it means each individual produces more than one new infected individual and hence the disease is able to invade the susceptible population. However, $\mathcal{R}_0 = 1$ is the threshold below which the generation of secondary cases is insufficient to maintain the infection with human community.

The basic reproduction number can not be determined from the structure of the mathematical model alone, but depends on the definition of infected and uninfected compartments. We define \mathbf{X}_s to be the set of all disease free states. That is

$$\mathbf{X}_s = \{x \geq 0 | x_i = 0, i = 1, \dots, m\}.$$

In the computation of \mathcal{R}_0 , it is important to distinguish new infection from all other changes in the population. Let \mathcal{F}_i be the rate of appearance of new infections in compartment i , $\mathcal{V}_i = \mathcal{V}_i^- - \mathcal{V}_i^+$ is the difference between the rate of transfer of individuals in the compartment i , (\mathcal{V}_i^-) , by all other means and the rate of transfer of individuals in the compartment i , (\mathcal{V}_i^+) by all other means, while x_0 be the disease-free equilibrium point. It is assumed that each function is continuously differentiable

at least twice in each variable. The disease transmission model consists of non-negative initial conditions together with the following system of equations:

$$\dot{x} = f_i(x) = \mathcal{F}_i(x) - \mathcal{V}_i(x), \quad i = 1, \dots, n.$$

Let

$$F = \left[\frac{\partial \mathcal{F}_i(x_0)}{\partial x_j} \right] \quad \text{and} \quad V = \left[\frac{\partial \mathcal{V}_i(x_0)}{\partial x_j} \right] \quad (2.11)$$

where $1 \leq i, j \leq m$.

Also, F is non-negative, V is a nonsingular M -matrix in which both are $m \times m$ matrix, where m is the number of infected classes.

Hence, \mathcal{R}_0 is the largest eigenvalue of FV^{-1} , where the (i, j) entry of F is the rate at which infected individuals in compartment j produce new infections i , the (j, k) entry of V^{-1} is the average length of time this individual spends in compartment j during its lifetime, assuming that the population remains near the DFE and barring reinfection.

Hence, the (i, k) entry of the product FV^{-1} is the expected number of new infections in compartment i produced by the infected individual originally introduced into compartment k . Following [48], FV^{-1} is called the next generation matrix for the model and we therefore say

$$\mathcal{R}_0 = \rho(FV^{-1}),$$

where $\rho(A)$ denotes the spectral radius of a matrix A .

In an attempt to calculate \mathcal{R}_0 for system (2.1), we start from the infected compartments for both populations; E_h, I_h, E_v, I_v and then followed by the uninfected classes; S_h, R_h, S_v . The two populations thus give

$$\begin{aligned}
\frac{dE_h}{dt} &= \frac{\beta\epsilon\kappa I_v}{N_h} S_h - (\eta_h + \mu_h) E_h \\
\frac{dI_h}{dt} &= \eta_h E_h - (\alpha + \gamma + \mu_h) I_h \\
\frac{dE_v}{dt} &= \frac{\xi\epsilon\kappa I_h}{N_h} S_v - (\eta_v + \mu_v) E_v \\
\frac{dI_v}{dt} &= \eta_v E_v - \mu_v I_v \\
\frac{dS_h}{dt} &= \Phi_h + qR_h - \frac{\beta\epsilon\kappa I_v}{N_h} S_h - \mu_h S_h \\
\frac{dR_h}{dt} &= \alpha I_h - (q + \mu_h) R_h \\
\frac{dS_v}{dt} &= \Gamma_v - \frac{\xi\epsilon\kappa I_h}{N_h} S_v - \mu_v S_v
\end{aligned} \tag{2.12}$$

UNIVERSITY of the
WESTERN CAPE

From equation (2.12), we show the rate of appearance of new infection in compartments; E_h and E_v using the next generation matrix as

$$\mathcal{F} = \begin{bmatrix} \frac{\beta\epsilon\kappa I_v}{N_h} S_h \\ 0 \\ \frac{\xi\epsilon\kappa I_h}{N_h} S_v \\ 0 \end{bmatrix}. \tag{2.13}$$

Differentiating the matrix above, with respect to the model variables using Jacobian matrix method at the disease-free equilibrium point E_0 , where $N_h \leq \frac{\Phi_h}{\mu_h}$ and $N_v \leq \frac{\Gamma_v}{\mu_v}$

to get Jacobian matrix;

$$F = \begin{bmatrix} 0 & 0 & 0 & \beta\epsilon\kappa \\ 0 & 0 & 0 & 0 \\ 0 & \frac{\xi\epsilon\kappa\Gamma_v\mu_h}{\Phi_h\mu_v} & 0 & 0 \\ 0 & 0 & 0 & 0 \end{bmatrix} \quad (2.14)$$

Calculating the transfer of individuals out of the compartments of the system (2.12) by all other means, we have

$$V = \begin{bmatrix} (\eta_h + \mu_h)E_h \\ (\alpha + \gamma + \mu_h)I_h - \eta_h E_h \\ (\eta_v + \mu_v)E_v \\ \mu_v I_v - \eta_v E_v \end{bmatrix}. \quad (2.15)$$

Hence, the Jacobian matrix of V evaluated at E_0 is given by

$$V = \begin{bmatrix} \eta_h + \mu_h & 0 & 0 & 0 \\ -\mu_h & \alpha + \gamma + \mu_h & 0 & 0 \\ 0 & 0 & \eta_v + \mu_v & 0 \\ 0 & 0 & -\eta_v & \mu_v \end{bmatrix}. \quad (2.16)$$

The inverse of above matrix gives

$$V^{-1} = \begin{bmatrix} \frac{1}{\eta_h + \mu_h} & 0 & 0 & 0 \\ \frac{\eta_h}{(\eta_h + \mu_h)(\alpha + \gamma + \mu_h)} & \frac{1}{(\alpha + \gamma + \mu_h)} & 0 & 0 \\ 0 & 0 & \frac{1}{\eta_v + \mu_v} & 0 \\ 0 & 0 & \frac{\eta_v}{\mu_v(\eta_v + \mu_v)} & \frac{1}{\mu_v} \end{bmatrix}. \quad (2.17)$$

We find the product of equation (2.14) and (2.17) to give

$$FV^{-1} = \begin{bmatrix} 0 & 0 & a_1 & a_2 \\ 0 & 0 & 0 & 0 \\ a_3 & a_4 & 0 & 0 \\ 0 & 0 & 0 & 0 \end{bmatrix}, \quad (2.18)$$

where

$$a_1 = \frac{\beta\epsilon\kappa\eta_v}{\mu_v(\eta_v + \mu_v)}, \quad a_2 = \frac{\beta\epsilon\kappa}{\mu_v}, \quad a_3 = \frac{\xi\epsilon\kappa\Gamma_v\eta_h\mu_h}{(\alpha + \gamma + \mu_h)(\eta_h + \mu_h)\Phi_h\mu_v}, \quad \text{and}$$

$$a_4 = \frac{\xi\epsilon\kappa\Gamma_v\mu_h}{(\alpha + \gamma + \mu_h)(\eta_h + \mu_h)\Phi_h\mu_v}.$$

Hence, we develop the matrix determinant $M = |FV^{-1} - I\lambda| = 0$

$$M = \begin{vmatrix} -\lambda & 0 & a_1 & a_2 \\ 0 & -\lambda & 0 & 0 \\ a_3 & a_4 & -\lambda & 0 \\ 0 & 0 & 0 & -\lambda \end{vmatrix}. \quad (2.19)$$

The eigenvalues from the matrix (2.18) gives

$$\begin{bmatrix} 0 \\ 0 \\ 0 \\ \frac{\sqrt{\mu_v \beta \xi \kappa^2 \epsilon^2 \eta_v \eta_h \left(\frac{\Gamma \mu_h}{\mu_v \Phi_h}\right) (\alpha + \gamma + \mu_h) (\eta_h + \mu_h) (\eta_v + \mu_v)}}{\mu_v (\alpha + \gamma + \mu_h) (\eta_h + \mu_h) (\eta_v + \mu_v)}} \\ - \frac{\sqrt{\mu_v \beta \xi \kappa^2 \epsilon^2 \eta_v \eta_h \left(\frac{\Gamma \mu_h}{\mu_v \Phi_h}\right) (\alpha + \gamma + \mu_h) (\eta_h + \mu_h) (\eta_v + \mu_v)}}{\mu_v (\alpha + \gamma + \mu_h) (\eta_h + \mu_h) (\eta_v + \mu_v)}} \end{bmatrix}. \quad (2.20)$$

Hence, the reproduction number, \mathcal{R}_0 , from the matrix (2.20), which is the spectral radius $\rho(FV^{-1})$, defined as the dominant eigenvalue of FV^{-1} is given by

$$\mathcal{R}_0 = \sqrt{\frac{\mu_v^2 \Phi_h \beta \xi \kappa^2 \epsilon^2 \eta_v \eta_h \Gamma \mu_h (\alpha + \gamma + \mu_h) (\eta_h + \mu_h) (\eta_v + \mu_v)}{(\mu_v^2 \Phi_h (\alpha + \gamma + \mu_h) (\eta_h + \mu_h) (\eta_v + \mu_v))^2}} \quad (2.21)$$

Simplifying equation (2.21) further we have

$$\mathcal{R}_0 = \sqrt{\frac{\beta \xi \kappa^2 \epsilon^2 \eta_v \eta_h \Gamma \mu_h}{\mu_v^2 \Phi_h (\alpha + \gamma + \mu_h) (\eta_h + \mu_h) (\eta_v + \mu_v)}} \quad (2.22)$$

The term $\frac{\eta_h}{\eta_h + \mu_h}$ is the probability of survival of individuals from exposed class to the infectious class. Similarly, $\frac{\eta_v}{\eta_v + \mu_v}$ is the probability of survival of mosquitoes from exposed class to the infectious class of the mosquito population. The term $\frac{\beta\epsilon\kappa\eta_v}{\mu_v(\eta_v + \mu_v)}$ describes the number of humans that one mosquito infects during the lifetime it survives as infectious, when all humans are susceptible. Also, the term $\frac{\xi\epsilon\kappa\eta_h}{(\alpha + \gamma + \mu_h)(\eta_h + \mu_h)}$ describes the number of mosquitoes that are infected through contacts with one infectious human, while the human survives as infectious, when no infection among vectors.

However, we can likewise say

$$\mathcal{R}_0 = \sqrt{\mathcal{R}_{0h} \times \mathcal{R}_{0v}} \quad (2.23)$$

where \mathcal{R}_{0h} is the number of humans that one mosquito infects through its infectious lifetime and defined as

$$\mathcal{R}_{0h} = \sqrt{\frac{\beta\epsilon\kappa\eta_h\mu_h}{\Phi_h(\alpha + \gamma + \mu_h)(\eta_h + \mu_h)}} \quad (2.24)$$

and \mathcal{R}_{0v} is the number of mosquitoes that one human infects through the duration of the infectious period.

$$\mathcal{R}_{0v} = \sqrt{\frac{\xi\epsilon\kappa\eta_v\Gamma_v}{\mu_v^2(\eta_v + \mu_v)}} \quad (2.25)$$

Hence,

$$\mathcal{R}_0 = \sqrt{\frac{\beta\epsilon\kappa\eta_h\mu_h}{\Phi_h(\alpha + \gamma + \mu_h)(\eta_h + \mu_h)} \cdot \frac{\xi\epsilon\kappa\eta_v\Gamma_v}{\mu_v^2(\eta_v + \mu_v)}} \quad (2.26)$$

2.5.2 Local stability of the disease-free equilibrium point

The local stability of the disease-free equilibrium (DFE) is computed by the next generation method of van den Driessche and Watwough [196] as in the basic repro-

duction number shown in equation (2.22), and can be discussed by examining the linearized form of the system (2.1) at the steady state E_0 .

Lemma 2.5.1. *The disease-free equilibrium point E_0 for the system (2.1) is locally asymptotically stable (LAS) if $\mathcal{R}_0 < 1$ and unstable if $\mathcal{R}_0 > 1$*

Proof: The Jacobian matrix of the system (2.1) with $S_h = N_h - (E_h + I_h + R_h)$ at the diseases-free equilibrium point is given by

$$\begin{bmatrix} -(\eta_h + \mu_h) & 0 & 0 & 0 & 0 & \beta\epsilon\kappa \\ \eta_h & -(\alpha + \gamma + \mu_h) & 0 & 0 & 0 & 0 \\ 0 & \alpha & -(q + \mu_h) & 0 & 0 & 0 \\ 0 & -\frac{\xi\epsilon\kappa\Gamma_v\mu_h}{\Phi_h\mu_v} & 0 & -\mu_h & 0 & 0 \\ 0 & \frac{\xi\epsilon\kappa\Gamma_v\mu_h}{\Phi_h\mu_v} & 0 & 0 & -(\eta_v + \mu_v) & 0 \\ 0 & 0 & 0 & 0 & \eta_v & -\mu_v \end{bmatrix} \quad (2.27)$$

The third and the fourth columns have diagonal entries, Therefore, we reduce the matrix by excluding the corresponding rows and columns of $-(q + \mu_h)$ and μ_v which are the eigenvalues of the Jacobian. The reduced matrix thus

$$\begin{bmatrix} -(\eta_h + \mu_h) & 0 & 0 & \beta\epsilon\kappa \\ \eta_h & -(\alpha + \gamma + \mu_h) & 0 & 0 \\ 0 & \frac{\xi\epsilon\kappa\Gamma_v\mu_h}{\Phi_h\mu_v} & -(\eta_v + \mu_v) & 0 \\ 0 & 0 & \eta_v & -\mu_v \end{bmatrix} \quad (2.28)$$

We calculate the remaining eigenvalues and the solutions of the characteristic equa-

tion of the reduced matrix (2.28) is given by

$$(x + \mu_v)(x + Q_1)(x + Q_2)(x + Q_3) - \frac{\beta\xi\eta_v\epsilon^2\kappa^2\Gamma_v\eta_h\mu_h}{\Phi_h\mu_v} \quad (2.29)$$

where

$$Q_1 = \eta_h + \mu_h, \quad Q_2 = \eta_v + \mu_v, \quad \text{and} \quad Q_3 = \alpha + \gamma + \mu_h$$

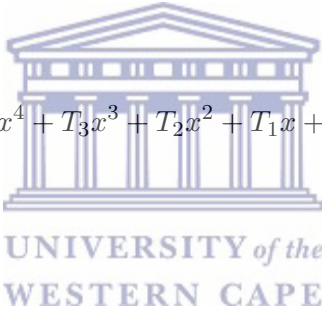
This reduces equation (2.22) to

$$\mathcal{R}_0^2 = \frac{\beta\xi\kappa^2\epsilon^2\eta_v\eta_h\Gamma_v\mu_h}{\mu_v^2\Phi_hQ_1Q_2Q_3} \quad (2.30)$$

and equation (2.29) to

$$x^4 + T_3x^3 + T_2x^2 + T_1x + T_0 = 0 \quad (2.31)$$

where



$$\begin{aligned} T_0 &= \mu_v Q_1 Q_2 Q_3 - \frac{\beta\xi\epsilon^2\kappa^2\Gamma_v\eta_h\eta_v\mu_h}{\Phi_h\mu_v} \\ T_1 &= \mu_v Q_2 Q_3 + Q_1 Q_3 (2\mu_v + \eta_v) + \mu_v Q_1 Q_2 \\ T_2 &= (Q_1 + Q_3)(2\mu_v + \eta_v) + \mu_v Q_2 + Q_1 Q_3 \\ T_3 &= Q_1 + Q_3 + 2\mu_v + \eta_v \end{aligned} \quad (2.32)$$

To ensure that all roots of the polynomial given by (2.31) have negative real parts, we introduce the Routh-Hurwitz conditions [33], which usually have different forms for sufficient and necessary conditions on the coefficients of a polynomial. The Routh-Hurwitz conditions for polynomial (2.31) are $T_0 > 0$, $T_1 > 0$, $T_2 > 0$, $T_3 > 0$, and

$$H_1 = T_3 > 0,$$

$$H_2 = \begin{vmatrix} T_3 & 1 \\ T_1 & T_2 \end{vmatrix} > 0, \quad (2.33)$$

$$H_3 = \begin{vmatrix} T_3 & 1 & 0 \\ T_1 & T_2 & T_3 \\ 0 & T_0 & T_1 \end{vmatrix} > 0, \quad (2.34)$$

$$H_3 = \begin{vmatrix} T_3 & 1 & 0 & 0 \\ T_1 & T_2 & T_3 & 1 \\ 0 & T_0 & T_1 & T_2 \\ 0 & 0 & 0 & T_0 \end{vmatrix} > 0. \quad (2.35)$$

It is clearly seen that $H_4 = T_0 H_3$.

Since $Q_1 > 0$, $Q_2 > 0$, $Q_3 > 0$, we have $T_i > 0$, $i = 1, 2, 3$. Moreover, if $R_0 < 0$, it follows that $T_0 > 0$. Hence we prove that $H_2 > 0$ and $H_3 > 0$. Clearly $H_3 = T_1(T_2 T_3 - T_1) - T_0 T_3^2$ and $H_2 = T_2 T_3 - T_1$.

We show further that

$$\begin{aligned} H_2 &= T_2 T_3 - T_1 \\ &= Q_3^2(\mu_v + Q_1 + Q_2) + Q_2 Q_3(2\mu_v + Q_1 + 2Q_2) \\ &\quad + \mu_v^2(Q_1 + Q_2 + Q_3) + Q_1^2(\mu_v + Q_2 + Q_3) \\ &\quad + 2\mu_v Q_1(Q_2 + Q_3) + Q_2^2(\mu_v + Q_1). \end{aligned} \quad (2.36)$$

It is seen that equation (2.36) above is positive.

Also we show that,

$$\begin{aligned}
 H_3 &= T_1(T_2T_3 - T_1) - T_0T_3^2 \\
 &= (Q_2 + Q_3)(Q_1 + Q_3)(Q_1 + Q_2)W \\
 &\quad + \frac{\beta\xi\epsilon^2\kappa^2\Gamma_v\eta_h\eta_v\mu_h}{\Phi_h\mu_v}
 \end{aligned} \tag{2.37}$$

where $W = (\mu_v + Q_1)(\mu_v + Q_2)(\mu_v + Q_3)$ is also positive. Hence, all of the eigenvalues of the Jacobian matrix have negative real parts when $\mathcal{R}_0 < 1$.

However, $\mathcal{R}_0 > 1$ implies that $T_0 < 0$; and since all of coefficients (T_1, T_2 , and T_3) of the polynomial (2.31) are positive, not all roots of this polynomial can have negative real parts. This means, $\mathcal{R}_0 > 1$, the disease-free equilibrium point is unstable.

2.5.3 The endemic equilibrium point E_1

In the presence of malaria, the model system (2.1) has an equilibrium point called the endemic equilibrium denoted by E_1 and is given by,

$$E_1 = (S_h^{**}, E_h^{**}, I_h^{**}, R_h^{**}, S_v^{**}, E_v^{**}, I_v^{**}).$$

That is, E_1 is a steady-state endemic equilibrium point whereby the disease persists in the population. Its coordinates should satisfy the following conditions for its existence and uniqueness of a particular point.

$$0 < S_h^{**}, 0 < E_h^{**}, 0 < I_h^{**}, 0 < R_h^{**}, 0 < S_v^{**}, 0 < E_v^{**}, 0 < I_v^{**}$$

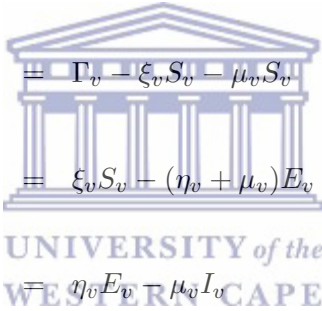
so, from the model system (2.1), we have the first order system of differential equations expressed as

$$S'_h = E'_h = I'_h = R'_h = S'_v = E'_v = I'_v = 0,$$

from which the model system (2.1) turns into the homogeneous system of differential

equations (2.38). So we compute the system (2.38) below for endemic equilibrium points in terms of β^{**} and ξ^{**} values.

$$\begin{aligned}
 0 &= \Phi_h + qR_h - \beta_h S_h - \mu_h S_h \\
 0 &= \beta_h S_h - (\eta_h + \mu_h) E_h \\
 0 &= \eta_h E_h - (\alpha + \gamma + \mu_h) I_h \\
 0 &= \alpha I_h - (q + \mu_h) R_h
 \end{aligned} \tag{2.38}$$



$$\begin{aligned}
 0 &= \Gamma_v - \xi_v S_v - \mu_v S_v \\
 0 &= \xi_v S_v - (\eta_v + \mu_v) E_v \\
 0 &= \eta_v E_v - \mu_v I_v
 \end{aligned}$$

Using Maple and Mathematica programming language, the model system (2.1) has an equilibrium point $E_1 = (S_h^{**}, E_h^{**}, I_h^{**}, R_h^{**}, S_v^{**}, E_v^{**}, I_v^{**})$ and the solutions (in terms of β_h^{**} and ξ_v^{**}) are presented in a simplified structure in equation (2.39) below,

$$\begin{aligned}
\frac{dS_h^{**}}{dt} &= \frac{(\eta_h + \mu_h)(\alpha + \gamma + \mu_h)\Phi_h(q + \mu_h)}{(\beta_h^{**} + \mu_h)(\eta_h + \mu_h)(\alpha + \gamma + \mu_h)(q + \mu_h) - q\alpha\eta_h\beta_h^{**}}, \\
\frac{dE_h^{**}}{dt} &= \frac{(\alpha + \gamma + \mu_h)\Phi_h(q + \mu_h)\beta_h^{**}}{(\beta_h^{**} + \mu_h)(\eta_h + \mu_h)(\alpha + \gamma + \mu_h)(q + \mu_h) - q\alpha\eta_h\beta_h^{**}}, \\
\frac{dI_h^{**}}{dt} &= \frac{\Phi_h(q + \mu_h)\beta_h^{**}\eta_h}{(\beta_h^{**} + \mu_h)(\eta_h + \mu_h)(\alpha + \gamma + \mu_h)(q + \mu_h) - q\alpha\eta_h\beta_h^{**}}, \\
\frac{dR_h^{**}}{dt} &= \frac{\alpha\Phi_h\beta_h^{**}\eta_h}{(\beta_h^{**} + \mu_h)(\eta_h + \mu_h)(\alpha + \gamma + \mu_h)(q + \mu_h) - q\alpha\eta_h\beta_h^{**}}, \quad (2.39) \\
\frac{dS_v^{**}}{dt} &= \frac{\Gamma_v}{\xi_v + \mu_v}, \\
\frac{dE_v^{**}}{dt} &= \frac{\xi_v\Gamma_v}{(\eta_v + \mu_v)(\xi_v + \mu_v)}, \\
\frac{dI_v^{**}}{dt} &= \frac{\xi_v\Gamma_v\eta_v}{(\eta_v + \mu_v)\mu_v(\xi_v + \mu_v)},
\end{aligned}$$

(2.41)

where, $\beta_h^{**} = \frac{\beta\epsilon\kappa I_v^{**}}{S_h^{**} + E_h^{**} + I_h^{**} + R_h^{**}}$.

Putting equation (2.39) into expression $\xi_v^{**} = \frac{\xi\epsilon\kappa I_h^{**}}{S_h^{**} + E_h^{**} + I_h^{**} + R_h^{**}}$, after some algebraic manipulations, the endemic equilibria of the malaria model (2.1) satisfy the

polynomial

$$P(\xi_v^{**}) = \xi_v^{**}(A_1(\xi_v^{**})^2 + A_2(\xi_v^{**})), \quad (2.42)$$

we have

$$A_1(\xi_v^{**}) + A_2 = 0, \quad (2.43)$$

where,

$$A_1 = \eta_h (q + \alpha + \mu_h) + (q + \mu_h) (\alpha + \gamma + \mu_h) \quad (2.44)$$

$$A_2 = \frac{(\alpha + \gamma + \mu_h) (\eta_h + \mu_h)^2 \phi_h^2}{\eta_h \mu_h^2} \left[1 - \frac{\Phi_h(\eta_h + \mu_h)}{\mu_h \eta_h} \mathcal{R}_{0h}^2 \right]. \quad (2.45)$$

Clearly, $A_1 > 0$ and $A_2 \geq 0$ whenever $\mathcal{R}_{0h} \leq 1$, implying that $\xi_v^{**} = \frac{-A_2}{A_1} \leq 0$. Therefore the mass action of the malaria model has no endemic equilibrium whenever $\mathcal{R}_{0h} \leq 1$ and one unique endemic equilibrium when $\mathcal{R}_{0h} > 1$.

2.6 Summary

In this chapter, a basic deterministic malaria model is formulated and analysed. The seven compartments model consist of four human and three adults mosquito compartments. The analysis of the model has shown that there exists a domain where the model is epidemiologically meaningful and mathematically well-posed. The model has been qualitatively analysed for the existence and stability of the disease-free equilibrium and endemic equilibrium points. Thereafter, the next generation method has been used to calculate the reproduction number, \mathcal{R}_0 , as an important parameter that plays a big role in the control of the malaria infection. The stability of the equilibrium points is also analyzed using \mathcal{R}_0 . We also showed that the disease-free equilibrium E_0 is locally asymptotically stable if $\mathcal{R}_0 < 1$, and become unstable, and there exists endemic equilibrium E_1 stable when $\mathcal{R}_0 > 1$.

Chapter 3

Modelling the impact of climatic variables on malaria transmission



Accepted for publication in *Haceteppe Journal of Mathematics and Statistics*.

Authors: G.J. Abiodun, P. Witbooi, K.O. Okosun

In this chapter, we develop and analyse mosquito-human malaria model similar to that in Chapter 2. We incorporate climate-dependent parameters of *Anopheles gambiae* into the model to understudy malaria transmission over Limpopo province in South Africa.

3.1 Abstract

Malaria is one of the most severe disease in the world. A projected climate change will probably alter the region and transmission potential of malaria in Africa. In

this study, a climate-based mathematical model to investigate the impact of temperature and rainfall on malaria transmission is developed and analysed. The basic reproduction number (\mathcal{R}_0) is derived along with stability analysis. The effect of the larval death rate on the reproduction number is also investigated. The model is validated on observed malaria transmission in Limpopo province, South Africa, giving a reasonable fit and in particular, detecting accurately all the spikes in malaria prevalence. The model provides a numerical basis for further refinement towards prediction of the impact of climate variability on malaria transmission.

3.2 Introduction

Malaria remains one of the largest killer diseases in Africa, and most of its victims are women and children [205]. Sub-Saharan Africa continues to carry an extremely high portion of the global malaria burden [208]. In South Africa, over 10% of the population are living in malaria-epidemic provinces and are posed to the danger of contacting the disease [128]. Malaria is caused by a protozoan from the genus *Plasmodium*, and it is spread through mosquitoes. A single bite by a malaria-carrying mosquito can lead to extreme sickness or death. Malaria starts with an extreme cold, followed by high fever and severe sweating. These can be accompanied by joint pain, abdominal pain, headaches, vomiting, and extreme fatigue.

Malaria is very sensitive to climatic conditions, which explains why it is most prevalent in tropical climates, where there is sufficient breeding sites and conducive temperatures for mosquitoes. The high sensitivity of malaria to climate cannot be over-emphasized. For instance, a slight change in temperature can drastically affect the lifespan and patterns of mosquitoes because they are cold-blooded, and moreover, the protozoan itself can only survive in certain temperatures. With higher temperatures, the mosquitoes can mature faster, and thus have more time to spread the disease. The malaria parasite also matures more quickly at warmer temperatures. However, if temperatures become too high, neither mosquitoes nor the malaria parasite can survive. In addition, water is also a major contributor to the spread of malaria, since the vector mosquitoes breed in small pools of water. More rainfall increases the possible breeding grounds for mosquito larvae, which eventually results

in more vectors to spread the disease. With little rainfall, there are few places for the mosquitoes to breed.

When attempting to control the mosquito population, it is important to examine the weather parameters such as temperature and rainfall which are imperative in determining the disease epidemics. Having accurate seasonal climate forecasts of these parameters, it is possible to utilize malaria models that account for early warning systems in endemic regions [175]. These models can also be used to evaluate the possible changes in malaria prevalence regions under climate change scenarios [93]. Malaria transmission models play a significant role in understanding the dynamics of the disease [119] and have long been applied to assess the possible means of intervention [89]. The dynamics have been investigated through deterministic models in many studies [36] and some through stochastic models [135, 175]. Some of these studies either neglect the impact of climate or incorporate it through the force-of-infection. For instance, Okosun and Makinde [141] derived and analyzed a model for the transmission of malaria disease that includes the class of individuals with drug resistance and treatment measures. These parameters were used to formulate optimal strategies for disease control in the population. The local stability of the disease free equilibrium and the existence of an endemic equilibrium were also established in the study.

In addition to these, many studies have also considered climate as a major factor of the disease epidemic. Craig *et al* [41], for instance examined both seasonal case totals and seasonal changes in cases aligned with a series of climatic indicators obtained from three weather stations in KwaZulu-Natal, South Africa. In the study, linear regression analysis with several climate variables is used to verify that seasonal changes are important. Eckhoff *et al* [52] also offered a new model for mosquito population dynamics with the effect of weather and impacts of multiple concurrent interventions. The model is set in large-scale individual-based simulation and results for local elimination of malaria are discussed. More dynamic models for vector life-cycle have been set up and designed to run on a local scale with treatment of water bodies. The Liverpool Malaria Model (LMM) has also been useful in forecasting and climate projection analysis [84]. It includes the effect of temperature on the sporogonic and gonotrophic cycles, and clearly explains the parasite and egg growth stages with consideration to temperature impact on vector death rates [80].

Although the model was made to run over a regional scale, it did not embrace a clear representation of the surface hydrology, and egg laying rates were proportional to the 10-day rain rate. The updated version of LMM (that is LMM₂₀₁₀) which works on daily mean temperature and rainfall was later introduced to fill the lapses above, [55]. In the previous study of Okosun and Makinde [142], the impact of climate on malaria transmission was not put into consideration. Hence this study aims to extend the work of [142] by examining the impact of climate variability on malaria epidemics over Limpopo province, South Africa.

3.3 Methodology

3.3.1 Model formulation

Our model sub-divides the total human population, denoted by N_h into sub-populations of susceptible individuals (S_h), those exposed to malaria parasite (E_h), individuals with malaria symptoms (I_h) and recovered humans (R_h) as illustrated in Fig. 3.1, such that $N_h = S_h + E_h + I_h + R_h$.

The total vector (mosquito) population is denoted by N_v and is sud-divided into susceptible mosquitoes (S_v), mosquitoes exposed to malaria parasite (E_v) and infectious mosquitoes (I_v). Hence, $N_v = S_v + E_v + I_v$.

Susceptible individuals are recruited (by birth or immigration) into the community at a rate Φ_h and acquire malaria through contact with infectious mosquitoes at a rate β_h . Exposed individuals move to infectious class at a rate η_h while infected individuals recover spontaneously at a rate α to join the immune class as some recovered due to treatment at a rate ς . Recovered individuals lose their immunity and return to susceptible class at a rate q while the natural death and disease-induced death rate are denoted by μ_h and γ respectively.

Susceptible mosquitoes (S_v) are recruited at the rate $\vartheta_v(T, R)N_v(1 - \frac{N_v}{P})(1 - \delta_v)$, where P is the larval carrying capacity and δ_v represent the proportion of larvae that died in the process of becoming adult mosquito. We assume that larvae become adult at the rate $\vartheta_v(T, R)$ which is dependent on temperature (T) and rainfall (R). Mosquitoes are assumed to suffer death due to natural causes at a rate $\mu_v(T)$

and their numbers are further reduced due to the use of insecticide spray at a rate ϱ .

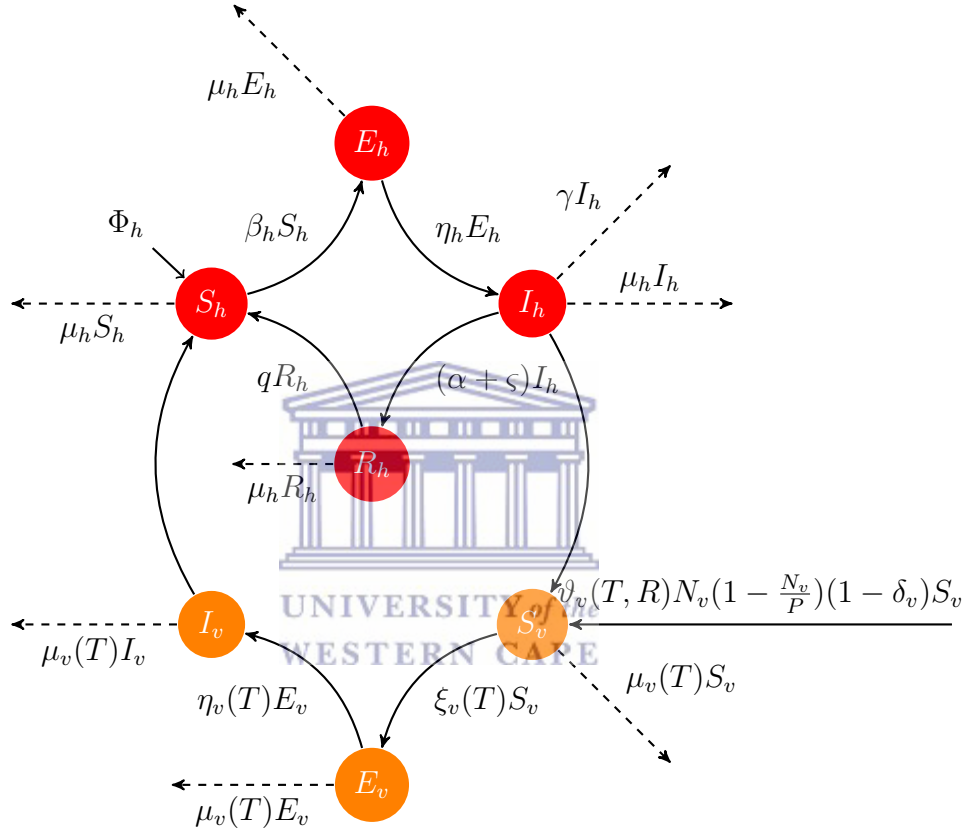
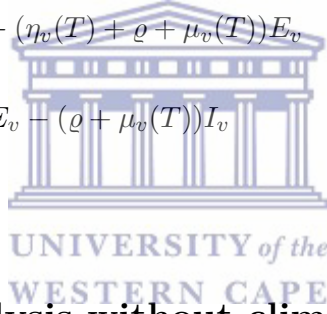


Figure 3.1: Flow diagram for malaria transmission model

The susceptible mosquitoes acquire malaria through contact with infected humans at a rate ξ_v and move to the exposed class (E_v), later to progress towards the infected class (I_v) at a rate $\eta_v(T)$. It is noted that $\beta_h = \frac{v\epsilon\kappa I_v}{N_h}$ and $\xi_v(T) = \frac{\xi\epsilon(T)\kappa I_h}{N_h}$, where v and ξ represent the transmission probability of humans and mosquitoes respectively, with contact rate κ of mosquito per human per unit time. We also assume that mosquito biting rate $\epsilon(T)$ and mortality rate $\mu_v(T)$ are temperature dependent [4, 137, 190]. The dynamics of the disease are described by the following

system of differential equations:

$$\begin{aligned}
 \frac{dS_h}{dt} &= \Phi_h + qR_h - \beta_h S_h - \mu_h S_h \\
 \frac{dE_h}{dt} &= \beta_h S_h - (\eta_h + \mu_h) E_h \\
 \frac{dI_h}{dt} &= \eta_h E_h - (\alpha + \gamma + \varsigma + \mu_h) I_h \\
 \frac{dR_h}{dt} &= (\alpha + \varsigma) I_h - (q + \mu_h) R_h \\
 \frac{dS_v}{dt} &= \vartheta_v(T, R) N_v \left(1 - \frac{N_v}{P}\right) (1 - \delta_v) - (\xi_v + \varrho + \mu_v(T)) S_v \\
 \frac{dE_v}{dt} &= \xi_v S_v - (\eta_v(T) + \varrho + \mu_v(T)) E_v \\
 \frac{dI_v}{dt} &= \eta_v(T) E_v - (\varrho + \mu_v(T)) I_v
 \end{aligned} \tag{3.1}$$



3.3.2 Model analysis without climate parameters

In this section, we begin our mathematical analysis without climate-dependent parameters. We assume all parameters are constant. The malaria model (3.1) will be analyzed in a biologically feasible region as follows. This region should be feasible for both human and vector populations. More precisely, we have

Theorem 3.3.1. *If $S_h(0), E_h(0), I_h(0), R_h(0), S_v(0), E_v(0)$ and $I_v(0)$ are non-negative, then so are $S_h(t), E_h(t), I_h(t), R_h(t), S_v(t), E_v(t)$ and $I_v(t)$ for all $t > 0$. Hence $\limsup_{t \rightarrow \infty} N_h(t) \leq \frac{\Phi_h}{\mu_h}$ and $\limsup_{t \rightarrow \infty} N_v(t) \leq P(1 + \frac{(\varrho + \mu_v)}{\vartheta_v(1 - \delta_v)})$.*

Furthermore, if in addition $N_h(0) \leq \frac{\Phi_h}{\mu_h}$ and $N_v(0) \leq P(1 + \frac{(\varrho + \mu_v)}{\vartheta_v(1 - \delta_v)})$ respectively, then $N_h(t) \leq \frac{\Phi_h}{\mu_h}$ and $N_v(t) \leq P(1 + \frac{(\varrho + \mu_v)}{\vartheta_v(1 - \delta_v)})$ respectively. In particular, the region $D = D_h \times D_v$ with,

$$D_h = \left\{ (S_h, E_h, I_h, R_h) \in \mathbb{R}_+^4 : S_h + E_h + I_h + R_h \leq \frac{\Phi_h}{\mu_h} \right\}$$

and

$$D_v = \left\{ (S_v, E_v, I_v) \in \mathbb{R}_+^3 : S_v + E_v + I_v \leq P \left(1 + \frac{(\varrho + \mu_v)}{\vartheta_v(1 - \delta_v)} \right) \right\}$$

is positively invariant.

Proof. Let $t_1 = \sup \{t > 0 : S_h, E_h, I_h, R_h, S_v, E_v, I_v \text{ are positive on } [0, t]\}$. Since $S_h(0) > 0, E_h(0) > 0, I_h(0) > 0, R_h(0) > 0, S_v(0) > 0, E_v(0) > 0, I_v(0) > 0$, then $t_1 > (0)$. If $t_1 < +\infty$, then by using the variation of constants formula to the first equation of the system 3.1, we have

$$S_h(t_1) = \mathcal{U}(t_1, 0)S_h(0) + \int_0^{t_1} \Lambda \mathcal{U}(t_1, \tau) d\tau$$

where $\mathcal{U}(t_1, \tau) = e^{-\int_\tau^{t_1} (\beta_h + \mu_h)(s) ds}$.

Clearly, $S_h(t_1) > 0$ and it can be shown in the same manner that this is the case for the other variables. This contradicts the fact that t_1 is the supremum because at least one of the variable should be equal to zero at t_1 . Therefore $t_1 = \infty$ which implies that $S_h, E_h, I_h, R_h, S_v, E_v, I_v$ are positive for all $t > 0$.

For the second part of the proof, we obtain by adding the first four equations and the last three equations of the system 3.1 gives

$$\begin{aligned} \frac{dN_h}{dt}(t) &= \Phi_h - \gamma I_h(t) - \mu_h N_h(t) \\ \frac{dN_v}{dt}(t) &= \vartheta_v(T, R)N_v(t) \left(1 - \frac{N_v(t)}{P} \right) (1 - \delta_v) - (\varrho + \mu_v)N_v(t) . \end{aligned} \quad (3.2)$$

Since $0 < I_h(t) \leq N_h(t)$

$$\Phi_h - (\gamma + \mu_h)N_h(t) \leq \frac{dN_h}{dt}(t) \leq \Phi_h - \mu_h N_h(t) \quad (3.3)$$

By using a standard comparison theorem [94], we obtain

$$N_h(0)e^{-(\gamma + \mu_h)t} + \frac{\Phi_h}{\gamma + \mu_h} (1 - e^{-(\gamma + \mu_h)t}) \leq N_h(0)e^{-\mu_h t} + \frac{\Phi_h}{\mu_h} (1 - e^{-\mu_h t})$$

$$N_v(t) = N_v(0)e^{-\vartheta_v(1-\delta_v)t} + P \left[1 + \frac{(\varrho + \mu_v)}{\vartheta_v(1-\delta_v)} \right] \left(1 - e^{-\vartheta_v(1-\delta_v)t} \right).$$

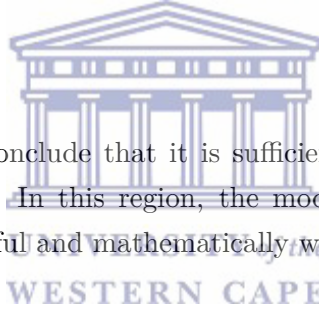
Therefore, if $N_h(0) \leq \frac{\Phi_h}{\mu_h}$ (resp. $N_v(0) \leq P \left[1 + \frac{(\varrho + \mu_v)}{\vartheta_v(1-\delta_v)} \right]$) then

$$N_h(t) \leq \frac{\Phi_h}{\mu_h} \text{ (resp. } N_v(t) \leq P \left[1 + \frac{(\varrho + \mu_v)}{\vartheta_v(1-\delta_v)} \right]).$$

Moreover

$$\limsup_{t \rightarrow \infty} N_h(t) \leq \frac{\Phi_h}{\mu_h} \text{ and } \limsup_{t \rightarrow \infty} N_v(t) \leq P \left[1 + \frac{(\varrho + \mu_v)}{\vartheta_v(1-\delta_v)} \right].$$

This establishes the invariance of D as required. □



From Theorem 3.3.1 we conclude that it is sufficient to consider the dynamics of the model in [125] on D . In this region, the model can be considered as being epidemiologically meaningful and mathematically well-posed [78].

3.3.2.1 Existence and stability of equilibria

Disease-free equilibrium (DFE)

The basic model (3.1) has a DFE given by,

$$\mathcal{E}_0 = (S_h^*, E_h^*, I_h^*, R_h^*, S_v^*, E_v^*, I_v^*) = \left(\frac{\Phi_h}{\mu_h}, 0, 0, 0, P \left(1 + \frac{(\varrho + \mu_v)}{\vartheta_v(1-\delta_v)} \right), 0, 0 \right) \quad (3.4)$$

At this point we find it convenient to introduce the symbol $\bar{\mu}$, $\bar{\mu} = \alpha + \gamma + \zeta + \mu_h$, in order to simplify a number of expressions. The linear stability of \mathcal{E}_0 is ascertained as in [196]. Using the next generation operator method on model (3.1) the basic

reproduction number, denoted by \mathcal{R}_0 , is found to be given by

$$\mathcal{R}_0 = r(FV^{-1}) = \sqrt{\mathcal{R}_{0h} \times \mathcal{R}_{0v}} = \sqrt{\frac{P\xi v(\epsilon\kappa)^2\eta_h\mu_h\eta_v(\vartheta_v(1-\delta_v) - (\varrho + \mu_v))}{\Phi_h\bar{\mu}\vartheta_v(1-\delta_v)(\varrho + \mu_v)(\eta_v + \varrho + \mu_v)}} \quad (3.5)$$

where r is the spectra radius (dominant eigenvalue in magnitude) of the next generation matrix FV^{-1} . The term \mathcal{R}_{0h} represents the number of humans that one mosquito infects through its infectious lifetime and it is defined as

$$\mathcal{R}_{0h} = \sqrt{\frac{v\epsilon\kappa\eta_h\mu_h}{\Phi_h\bar{\mu}(\eta_h + \mu_h)}} \quad (3.6)$$

and \mathcal{R}_{0v} is the the number of mosquitoes that one human infects through the duration of the infectious period, which is also defined as

$$\mathcal{R}_{0v} = \sqrt{\frac{P\xi\epsilon\kappa\eta_v(\vartheta_v(1-\delta_v) - (\varrho + \mu_v))}{\vartheta_v(1-\delta_v)(\varrho + \mu_v)(\eta_v + \varrho + \mu_v)}}. \quad (3.7)$$

Furthermore, using Theorem 2 of [196], the following result is established.

Theorem 3.3.2. *The disease free equilibrium, \mathcal{E}_0 , of the model (3.1), is locally asymptotically stable (LAS) if $\mathcal{R}_0 < 1$ and unstable otherwise.*

We refer readers to other studies (e.g., [138, 141, 142]) for the proof of this theorem. The basic reproduction number \mathcal{R}_0 measures the average number of new infections generated by a single infected individual in a completely susceptible population [5, 47, 196]. Thus, Theorem 3.3.2 implies that malaria can be eliminated from human population (when $\mathcal{R}_0 < 1$) if the initial sizes of the sub-populations are in the basin of attraction of the DFE.

3.3.2.2 Existence of endemic equilibria

In search of an endemic equilibrium point of model (3.1) (that is, equilibria where at least one of the infected components in model (3.1) is non-zero), we take the

following steps. Let $\mathcal{E}_1 = (S_h^{**}, E_h^{**}, I_h^{**}, R_h^{**}, S_v^{**}, E_v^{**}, I_v^{**})$ represent any arbitrary endemic equilibrium of model (3.1). Also let

$$\beta_h^{**} = \frac{v\epsilon\kappa I_v^{**}}{N_h^{**}}, \quad \text{and} \quad \xi_v^{**} = \frac{\xi\epsilon\kappa I_h^{**}}{N_h^{**}} \quad (3.8)$$

be the forces of infection of human and vectors at steady state, respectively. Setting the right hand side of equation (3.1) to zero gives the following expressions.

$$\left. \begin{aligned} S_h^{**} &= \frac{\Phi_h + qR_h^{**}}{\beta_h^{**} + \mu_h}, \\ E_h^{**} &= \frac{\beta_h^{**} S_h^{**}}{\eta_h + \mu_h}, \\ I_h^{**} &= \frac{\eta_h E_h^{**}}{\bar{\mu}}, \\ R_h^{**} &= \frac{(\alpha + \zeta) I_h^{**}}{q + \mu_h}, \\ S_v^{**} &= \frac{P \mu_v (\vartheta_v (1 - \delta_v) + (\varrho + \mu_v))}{\vartheta_v (1 - \delta_v) ((\varrho + \mu_v) + \xi_v^{**})}, \\ E_v^{**} &= \frac{\xi_v^{**} S_v^{**}}{\eta_v + \varrho + \mu_v}, \\ I_v^{**} &= \frac{\eta_v E_v^{**}}{\varrho + \mu_v}. \end{aligned} \right\} \quad (3.9)$$

Substituting (3.9) in (3.8) gives,

$$\xi_v^{**} = \frac{\epsilon \kappa \xi \beta_h^{**} \eta_h \mu_h (q + \mu_h) \Phi_h}{((\bar{\mu}) \mu_h (q + \mu_h) (\eta_h + \mu_h) + \beta_h^{**} ((\bar{\mu}) \mu_h (q + \mu_h) + \eta_h (q(\gamma + \mu) + (\bar{\mu}) \mu_h))) - (\gamma \beta_h^{**} \eta_h (q + \mu_h) \Phi_h)} \quad (3.10)$$

It can be shown that the non-zero equilibria of the model satisfy the following polynomial (in terms of β_h^{**})

$$P(\beta_h^{**}) = A(\beta_h^{**})^3 + B(\beta_h^{**})^2 + C(\beta_h^{**})$$

$$A(\beta_h^{**})^2 + B(\beta_h^{**}) + C = 0, \quad (3.11)$$

where,

$$\begin{aligned} A &= \vartheta_v(1 - \delta_v) [(\bar{\mu})\mu_h(q + \mu_h) + \eta_h(q\mu_h + (\alpha + \mu_h)\mu_h)] (\eta_v + \mu_v) \\ &\quad [(\bar{\mu})\mu_h(q + \mu_h)\mu_v + \eta_h(\epsilon\kappa\xi\mu_h(q + \mu_h) + (q\mu_h + (\alpha + \mu_h)\mu_h)(\varrho + \mu_v))] \Phi_h \\ B &= \mu_h(q + \mu_h)\vartheta_v(1 - \delta_v)(\bar{\mu})(\eta_h + \mu_h)(\eta_v + \varrho + \mu_v)\Phi_h [\mathcal{R}_k - \mathcal{R}_0^2] G_1 \\ C &= (\bar{\mu})^2\mu_h^2(q + \mu_h)^2(\eta_h + \mu_h)^2\vartheta_v(1 - \delta_v)(\eta_v + \varrho + \mu_v)\Phi_h [1 - \mathcal{R}_0^2], \end{aligned} \quad (3.12)$$

where,

$$\mathcal{R}_k = \frac{\epsilon\kappa\xi\eta_h\mu_h(q + \mu_h) + 2[(\bar{\mu})\mu_h(q + \mu_h) + \eta_h(q\mu_h + (\bar{\mu}))](\varrho + \mu_v)}{(\varrho + \mu_v)[(\bar{\mu})\mu_h(q + \mu_h)\eta_h(q(\gamma + \mu_h) + (\bar{\mu})\mu_h)]}$$

and

$$G_1 = (\bar{\mu})\mu_h(q + \mu_h)\eta_h(q(\gamma + \mu_h) + (\bar{\mu})\mu_h).$$

It is noted that coefficient A is always positive and C is positive if \mathcal{R}_0 is less than 1 (resp $\sqrt{\mathcal{R}_k}$) respectively.

We have the following results:

Proposition 3.3.3.

1. If $\mathcal{R}_k \geq 1$ then system (3.1) exhibits a forward bifurcation.
2. If $\mathcal{R}_k < 1$ then system (3.1) exhibits a backward bifurcation.

Proof:

1. For $\mathcal{R}_k \geq 1$ we obtain when $\mathcal{R}_0 > 1$ that $C < 0$. This implies that system (3.1) has a unique endemic steady state. If $\mathcal{R}_0 \leq 1$, then $C \geq 0$ and $B \geq 0$. In this case system (3.1) has no endemic steady states.
2. For $\mathcal{R}_k < 1$ we discuss the following cases:
 - i. $\mathcal{R}_0 > 1$, in this case $C < 0$ and system (3.1) has a unique endemic steady state.
 - ii. $\mathcal{R}_0 \leq \sqrt{\mathcal{R}_k}$, in this case both B and C are positive implying that system (3.1) has no endemic steady states.
 - iii. $\sqrt{\mathcal{R}_k} < \mathcal{R}_0 < 1$, here $C > 0$ and $B < 0$ while the discriminant of (3.11), $\Delta(\mathcal{R}_0) = B^2 - 4AC$, can be either positive or negative. We have $\Delta(1) = B^2 > 0$ and $\Delta(\sqrt{\mathcal{R}_k}) = -4AC < 0$, then there exists R_{0c} such that $\Delta(R_{0c}) = 0$, $\Delta(\mathcal{R}_0) < 0$ for $\sqrt{\mathcal{R}_k} < \mathcal{R}_0 < R_{0c}$ and $\Delta(\mathcal{R}_0) > 0$ for $R_{0c} < \mathcal{R}_0$. This together with the signs of B and C imply that system (3.1) has no endemic steady states when $\sqrt{\mathcal{R}_k} < \mathcal{R}_0 < R_{0c}$, one endemic steady state when $\mathcal{R}_0 = R_{0c}$ and two endemic steady states when $R_{0c} < \mathcal{R}_0 < 1$. ■

3.3.3 Model analysis with climate-dependent parameters

3.3.3.1 Study case and data

Over the years, *Plasmodium falciparum* has been identified as the main causes of malaria in three northeastern provinces of South Africa namely; Mpumalanga, KwaZulu-Natal and Limpopo [41, 105]. In this study, we validate our model against the malaria transmission case in Limpopo Province. The province is situated in the northernmost corner of South Africa (as in Fig. 3.2). It experiences long sunny days and dry weather on most days with high rainfall between October - March every year [60] as shown in Fig. 3.3. In Fig. 3.3a, four peaks with three nadirs are observed for temperature between January

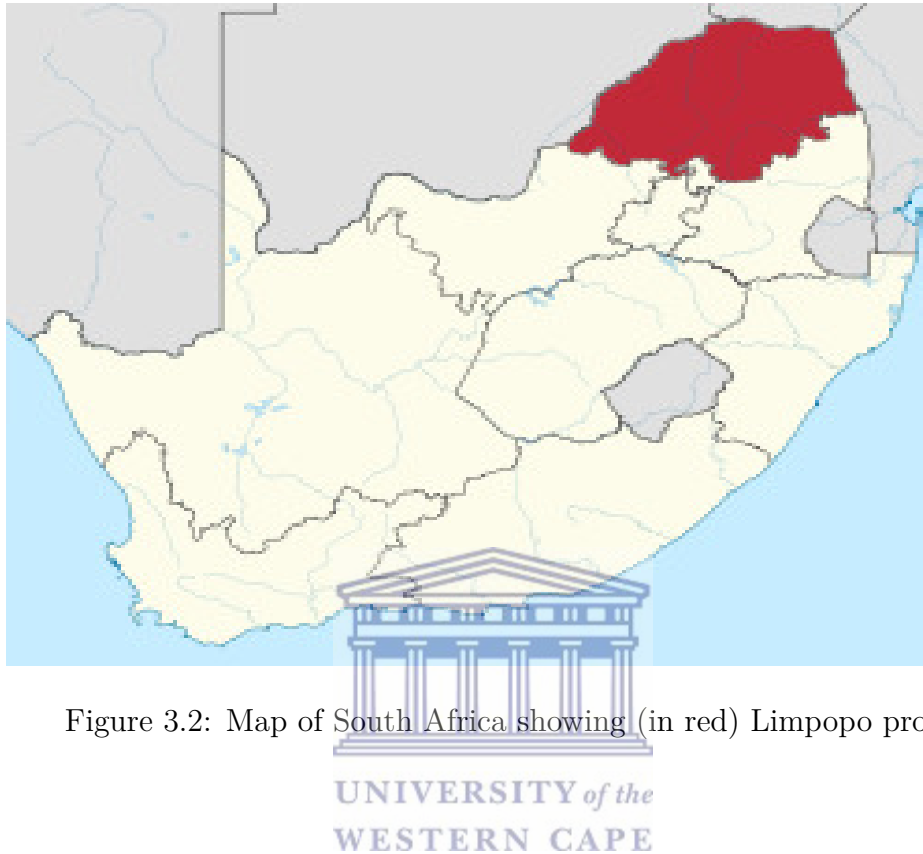


Figure 3.2: Map of South Africa showing (in red) Limpopo province.

2002 - December 2004. The peaks occur between December-February while the nadirs falls within June - August each year. Similar patterns are observed for rainfall in Fig. 3.3b. This implies that the province simultaneously experiences high temperature and rainfall between December - February with low temperature and rainfall between June-August every year. Also, malaria transmission in this province is seasonal with climatic conditions affecting the development of mosquitoes and malaria parasites [60, 177]. Hence, we limit our study on the effects of temperature and rainfall on the transmission of malaria in Limpopo province. The input climate data used for this study is obtained from the South African Weather Service (SAWS). The data consists of daily rainfall, minimum and maximum temperature that spans the period of 2002 to 2004, while the monthly malaria cases for the same period were obtained from the South African Department of Health.

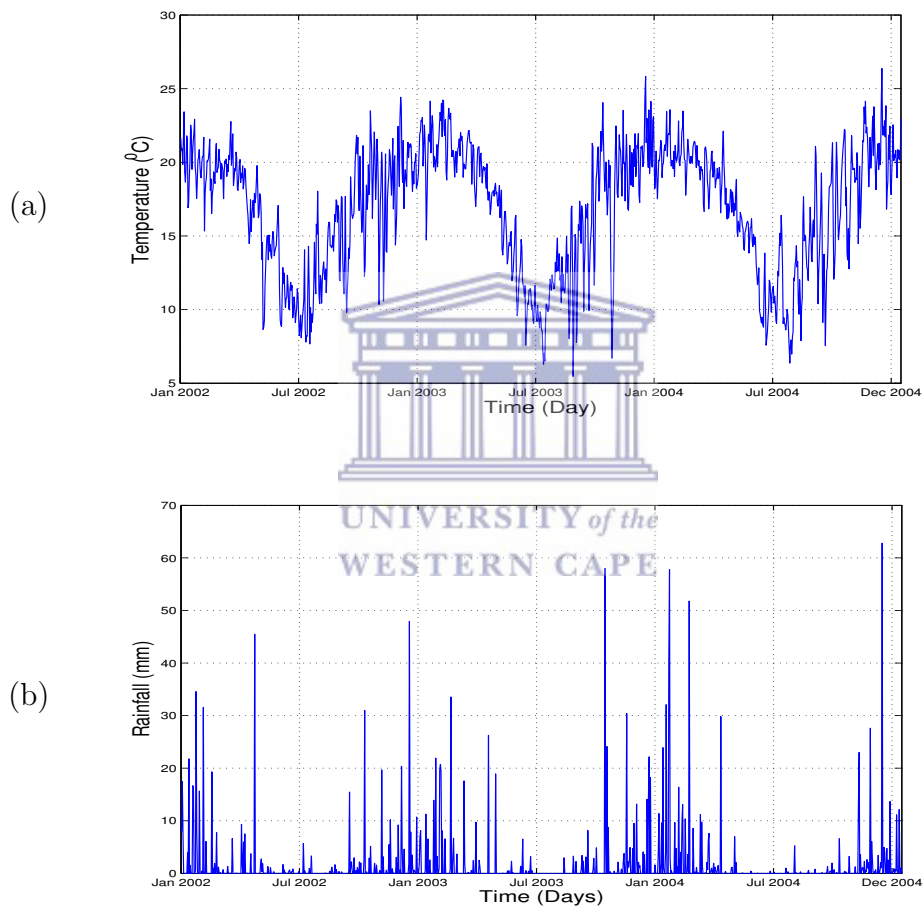


Figure 3.3: (a) Daily mean temperature and (b) rainfall of Limpopo province between January 2002 - December 2004.

3.3.3.2 Parameter estimates

Some of the parameters relevant to our study has also featured in previous studies of malaria transmission modeling such as in [35, 105, 106, 141]. In these papers the authors have obtained fairly good numerical values for these parameters and we reference such parameter values in Table 3.1. Following the approach of [105], we estimate below the death and birth rate of humans in Limpopo province.

Human death rate μ_h

According to the World Health Organization (WHO) report, the life expectancy for South Africa in 2002 was 49.1 years. Hence, the human death rate is calculated as



$$\mu_h = \frac{1}{49.1 \times 365} = 0.000056 \text{ Day}^{-1} \quad (3.13)$$

Human birth rate Φ_h

The South Africa Census for 2001 stated that the total human population for Limpopo province was 5,273,642 [179]. Therefore, the human birth rate for Limpopo province is estimated as

$$\Phi_h = \mu_h \times 5,273,642 = 295 \text{ Human/day} \quad (3.14)$$

The climate-dependent parameters affect the processes occurring during either the larva or adult stage. For instance, adequate rainfall is essential for survival of eggs, larva and pupae, while temperature is influential in the gonotrophic cycle, a period between blood meal and oviposition [4].

Mosquito birth rate

We assume that the mosquito birth rate depends on temperature and rainfall (through the dependence on breeding site availability). From the study of Parham and Michael [150], we adopt the mosquito birth rate ϑ_v as

$$\vartheta_v(T, R) = \frac{n_e p_e(R) p_l(R, T) p_p(R)}{t_e + t_l(T) + t_p} \quad (3.15)$$

where n_e is the number of eggs laid per adult female mosquito, per oviposition, $p_e(R)$, $p_l(R, T)$ and $p_p(R)$ are the survival probabilities of eggs, larvae and pupae respectively. The duration of each development stage is given as t_e , $t_l(T)$ and t_p and the average larval duration $t_l(T) = 1/(0.0554T - 0.06737)$. We assume that temperature and rainfall act independently on the survival probability p_l of larvae (cf. [150]) such that $p_l(R, T) = \pi_1(T)\pi_2(R)$. In this product the first factor is taken as

$$\pi_1(T) = e^{-(0.0554T - 0.06737)}. \quad (3.16)$$

Rainfall has been shown to positively correlate with malaria incidence [145], although excessive rainfall may flush out larvae and breeding sites [45, 190]. Hence we assume a quadratic relationship between the survival probabilities of eggs, larvae and pupae and rainfall. For larvae, we assume

$$\pi_2(R) = \left[\frac{4p_l^*}{R_l^2} \right] R(R_l - R), \quad (3.17)$$

where R_l is the rainfall limit beyond which breeding site get flushed out and no immature stages survive [150]. The constant p_l^* is the maximum survival probability.

Mosquito mortality rate

To estimate the temperature-dependent mortality rate of adult mosquito, we adopt the expression of [4, 110, 137] that;

$$\mu_v(T) = \frac{1}{(-4.4 + 1.31T - 0.03T^2)} \text{Day}^{-1} \quad (3.18)$$

Larval carrying capacity

We assume that rainfall generates available water for larval development, and that the carrying capacity P evolves according to a dynamical equation that takes into account habitable per unit area and unit time [4]. It is measured in terms of an effective maximum number of larvae available in a given region and we say



$$P = \frac{P_A}{P_E} R \quad (3.19)$$

where $P_E = 10^{-3} < P_E < 10^0$ is the carrying capacity decaying rate, and the conversion factor P_A varies between 0 and 10^4 . Other parameters are shown in Table 3.1 with references.

3.4 Results and discussion

3.4.1 Effects of temperature-dependent parameters

In this section, we illustrate the relationship between temperatures and mosquito death rate, biting rate, progression rate and reproduction number in Fig. 3.4. The U-curve in Fig. 3.4a explains in line with [137, 168], that the mosquito death rate is high at low temperature (below 18°C), low between $18 - 25^\circ\text{C}$ and

increases at temperature beyond 25°C. Fig. 3.4b and Fig. 3.4d show unimodal curves (as also appeared in [128, 137]) which are thermally constrained at both low and high temperature. Fig. 3.4b demonstrates low mosquito biting rate at temperatures below 12°C, gradually increasing with a slight declination at upper thermal limit of 35°C. Although the limit is considerably different from that obtained in the study [21] which is 30°C, it matches the findings of [128, 137] which is 35°C. However, the reproduction number \mathcal{R}_0 in Fig. 3.4d indicates that the optimal temperature for malaria transmission is 30°C, with threshold where $\mathcal{R}_0 > 1$ between 18 – 38°C. The transmission range is closer to the new estimate of [128] which is 15 – 35°C, while the optimal temperature and the threshold is similar to the findings of [137] which are 31.5°C and 22.34 – 38.6°C respectively. Over a certain temperature interval, the parasite development rate in Fig. 3.4c increases with temperature.

In Fig. 3.5, the incidence cases of malaria infection is simulated by our model and compared with malaria monthly cases for Limpopo province as reported by South African Department of Health. The figure shows a good fit between the observed and predicted incidence over wide range of time. It can be seen in both results that malaria is climate-driven with epidemic peaks between December-February when temperature and rainfall is high in the province (as shown in Fig. 3.3). The results indicate a seasonal pattern as both curves decrease progressively from February through August and then gradually increase from September through January. However, we observe high temperature and rainfall in December 2002 resulting in an epidemic peak (in Fig. 3.5) in January 2003. At the ideal temperature (28°C) and conditions, the development of *Anopheles* from juvenile to adult stage takes about 14 days [45, 190], while symptoms of falciparum malaria arise between 7-15 days depending on immunity of the host [55].

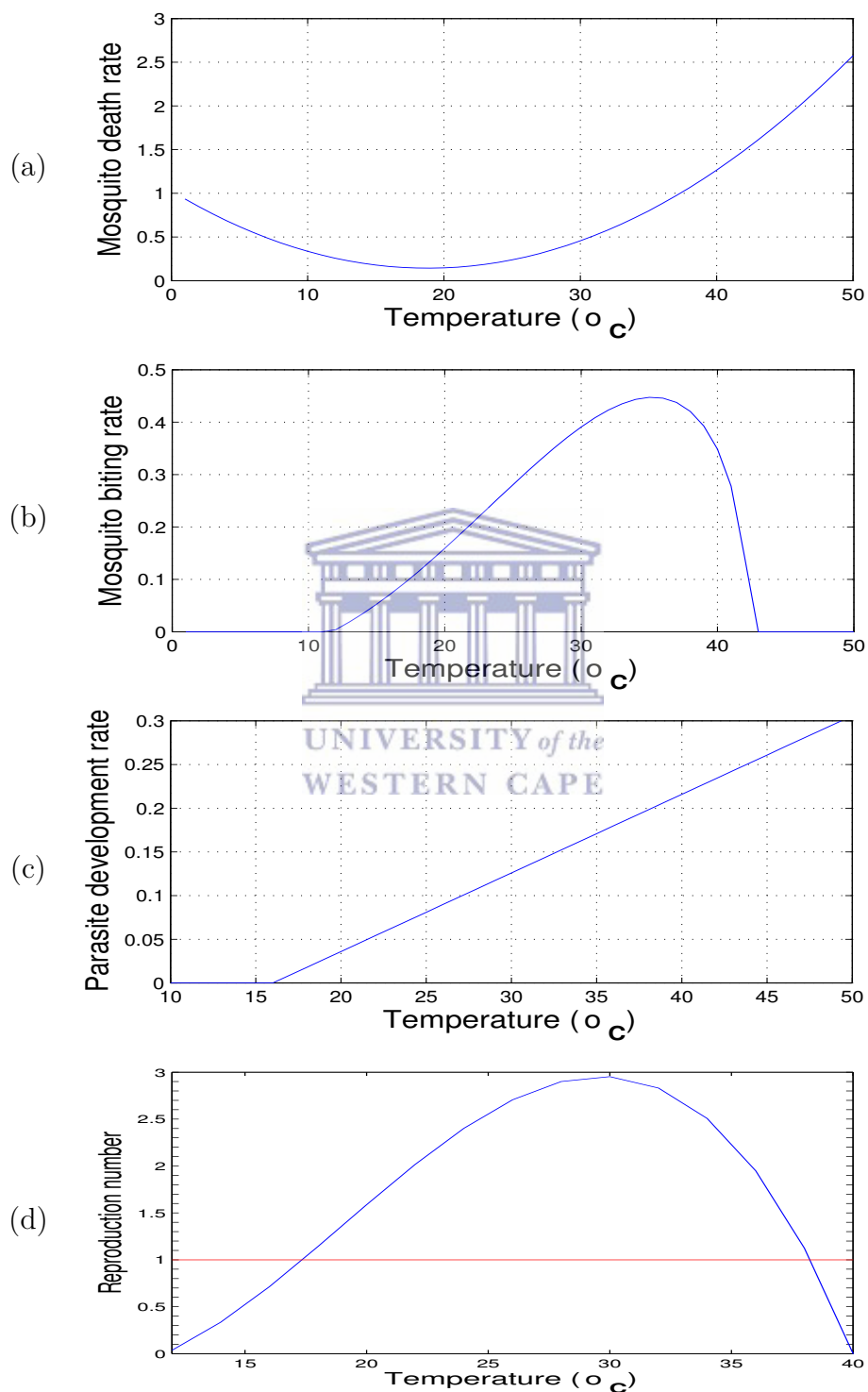


Figure 3.4: Simulation of (a) mosquito death rate, (b) mosquito biting rate, (c) progression rate of mosquitoes, and (d) \mathcal{R}_0 versus temperature.

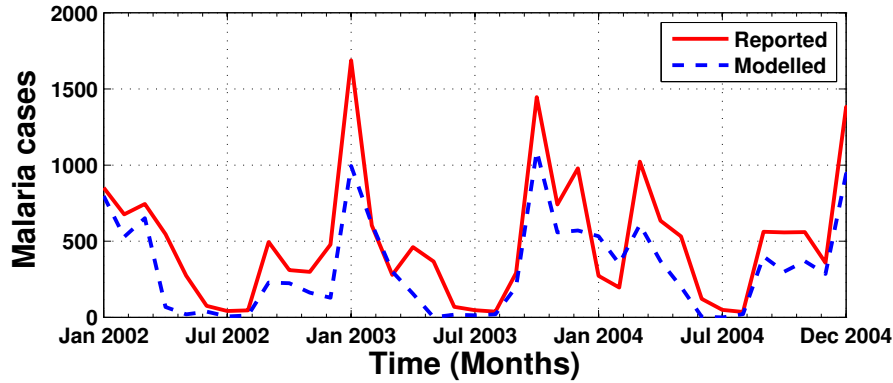


Figure 3.5: The reported cases and modelled cases for Limpopo province, South Africa 2002 - 2004.

3.4.2 Spatial distribution of malaria reproduction number over Limpopo

In rainy summer, we assume several water pools serving as mosquito breeding sites are generated by rainwater. This allows mosquitoes to lay their eggs, which later develop to adult mosquitoes if the pools are sustained for at least 14 days. We also assumed that additional pools are intentionally created for the purpose of cattle watering, irrigation and so on [210]. Using our model with Observational–Reanalysis hybrid datasets for daily temperature, we numerically calculate a time-varying approximation to the basic reproduction number ($\hat{\mathcal{R}}_0$) over Limpopo between December 2002 and December 2003 with the assumption that \mathcal{R}_0 varies with time. To achieve this, we incorporate the climate-dependent parameters into expression (3.5). The 1.0–degree spatial resolution and Global Meteorological Forcing Dataset for land surface modelling, are produced by the Terrestrial Hydrology Research Group at Princeton University (hereafter, [174]). The results in Fig. 3.6 and Fig. 3.7 show that malaria transmission in South Africa is distinctly seasonal, with high transmission limited to the warm and rainy summer months (September to May) with very low cases in June, July and August [60]. We further investigate the impact of larval population abundance on the reproductive number by consid-

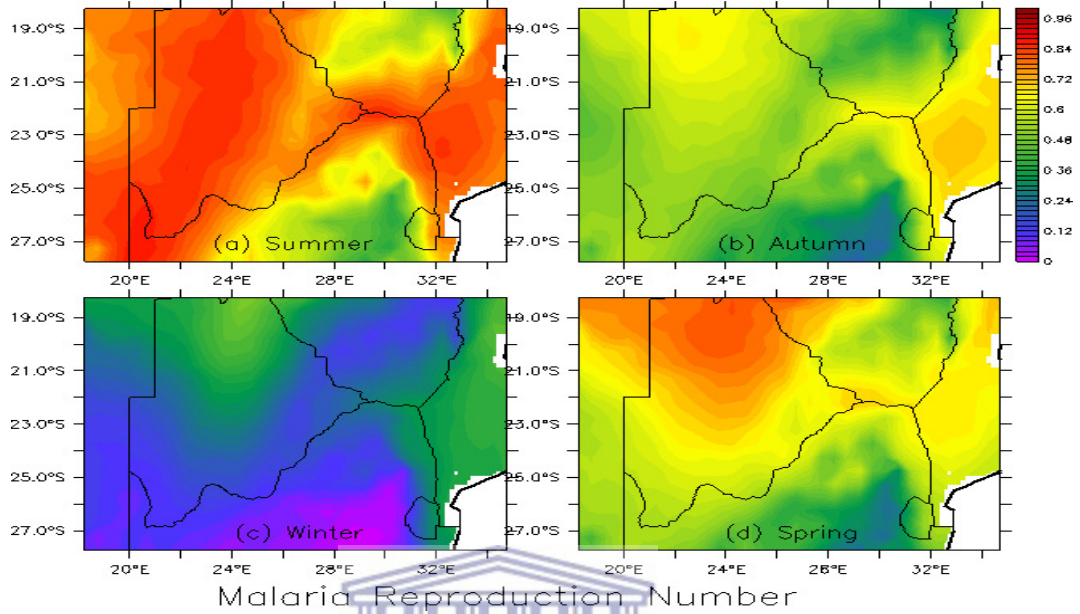


Figure 3.6: Simulation of basic reproduction number when δ_v is low ($\delta_v = 0.2$).

ering a low and high proportion of larva that died in the process of becoming adult. It is observed in Fig. 3.6 that when the proportion $\delta_v = 0.2$, the maximum value of $\hat{\mathcal{R}}_0$ over Limpopo, which is found in summer is 0.84. The value reduces to 0.48 when $\delta_v = 0.9$. This implies that when δ_v is low, it increases the proportion of larvae ($1 - \delta_v$) that made it to the adult stage, thus increases the number of mosquitoes available for transmission. On the other hand, high δ_v reduces the proportion of adult mosquitoes available for transmission, thus reduces the reproduction number.

3.5 Conclusion

In this study, a deterministic malaria model to explore the impact of temperature and rainfall on malaria transmission is presented and analysed. We derived the basic reproduction number and examined the model for the existence of disease-free and endemic equilibrium points. The system has an

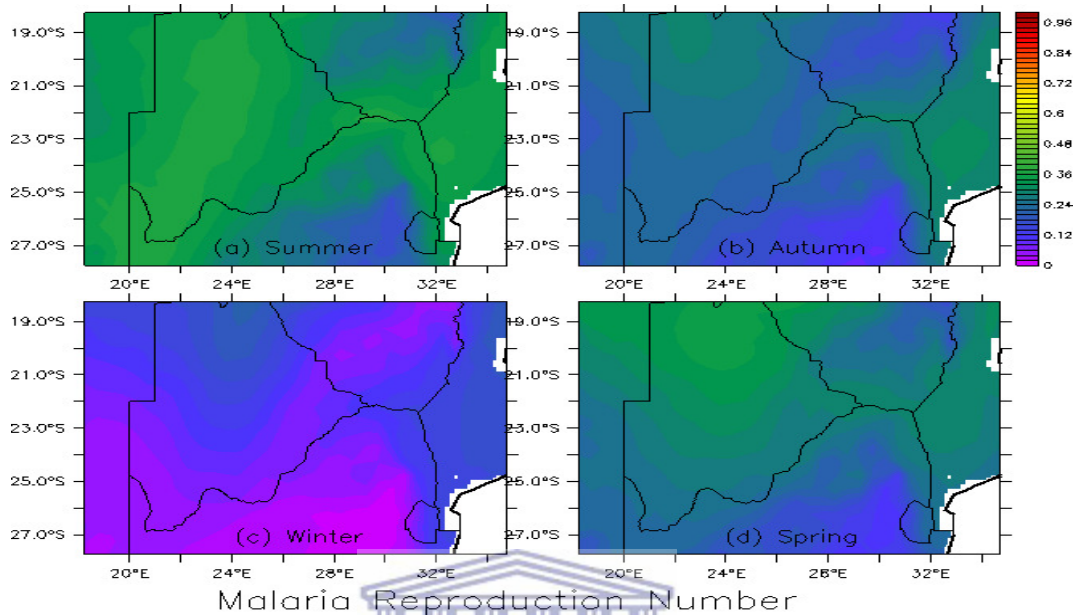


Figure 3.7: Simulation of basic reproduction number when δ_v is high ($\delta_v = 0.9$).

equilibrium point in which the disease persist in the population.

In Section 3.4.1, we examined the effect of temperature on mosquito death, biting rate, parasite development rate and reproduction number. It is verified that parasite development rate increases along with temperature, while mosquito biting rate and reproduction number are thermally constrained at both low and high temperatures. In the same section, the model is validated against malaria transmission in Limpopo province, South Africa for 2002-2004. The results indicate that malaria transmission in the province is seasonal with epidemic peak between December-February when temperature and rainfall are relatively high.

We further investigate the effect of larva death rate on the reproduction number over the entire South Africa for 2003 in Section 3.4.2. Our findings show that a high rate of larva mortality reduces the reproduction number, and increases it when low. This suggests that destruction of mosquitoes breeding sites and regular use of larvicides have high potential to reduce malaria

Table 3.1: Parameters of the malaria model 3.1

Description	Symbol	Value	Ref
Mosquito biting rate	$\epsilon(T)$	$0.000203D_1D_2$ $D_1 = T^2 - 11.7T$ $D_2 = \sqrt{42.3 - T}$	[137, 148]
Adult mosquito death rate	$\mu_v(T)$	$\frac{1}{(-4.4+1.31T-0.03T^2)}$	[4, 137]
Progression rate of mosquitoes	$\eta_v(T)$	$\frac{(T-T_{min})}{111}$	[137, 150]
Duration of egg development	t_e	1 (days)	[150]
Duration of pupa development	t_p	1 (days)	[150]
Maximum survival probability of egg	p_e^*	0.9	[150]
Maximum survival probability of pupa	p_p^*	0.25	[150]
Maximum survival probability of larva	p_l^*	0.75	[150]
Rainfall limit to flushing	R_l	50 (mm)	[150]
Num. of eggs laid per adult per ovip.	n_e	200	[137, 150]
Min. temp. for <i>P. falciparum</i> survival	T_{min}	16 ($^{\circ}C$)	[150]
Carrying capacity of larva	P	1000000	Est.
Induced death rate	γ	0.0004	[36, 137]
Loss of immunity	α	0.00014	[137]
Recovery rate of humans	q	0.005	[36, 137]
Progression rate of humans from the exposed class to infectious class	η_h	1/14	[36, 137]
Natural death rate of humans	μ_h	0.000056	Est.
Rate of treatment	ϱ	0.01-0.7	Est.
Probability of transmission of infection from an infectious human to a susceptible mosquito	ν	0.09	[137, 150]
Probability of transmission of infection from an infectious mosquito to a susceptible human	ξ	0.04	[137, 150]
Birth rate of humans	Φ_h	295 human/day	Est.
Contact rate	κ	0.6	[106]
Carrying capacity decaying rate	P_E	0.01	[150]
Conversion factor	P_A	1000	[150]

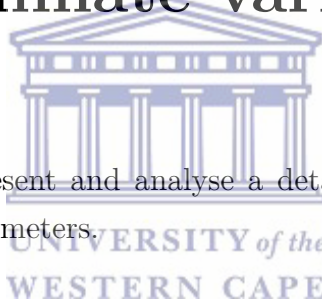
transmission. Further activities like spraying, use of treated bed nets that contribute to mosquitoes death should be encouraged mostly between September and May when the climatic conditions are favourable for mosquitoes' development in South Africa.

However, there are other factors aside climatic reasons which need to be considered in studying malaria transmission. Some of these factors include; migration of infected human, economic development and so on. We leave these aspects for future studies.



Chapter 4

Analysis of mosquito model without climate variables



In this chapter, we present and analyse a detailed mosquito model without climate-dependent parameters.

4.1 Model formulation

The mosquito population model is based and developed around phases of the mosquito life cycle in the study of Lutambi *et al* [103, 104]. A Mosquito's life begins with eggs, which hatch into larvae under a conducive condition. The larvae further develop into pupae that advance and emerge into adults. The model consists of three aquatic stages; Eggs (E), Larvae (L), and Pupae (P), and three adult classes; Adult searching for host (A_h), Adult at resting state (A_r) and Adult searching for oviposition site. The compartmental model is based on a system of six ordinary differential equations with the assumption that the dynamics are mainly driven by temperature and rainfall. Temperature has a strong impact on the progression rates at the aquatic stage and on the survival of adult populations [164] while; rainfall plays a significant role in

provision of the breeding sites. Female mosquitoes feed on human or animal blood to produce protein for their eggs. After biting, the female mosquitoes rest a while in order to develop their eggs. Once the eggs are fully developed, they find a suitable breeding site to lay their eggs and then proceed to find another blood meal. This completes the mosquito feeding cycle [35, 103, 104]. We ignore the effects of hibernation and breaks in the reproductive cycle, and assumed that eggs deposited at breeding sites proceed through development immediately (as in [103, 104, 172]). We also overlook the male population in this model since only female mosquitoes are involved in the transmission of vector-borne diseases. The six subgroups have diverse mortality and progression rates. Each subgroup is affected by three processes: (i) increase due to recruitment, (ii) decrease due to mortality, and (iii) development or progression of survivors into the next state. The parameter n is the average number of eggs which are expected to hatch into female mosquitoes laid during an oviposition and ρ_{A_o} (day^{-1}) is the rate at which new eggs are oviposited (i.e. reproduction rate). Exit from the egg stage is either due to mortality at μ_e (day^{-1}), or hatching into larvae, ρ_e (day^{-1}). In the larval stage, individuals exit by death or progress to pupal stage at a rate, ρ_L (day^{-1}). Assuming a stable environment, inter-competition for food and other resources for larvae may occur, leading to density-dependent mortality, $\frac{\mu_L L}{K}$ ($\text{day}^{-1} \text{ mosquito}^{-1}$) or natural death at an intrinsic rate, μ_L (day^{-1}), where K is the carrying capacity of the breeding site. Pupae die at a rate, μ_P (day^{-1}), and survivors progress and emerge as adults at rate ρ_P (day^{-1}). In the adult stage, host seeking mosquitoes die at a rate μ_{A_h} (day^{-1}). Those surviving this stage, and if they are successful in feeding, enter the resting stage at a rate ρ_{A_h} (day^{-1}). In the resting stage, mosquitoes die at a rate, μ_{A_r} (day^{-1}). Survivors progress to the oviposition site searching stage at a rate ρ_{A_r} (day^{-1}). Oviposition site seekers die at rate μ_{A_o} (day^{-1}) and after laying eggs return to the host seeking stage. We assume an additional mortality rate of adult mosquito μ_r (day^{-1}) related to seeking behaviour. Hence, the dynamics of the mosquito population are described by the following flow diagram in Fig. 4.1 and the system of differential equations 4.1:

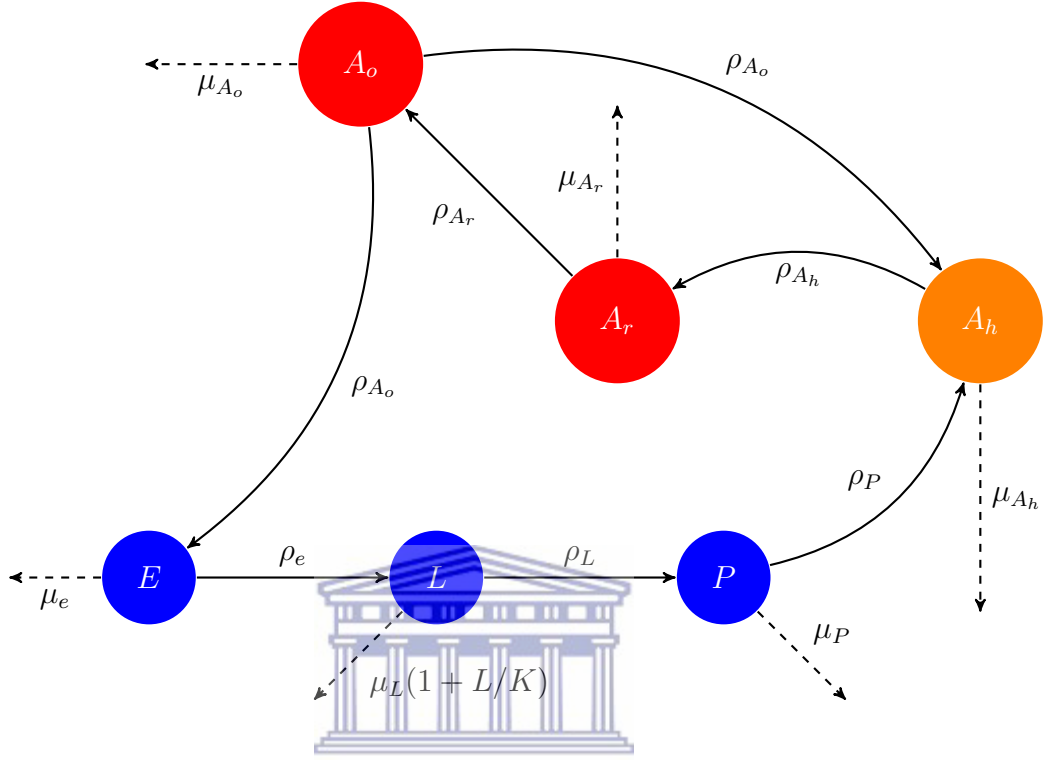


Figure 4.1: Flow diagram of the mosquito population model

$$\begin{aligned}
 \frac{dE}{dt} &= n\rho_{A_o}A_o - (\rho_e + \mu_e)E \\
 \frac{dL}{dt} &= \rho_e E - (\rho_L + \mu_L(1 + \frac{L}{K}))L \\
 \frac{dP}{dt} &= \rho_L L - (\rho_P + \mu_P)P \\
 \frac{dA_h}{dt} &= \rho_P P + \rho_{A_o}A_o - (\rho_{A_h} + \mu_{A_h} + \mu_r)A_h \\
 \frac{dA_r}{dt} &= \rho_{A_h}A_h - (\rho_{A_r} + \mu_{A_r})A_r \\
 \frac{dA_o}{dt} &= \rho_{A_r}A_r - (\rho_{A_o} + \mu_{A_o} + \mu_r)A_o
 \end{aligned} \tag{4.1}$$

with initial conditions $E(0), L(0), P(0), A_h(0), A_r(0)$, and $A_o(0)$, where the carrying capacity, K is assumed to be constant. Mosquito survival in each stage and the progression period from one stage to the next are assumed to be exponentially distributed. Since the system (4.1) monitors populations in each stage of mosquito development and because all model parameters are positive, there exists a region \mathbb{D} such that

$$\mathbb{D} = \{E, L, P, A_h, A_r, A_o \in \mathbb{R}^6 \mid E \geq 0, L \geq 0, P \geq 0, A_h \geq 0, A_r \geq 0, A_o \geq 0\},$$

where the model is mathematically and biologically meaningful and all solutions of the system (4.1) with non-negative initial data will remain non-negative in the feasible region \mathbb{D} for all time $t \geq 0$. We use the notation X' to represent $\frac{dX}{dt}$ here and denote the boundary of \mathbb{D} by $\partial\mathbb{D}$.

Theorem 4.1.1. *If the initial conditions of system (4.1) lie in region \mathbb{D} , then there exists a unique solution for (4.1), giving $E(t), L(t), P(t), A_h(t), A_r(t)$, and $A_o(t)$ that remains in \mathbb{D} for all time $t \geq 0$.*

Proof. The right hand side of the system (4.1) is continuous with continuous partial derivatives in \mathbb{D} , therefore (4.1) has a unique solution that exists for all time. It remains to be shown that \mathbb{D} is forward-invariant. We see from system (4.1) that if $E = 0$, then $E' = n\rho_{A_o}A_o \geq 0$; if $L = 0$, then $L' \geq 0$; if $P = 0$, then $P' \geq 0$; if $A_h = 0$, then $A_h' \geq 0$; if $A_r = 0$, then $A_r' \geq 0$; and if $A_o = 0$, then $A_o' \geq 0$. Therefore all solutions of the system of equations (4.1) are contained in the region \mathbb{D} . \square

4.2 Existence and stability of equilibria

4.2.1 Existence of equilibrium points

Theorem 4.2.1. *The model in (4.1) has exactly one equilibrium point on $\partial\mathbb{D}$ given by $\mathcal{P}_0 = (0, 0, 0, 0, 0, 0)$. We label \mathcal{P}_0 the mosquito-free equilibrium point.*

Proof. It is easy to check that \mathcal{P}_0 is the only equilibrium point on $\partial\mathbb{D}$. The linear stability of \mathcal{P}_0 is ascertained (as in [196]) using next generation operator method on model (4.1). We calculate spectral radius r (dominant eigenvalue in magnitude) of the next generation matrix FV^{-1} , where

$$F = \begin{bmatrix} 0 & 0 & 0 & 0 & 0 & n\rho_{A_o} \\ 0 & 0 & 0 & 0 & 0 & 0 \\ 0 & 0 & 0 & 0 & 0 & 0 \\ 0 & 0 & 0 & 0 & 0 & 0 \\ 0 & 0 & 0 & 0 & 0 & 0 \\ 0 & 0 & 0 & 0 & 0 & 0 \end{bmatrix} \quad (4.2)$$

and

$$V = \begin{bmatrix} Z_1 & 0 & 0 & 0 & 0 & 0 \\ -\rho_e & Z_2 & 0 & 0 & 0 & 0 \\ 0 & -\rho_L & Z_3 & 0 & 0 & 0 \\ 0 & 0 & -\rho_P & Z_4 & 0 & -\rho_{A_o} \\ 0 & 0 & 0 & -\rho_{A_h} & Z_5 & 0 \\ 0 & 0 & 0 & 0 & -\rho_{A_r} & Z_6 \end{bmatrix} \quad (4.3)$$

where,

$$Z_1 = (\rho_e + \mu_e), \quad Z_2 = (\rho_L + \mu_L), \quad Z_3 = (\rho_P + \mu_P), \quad Z_4 = (\rho_{A_h} + \mu_{A_h} + \mu_r), \\ Z_5 = (\rho_{A_r} + \mu_{A_r}) \text{ and } Z_6 = (\rho_{A_o} + \mu_{A_o} + \mu_r).$$

Then the basic reproduction number, denoted by \mathcal{R}_0 is given by

$$\mathcal{R}_0 = \frac{n\rho_e\rho_L\rho_P\rho_{A_h}\rho_{A_r}\rho_{A_o}}{Z_1Z_2Z_3Z_4Z_5Z_6}. \quad (4.4)$$

In search of a persistence equilibrium point of system (4.1), we take the following steps. Let $\mathcal{P}_e = (E^*, L^*, P^*, A_h^*, A_r^*, A_o^*)$ be a persistence equilibrium of model (4.1). Setting the right hand side of equation (4.1) to zero gives the

following expression.

$$\left. \begin{aligned}
 E^* &= \frac{nA_o^* \rho_{A_o}}{Z_1}, \\
 L^* &= \frac{Z_2(\mathcal{R}_0 - 1)}{\varphi_4}, \\
 P^* &= \frac{\rho_L(K Z_1 Z_2 + \varphi_1)}{2\mu_L Z_1 Z_3}, \\
 A_h^* &= \frac{2A_o^* \mu_L Z_1 Z_3 \rho_{A_o} + \rho_L \rho_P (K Z_1 Z_2 + \varphi_1)}{2\mu_L Z_1 Z_3 Z_4}, \\
 A_r^* &= \frac{\rho_{A_h}((\rho_L \rho_P \varphi_1) + Z_1(K \rho_L Z_2 \rho_P + 2A_o^* \mu_L Z_3 \rho_{A_o}))}{2\mu_L Z_1 Z_3 Z_4 Z_5}, \\
 A_o^* &= \frac{K \rho_L \rho_P \rho_{A_h} \rho_{A_r} (\rho_e (\mu_{A_r} Z_2 Z_3 Z_4 Z_6 + \varphi_2 \rho_{A_r}) + \mu_e \varphi_3)}{\mu_L Z_1 Z_3^2 (\mu_{A_h} Z_6 Z_5 + \rho_{A_h} (\mu_{A_r} \rho_{A_o} + \mu_{A_o} Z_5))^2}
 \end{aligned} \right\} \quad (4.5)$$

where,

$$\begin{aligned}
 \varphi_1 &= \sqrt{K Z_1 (K Z_1 Z_2^2 + 4nA_o^* \mu_L \rho_e \rho_{A_o})}, \\
 \varphi_2 &= (\mu_{A_o} Z_2 Z_3 Z_4 + (\mu_{A_h} Z_2 Z_3 + n \rho_L \rho_P \rho_{A_h}) \rho_{A_o}), \\
 \varphi_3 &= Z_2 Z_3 (\mu_{A_h} Z_6 Z_5 + \rho_{A_h} (\mu_{A_r} Z_6 + \mu_{A_o} \rho_{A_r})) \\
 \varphi_4 &= \frac{L}{K}.
 \end{aligned}$$

Substituting $\mathcal{P}_e = (E^*, L^*, P^*, A_h^*, A_r^*, A_o^*)$ into 4.1 shows that \mathcal{P}_e is an equilibrium point of 4.1. If $\mathcal{R}_0 > 1$, we see that all components \mathcal{P}_e are positive. Thus, \mathcal{P}_e exist in the interior of \mathbb{D} if $\mathcal{R}_0 > 1$.

4.2.2 Stability of the equilibrium points

Theorem 4.2.2. *The persistence equilibrium is locally asymptotically stable whenever $\mathcal{R}_0 > 1$ and unstable when $\mathcal{R}_0 < 1$. When $\mathcal{R}_0 = 1$, $\mathcal{P}_e = \mathcal{P}_o$*

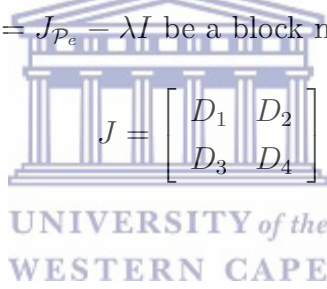
Proof. Let $J_{\mathcal{P}_e}$ be the Jacobian matrix of system (4.1) at the mosquito per-

sistent equilibrium given by

$$J_{\mathcal{P}_e} = \begin{bmatrix} -Z_1 & 0 & 0 & 0 & 0 & n\rho_{A_o} \\ \rho_e & -Q_1 & 0 & 0 & 0 & 0 \\ 0 & \rho_L & -Z_3 & 0 & 0 & 0 \\ 0 & 0 & \rho_P & -Z_4 & 0 & \rho_{A_o} \\ 0 & 0 & 0 & \rho_{A_h} & -Z_5 & 0 \\ 0 & 0 & 0 & 0 & \rho_{A_r} & -Z_6 \end{bmatrix} \quad (4.6)$$

where,

$Q_1 = Z_2 - Q_3$ and $Q_3 = 2Z_2(\mathcal{R}_0 - 1)$. In order to obtain the eigenvalues of $J_{\mathcal{P}_e}$, we solve $\det(J_{\mathcal{P}_e} - \lambda I) = 0$. Using the concept of block matrices to compute this determinant, let $J = J_{\mathcal{P}_e} - \lambda I$ be a block matrix given by



$$J = \begin{bmatrix} D_1 & D_2 \\ D_3 & D_4 \end{bmatrix} \quad (4.7)$$

where

$$D_1 = \begin{pmatrix} -Z_1 - \lambda & 0 & 0 \\ \rho_e & -Z_2 - Q_3 - \lambda & 0 \\ 0 & \rho_L & -Z_3 - \lambda \end{pmatrix},$$

$$D_2 = \begin{pmatrix} 0 & 0 & b\rho_{A_o} \\ 0 & 0 & 0 \\ 0 & 0 & 0 \end{pmatrix},$$

$$D_3 = \begin{pmatrix} 0 & 0 & \rho_P \\ 0 & 0 & 0 \\ 0 & 0 & 0 \end{pmatrix}, \text{ and}$$

$$D_4 = \begin{pmatrix} -Z_4 - \lambda & 0 & \rho_{A_o} \\ \rho_{A_h} & -Z_5 - \lambda & 0 \\ 0 & \rho_{A_r} & -Z_6 - \lambda \end{pmatrix}.$$

It follows from the concept of block matrices that $\det(J) = \det(D_1 D_4 - D_2 D_3)$. But here, $D_2 D_3$ is a zero matrix leading to $\det(J_{P_e} - \lambda I) = \det(J) = \det(D_1 D_4) = 0$. Solving the equation gives three eigenvalues $\lambda_1 = -(\mu_e + \rho_e)$, $\lambda_2 = -Z_2 - Q_3$ and $\lambda_3 = -Z_3$. When $\mathcal{R}_0 > 1$, then $\lambda_2 < 0$, which forms the necessary condition for a stable equilibrium point. When $\mathcal{R}_0 < 1$, then $\lambda_2 > 0$, and P_e is unstable. The remaining three eigenvalues are obtained as the roots of the following equation:

$$c_0 \lambda^3 + c_1 \lambda^2 + c_2 \lambda + c_3 = 0$$


where

$$c_0 = 1,$$

$$c_1 = \mu_{A_h} + \mu_{A_o} + \mu_{A_r} + 2(\mu_r + \rho_{A_h} + \rho_{A_o} + \rho_{A_r}),$$

$$c_2 = Z_4 Z_5 Z_6$$

$$c_3 = 2\mu_{A_r} \mu_r + \mu_r^2 + \mu_{A_r} \rho_{A_h} + \mu_r \rho_{A_h} + \mu_{A_r} \rho_{A_o} + \mu_r \rho_{A_o} + \rho_{A_h} \rho_{A_o} \\ + (2\mu_r + \rho_{A_h} + \rho_{A_o}) \rho_{A_r} + \mu_{A_o} (\mu_{A_r} + \mu_r + \rho_{A_h} + \rho_{A_r}) \\ + \mu_{A_h} (Z_5 + Z_6).$$

It is clear that $c_0 > 0$, $c_1 > 0$, $c_2 > 0$, and $c_3 > 0$ always. Also, by the Routh-Hurwitz criteria (Meinsma, 1995), we show that $c_1 c_2 - c_3 > 0$ since

$$c_1 c_2 - c_3 = Z_5 + Z_6 + Z_5 Z_6 + Z_4 + Z_4 Z_5 + Z_5 Z_6 (\mathcal{R}_0 - 1).$$

Thus, the roots of the polynomial have negative real parts. Therefore, when $\mathcal{R}_0 > 1$, the six eigenvalues have negative real parts and the persistence equilibrium points is locally asymptotically stable. \square

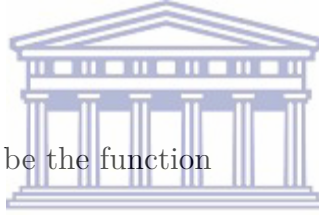
4.2.3 Global stability of mosquito-free equilibrium

Theorem 4.2.3. *Given Z_1, Z_2, \dots, Z_6 as defined above. If $\frac{Z_1}{Z_2} < 1$, $\frac{Z_2}{Z_3} < 1$, $\frac{Z_3}{Z_4} < 1$, $Z_4 < 1$, and $\mathcal{R}_0 \leq 1$, then the mosquito-free equilibrium of the system (4.1) is globally asymptotically stable on \mathbb{D} .*

Proof. We construct a Lyapunov function by introducing the following positive constants $\alpha_1, \alpha_2, \alpha_3, \alpha_4, \alpha_5$ and α_6 . We let

$$\alpha_1 = \frac{\rho_e \rho_L \rho_P \rho_{A_h} \rho_{A_r}}{Z_2 Z_3 Z_4 Z_5}, \quad \alpha_2 = \frac{\rho_L \rho_P \rho_{A_h} \rho_{A_r}}{Z_3 Z_4 Z_5}, \quad \alpha_3 = \frac{\rho_P \rho_{A_h} \rho_{A_r}}{Z_4 Z_5}, \quad \alpha_4 = \frac{\rho_{A_h} \rho_{A_r}}{Z_5}$$

$$\text{and } \alpha_5 = \frac{\rho_{A_r} Z_4}{Z_5}.$$



We then define $V(t)$ to be the function

$$V(t) = \alpha_1 E(t) + \alpha_2 L(t) + \alpha_3 P(t) + \alpha_4 A_h(t) + \alpha_5 A_r(t) + A_o(t). \quad (4.8)$$

Calculating the Lyapunov derivative of V along the solutions of system (4.1), we obtain

$$\begin{aligned} V'(t) &= \alpha_1 [n\rho_{A_o} A_o - Z_1 E] + \alpha_2 [\rho_e E - Z_2 L] + \alpha_3 [\rho_L L - Z_3 P] \\ &+ \alpha_4 [\rho_P P + \rho_{A_o} A_o - Z_4 A_h] + \alpha_5 [\rho_{A_h} A_h - Z_5 A_r] + [\rho_{A_r} A_r - Z_6 A_o] \end{aligned}$$

where $'$ denotes the derivative. We prove that $V'(t)$ is a negative-definite function in the variable $(E(t), L(t), P(t), A_h(t), A_r(t), A_o(t))$, such that

$$V'(t) = \chi_1 E(t) + \chi_2 L(t) + \chi_3 P(t) + \chi_4 A_h(t) + \chi_5 A_r(t) + \chi_6 A_o(t), \quad (4.9)$$

where,

$$\chi_1 = \alpha_2 \rho_e - \alpha_1 Z_1, \quad \chi_2 = \alpha_3 \rho_L - \alpha_2 Z_2, \quad \chi_3 = \alpha_4 \rho_P - \alpha_3 Z_3,$$

$$\chi_4 = \alpha_5 \rho_{A_h} - \alpha_4 Z_4, \quad \chi_5 = \rho_{A_r} - \alpha_5 Z_5, \quad \chi_6 = n\alpha_1 \rho_{A_o} + \alpha_4 \rho_{A_o} - Z_6.$$

Now we prove that coefficients $\chi_1, \chi_2, \chi_3, \chi_4, \chi_5,$ and χ_6 are negative.

From above expressions, we note that

$$\begin{aligned} \chi_1 &< \alpha_1 Z_1 - \alpha_2 \rho_e < 0 \\ &= \frac{\rho_e \rho_L \rho_P \rho_{A_h} \rho_{A_r} Z_1}{Z_2 Z_3 Z_4 Z_5} - \frac{\rho_e \rho_L \rho_P \rho_{A_h} \rho_{A_r}}{Z_3 Z_4 Z_5} = \frac{\rho_e \rho_L \rho_P \rho_{A_h} \rho_{A_r}}{Z_3 Z_4 Z_5} \left[\frac{Z_1}{Z_2} - 1 \right] < 0. \end{aligned}$$

Similarly,

$$\chi_2 < \frac{\rho_L \rho_P \rho_{A_h} \rho_{A_r}}{Z_4 Z_5} \left[\frac{Z_2}{Z_3} - 1 \right] < 0, \quad \chi_3 = \frac{\rho_L \rho_P \rho_{A_h} \rho_{A_r}}{Z_5} \left[\frac{Z_3}{Z_4} - 1 \right] < 0,$$

$$\chi_4 < \alpha_4 Z_4 - \alpha_5 \rho_{A_h} = 0, \quad \chi_5 < \rho_{A_r} [Z_4 - 1] < 0, \quad \text{and}$$

$$\chi_6 < -\frac{\rho_{A_h} \rho_{A_r} \rho_{A_o}}{Z_5} + \frac{n \rho_e \rho_L \rho_P \rho_{A_h} \rho_{A_r}}{Z_2 Z_3 Z_4 Z_5} [\mathcal{R}_0 - 1] < 0.$$

Thus $V'(t)$ is negative if $\mathcal{R}_0 \leq 1$. Also note that $V'(t) = 0$ if and only if $E = L = P = A_h = A_r = A_o = 0$. That is, the region \mathbb{D} is positively-invariant, hence, the mosquito-free equilibrium is globally asymptotically stable in \mathbb{D} if $\mathcal{R}_0 \leq 1$. □

4.3 Numerical analysis of the model

To explore the behavior of system (4.1) and to demonstrate the stability of the mosquito-free and persistence equilibrium, we examine the time series plot of the mosquito population with constant parameter values as shown in Fig. 4.2-4.5. We observe in Fig. 4.2a-c and Fig. 4.3a-c that each population tends to zero with time when $\mathcal{R}_0 = 0.55$. This is an evidence to Theorem 4.2.3, that at mosquito-free equilibrium, the system converges and is globally stable whenever $\mathcal{R}_0 < 1$, which implies that the population is eradicated. On the other hand, in Fig. 4.4a-c and Fig. 4.5a-c, the mosquito-free equilibrium of the system becomes unstable as $\mathcal{R}_0 > 1$. To achieve this, we double the progression rate (ρ_P) of pupa to adult searching for host, that is from 0.04 to

0.08. This increment gives rise to the previous value of \mathcal{R}_0 from 0.55 to 1.01, thus makes mosquito-persistence equilibrium to be stable as stated in Theorem 4.2.2.



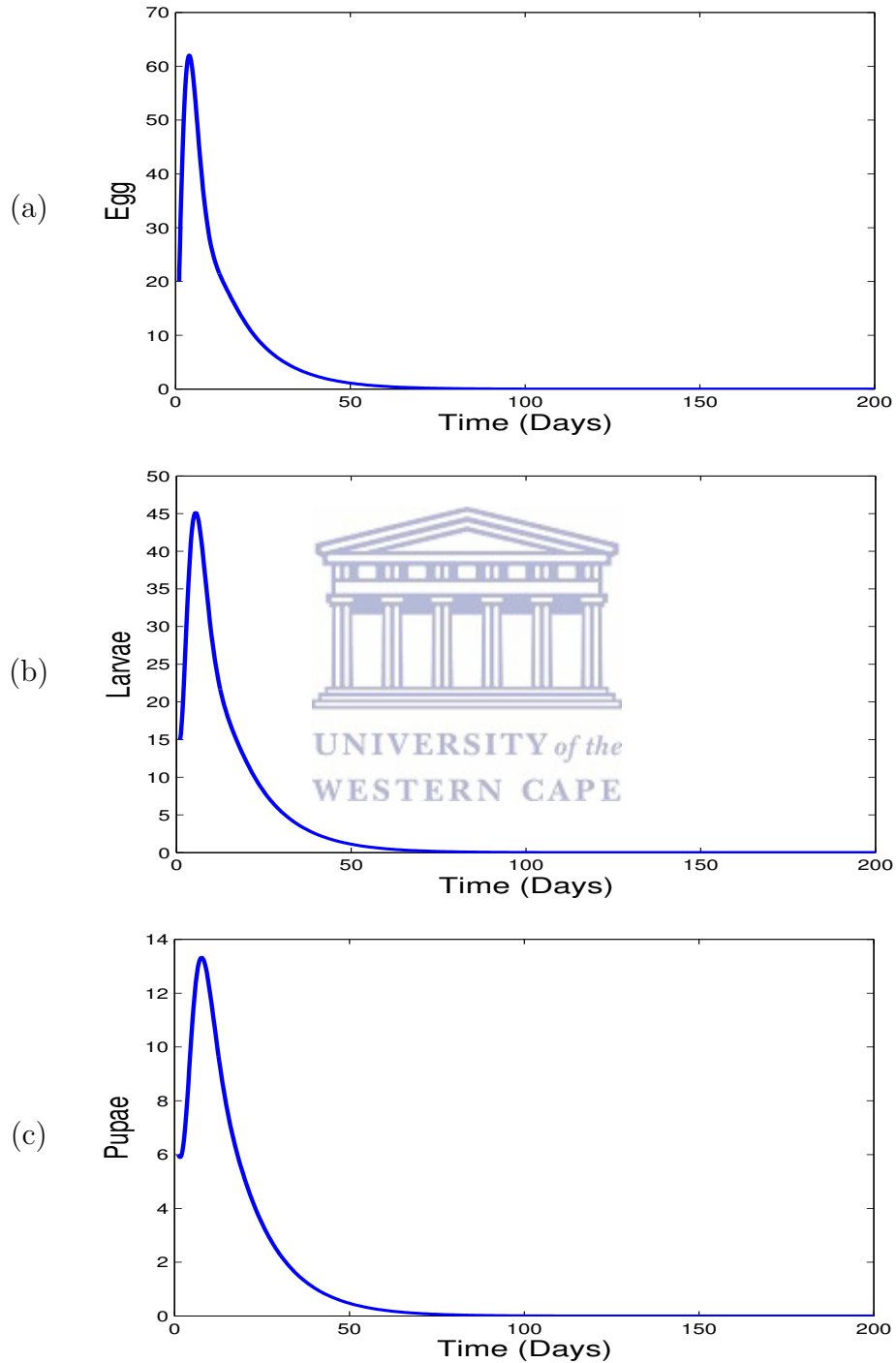


Figure 4.2: Simulated aquatic-stage mosquito population with low progression rate of pupa; $n = 100$, $\rho_E = 0.5$, $\rho_L = 0.14$, $\rho_P = 0.04$, $\mu_E = 0.56$, $\mu_L = 0.44$, $\mu_P = 0.37$, $\rho_{Ah} = 0.46$, $\rho_{Ar} = 0.43$, $\rho_{Ao} = 0.5$, $\mu_{Ah} = 0.18$, $\mu_{Ar} = 0.0043$, $\mu_{Ao} = 0.41$, $\mu_r = 0.043$, $\mathcal{R}_0 = 0.55$.

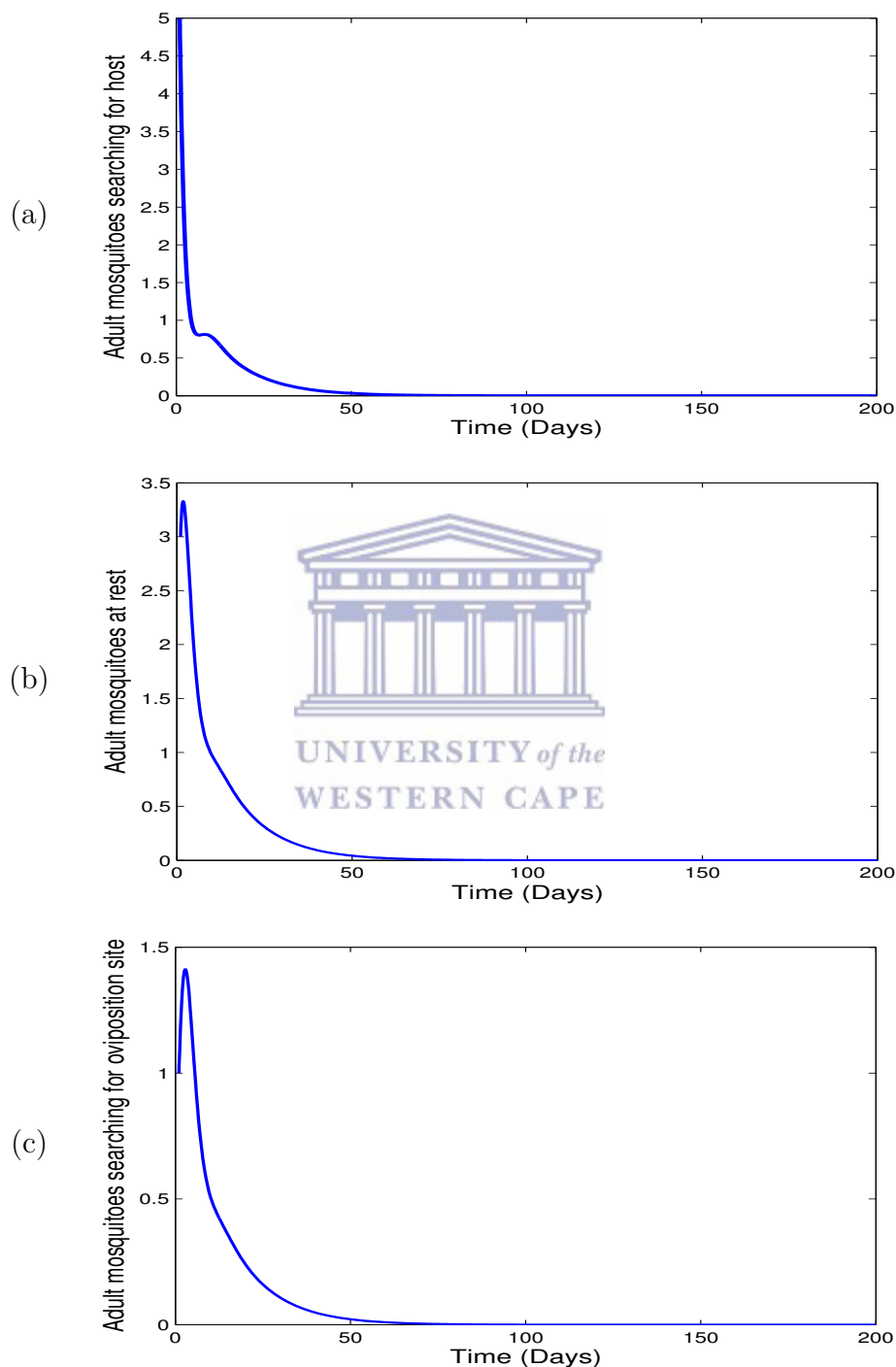


Figure 4.3: Simulated adult-stage mosquito population with low progression rate of pupa; $n = 100$, $\rho_E = 0.5$, $\rho_L = 0.14$, $\rho_P = 0.04$, $\mu_E = 0.56$, $\mu_L = 0.44$, $\mu_P = 0.37$, $\rho_{Ah} = 0.46$, $\rho_{Ar} = 0.43$, $\rho_{Ao} = 0.5$, $\mu_{Ah} = 0.18$, $\mu_{Ar} = 0.0043$, $\mu_{Ao} = 0.41$, $\mu_r = 0.043$, $\mathcal{R}_0 = 0.55$.

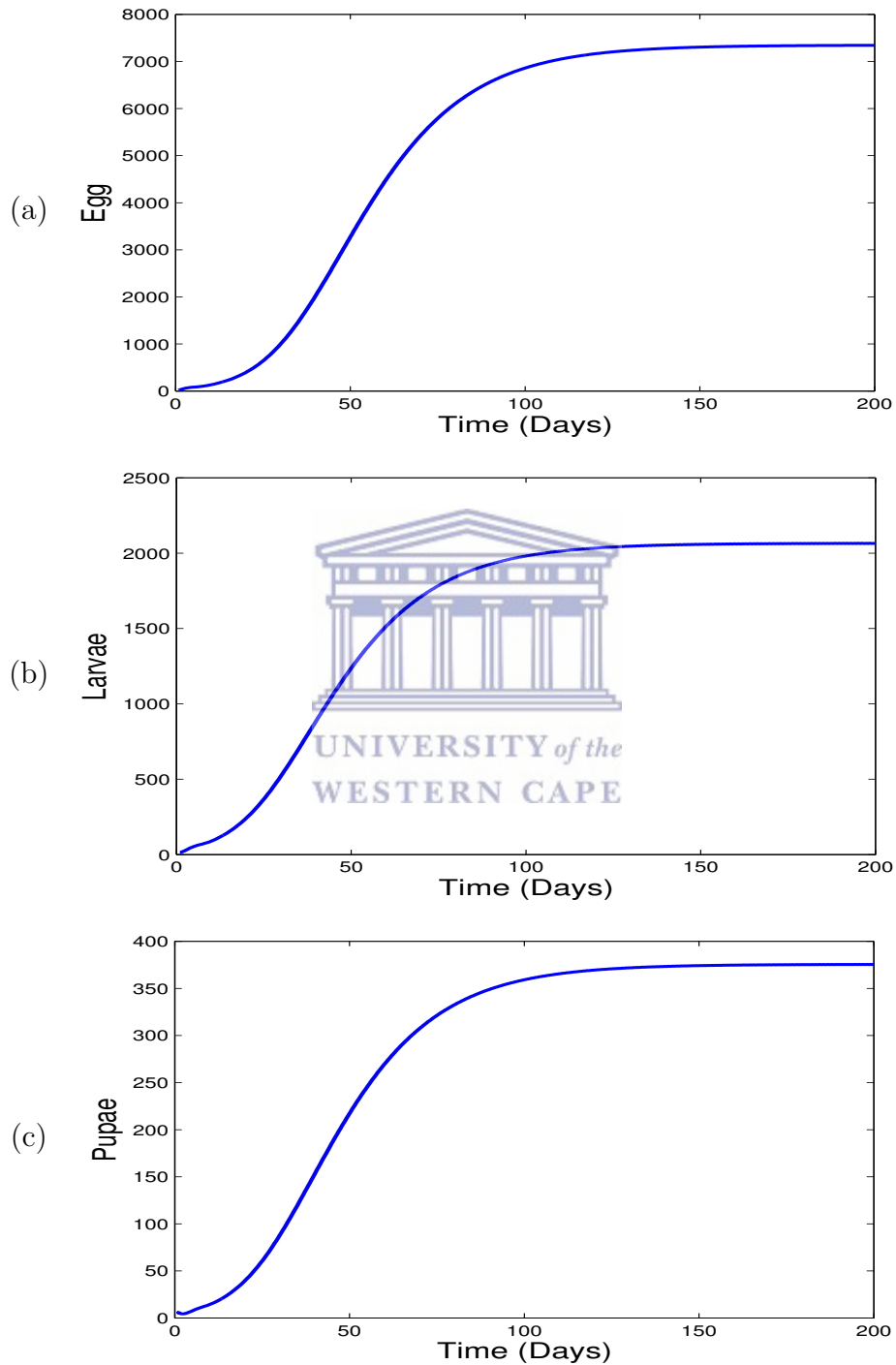


Figure 4.4: Simulated aquatic-stage mosquito population with high progression rate of pupa; $n = 100$, $\rho_E = 0.5$, $\rho_L = 0.14$, $\rho_P = 0.08$, $\mu_E = 0.56$, $\mu_L = 0.44$, $\mu_P = 0.37$, $\rho_{Ah} = 0.46$, $\rho_{Ar} = 0.43$, $\rho_{Ao} = 0.5$, $\mu_{Ah} = 0.18$, $\mu_{Ar} = 0.0043$, $\mu_{Ao} = 0.41$, $\mu_r = 0.043$, $\mathcal{R}_0 = 1.01$.

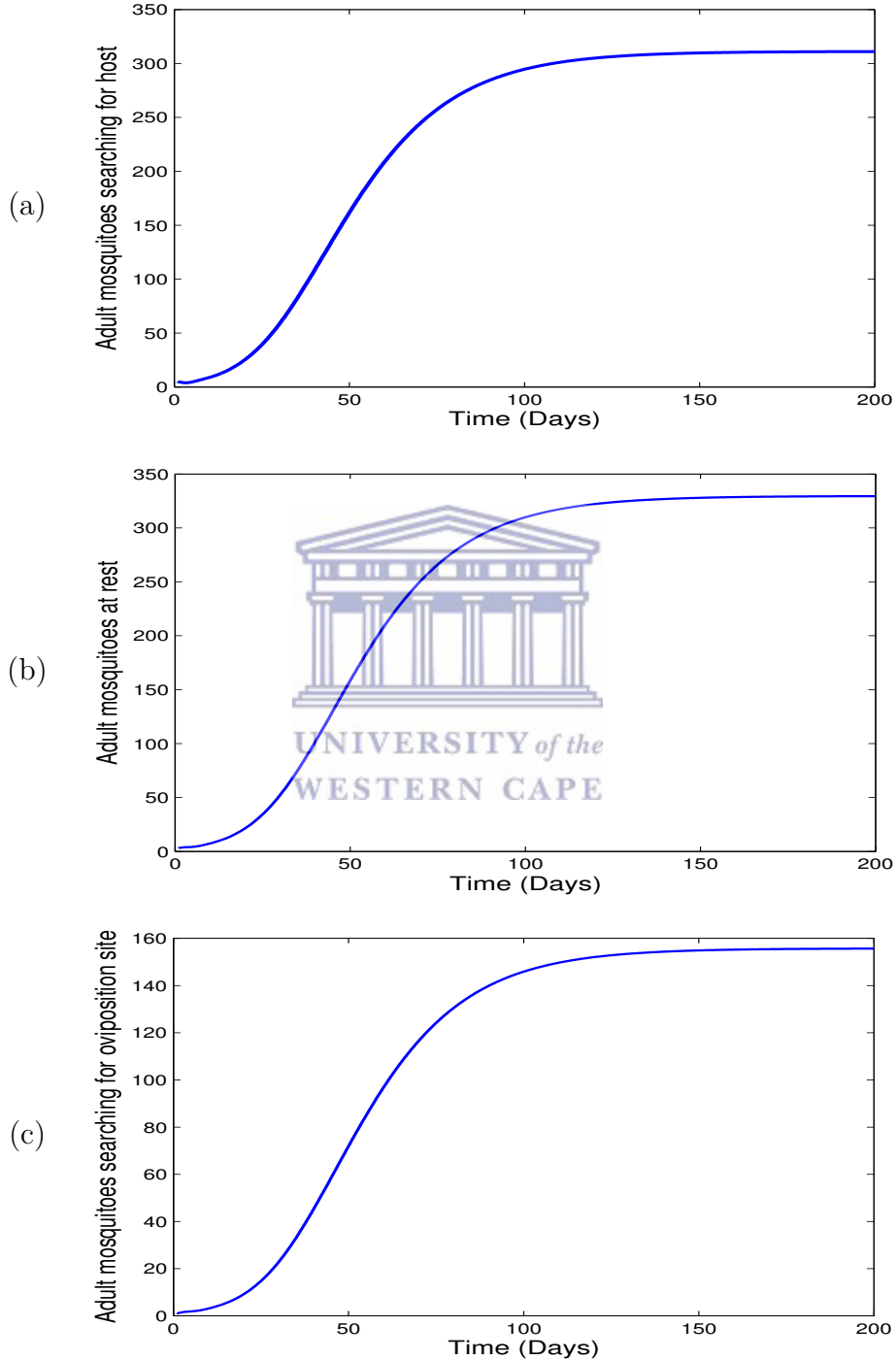
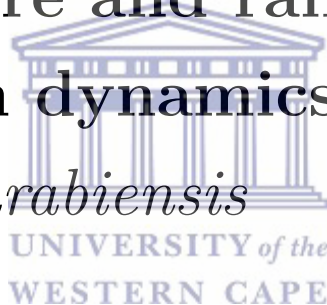


Figure 4.5: Simulated adult-stage mosquito population with high progression rate of pupa; $n = 100$, $\rho_E = 0.5$, $\rho_L = 0.14$, $\rho_P = 0.08$, $\mu_E = 0.56$, $\mu_L = 0.44$, $\mu_P = 0.37$, $\rho_{Ah} = 0.46$, $\rho_{Ar} = 0.43$, $\rho_{Ao} = 0.5$, $\mu_{Ah} = 0.18$, $\mu_{Ar} = 0.0043$, $\mu_{Ao} = 0.41$, $\mu_r = 0.043$, $\mathcal{R}_0 = 1.01$.

Chapter 5

Modelling the influence of temperature and rainfall on the population dynamics of *Anopheles arabiensis*



Published in Malaria Journal, 2016

Authors: G.J. Abiodun, R. Maharaj, P. Witbooi, K.O. Okosun

In this chapter, we incorporate climate-dependent parameters into the mosquito model in Chapter 4 with an additional mosquito compartments. Hence, the model is used to study the population dynamics of *An. arabiensis* over Kwa-Zulu Natal province.

5.1 Abstract

Malaria continues to be one of the most devastating diseases in the world, killing more humans than any other infectious disease. Malaria parasites are entirely dependent on *Anopheles* mosquitoes for transmission. For this reason, vector population dynamics is a crucial determinant of malaria risk. Consequently, it is important to understand the biology of malaria vector mosquitoes in the study of malaria transmission. Temperature and precipitation also play a significant role in both aquatic and adult stages of the *Anopheles*. In this study, a climate-based, ordinary-differential-equation model is developed to analyse how temperature and the availability of water affect mosquito population size. In the model, the influence of ambient temperature on the development and the mortality rate of *Anopheles arabiensis* is considered over a region in KwaZulu-Natal province, South Africa. In particular, the model is used to examine the impact of climatic factors on the gonotrophic cycle and the dynamics of the mosquito population over the study region. The results fairly accurately quantify the seasonality of the population of *Anopheles arabiensis* over the region and also demonstrate the influence of climatic factors on the vector population dynamics. The model simulates the population dynamics of both immature and adult *Anopheles arabiensis*. The simulated larval density produces a curve which is similar to observed data obtained from another study. The model is efficiently developed to predict *Anopheles arabiensis* population dynamics, and to assess the efficiency of various control strategies. In addition, the model framework is built to accommodate human population dynamics with the ability to predict malaria incidence in future.

5.2 Introduction

Malaria is still one of the deadliest mosquito-borne diseases in the world. In 2015, an estimated 214 million malaria cases occurred, leading to almost 438,000 deaths [208]. Malaria is not present on all continents, mainly occur-

ring in Africa, South-east Asia, Central and South America. It is caused by the protozoan *Plasmodium*, which is transmitted by mosquitoes of the genus *Anopheles* [4, 9, 35, 41, 141, 190]. In Africa, three *Anopheles* species, namely *Anopheles gambiae*, *Anopheles arabiensis* and *Anopheles funestus* are considered to be the major vectors responsible for malaria transmission. The first two species are considered to be the most effective malaria vectors in the world and are classified as a group called the *An. gambiae* complex [55, 97]. *Anopheles arabiensis* and *An. funestus* are found in South Africa, living in sympatry.

Malaria as a mosquito-borne disease is strongly influenced by climate variables (temperature, rainfall and humidity). It is well established that weather fluctuations significantly affect not only the life expectancy or completion of the life-cycle of the mosquito, but also the development of sporogonic stages of the malarial parasite within the mosquito's body [55, 157]. The biting rate and gonotrophic processes are also temperature dependent [55, 145, 190]. For these reasons, a qualitative relationship between the vector abundance and the climate variables can help to identify the peaks of the vector population through meteorological monitoring and forecast [55, 170].

Although many studies have explored the impact of climate variables on *An. gambiae* at global and regional levels, little research has been carried out on *An. arabiensis*. For instance on *An. gambiae*, Ronald Ross [165] developed a simple mathematical model to describe the relationship between the number of mosquitoes and incidence of malaria in humans. Parham and Edwin [150] used published, as well as unpublished field and experimental data to examine the relationships between vector ecology and environmental variables. These relationships are incorporated within a validated deterministic model of *An. gambiae s.s.* population dynamics to offer a valuable tool for highlighting vector response to biotic and abiotic variables. Minakawa *et al* [124] examined the dynamics of adult *An. gambiae* mosquitoes, their larval habitats, and egg survival potential during the dry season in the basin region of Lake Victoria, western Kenya. In the study, *An. gambiae* showed a strong inclination for wet soil as an oviposition substrate rather than dry soil substrate under the

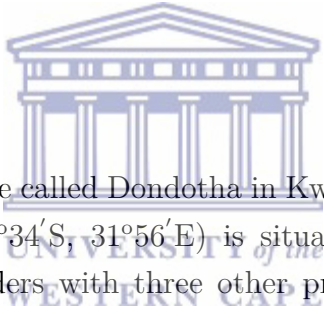
insectary surroundings. Also their findings show that in the dry season, eggs remain latent in the wet soil to resist dryness, and are hatched shortly after they are sufficiently wetted. This suggests why anopheline mosquitoes do not necessarily suffer a severe population bottleneck during the dry season and thus maintain a large effective population size [124]. Craig *et al* [41] developed a climate-based distribution model to investigate the impact of climate change on *An. gambiae* and malaria transmission over Sub-Saharan Africa. Their model in conjunction with population, morbidity and mortality data is used to estimate the burden of disease and to support strategic control of malaria. Also, Martens *et al* [108] used a rules-based modelling method to explore how climate change might affect vector abundance and global malaria transmission. Lindsay and Martens [101] extended this study by investigating the implications of climate change scenarios on *An. gambiae* and highland malaria in Africa and, more specifically, in Zimbabwe. Hoshen and Morse [80] also developed a mathematical-biological model, comprising both the climate-dependent within-vector (*An. gambiae s.l.*) stages and the climate-independent within host stages to simulate malaria incidence in Zimbabwe. The model shows a qualitative reconstruction of infection prevalence and a suitable prediction of malaria transmission based on seasonal climate forecasts.

Anopheles arabiensis is generally found in Africa, mostly in southern Africa. They live long enough to become infected and infective with *Plasmodium falciparum* [114]. Studies have also shown that their life expectancy is highly influenced by climate variables. In the study of Maharaj [114], it is established in laboratory experiments that *An. arabiensis* feeds and produces eggs but does not oviposit during winter. This is also in line with the study of Omer and Cloudsley-Thompson [144]. Although Le Sueur [182] found some first instar larvae during winter, this suggests that to a lesser extent, oviposition may occur in the field [114, 182]. The laboratory experiments further suggest that *An. arabiensis* could possibly transmit malaria during winter since they do feed during this period. The sporogonic process would be faster during summer than winter period [114]. This suggestion is in line with the previous study of [158] that malaria incidence is directly attributable to the vector

feeding habits, abundance and survivorship. However, these studies are laboratory experiments with a limited number of *An. arabiensis* used as samples. Also, the breeding site is assumed to be stagnant. The aim of this study is to develop a deterministic mosquito model that gives a detailed account of the impact of climate variables on the population dynamics of *An. arabiensis*, and to consider a dynamical breeding site being influenced by rainfall and temperature. The laboratory experimental data obtained from the study of Maharaj [114] is used in calibrating the model.

5.3 Methods

5.3.1 Study area



The study area is a village called Dondotha in KwaZulu-Natal province, South Africa. The village ($28^{\circ}34'S$, $31^{\circ}56'E$) is situated in the northeast of the province that share borders with three other provinces (Mpumalanga, Free State and Eastern Cape) and countries (Mozambique, Swaziland and Lesotho) as shown in Fig. 5.3.1. It experiences long sunny days and dry weather on most days with high rainfall during December - April (see Fig. 5.2). In the study period (January 2002 to December 2004), the heaviest rainfall occurred around December 2002 (78 mm); whereas the highest temperature occurred around January 2003 (mean = $32^{\circ}C$). Also from Fig. 5.3, the average daily mean temperature and rainfall increased from January and peaked in February before declining gradually toward June every year.

5.3.2 Entomological data

The entomological data used in this study is based on laboratory experiments in the study of Maharaj [114]. In the experiment, *An.arabiensis* were collected from Dondotha village. Fresh breeding stock was caught at the start of each



Figure 5.1: Map showing the location of Dondotha in KwaZulu-Natal province. Source: GIS unit of the Medical Research Council of South Africa.

set of experiments and newly laid eggs were kept under insectary conditions of temperature ($27 \pm 2^\circ\text{C}$), relative humidity ($70 \pm 10\%$) and photoperiod (12L:12D with 1 hour simulated crepuscular period) [114]. Identification was obtained by using the Polymerase Chain Reaction (PCR) method on samples of the first larval instars of each female [114, 153]. Also, in their studies, all experiments were conducted in a Specht Scientific programmable growth cabinet (model SFPGR066) fitted with a Dumo Dicon P temperature and humidity control unit [114]. The development and survivorship of immature *An. arabiensis* were studied at four fluctuations temperatures. Temperature levels with mean values (17.9, 23.2, 26.1 and 21.4°C) were used to represent winter, spring, summer and autumn profiles respectively. The output data were used in their study to describe the life table characteristics of *An. arabiensis*.

5.3.3 Climate data

In the present study, the Observational-Reanalysis hybrid datasets for the daily precipitation, minimum and maximum daily temperature are considered over

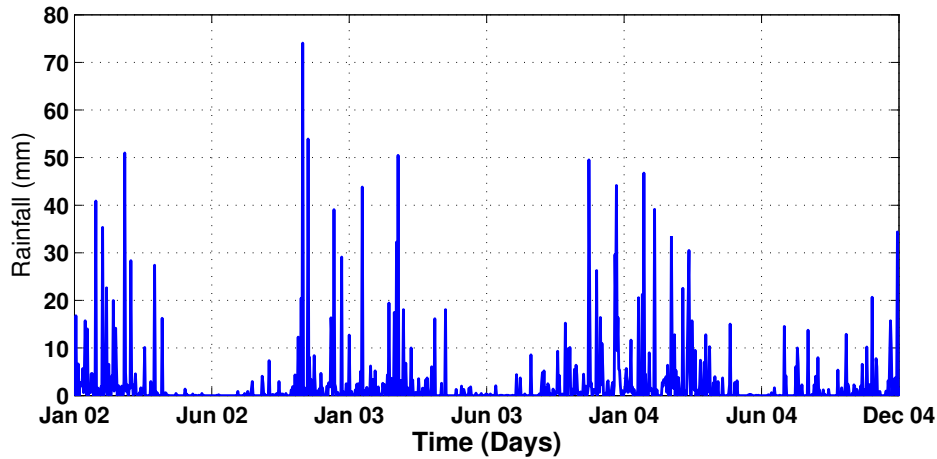


Figure 5.2: Daily rainfall over calibration period showing the daily rainfall of the study area; Dondotha village in KwaZulu-Natal province, South Africa between January 2002 and December 2004.

the study region for the period 2002 – 2004. The Princeton University Global Meteorological Forcing Datasets for land surface modelling are produced by the Terrestrial Hydrology Research Group at Princeton University (hereafter, [174]). Also in this study, it is assumed in line with previous studies (e.g., [55, 190]) that the population dynamics of *Anopheles* is mainly driven by two major factors: (i) temperature - has a strong impact on the survival of *An. arabiensis* populations, and on the development of aquatic stages (e.g., [114]); (ii) precipitation - provides breeding sites for immature *Anopheles*. However, excess rainfall can flush away the breeding sites (e.g., [55, 190]).

5.3.4 Model formulation

The vector population dynamics model used in the present study is based on previously developed models by others [24, 81, 103, 104, 193]. The compartmental models of [103], Lutambi2013thesis consists of three aquatic stages; Eggs (E), Larvae (L), and Pupae (P), and three adult classes; Adult searching for host (A_h), Adult at resting state (A_r) and Adult searching for oviposition

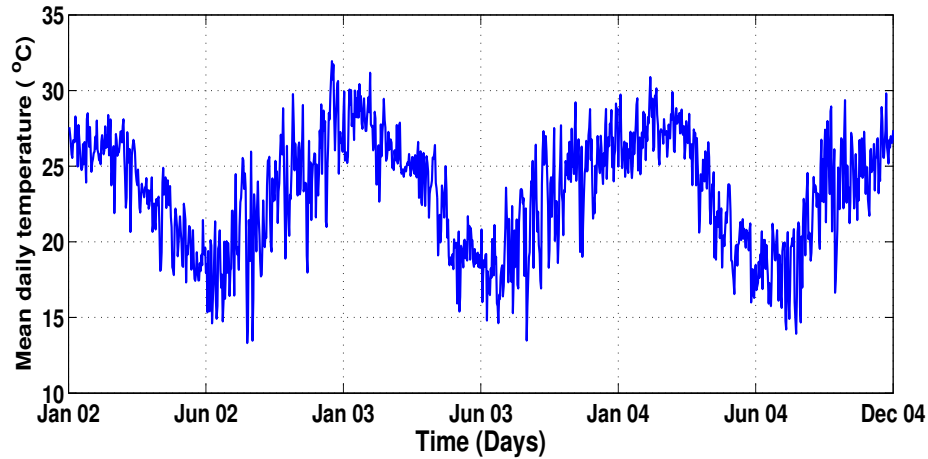


Figure 5.3: Daily mean temperature over calibration period showing the daily mean temperature of the study area; Dondotha village in KwaZulu-Natal province, South Africa between January 2002 and December 2004.

site (A_o). One more compartment of adult female *An. arabiensis* searching for mating (A_m) is added as shown in Fig. 5.4. Temperature has a strong impact on the progression rates at the aquatic stage and on the survival of adult populations [164], while rainfall plays a significant role in provision of the breeding sites. In this study, the impact of these factors were incorporated into the model, and additional attention is given to the dynamics of the mosquito breeding sites (puddle dynamics). A Mosquito's life begins with eggs, which hatch into larvae under conducive conditions. The larvae further develop into pupae that advance and emerge into adults. Adult female mosquitoes feed on human or animal blood to produce eggs. After biting, the female mosquitoes rest a while in order to develop their eggs. Once the eggs are fully developed, they find a suitable breeding site to lay their eggs and then proceed to find another blood meal. This completes the mosquito feeding cycle [35, 103, 104]. The effects of hibernation and breaks in the reproductive cycle is ignored, and it is assumed that eggs deposited at breeding sites proceed through development immediately (as in [103, 104, 172]). The male population in this model is also overlooked since only female mosquitoes are involved in

the transmission of malaria. The seven subgroups have diverse mortality and progression rates. Each subgroup is affected by three processes: (i) increase due to recruitment, (ii) decrease due to mortality, and (iii) development or progression of survivors into the next state. The parameter n is the average number of eggs which are expected to hatch into female mosquitoes laid during an oviposition and ρ_{A_o} (day^{-1}) is the rate at which new eggs are oviposited (i.e. reproduction rate). Exit from the egg stage is either due to mortality at μ_e (day^{-1}), or hatching into larvae, ρ_e (day^{-1}). In the larval stage, individuals exit by death or progress to pupal stage at a rate, ρ_L (day^{-1}). Assuming a stable environment, inter-competition for food and other resources for larvae may occur, leading to density-dependent mortality, $\frac{\mu_L L}{K}$ ($\text{day}^{-1} \text{ mosquito}^{-1}$) or natural death at an intrinsic rate, μ_L (day^{-1}), where K is the carrying capacity of the breeding site. Pupae die at a rate, μ_P (day^{-1}), and survivors progress and emerge as adults at a rate ρ_P (day^{-1}). In the adult stage, mate seeking mosquitoes die at a rate μ_{A_m} (day^{-1}) while the survivors proceed to search for blood meal at a rate ρ_{A_m} (day^{-1}). Host seeking mosquitoes die at a rate μ_{A_h} (day^{-1}). Those surviving this stage, and if they are successful in feeding, enter the resting stage at a rate ρ_{A_h} (day^{-1}). In the resting stage, mosquitoes die at a rate, μ_{A_r} (day^{-1}). Survivors progress to the oviposition site searching stage at a rate ρ_{A_r} (day^{-1}). Oviposition site seekers will lay their eggs and return to the host seeking stage or die at a rate μ_{A_o} (day^{-1}). An additional mortality rate of adult mosquitoes μ_r (day^{-1}) related to seeking behaviour is also considered. In line with other studies (e.g., [55, 190]), it is assumed in this study that *Anopheles* female mosquitoes require a blood meal to produce eggs.

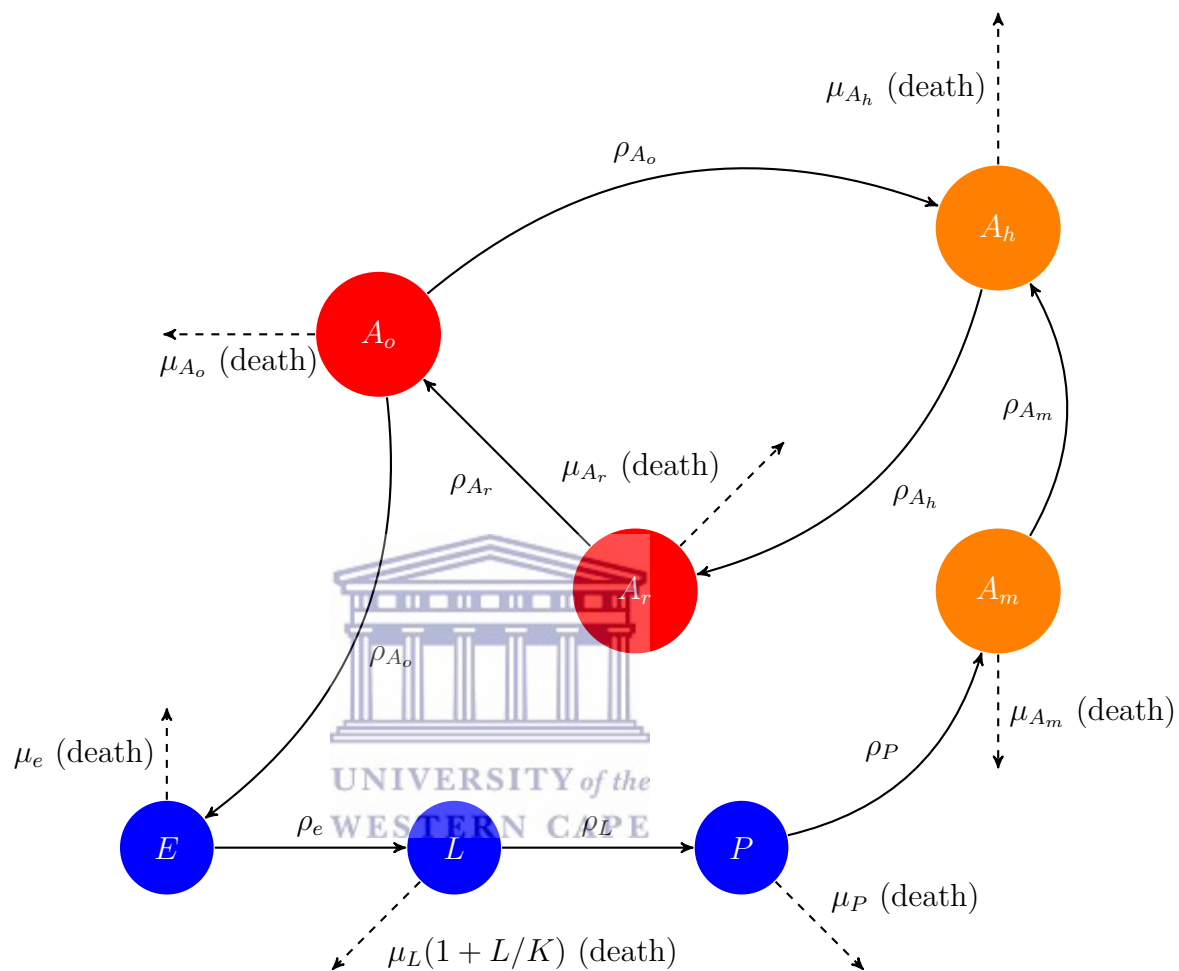
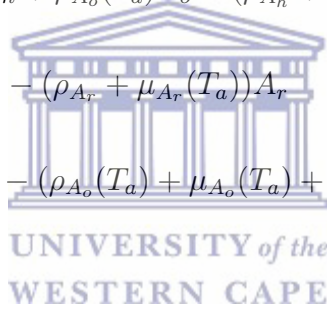


Figure 5.4: Flow diagram of the mosquito population model

Hence, the dynamics of the mosquito population are described by the following system of differential equations:

$$\begin{aligned}
 \frac{dE}{dt} &= n\rho_{A_o}(T_a)A_o - (\rho_e(T_w) + \mu_e(T_w))E \\
 \frac{dL}{dt} &= \rho_e(T_w)E - (\rho_L(T_w) + \mu_L(T_w)(1 + \frac{L}{K}))L \\
 \frac{dP}{dt} &= \rho_L(T_w)L - (\rho_P(T_w) + \mu_P(T_w))P \\
 \frac{dA_m}{dt} &= \rho_P(T_w)P - (\rho_{A_m} + \mu_{A_m}(T_a) + \mu_r)A_m \\
 \frac{dA_h}{dt} &= \rho_{A_m}A_m + \rho_{A_o}(T_a)A_o - (\rho_{A_h} + \mu_{A_h}(T_a) + \mu_r)A_h \\
 \frac{dA_r}{dt} &= \rho_{A_h}A_h - (\rho_{A_r} + \mu_{A_r}(T_a))A_r \\
 \frac{dA_o}{dt} &= \rho_{A_r}A_r - (\rho_{A_o}(T_a) + \mu_{A_o}(T_a) + \mu_r)A_o
 \end{aligned} \tag{5.1}$$



with initial conditions $E(0), L(0), P(0), A_h(0), A_r(0)$, and $A_o(0)$, where T_w and T_a are water and air temperatures respectively.

5.3.4.1 Puddle dynamics

In this study, it is assumed in line with [45, 102] that the larval carrying capacity K is a function of water availability at the breeding site; that is, the water volume of the pond, V_{pond} , is such that $K = L_{max} \times V_{pond}$, where L_{max} is the maximum larval biomass per surface area. The L_{max} is set to 300 mg m^{-2} , following [45, 190]. Although *An. arabiensis* is associated with small ponds [63], it is also established that, aside rainfall, rivers and human activities (such as irrigation, pipe leakage) could serve as water source to the breeding sites [102, 210]. In an irrigated area, one can expect to have pools of water even outside the raining season. Other studies [108, 145, 190] have also

suggested that heavy rainfall can flush off the breeding sites, leading to high larvae mortality. For these reasons, in this study, the puddle dynamics of [190] is considered for the breeding site, that is

$$\frac{dV_{pond}}{dt} = K_v [R_f(V_{max} - V_{pond}) - V_{pond}(\varrho + I_f)], \quad (5.2)$$

such that $V_{min} \leq V_{pond} \leq V_{max}$, where, V_{min} and V_{max} respectively represent the pond minimum and maximum water volume. The rainfall or precipitation rate is denoted as R_f , while K_v represents the puddle geometry. Evaporation and infiltration rates are hence denoted by ϱ and I_f respectively. A cylindrical shape puddle of 1.2m diameter and 0.5m height is considered for the puddle geometry with the assumption that water depth is much less than puddle height. In line with [190], a fixed constant parameter is assigned for the infiltration rate as shown in Table 5.1. The evaporation rate by Hamon's equation [73] is similarly considered as used in other studies (e.g., [3, 72, 146, 156]). The effect of waves in the puddle is ignored since *An. arabiensis* is less common in the areas that are exposed to waves [124]. In the expression for ϱ below,

$$\varrho = 2.1 \times H_t^2 \times \left(\frac{e_s}{T_a + 273.3} \right). \quad (5.3)$$

H_t is the average number of daylight hours per day during the month in which day t falls. Also, e_s denotes saturation vapor pressure, given by

$$e_s(T_a) = 0.6108e^{\left(\frac{17.27T_a}{T_a+237.3}\right)} \quad (5.4)$$

In addition to pond dimension the other important parameter of water bodies is the temperature of the water near the surface [190]. For small ponds and puddles the temperature is often one or two degrees warmer than the air temperature [45, 146, 147]. We therefore assumed the temperature of puddles to have a fixed offset relative to the air temperature (such that $T_w = T_a + 2^\circ\text{C}$).

5.3.4.2 Parameters and functions of the model

The parameters used for this model are adopted from the data generated from the laboratory experiments of Maharaj [114]. The extensive data highlight the impact of temperature on developmental attributes of immature *An. arabiensis* under simulated seasonal conditions. The results from the study is used to estimate the parameters and the forcing functions for the gonotrophic rate (ρ_{A_o}), development and mortality rate of immature *An. arabiensis*.

Using MATLAB software, the best fit curves are found (as seen in Fig. 5.5 and Additional file 1) for the gonotrophic rate (ρ_{A_o}), development and mortality rate of immature stages. Their parameter functions were further derived as given in the Table 5.1.



5.4 Results and discussion

5.4.1 Model validation

Although it is difficult to find mosquito data to validate the model, in order to ascertain the robustness of the model, the model output is compared with the results obtained from the study of Himeidan and Rayah [79]. In the study, larvae are collected over different breeding sites and sources in New Halfa town, eastern Sudan. The collection was done between March 1999 and March 2000. In the town, temperature is noted to be high in summer (March - June) as shown in Fig. 5.6b. During this period, rainfall is noted to be minimal (see Fig. 5.6a). In the raining season (July - September), temperature reaches a minimum as indicated in Fig. 5.6a. Based on the observed temperature and rainfall during the study period, the dynamics of larvae population at time t (red line) is simulated and compared with the mean number of larvae collected (dashed blue line) over New Halfa town as shown in Fig. 5.6c. The model produces a similar curve (in red) with the observed larvae populations. Also,

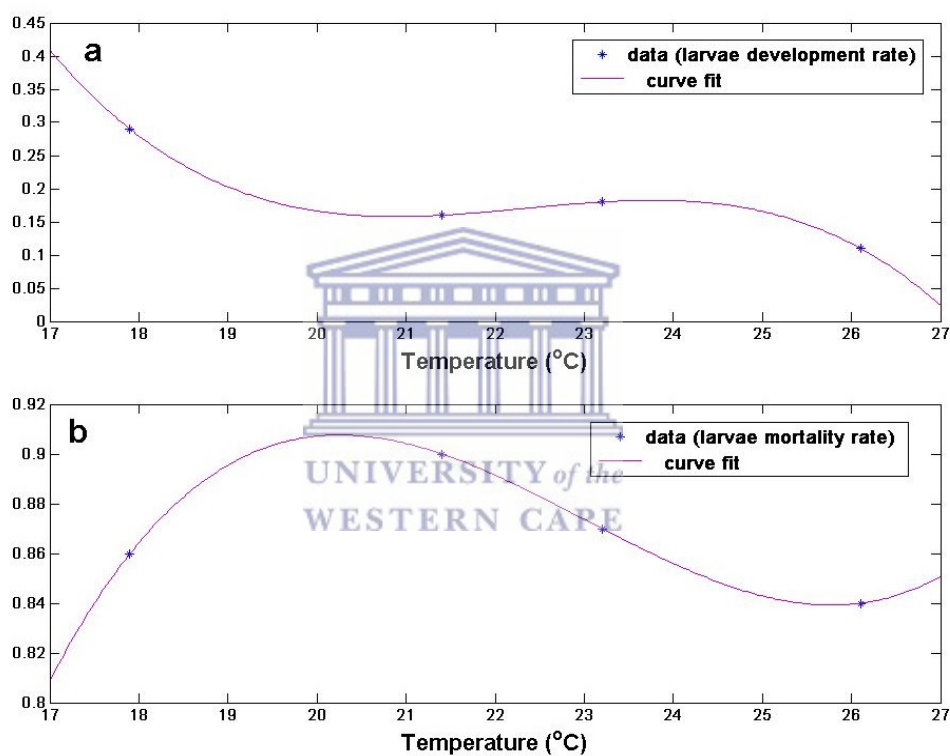
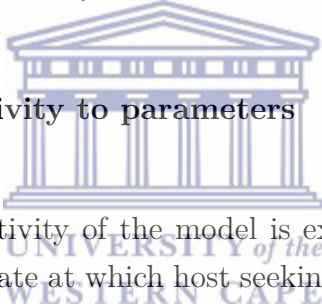


Figure 5.5: Parameter estimates and curves fit for (a) larvae development rate, (b) larvae mortality rate of *An. arabiensis*. See additional files in Appendices for other parameters.

both graphs (in Fig. 5.6c) indicate that larvae abundance reaches a minimum between October and June, increases between June and October while reaching the peak in August. The reason for this could easily be linked to low and high rainfall in October - June and June - October respectively. High temperature in summer negatively impacts the larvae and other immature *An. arabiensis* as the breeding sites dry up quickly during this period.

5.4.2 Sensitivity analysis

5.4.2.1 Model sensitivity to parameters



In this section, the sensitivity of the model is examined with two important parameters, that is, the rate at which host seeking adult *An. arabiensis* enters the resting state (ρ_{A_h}) and the rate at which resting adult *An. arabiensis* enters the oviposition searching state (ρ_{A_r}). To accomplish this, parameter ρ_{A_h} is held constant at $\rho_{A_h} = 0.3$, while varying ρ_{A_r} between 0.3 - 0.9 in Fig. 5.7a. Similarly, ρ_{A_h} is held constant at $\rho_{A_h} = 0.5$, as ρ_{A_r} is varied between 0.3 - 0.9 in Fig. 5.7b. Finally, in Fig. 5.7c, ρ_{A_h} is held constant at $\rho_{A_h} = 0.9$ as ρ_{A_r} varies between 0.3 - 0.9. All figures show a good correlation between the modelled and observed larvae. Also, the results show that the model is sensitive to both parameters, but more sensitive to ρ_{A_h} than ρ_{A_r} . For instance, in Fig. 5.7a, when $\rho_{A_h} = 0.3$ and $\rho_{A_r} = 0.9$ (in green), there is a significant difference of about 90 larvae between the peaks of the modelled and collected larvae. The peak difference reduces to about 30 larvae when $\rho_{A_h} = 0.5$ and $\rho_{A_r} = 0.9$ in Fig. 5.7b. The number of simulated larvae overshoots that of observed in Fig. 5.7c by 50 when $\rho_{A_h} = \rho_{A_r} = 0.9$. For all the simulations, these were considered $\rho_{A_h} = 0.9$ and $\rho_{A_r} = 0.5$ because it produces the closest simulation to observed larvae data.

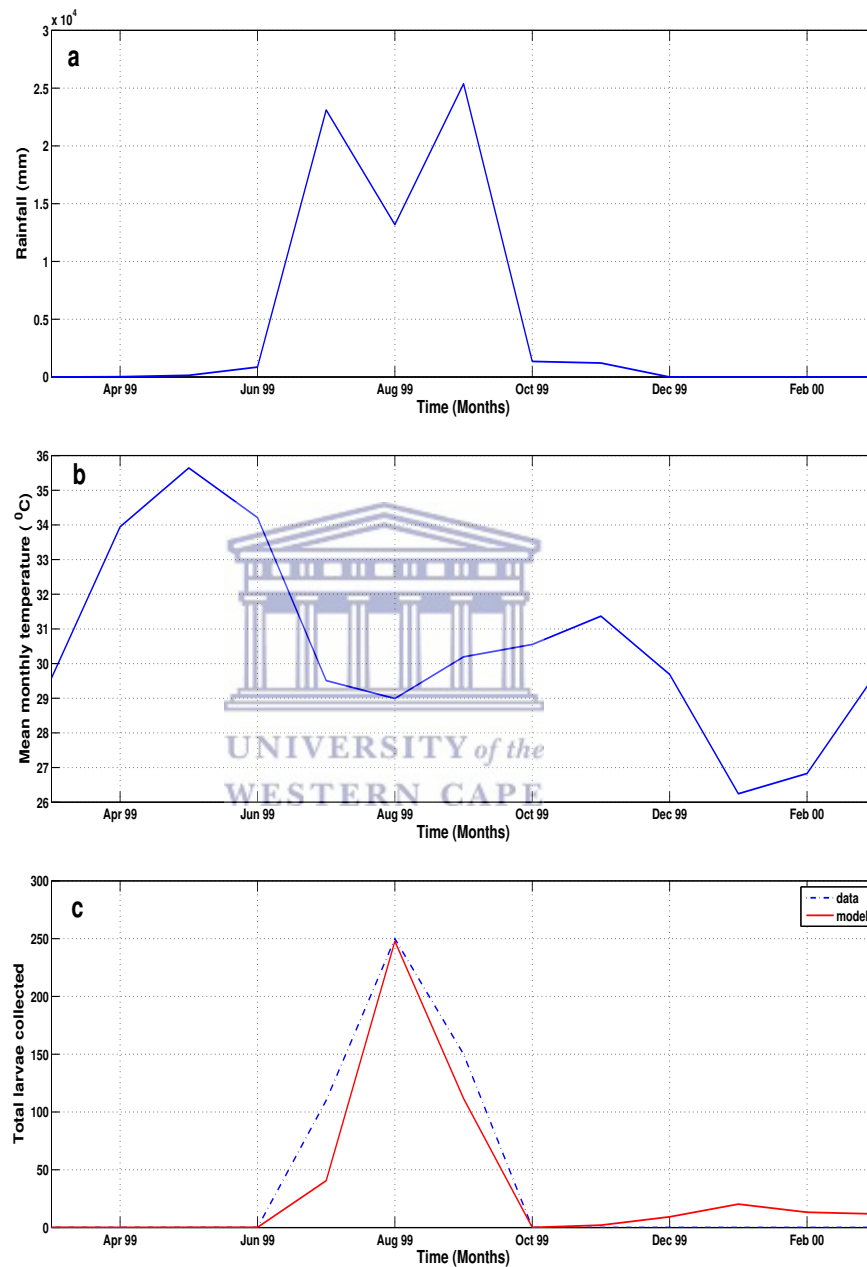


Figure 5.6: Model validation and climate monthly data of New Halfa town, eastern Sudan. (a) Monthly rainfall, (b) mean monthly temperature, and (c) showing the simulated and observed collected larvae over the study area and period.

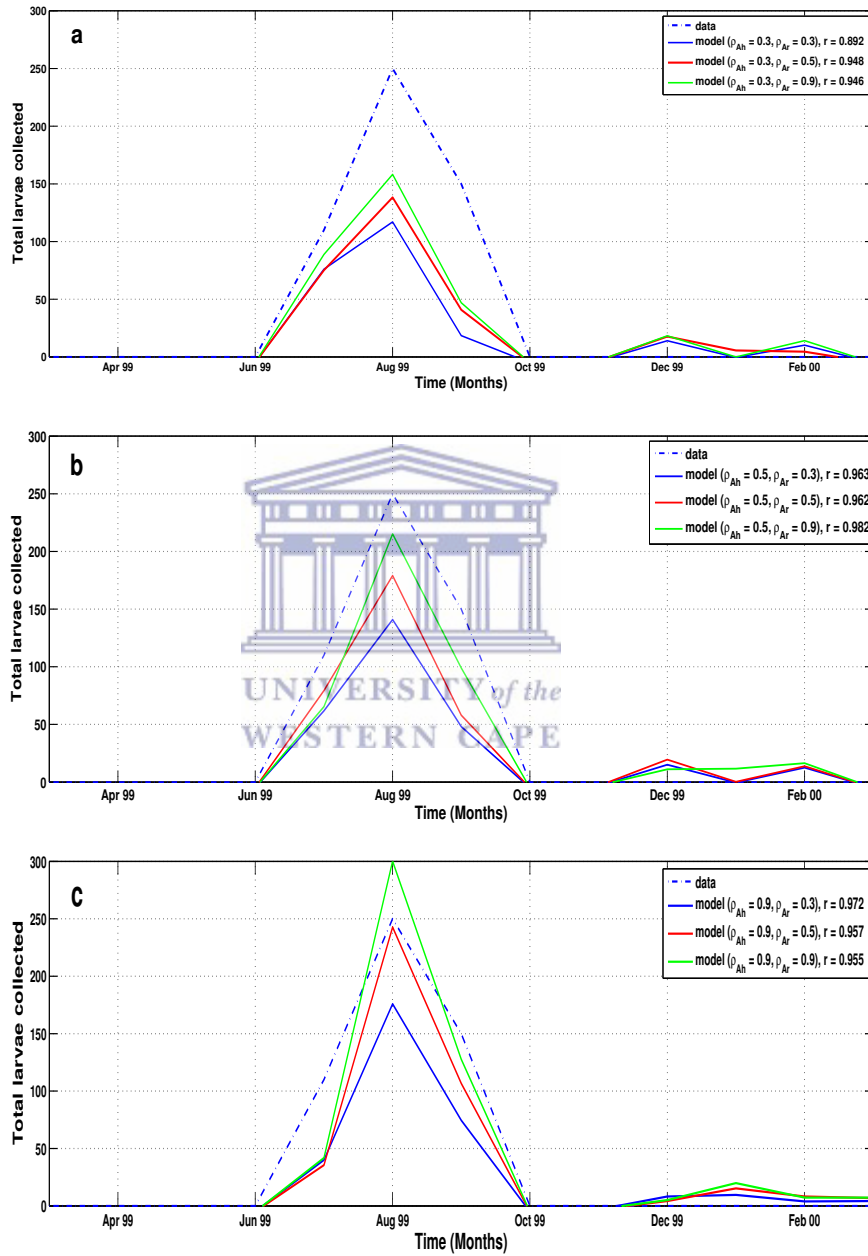


Figure 5.7: Model sensitivity to parameters. This highlights the sensitivity of the model to parameters. See main text for details.

5.4.2.2 Model sensitivity to temperature

For better understanding of the relationship between temperature and vector dynamics, the sensitivity to temperature on both immature and adult mosquito population is examined in Fig. 5.8 and Fig. 5.9 respectively. To analyse this, it is assumed that rainfall is constant for the first 30 days with varied temperature. In each class, the dynamics is checked when the temperature is 10°C, 15°C, 20°C, 25°C, 30°C and 35°C. It is noticed in both figures (Fig. 5.8 and Fig. 5.9) that the aquatic mosquitoes are more sensitive to temperatures at 25°C than the adult. It is also noticed that temperatures below 15°C have negative impact on *An. arabiensis*. Consequently, the dynamics are negatively influenced by temperatures above 30°C as specified in other studies (e.g., [190]).

Incorporating the daily climate data of Dondotha village between January 2002 - December 2004, the model is used to simulate the dynamics of *An. arabiensis* populations in the region. The model simulates well the abundance of mosquitoes per stage ($E, L, P, A_m, A_h, A_r, A_o$) over time and presents a strong seasonal variability as shown in Fig. 5.10 and 5.11.

With the assumption that the first eggs of the year are laid at the beginning of January, eggs density reaches a maximum in mid-January, February and early March as shown in Fig. 5.10a. Oviposition activity decreases between June and mid-August of every year. Larvae and pupae populations follow the same pattern for each year through the study period. Due to human activities such as irrigation and water leakage leading to creation of breeding sites, the model allows the immature *An. arabiensis* population to remain non-zero even in unfavourable conditions between June and August. Differences between years were due to differences in climate variables, the model being otherwise deterministic.

Similar results of the aquatic stages over the adult group were observed as shown in Fig. 5.11a-d. It is noted that the adult populations also present a strong seasonal variability with a 6-month period of adult activity as mosquito density is minimal through June, July and August. This suggests that the

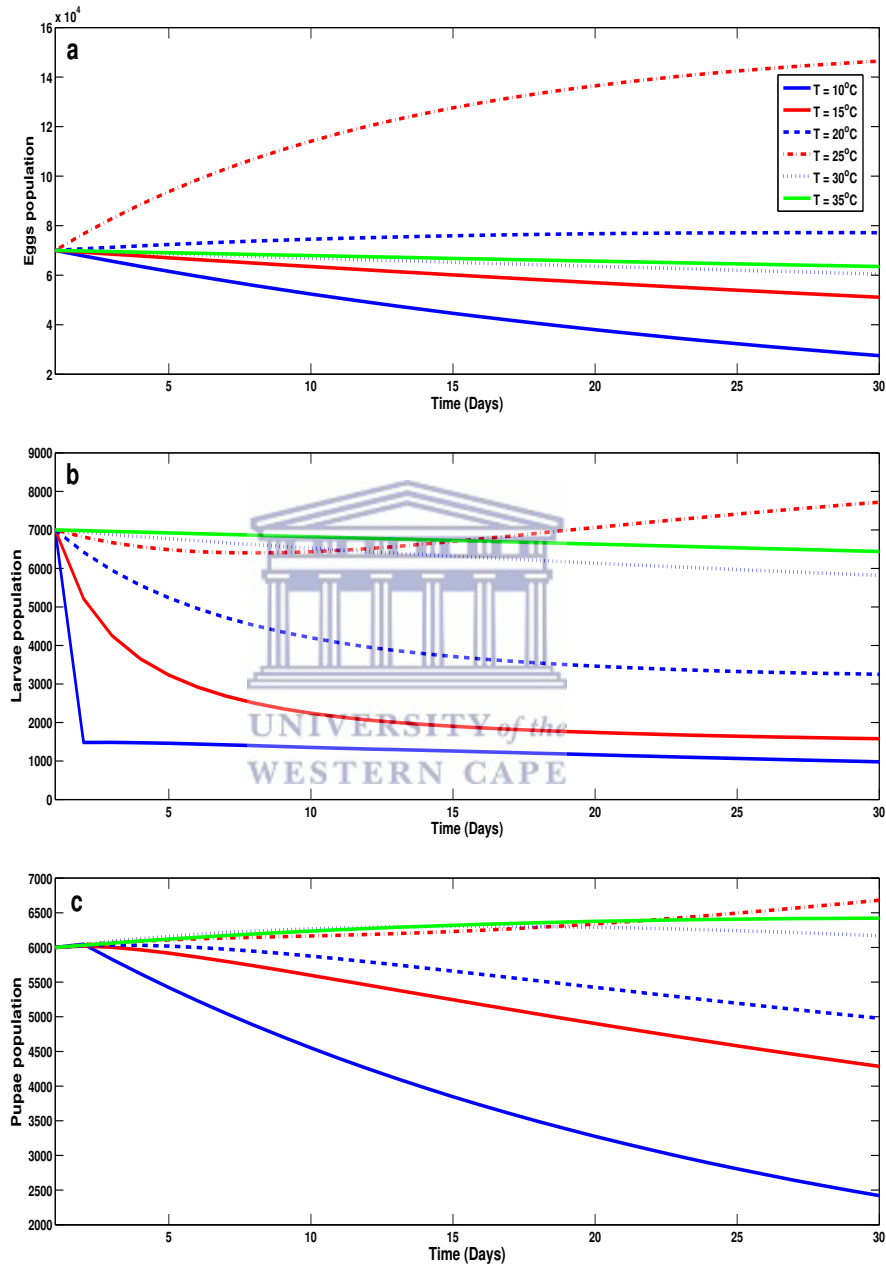


Figure 5.8: Sensitivity of aquatic-stage mosquito population dynamics to temperature. Effect of constant temperature on (a) eggs, (b) larvae, and (c) pupa *An. arabiensis*.

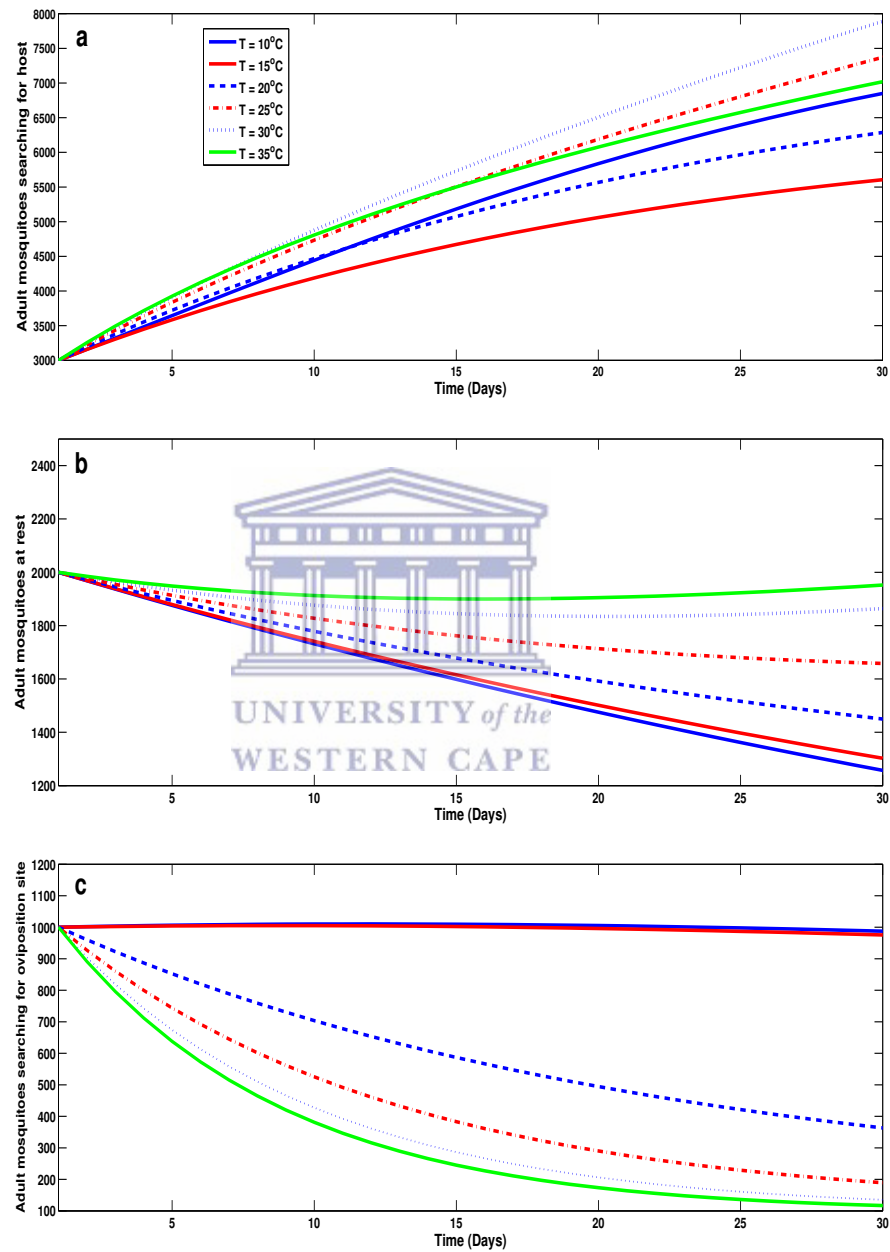


Figure 5.9: Sensitivity of adult mosquito population dynamics to temperature. Effect of constant temperature on adult *An. arabiensis* (a) searching for host, (b) resting, and (c) searching for oviposition site.

number of adults old enough to transmit malaria is intensely influenced by the aquatic stage dynamics, which is in line with the study of [9]. The results also indicate that *An. arabiensis* mosquitoes are present in the region over the study periods, and that the population of *An. arabiensis* in the province is highly seasonal with the peak in summer and minimal in winter as shown in Fig. 5.11a-d.

Also, temperature is noted to have a stronger influence on adult *An. arabiensis* abundance than precipitation, and it is also the main driver of the model. In fact, most of the mortality and progression rates are temperature-dependent functions. Temperature drives the mortality and transition rates functions in two different ways: higher temperatures favour higher transition rates between stages, although mortality rates decrease with temperature. Yet, according to the simulations in the province, the impact of temperatures is rather favourable to *An. arabiensis* populations as the peak of abundance occurs with the highest temperatures observed in summer period.

Running the model over the daily temperature of the 1.0-degree spatial resolution dataset, the oviposition rate is spatially simulated over South Africa for December 2001 to December 2002. The results as shown in Fig. 5.12 suggest why malaria transmission in South Africa is distinctly seasonal. It is noticed that more eggs are produced in summer (December - February) than winter (June - August) period (see Fig. 5.12b). Some eggs are also produced in Spring (September - November) and Autumn (March - May). This is in line with previous studies [114, 144, 182] that *An. arabiensis* do not oviposit in dry and cold conditions. Similarly, as a result of high temperature in summer, it is established that gonotrophic activities are faster during this period as mosquitoes bite more aggressively for survival and oviposition (e.g., [190]).

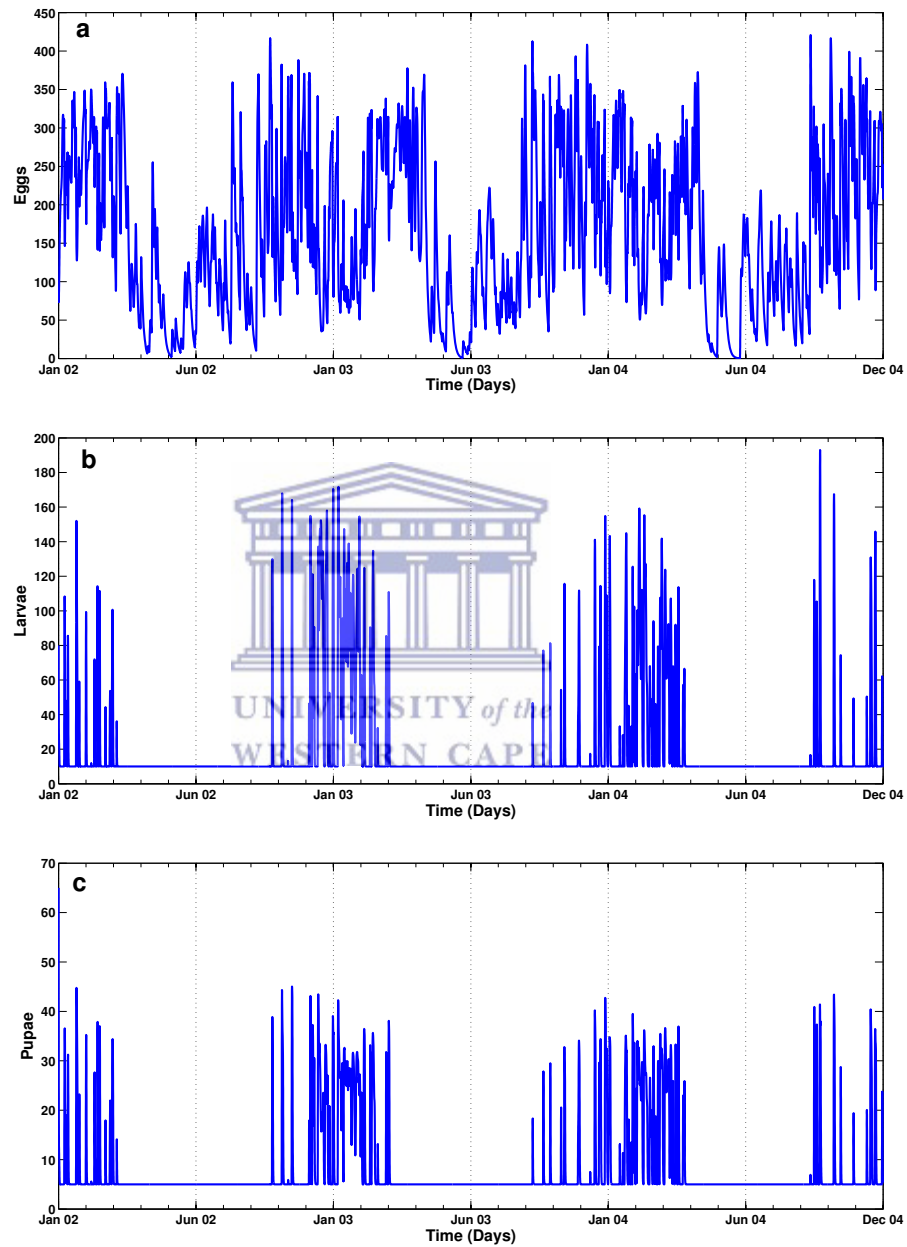


Figure 5.10: Simulated population of immature *An. arabiensis*. Simulations of (a) eggs, (b) larvae, and (c) pupae population dynamics with climate variables.

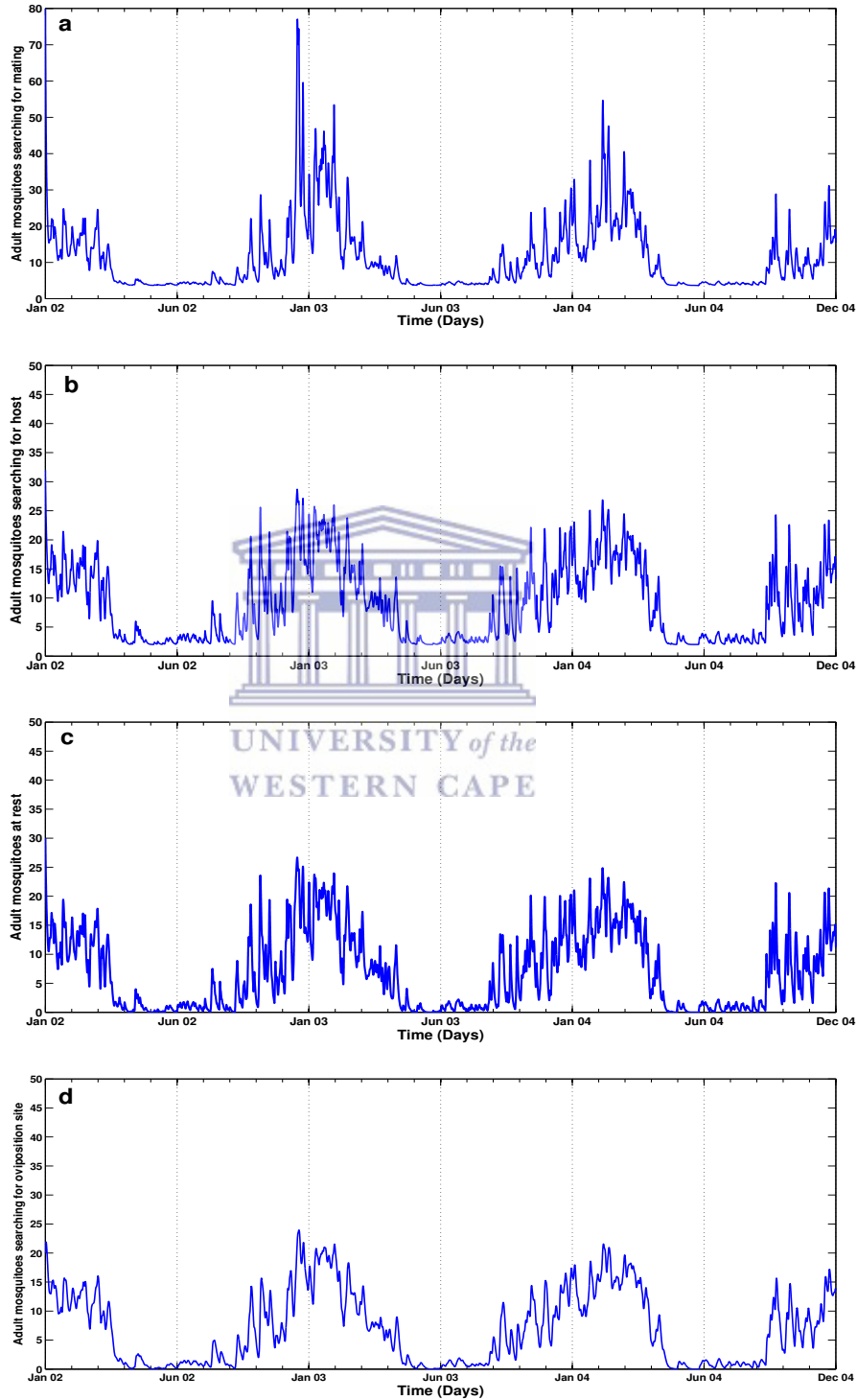


Figure 5.11: Simulated population of adult *An. arabiensis*. Simulations of adult mosquitoes (a) searching for mating, (b) searching for host, (c) resting, and (d) searching for oviposition site with climate variables.

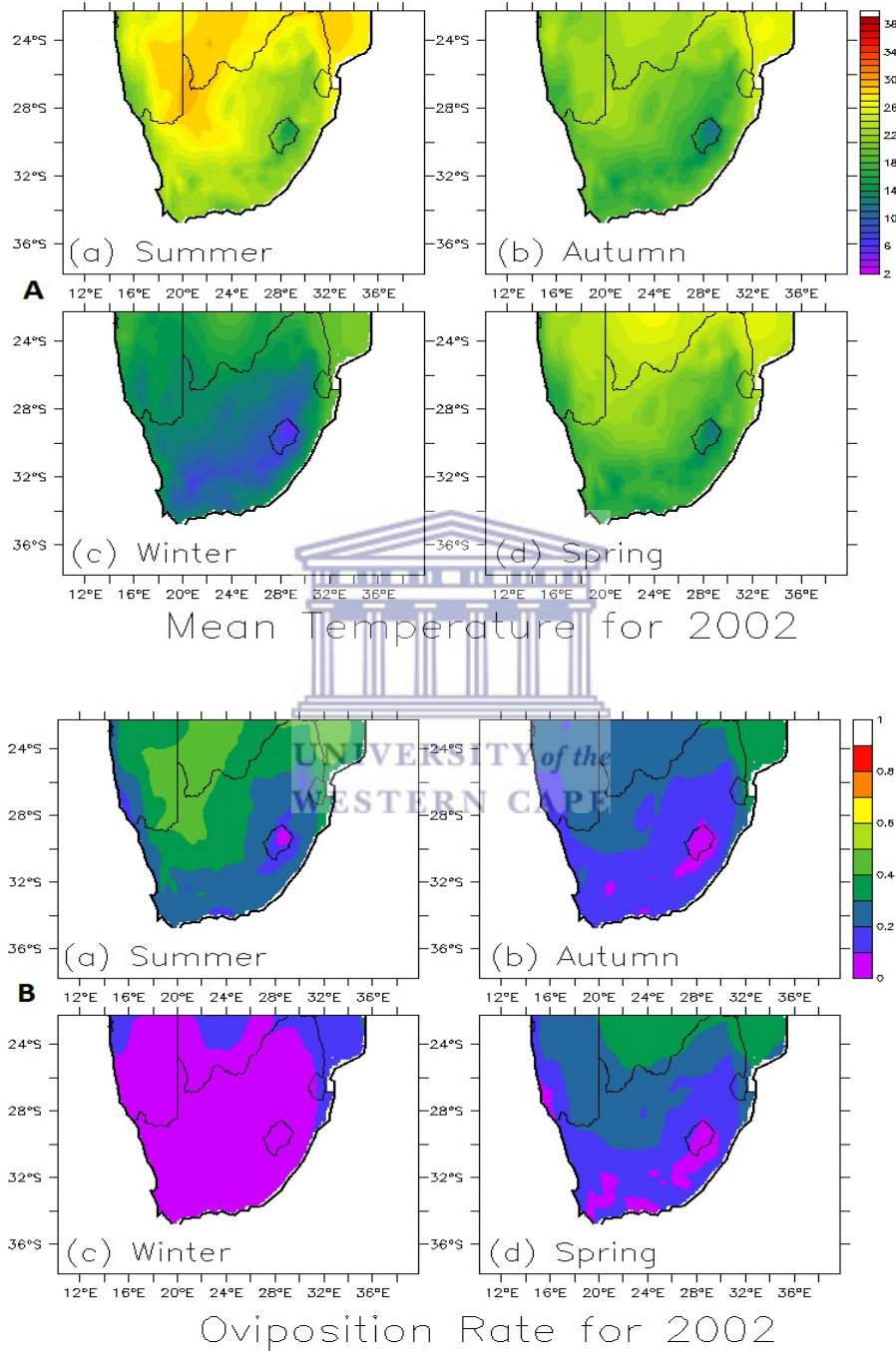


Figure 5.12: Spatial distribution of temperature and oviposition rate over South Africa. This highlights the spatial distribution of (a) observed temperature, and (b) simulated oviposition rate over South Africa.

5.5 Conclusion

In this paper, a mathematical mosquito model is presented and analysed, this was motivated by the compartmental model of [103], Lutambi2013thesis. Two climatic factors (rainfall and temperature) and puddle dynamics are incorporated into the model to understudy the dynamics of immature *An. arabiensis*.

The forcing functions for gonotrophic cycle, progression and mortality rate of eggs, larvae and pupae are also derived from the laboratory experiment in the study of Maharaj [114]. The efficiency of the model are also verified by comparing the simulated larvae with total average number of larvae collected over a town in eastern Sudan from the study of Himeidan and Rayah [79]. Furthermore, the model sensitivity analysis is carried out to examine the sensitivity of the model to parameters.

In addition, the climate data of Dondotha village in KwaZulu-Natal province are incorporated into the model to simulate the dynamics of the mosquito population over the region. The results highlight the importance of climate on *An. arabiensis* which is accountable for malaria transmission in Africa. It also increases the understanding of significance of the role of mosquito biology in malaria models. The model structure demonstrates a level of robustness as it can be tested on varied climate conditions and on various other species. In particular, the model can be used to study the effect of climate change and variability on vector population dynamics.

Additionally, the model can be developed further by incorporating other processes such as malaria infection. Also, since all mosquito vectors share the same basic life cycle, the model can be converted to other mosquito-borne disease systems, such as Dengue Fever and West Nile Virus. It can be used efficiently as a tool to predict *An. arabiensis* population dynamics. The framework of the model is also designed to accommodate human population dynamics, with the ability to predict malaria incidence in future.

However, the model neglects other important factors influencing the dy-

namics of the vector population. For instance, humidity has been identified to play a crucial role in both vector and puddle dynamics [102]. Low levels of relative humidity are known to decrease the lifespan of mosquitoes [209]. It has also been established that land cover affects the duration of larval development through its effect on water temperature [44]. Other missing factors in the model includes irrigation [71], deforestation [65], and so on. Hence, the present study leaves these factors for future consideration.

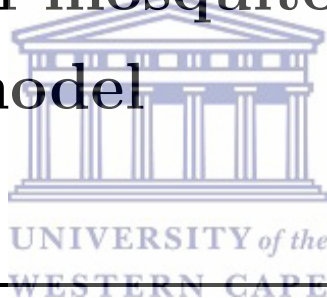


Table 5.1: Parameters of the model for *An. arabiensis*

Description	Parameters/Functional form	Ref.
Number of eggs, $n(T_a)$	$-0.61411T_a^3 + 38.93T_a^2 - 801.27T_a + 5391.4$	Derived from [114]
Egg development rate, $\rho_e(T_w)$	$0.0127T_w^3 - 0.81T_w^2 + 18T_w - 135.93$	Derived from [114]
Larva development rate, $\rho_L(T_w)$	$-0.002T_w^3 + 0.14T_w^2 - 3T_w + 22$	Derived from [114]
Pupa development rate, $\rho_P(T_w)$	$-0.0018T_w^3 + 0.12T_w^2 - 2.7T_w + 20$	Derived from [114]
Egg mortality rate, $\mu_e(T_w)$	$0.00337T_w^3 - 0.23T_w^2 + 5.3T_w - 40$	Derived from [114]
Larva mortality rate, $\mu_L(T_w)$	$0.000817T_w^3 - 0.056T_w^2 + 1.3T_w - 8.6$	Derived from [114]
Pupa mortality rate, $\mu_P(T_w)$	$0.0034T_w^3 - 0.22T_w^2 - 4.9T_w - 34$	Derived from [114]
Gonotrophic rate, $\rho_{A_0}(T_a)$	$0.00054T_a^3 - 0.038T_a^2 + 0.88T_a$	Derived from [114]
Rate adult seeks mating, ρ_{A_m}	0.5	assumed
Rate adult seeks blood meal, ρ_{A_b}	0.3 - 0.5	[103], Lutambi2013thesis
Rate adult seeks resting site, ρ_{A_r}	0.3 - 0.5	[103], Lutambi2013thesis
Rate adult seeks to mate, ρ_{A_m}	0.5	Nominal
Infiltration rate, I_f	5mm/day	[190]
Maximum volume of puddle, V_{max}	$0.57m^3/day$	Nominal
Minimum volume of puddle, V_{min}	$0.001m^3/day$	Nominal
Daylight hours per day, H_t	10-14 hrs/day	Nominal
Maximum larval biomass, L_{max}	300 mg m ⁻²	[17, 45, 190]

Chapter 6

Mathematical modelling and analysis of mosquito-human malaria model



Submitted for publication.

Authors: G.J. Abiodun, P. Witbooi, K.O. Okosun

Ignoring the impact of climate in this chapter, we further modify the mosquito model in Chapter 4 by incorporating into the model exposed and infected mosquitoes and human compartments. The detailed mosquito-human malaria model is analytically and numerically analysed with presented results.

6.1 Abstract

In this study, we derive and analyse a deterministic model for the transmission of malaria disease. We consider in detailed the human population and both stages (aquatic and adult) of mosquito population are also included. We analyse the basic reproduction number, \mathcal{R}_0 , and investigate the existence and stability of equilibria. In an attempt to examine the effectiveness of control measure, we study the sensitivity analysis of the reproductive number and highlight the importance of mosquito biting rate on malaria transmission. Finally, we perform the numerical simulations to verify the global stability of both disease-free and endemic equilibrium.

6.2 Introduction



Malaria as one of the oldest and lethal infectious diseases in humans mostly infects the infants and the poor in sub-Saharan Africa [207]. Over the world in 2006, an estimated 247 million malaria cases which led to almost a million deaths, mostly of children under-five were recorded [205]. More recently in 2013, it was also recorded that over 437 000 African children lost their lives to malaria before their fifth birthday, while an estimated 453 000 children of the same age group died globally in the same year [208]. However, the population dynamics of adult anopheles; the main carrier of malaria is highly dependent on the dynamics of the aquatic-stage. For this reason, a detailed malaria model incorporating a complete mosquito life cycle could be a crucial tool for providing early warning on malaria outbreaks.

Mathematical modelling of the spread of infectious diseases continues to offer important perceptions into diseases behaviour and control [141]. It has also become an important tool in understanding the dynamics of diseases and also in decision making processes in many countries over the years. Several efforts have also been made in the past to develop a mathematical model to analyse

the interaction between human and mosquito population and the transmission of the disease within the host. For instance, Ronald Ross [166] discovered that mosquitoes transmit malaria and used mathematical model to examine the dynamics of disease transmission. Kribs-Zaleta and Velasco-Hernandez [91] derived a simple two-dimensional SIS (susceptible-infected-susceptible) model with vaccination and multiple endemic states. Dietz *et al* [49] developed a model that accounts for acquired immunity in a mass action model. Also, Chiyaka *et al* [36] formulated a deterministic model with two latent periods in the hosts and vector populations. Li [99] examined a compartmental model for malaria transmission that includes incubation periods for both infected human hosts and mosquitoes. Okosun and Makinde [142] derived and analysed a deterministic model for the transmission of malaria disease with drug resistance in the infectives. In the study, they calculated the basic reproduction number, and investigated the existence and stability of equilibria.

Incorporating mosquito aquatic stage into models becomes more important when considering other factors (such as, climate variables) affecting mosquito abundance. In such cases, all stages are paramount to the study of mosquito population dynamics. However, most models often ignore a complete mosquito life cycle since eggs, larvae and pupae are not directly involved in the transmission cycle. Also, based on the assumption that eggs, larvae, and pupa have similar development and mortality rate, some studies have used only the larval stage to represent the entire immature stage. For instance, Ngarakana-Gwasira *et al* [137] developed and analysed a mosquito-human model to assess the impact of temperature on transmission of malaria. In the study, one compartment was used to represent the juvenile stages. However, the assumption contradicts the findings of other studies. For example, in the study of Maharaj [114], the laboratory experiment highlighted the differences in progression and mortality rate of each stage. In this study, we adopt and modify the model of Lutambi *et al* [103]. We aim to develop a detailed mosquito-human malaria model that overcomes the weakness of conventional malaria models. Since several factors such as climate and ecology affect the dynamics of aquatic-stage mosquitoes, we include this stage in our model and analysis. This is to prepare

a strong frame-work that can easily incorporate the impact of these factors in future. Also to carefully monitor the development in each of the mosquito stages for helpful interventions and control strategies.

6.3 Model formulation

The total human population, denoted by N_h is sub-divided into susceptible individuals (S_h), those exposed to malaria parasite (E_h), individuals with malaria symptoms (I_h) and recovered human (R_h) such that $N_h = S_h + E_h + I_h + R_h$. Susceptible individuals are recruited (by birth or immigration) into the community at a rate ϕ_h and acquire malaria through contact with infectious mosquitoes at a rate β_h . Exposed individuals move to infectious class at a rate ρ_{E_h} . Infectious individuals move to the recovered class at a rate ρ_{I_h} while infected individuals die at a rate α . Recovered individuals loose immunity at a rate ρ_{R_h} and become susceptible again and the natural death rate is denoted by μ_h .

The mosquito population model is based and developed on phases of the mosquito life cycle. Mosquito life begins with eggs, which hatch into larvae under suitable conditions. The larvae develop into pupae that mature and emerge into adults. The total mosquito population is denoted by N_v and is sud-divided into three aquatic stages; Eggs (E), Larvae (L), and Pupae (P), and five adult classes; Susceptible adult searching for host (A_h), Adult at resting state (A_r), Adult searching for oviposition site (A_o), Adult exposed to malaria parasite (E_v) and infectious mosquitoes (I_v). Hence, $N_v = E + L + P + A_h + A_r + A_o + E_v + I_v$ as shown in Figure 6.1. Female mosquitoes then feed on human or animal blood to provide protein for their eggs. After biting, female mosquitoes rest while their eggs develop. Once eggs are fully developed, the females oviposit and then proceed to find another blood meal thus completing the mosquito feeding cycle [35].

We ignore the effects of hibernation and breaks in the reproductive cycle, and assumed that eggs deposited at breeding sites proceed through development

immediately [103, 104, 172]. In contrast to other models [99], we distinguish all of these stages because interventions may be applied to any one (or more) of them. We also ignore the male population in this model since only female mosquitoes are involved in the transmission of vector-borne diseases. The six subgroups have different mortality and progression rates. Each subgroup is affected by three processes: increase due to recruitment, decrease due to mortality, and development or progression of survivors into the next state. The parameter n is the average number of eggs which are expected to hatch into female mosquitoes laid during an oviposition and ρ_{A_o} (day^{-1}) is the rate at which new eggs are oviposited (i.e. reproduction rate). Exit from the egg stage is either due to mortality, μ_e (day^{-1}), or hatching into larvae, ρ_e (day^{-1}). In the larval stage, individuals exit by death or progress to pupal stage at a rate, ρ_L (day^{-1}). Assuming a stable environment, inter-competition for food and other resources for larvae may occur, leading to density-dependent mortality, $\frac{\mu_L L}{K}$ ($\text{day}^{-1} \text{ mosquito}^{-1}$) or natural death at an intrinsic rate, μ_L (day^{-1}), where K is the carrying capacity of the breeding site. Pupae die at a rate, μ_P (day^{-1}), and survivors progress and emerge as adults at rate ρ_P (day^{-1}). In the adult stage, host seeking mosquitoes die at a rate μ_{A_h} (day^{-1}). Those surviving this stage, and if they are successful in feeding, enter the resting stage at a rate ρ_{A_h} (day^{-1}). In the resting stage, mosquitoes die at a rate, μ_{A_r} (day^{-1}). Survivors progress to the oviposition site searching stage at a rate ρ_{A_r} (day^{-1}). Oviposition site seekers die at rate μ_{A_o} (day^{-1}) and after laying eggs return to the host seeking stage. Although mosquitoes might require more than one blood meal to produce eggs [10, 103, 104], this model assumes the simplified case where only one blood meal is enough for eggs to mature. After feeding, we assume that some proportion ($D_v A_h$) of susceptible mosquito move to resting class A_r for gonotrophic process without being infected while others ($\beta_v A_h$) move to exposed class (E_v) for sporogonic process. They acquire malaria through contact with infected humans at rate β_v , and later progress to the infected class (I_v) at a rate ρ_{E_v} . It is noted that $\beta_h = \frac{\beta_1 \epsilon \kappa I_v}{N_h}$, $\beta_v = \frac{\beta_2 \epsilon \kappa I_h}{N_h}$ and $D_v = \frac{\epsilon \kappa A_h}{N_h}$, where β_1 and β_2 represent the transmission probability of human and mosquito respectively with contact rate κ of mosquito per human per unit time.

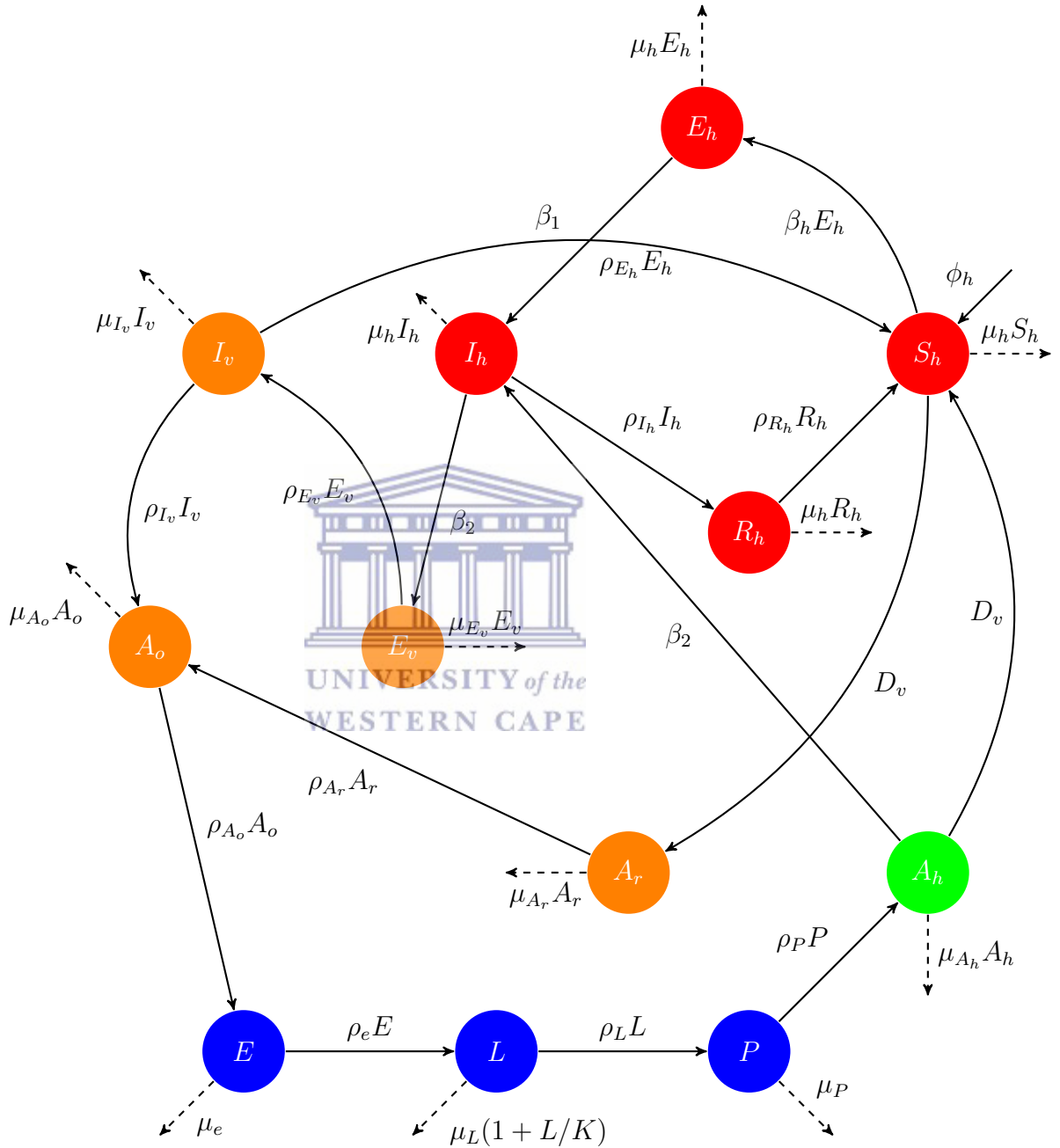


Figure 6.1: Flow diagram for malaria transmission model

The dynamics of the mosquito population are described by the following system of differential equations:

$$\begin{aligned}
\frac{dS_h}{dt} &= \phi_h + \rho_{R_h} R_h - (\beta_h + \mu_h) S_h \\
\frac{dE_h}{dt} &= \beta_h S_h - (\rho_{E_h} + \mu_h) E_h \\
\frac{dI_h}{dt} &= \rho_{E_h} E_h - (\rho_{I_h} + \mu_h + \alpha) I_h \\
\frac{dR_h}{dt} &= \rho_{I_h} I_h - (\rho_{R_h} + \mu_h) R_h \\
\frac{dE}{dt} &= n(\rho_{A_o} A_o + \rho_{I_v} I_v) - (\rho_e + \mu_e) E \\
\frac{dL}{dt} &= \rho_e E - (\rho_L + \mu_L(1 + L/K)) L \\
\frac{dP}{dt} &= \rho_L L - (\rho_P + \mu_P) P \\
\frac{dA_h}{dt} &= \rho_P P + \rho_{A_o} A_o - (\beta_v + D_v + \mu_{A_h}) A_h \\
\frac{dA_r}{dt} &= D_v A_h - (\rho_{A_r} + \mu_{A_r}) A_r \\
\frac{dA_o}{dt} &= \rho_{A_r} A_r - (\rho_{A_o} + \mu_{A_o}) A_o \\
\frac{dE_v}{dt} &= \beta_v A_h - (\rho_{E_v} + \mu_{E_v}) E_v \\
\frac{dI_v}{dt} &= \rho_{E_v} E_v - \mu_{I_v} I_v
\end{aligned} \tag{6.1}$$

In the model, the term $\frac{\beta_2 \epsilon \kappa I_h A_h}{N_h}$ denotes the rate at which the susceptible mosquitoes searching for host A_h are infected by human I_h and $\frac{\beta_1 \epsilon \kappa I_v S_h}{N_h}$ refers to the rate at which the susceptible humans S_h , become infected by infectious female *Anopheles* mosquito I_v . It is important to note that the rate of infection of susceptible humans S_h by infected mosquito I_v is dependent on the total

number of humans N_h available per vector.

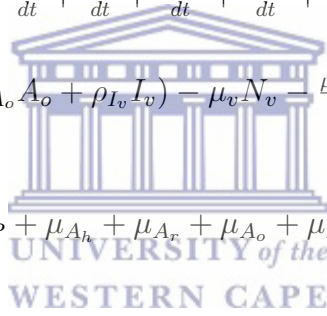
The total population sizes are $N_h = S_h + E_h + I_h + R_h$ and $N_v = E + L + P + A_h + A_r + A_o + E_v + I_v$ with their differential equations

$$\begin{aligned} \frac{dN_h}{dt} &= \frac{dS_h}{dt} + \frac{dE_h}{dt} + \frac{dI_h}{dt} + \frac{dR_h}{dt} \\ &= \phi_h - \mu_h N_h - \alpha I_h \end{aligned} \tag{6.2}$$

and

$$\begin{aligned} \frac{dN_v}{dt} &= \frac{dE}{dt} + \frac{dL}{dt} + \frac{dP}{dt} + \frac{dA_h}{dt} + \frac{dA_r}{dt} + \frac{dA_o}{dt} + \frac{dE_v}{dt} + \frac{dI_v}{dt} \\ &= n(\rho_{A_o} A_o + \rho_{I_v} I_v) - \mu_v N_v - \frac{\mu_L L^2}{K} \end{aligned} \tag{6.3}$$

where $\mu_v = \mu_e + \mu_L + \mu_P + \mu_{A_h} + \mu_{A_r} + \mu_{A_o} + \mu_{E_v} + \mu_{I_v}$.



6.4 Mathematical analysis of the model

We analyse the model to check if intervention strategies have any impact on the diseases, that is, whether the disease can be eradicated or not. The thresholds parameters which determine persistence or elimination of malaria will be determined and studied. Therefore, we start by determining the invariant region to check whether the model is biologically meaningful and showing that all solutions of (6.1) are positive for all $t \geq 0$ and are attracted in that region.

6.4.1 Invariant region

This region can be obtained by the following theorem.

Theorem 6.4.1. *The solutions of the system (6.1) are feasible for all $t > 0$ if*

they enter the invariant region $\Omega = \Omega_h \times \Omega_v$

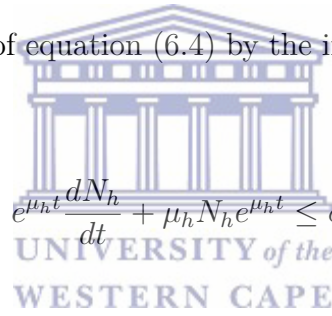
Proof: Let $\Omega = (S_h, E_h, I_h, R_h, E, L, P, A_h, A_r, A_o, E_v, I_v) \in R_+^{12}$ be any solution of the system (6.1) with non-negative initial conditions.

In absence of the disease, that is $I_h = 0$, equation (6.2) becomes

$$\frac{dN_h}{dt} \leq \phi_h - \mu_h N_h,$$

$$\frac{dN_h}{dt} + \mu_h N_h \leq \phi_h \quad (6.4)$$

Multiplying both side of equation (6.4) by the integrating factor $e^{\int \mu_h dt} = e^{\mu_h t}$ gives



$$e^{\mu_h t} \frac{dN_h}{dt} + \mu_h N_h e^{\mu_h t} \leq \phi_h e^{\mu_h t},$$

$$\frac{d}{dt}(N_h e^{\mu_h t}) \leq \phi_h e^{\mu_h t} \quad (6.5)$$

integrating both sides of equation (6.5), we have

$$N_h e^{\mu_h t} \leq \frac{\phi_h}{\mu_h} e^{\mu_h t} + C \quad (6.6)$$

where C is integration constant.

Dividing equation (6.6) through by $e^{\mu_h t}$ gives

$$N_h \leq \frac{\phi_h}{\mu_h} + C e^{-\mu_h t}$$

Using the initial conditions at $t = 0$, $N_h(0) = N_{h0}$:

$$N_{h0} \leq \frac{\phi_h}{\mu_h} + C \Rightarrow N_{h0} - \frac{\phi_h}{\mu_h} \leq C,$$

$$N_h \leq \frac{\phi_h}{\mu_h} + (N_{h0} - \frac{\phi_h}{\mu_h})e^{-\mu_h t} \quad (6.7)$$

Applying the theorem of differential inequality [13], we obtain

$$0 \leq N_h \leq \frac{\phi_h}{\mu_h}$$

Therefore, as $t \rightarrow \infty$ in (6.7), the human population $N_h \leq \frac{\phi_h}{\mu_h}$.

Hence all feasible solutions set of the human population of the model (6.1) enters region

$$\Omega_h = \left\{ (S_h, E_h, I_h, R_h) \in R_+^4 : S_h > 0, E_h \geq 0, I_h \geq 0, R_h \geq 0, N_h \leq \frac{\phi_h}{\mu_h} \right\}$$

Similarly, the feasible solutions set of the mosquito population enters the region

$$\Omega_v = \{(E, L, P, A_h, A_r, A_o, E_v, I_v) \in R_+^8 :$$

$$E > 0, L \geq 0, P \geq 0, A_h \geq 0, A_r \geq 0, A_o \geq 0, E_v \geq 0, I_v \geq 0,$$

$$N_v \leq \frac{nK(\rho_{A_o}A_o + \rho_{I_v}I_v) - \mu_L L^2}{K\mu_v} \leq \frac{nK\rho_{A_o}A_o - \mu_L L^2}{K\mu_v}\}.$$

Therefore, the feasible solution set for model (6.1) is given by

$$\Omega = \{(S_h, E_h, I_h, R_h, E, L, P, A_h, A_r, A_o, E_v, I_v) \in R_+^{12} :$$

$$(S_h, E) > 0, (E_h, I_h, R_h, L, P, A_h, A_r, A_o, E_v, I_v) \geq 0 :$$

$$N_h \leq \frac{\phi_h}{\mu_h} : N_v \leq \frac{nK\rho_{A_o}A_o - \mu_L L^2}{K\mu_v}\}.$$

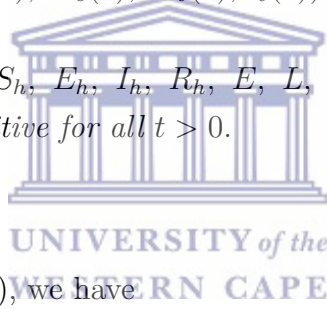
Therefore, the region Ω is positive-invariant (i.e. solutions remain positive for all times, t) and the model (6.1) is biologically meaningful and mathematically well-posed in the domain Ω \square

6.4.2 Positivity of solutions

Lemma 6.4.2. *Let the initial conditions be*

$$\{(S_h(0), E(0)) > 0, (E_h(0), I_h(0), R_h(0), L(0), P(0), A_h(0), A_r(0), A_o(0), E_v(0), I_v(0)) \geq 0\} \in \Omega.$$

Then the solution set $\{S_h, E_h, I_h, R_h, E, L, P, A_h, A_r, A_o, E_v, I_v\}(t)$ of the system (6.1) is positive for all $t > 0$.



Proof

From the equation (6.1), we have

$$\begin{aligned} \frac{dS_h}{dt} &= \phi_h + \rho_{R_h} R_h - (\beta_h + \mu_h) S_h \geq -(\beta_h + \mu_h) S_h \\ \int \frac{1}{S_h} dS_h &\geq - \int (\beta_h + \mu_h) dt \Rightarrow \ln S_h \geq -(\beta_h + \mu_h)t + C \Rightarrow S_h(t) = e^{[-(\beta_h + \mu_h)t + C]} \\ &\Rightarrow S_h(t) \geq e^{-(\beta_h + \mu_h)t} \times A = A e^{-(\beta_h + \mu_h)t}, \quad A = e^C \\ &\Rightarrow S_h(t) \geq A e^{-(\beta_h + \mu_h)t} \end{aligned}$$

At $t = 0$,

$$S_h(0) \geq A \Rightarrow S_h(t) \geq S_h(0) e^{-(\beta_h + \mu_h)t} \geq 0$$

Therefore,

$$S_h(t) \geq S_h(0) e^{-(\beta_h + \mu_h)t} \geq 0.$$

Similarly, it can be shown that the remaining equation of system (6.1) are also positive for all $t > 0$, because $e^\eta > 0 \quad \forall \eta \in \mathbb{R}$. \square

6.4.3 Disease-free equilibrium and stability analysis

The disease-free equilibrium of model (6.1) is given by,

$$\begin{aligned} \varepsilon_0 &= (S_h^0, E_h^0, I_h^0, R_h^0, E^0, L^0, P^0, A_h^0, A_r^0, A_o^0, E_v^0, I_v^0) \\ &= \left(\frac{\phi_h}{\mu_h}, 0, 0, 0, \frac{nK\rho_{A_o}A_o - \mu_L L^2}{K\mu_v}, 0, 0, 0, 0, 0, 0, 0 \right) \end{aligned}$$

We use the next generation operator approach as described by Diekmann *et al* [47] to define the basic reproduction number, \mathcal{R}_0 , as the number of secondary infections that one infectious individual would create over the duration of the infectious period, provided that everyone else is susceptible. The basic reproduction number (reproduction ratio) \mathcal{R}_0 is given by

$$\mathcal{R}_0 = \varphi(FV^{-1}),$$

where $\varphi(M)$ denotes the spectral radius of a matrix M ,

$$F = \begin{bmatrix} 0 & 0 & 0 & \beta_1 \epsilon \kappa \\ 0 & 0 & 0 & 0 \\ 0 & \frac{\beta_2 \epsilon \kappa \mu_h \theta_1}{\phi_h \theta_2} & 0 & 0 \\ 0 & 0 & 0 & 0 \end{bmatrix} \quad (6.8)$$

where $\theta_1 = nK\rho_{A_o}A_o - \mu_L L^2$, and $\theta_2 = K\mu_v$. Also,

$$V = \begin{bmatrix} (\rho_{E_h} + \mu_h) & 0 & 0 & 0 \\ -\rho_{E_h} & (\rho_{I_h} + \mu_h + \alpha) & 0 & 0 \\ 0 & 0 & (\rho_{E_v} + \mu_{E_v}) & 0 \\ 0 & 0 & -\rho_{E_v} & \mu_{I_v} \end{bmatrix}, \quad (6.9)$$

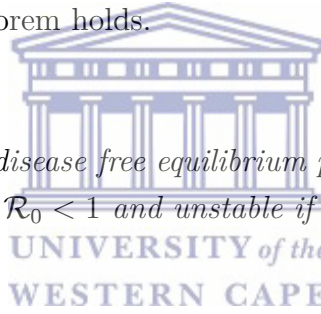
such that

$$\mathcal{R}_0 = \sqrt{\frac{\rho_{E_h} \rho_{E_v} \beta_1 \beta_2 (\epsilon \kappa)^2 \mu_h \theta_1}{\phi_h \theta_2 \mu_{I_v} (\rho_{E_h} + \mu_h) (\rho_{I_h} + \mu_h + \alpha) (\rho_{E_v} + \mu_{E_v})}} \quad (6.10)$$

6.4.4 Local stability of the disease-free equilibrium

We analyse the local stability of the disease-free equilibrium using the Jacobian matrix of the malaria model (6.1) at the disease free equilibrium point. Using [196], the following theorem holds.

Theorem 6.4.3. *The disease free equilibrium point for system (6.1) is locally asymptotically stable if $\mathcal{R}_0 < 1$ and unstable if $\mathcal{R}_0 > 1$.*



Proof:

Setting $C_1 = \mu_{I_v}$, $C_2 = \rho_{E_v} + \mu_{E_v}$, $C_3 = \rho_{I_h} + \mu_h + \alpha$ and $C_4 = \rho_{E_h} + \mu_h$, the Jacobian matrix (J) of the malaria model (6.1) with $S_h = N_h - (E_h + I_h + R_h)$ and $A_h = N_v - (E_v + I_v)$ at the disease-free equilibrium point is given by

$$\begin{bmatrix} -C_4 & 0 & 0 & 0 & \beta_1 \epsilon \kappa \\ \rho_{E_h} & -C_3 & 0 & 0 & 0 \\ 0 & \rho_{I_h} & -(\rho_{R_h} + \mu_h) & 0 & 0 \\ 0 & \frac{\beta_2 \epsilon \kappa \mu_h \theta_1}{\phi_h \theta_2} & 0 & -C_2 & 0 \\ 0 & 0 & 0 & \rho_{E_v} & -C_1 \end{bmatrix} \quad (6.11)$$

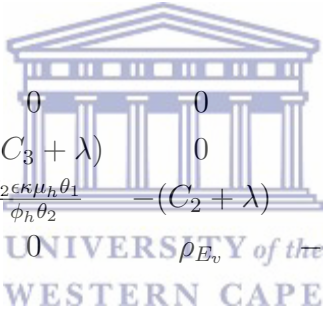
The eigenvalues of the Jacobian matrix are the solutions of the characteristics equation

$$|J - \lambda I| = 0.$$

That is

$$\begin{bmatrix} -(C_4 + \lambda) & 0 & 0 & 0 & \beta_1 \epsilon \kappa \\ \rho_{E_h} & -(C_3 + \lambda) & 0 & 0 & 0 \\ 0 & \rho_{I_h} & -(\rho_{R_h} + \mu_h + \lambda) & 0 & 0 \\ 0 & \frac{\beta_2 \epsilon \kappa \mu_h \theta_1}{\phi_h \theta_2} & 0 & -(C_2 + \lambda) & 0 \\ 0 & 0 & 0 & \rho_{E_v} & -(C_1 + \lambda) \end{bmatrix} = 0 \quad (6.12)$$

The third column has diagonal entry, therefore one of the eigenvalues of the Jacobian matrix is $(\rho_{R_h} + \mu_h)$. The remaining eigenvalues can be obtained as follows:



$$\begin{bmatrix} -(C_4 + \lambda) & 0 & 0 & \beta_1 \epsilon \kappa \\ \rho_{E_h} & -(C_3 + \lambda) & 0 & 0 \\ 0 & \frac{\beta_2 \epsilon \kappa \mu_h \theta_1}{\phi_h \theta_2} & -(C_2 + \lambda) & 0 \\ 0 & 0 & \rho_{E_v} & -(C_1 + \lambda) \end{bmatrix} = 0 \quad (6.13)$$

$$(C_4 + \lambda)(C_3 + \lambda)(C_2 + \lambda)(C_1 + \lambda) - Q_1 = 0 \quad (6.14)$$

where, $Q_1 = \frac{\rho_{E_h} \rho_{E_v} \beta_1 \beta_2 (\epsilon \kappa)^2 \mu_h \theta_1}{\phi_h \theta_2 \mu_{I_v}}$. Hence,

$$\lambda^4 + D_1 \lambda^3 + D_2 \lambda^2 + D_3 \lambda + D = 0, \quad (6.15)$$

where,

$$\begin{aligned} D_1 &= C_1 + C_2 + C_3 + C_4 \\ D_2 &= C_1 C_2 + C_3(C_1 + C_2) + C_4(C_1 + C_2 + C_3) \\ D_3 &= C_1 C_2 C_3 + C_1 C_2 C_4 + C_1 C_3 C_4 + C_2 C_3 C_4 \\ D_4 &= C_1 C_2 C_3 C_4 - Q_1 \end{aligned} \quad (6.16)$$

Also from (6.10),

$$\mathcal{R}_0^2 = \frac{\rho_{E_h} \rho_{E_v} \beta_1 \beta_2 (\epsilon \kappa)^2 \mu_h \theta_1}{\phi_h \theta_2 C_1 C_2 C_3 C_4} \quad (6.17)$$

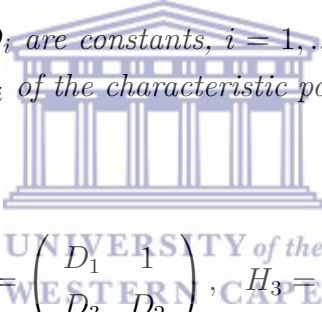
Using the Routh-Hurwitz Criteria on polynomial, we prove that all roots of the polynomial (6.15) have negative real part.

Theorem 6.4.4. Routh-Hurwitz Criteria

Given the polynomial

$$P(\lambda) = \lambda^n + D_1 \lambda^{n-1} + \dots + D_{n-1} \lambda + D_n,$$

where the coefficients D_i are constants, $i = 1, \dots, n$ define n Hurwitz matrices using the coefficients D_i of the characteristic polynomial



$$H_1 = (D_1), \quad H_2 = \begin{pmatrix} D_1 & 1 \\ D_3 & D_2 \end{pmatrix}, \quad H_3 = \begin{pmatrix} D_1 & 1 & 0 \\ D_3 & D_2 & D_1 \\ D_5 & D_4 & D_3 \end{pmatrix} \quad \text{and}$$

$$H_n = \begin{pmatrix} D_1 & 1 & 0 & 0 & \dots & 0 \\ D_3 & D_2 & D_1 & 1 & \dots & 0 \\ D_5 & D_4 & D_3 & D_2 & \dots & 0 \\ \vdots & \vdots & \vdots & \vdots & \dots & \vdots \\ 0 & 0 & 0 & 0 & \dots & D_n \end{pmatrix}$$

where

$D_j = 0$ if $j > n$. All of the roots of the polynomial $P(\lambda)$ are negatives or have negative real parts if and only if the determinants of all Hurwitz matrices are positive:

$$\det(H_j) > 0, j = 1, 2, \dots, n.$$

For the characteristic polynomial in equation (6.15), where $n = 4$, the Routh-

Hurwitz Criteria are

$$D_1 > 0, D_2 > 0, D_3 > 0, D_4 > 0,$$

$$\det(H_1) = D_1 = C_1 + C_2 + C_3 + C_4 > 0$$

$$\det(H_2) = \begin{pmatrix} D_1 & 1 \\ 0 & D_2 \end{pmatrix} = D_1 D_2 > 0,$$

$$= 3C_3 C_4 (C_1 + C_2) + 3C_2 C_1 (C_3 + C_4) + C_4^2 (C_1 + C_2 + C_3 + C_4)$$

$$+ C_3^2 (C_1 + C_2 + C_4) + C_2^3 (C_1 + C_3 + C_4) + C_1^2 (C_2 + C_3 + C_4) > 0$$

$$\det(H_3) = \begin{pmatrix} D_1 & 1 & 0 \\ D_3 & D_2 & D_1 \\ D_5 & D_4 & D_3 \end{pmatrix} = D_1 D_2 D_3 - D_3^2 = D_1 D_2 - D_3$$

$$= 2C_3 C_4 (C_1 + C_2) + 2C_1 C_2 (C_3 + C_4) + C_4^2 (C_1 + C_2 + C_3)$$

$$+ C_3^2 (C_1 + C_2 + C_4) + C_2^2 (C_1 + C_3 + C_4) + C_1^2 (C_2 + C_3 + C_4) > 0$$

and

$$\det(H_4) = \begin{pmatrix} D_1 & 1 & 0 & 0 \\ D_3 & D_2 & D_1 & 1 \\ 0 & D_4 & D_3 & D_2 \\ 0 & 0 & 0 & D_4 \end{pmatrix} = D_3 (D_1 D_2 - D_3) - D_4 D_1^2$$

$$= D_3 (D_1 D_2 - D_3) - D_4 D_1^2 = D_3 Q_2 + Q_1 D_1^2 - C_1 C_2 C_3 C_4 D_1^2 > 0$$

where, $Q_2 = D_1 D_2 D_3$.

Since all determinants of the Hurwitz matrices are positive, which means all the eigenvalues of the Jacobian (6.15) have negative real part and $\mathcal{R}_0 < 1$. Therefore, disease-free equilibrium point is stable. Conversely, if $\mathcal{R}_0 > 1$, it implies that $D_4 < 0$, and since the remaining coefficients (D_1, D_2 and D_3) of the polynomial (6.15) are positive, then all the roots of this polynomial cannot have negative real parts. Therefore, the DFE point is unstable. \square

6.4.5 Endemic equilibria and stability analysis

The endemic equilibrium (ε_1) of the model is given by

$$\varepsilon_1 = (S_h^*, E_h^*, I_h^*, R_h^*, E^*, L^*, P^*, A_h^*, A_r^*, A_o^*, E_v^*, I_v^*), \text{ where,}$$

$$\begin{aligned}
 S_h^* &= \frac{\phi_h(\rho_{R_h} + \mu_h) + \rho_{R_h} \rho_{I_h} I_h^*}{(\rho_{R_h} + \mu_h)(\beta_h^* + \mu_h)} \\
 E_h^* &= \frac{\beta_h^* [\phi_h(\rho_{R_h} + \mu_h) + \rho_{R_h} \rho_{I_h} I_h^*]}{(\rho_{E_h} + \mu_h)(\rho_{R_h} + \mu_h)(\beta_h^* + \mu_h)} \\
 I_h^* &= \frac{\rho_{E_h} E_h^*}{(\rho_{I_h} + \mu_h + \alpha) I_h^*} \\
 R_h^* &= \frac{I_h^* \rho_{I_h}}{\mu_h + \rho_{R_h}} \\
 E^* &= \frac{n(\rho_{A_o} A_o^* + \rho_{I_v} I_v^*)}{(\rho_e + \mu_e)} \\
 L^* &= \frac{\sqrt{4E^* K \mu_L \rho_e + (K(\mu_L + \rho_L))^2} - (K(\mu_L + \rho_L))}{\mu_L} \\
 P^* &= \frac{\rho_L L^*}{(\rho_P + \mu_P)} \\
 A_h^* &= \frac{\rho_P P^* + \rho_{A_o} A_o^*}{D_v + \epsilon \kappa I_h^* \beta_2 + \mu_r + \mu_{A_h}} \\
 A_r^* &= \frac{D_v (\rho_P P^* + \rho_{A_o} A_o^*)}{(D_v + \epsilon \kappa I_h^* \beta_2 + \mu_r + \mu_{A_h}) Z_5} \\
 A_o^* &= \frac{D_v (\rho_P P^* + \rho_{A_r} A_r^*)}{(D_v + \epsilon \kappa I_h^* \beta_2 + \mu_r + \mu_{A_h}) (\mu_r + \mu_{A_o} + \rho_{A_o}) Z_5} \\
 E_v^* &= \frac{\epsilon \kappa I_h^* \beta_2 (\rho_P P^* + \rho_{A_o} A_o^*)}{(D_v + \epsilon \kappa I_h^* \beta_2 + \mu_r + \mu_{A_h}) (\mu_{E_v} + \rho_{E_v})} \\
 I_v^* &= \frac{\epsilon \kappa I_h^* \beta_2 (\rho_P P^* + \rho_{A_o} A_o^*) \rho_{E_v}}{\mu_{I_v} (D_v + \epsilon \kappa I_h^* \beta_2 + \mu_r + \mu_{A_h}) (\mu_{E_v} + \rho_{E_v})}
 \end{aligned} \tag{6.18}$$

The endemic equilibrium satisfies the following polynomial

$$G_1(I_h^*)^2 + G_2(I_h^*) + G_3 = 0, \quad (6.19)$$

with

$$G_1 = \beta_2 \rho_{I_h} \rho_{R_h} \mu_h N_h \mathcal{R}_0^2 - (\epsilon \kappa)^2 \beta_h \mu_h (\rho_{R_h} + \mu_h) (\theta_2 \mu_{I_v} + \beta_2 \mu_h N_h)$$

$$G_2 = \rho_{I_h} \rho_{R_h} \mu_h N_h^2 (\theta_2 \mu_{I_v}) \mathcal{R}_0^2 - M_1 \left[\beta_2 \mu_h N_h (\phi_h \mathcal{R}_0^2 - \phi_h - \mu_h N_h) - M_2 \mathcal{R}_{0v} \right]$$

$$G_3 = \mu_h (\theta_2 \mu_{I_v})^2 N_h^2 \phi_h (\rho_{R_h} + \mu_h) \left[\mathcal{R}_0^2 - 1 \right],$$

where

$$M_1 = \theta_2 \mu_{I_v} \epsilon \kappa (\rho_{R_h} + \mu_h), \quad M_2 = \phi_h \theta_2 \mu_{I_v} \beta_2 \quad \text{and} \quad \mathcal{R}_{0v} = \frac{\rho_{E_v} \beta_2 \epsilon \kappa \theta_1}{\theta_2 \mu_{I_v} (\rho_{E_v} + \mu_{E_v})}.$$

Hence, the model has:

Theorem 6.4.5.

1. A unique endemic equilibrium if $G_3 < 0$, it implies that $\mathcal{R}_0 < 1$.
2. A unique endemic equilibrium if $G_2 < 0$ and $G_3 = 0$ or $G_2 - 4G_1G_3 > 0$.
3. Two endemic equilibria if $G_3 > 0$, $G_2 < 0$ and
4. No endemic otherwise.

6.4.6 Local stability of the endemic equilibrium

The stability of the endemic equilibrium of the model (6.1) is analysed using the Centre Manifold Theory described by Castillo-Chavez and Song, 2004 [27].

Theorem 6.4.6. *Castillo-Chavez and Song [141]*

Consider the following general system of ordinary differential equations with a parameter Ψ .

$$\frac{dx}{dt} = h(x, \Psi), \quad h : \mathbb{R}^n \times \mathbb{R} \rightarrow \mathbb{R} \quad \text{and} \quad h \in \mathcal{C}^2(\mathbb{R}^n \times \mathbb{R}) \quad (6.20)$$

where 0 is an equilibrium point of the system, that is, $h(0, \Psi) \equiv 0$ for all Ψ and

1. $A = D_x h(0, 0) = \left(\frac{\partial h_i}{\partial x_i}(0, 0) \right)$ is the linearization matrix of the system around the equilibrium 0 with Ψ evaluated at 0 .
2. Zero is a simple eigenvalue of A and other eigenvalues of A have negative real parts.
3. Matrix A has a nonnegative right eigenvector w and a left eigenvector v corresponding to the zero eigenvalue.

Let h_k be the k th component of h and

$$a = \sum_{k,i,j=1}^n v_k w_i w_j \frac{\partial^2 h_k}{\partial x_i \partial x_j}(0, 0)$$

and

$$b = \sum_{k,i=1}^n v_k w_i \frac{\partial^2 h_k}{\partial x_i \partial \Psi}(0, 0)$$

then the local dynamics of the system (6.20) around 0 is totally determined by the sign of a and b .

1. $a > 0$, $b > 0$. When $\Psi < 0$ with $|\Psi| \ll 1$, 0 is locally asymptotically stable and there exists a positive unstable equilibrium; when $0 < \Psi \ll 1$, 0 is unstable and there exists a negative, locally asymptotically stable equilibrium.
2. $a < 0$, $b < 0$. When $\Psi < 0$ with $|\Psi| \ll 1$, 0 is unstable; when $0 < \Psi \ll 1$, 0 is locally asymptotically stable, and there exists a positive unstable equilibrium.
3. $a > 0$, $b < 0$. When $\Psi < 0$ with $|\Psi| \ll 1$, 0 is unstable, and there exists a locally asymptotically stable negative equilibrium; when $0 < \Psi \ll 1$, 0 is stable, and a positive unstable equilibrium appears.

4. $a < 0$, $b > 0$, when Ψ changes from negative to positive, 0 changes its stability from stable to unstable. Correspondingly a negative unstable equilibrium becomes positive and locally asymptotically stable.

To apply this theorem we make the following changes of variables in the system (6.1).

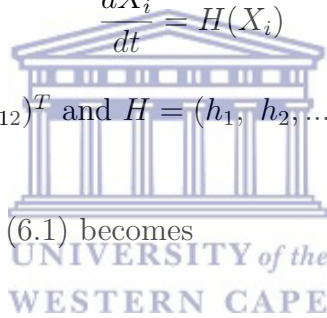
Let $x_1 = S_h$, $x_2 = E_h$, $x_3 = I_h$, $x_4 = R_h$, $x_5 = E$, $x_6 = L$, $x_7 = P$, $x_8 = A_h$, $x_9 = A_r$, $x_{10} = A_o$, $x_{11} = E_v$, $x_{12} = I_v$

The system (6.1) is written in vector form as

$$\frac{dX_i}{dt} = H(X_i)$$

where $X_i = (x_1, x_2, \dots, x_{12})^T$ and $H = (h_1, h_2, \dots, h_{12})^T$ are transposed matrices.

The system of equations (6.1) becomes



$$\begin{aligned}
\frac{dx_1}{dt} &= \phi_h + \rho_{R_h} x_4 - \left(\frac{\Psi^* \epsilon \kappa \mu_h x_{12}}{\phi_h} + \mu_h \right) x_1 = h_1 \\
\frac{dx_2}{dt} &= \frac{\Psi^* \epsilon \kappa \mu_h x_{12}}{\phi_h} x_1 - (\rho_{E_h} + \mu_h) x_2 = h_2 \\
\frac{dx_3}{dt} &= \rho_{E_h} x_2 - (\rho_{I_h} + \mu_h + \alpha) x_3 = h_3 \\
\frac{dx_4}{dt} &= \rho_{I_h} x_3 - (\rho_{R_h} + \mu_h) x_4 = h_4 \\
\frac{dx_5}{dt} &= n(\rho_{A_o} x_{10} + \rho_{I_v} x_{12}) - (\rho_e + \mu_e) x_5 = h_5 \\
\frac{dx_6}{dt} &= \rho_e x_5 - (\rho_L + \mu_L (1 + x_6/K)) x_6 = h_6 \\
\frac{dx_7}{dt} &= \rho_L x_6 - (\rho_P + \mu_P) x_7 = h_7 \\
\frac{dx_8}{dt} &= \rho_P x_7 + \rho_{A_o} x_{10} - \left(\frac{\beta_2 \epsilon \kappa \mu_h x_3}{\phi_h} + D_v + \mu_{A_h} + \mu_r \right) x_8 = h_8 \\
\frac{dx_9}{dt} &= D_v x_8 - (\rho_{A_r} + \mu_{A_r}) x_9 = h_9 \\
\frac{dx_{10}}{dt} &= \rho_{A_r} x_9 - (\rho_{A_o} + \mu_{A_o} + \mu_r) x_{10} = h_{10} \\
\frac{dx_{11}}{dt} &= \frac{\beta_2 \epsilon \kappa \mu_h x_3}{\phi_h} x_8 - (\rho_{E_v} + \mu_{E_v}) x_{11} = h_{11} \\
\frac{dx_{12}}{dt} &= \rho_{E_v} x_{11} - \mu_{I_v} x_{12} = h_{12}
\end{aligned} \tag{6.21}$$

where $N_h = x_1 + x_2 + x_3 + x_4$ and $N_v = x_5 + x_6 + x_7 + x_8 + x_9 + x_{10} + x_{11} + x_{12}$ with $\Psi^* = \beta_1$.

Let Ψ^* be the bifurcation parameter, the system (6.21) is linearized at disease free equilibrium point when $\Psi = \Psi^*$ with $\mathcal{R}_0 = 1$. Thus Ψ^* can be solved from (6.10) when $\mathcal{R}_0 = 1$ as

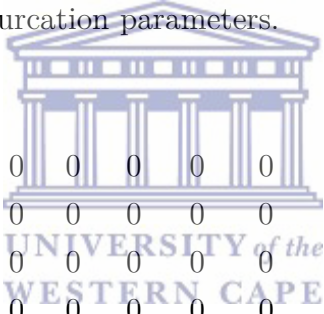
such that

$$\mathcal{R}_0 = \sqrt{\frac{\rho_{E_h} \rho_{E_v} \beta_1 \beta_2 (\epsilon \kappa)^2 \mu_h \theta_1}{\phi_h \theta_2 \mu_{I_v} (\rho_{E_h} + \mu_h) (\rho_{I_h} + \mu_h + \alpha) (\rho_{E_v} + \mu_{E_v})}}$$

$$1^2 = \frac{\Psi^* \rho_{E_h} \rho_{E_v} \beta_1 \beta_2 (\epsilon \kappa)^2 \mu_h \theta_1}{\phi_h \theta_2 \mu_{I_v} (\rho_{E_h} + \mu_h) (\rho_{I_h} + \mu_h + \alpha) (\rho_{E_v} + \mu_{E_v})}$$

$$\Psi^* = \frac{\phi_h \theta_2 \mu_{I_v} (\rho_{E_h} + \mu_h) (\rho_{I_h} + \mu_h + \alpha) (\rho_{E_v} + \mu_{E_v})}{\rho_{E_h} \rho_{E_v} \beta_1 \beta_2 (\epsilon \kappa)^2 \mu_h \theta_1} \quad (6.22)$$

Then zero is a simple eigenvalue of the following Jacobian matrix, J_{bif} with the application of the bifurcation parameters.



$$\begin{bmatrix} z_1 & 0 & 0 & \rho_{R_h} & 0 & 0 & 0 & 0 & 0 & 0 & 0 & -\Psi \epsilon \kappa \\ 0 & z_2 & 0 & 0 & 0 & 0 & 0 & 0 & 0 & 0 & 0 & \Psi \epsilon \kappa \\ 0 & \rho_{E_h} & z_3 & 0 & 0 & 0 & 0 & 0 & 0 & 0 & 0 & 0 \\ 0 & 0 & \rho_{I_h} & z_4 & 0 & 0 & 0 & 0 & 0 & 0 & 0 & 0 \\ 0 & 0 & 0 & 0 & z_5 & 0 & 0 & 0 & 0 & n \rho_{A_o} & 0 & n \rho_{I_v} \\ 0 & 0 & 0 & 0 & \rho_e & z_6 & 0 & 0 & 0 & 0 & 0 & 0 \\ 0 & 0 & 0 & 0 & 0 & \rho_L & z_7 & 0 & 0 & 0 & 0 & 0 \\ 0 & 0 & z_{13} & 0 & 0 & 0 & \rho_P & z_8 & 0 & \rho_{A_o} & 0 & 0 \\ 0 & 0 & 0 & 0 & 0 & 0 & 0 & D_v & z_9 & 0 & 0 & 0 \\ 0 & 0 & 0 & 0 & 0 & 0 & 0 & 0 & \rho_{A_r} & z_{10} & 0 & 0 \\ 0 & 0 & 0 & 0 & 0 & 0 & 0 & z_{14} & 0 & 0 & z_{11} & 0 \\ 0 & 0 & 0 & 0 & 0 & 0 & 0 & 0 & 0 & 0 & \rho_{E_v} & z_{12} \end{bmatrix} \quad (6.23)$$

where,

$$z_1 = -\mu_h, \quad z_2 = -(\rho_{E_h} + \mu_h), \quad z_3 = -(\rho_{I_h} + \mu_h + \alpha), \quad z_4 = -(\rho_{R_h} + \mu_h), \quad z_5 = -(\rho_e + \mu_e),$$

$$z_6 = -(\rho_L + \mu_{L_1} + \mu_{L_2}), \quad z_7 = -(\rho_P + \mu_P), \quad z_8 = -(D_v + \mu_{A_h} + \mu_r), \quad z_9 = -(\rho_{A_r} + \mu_{A_r}),$$

$$z_{10} = -(\rho_{A_o} + \mu_{A_o} + \mu_r), \quad z_{11} = -(\rho_{E_v} + \mu_{E_v}), \quad z_{12} = -\mu_{I_v}, \quad z_{13} = -\frac{\beta_2 \epsilon \kappa \mu_h \theta_1}{\phi_h \theta_2} \text{ and}$$

$$z_{14} = \frac{\beta_2 \epsilon \kappa \mu_h \theta_1}{\phi_h \theta_2}.$$

A right eigenvector associated with the eigenvalue zero is $w = (w_1, w_2, w_3, \dots, w_{12})$.

We get

$$\begin{aligned} -\mu_h w_1 + \rho_{R_h} w_4 - \Psi \epsilon \kappa w_{12} &= 0 \\ -(\rho_{E_h} + \mu_h) w_2 + \Psi \epsilon \kappa w_{12} &= 0 \\ \rho_{E_h} w_2 - (\rho_{I_h} + \mu_h + \alpha) w_3 &= 0 \\ \rho_{I_h} w_3 - (\rho_{R_h} + \mu_h) w_4 &= 0 \\ -(\rho_e + \mu_e) w_5 + n \rho_{A_o} w_{10} + n \rho_{I_v} w_{12} &= 0 \\ \rho_e w_5 - (\rho_L + \mu_{L_1} + \mu_{L_2}) w_6 &= 0 \\ \rho_L w_6 - (\rho_P + \mu_P) w_7 &= 0 \\ -\frac{\beta_2 \epsilon \kappa \mu_h \theta_1}{\phi_h \theta_2} w_3 + \rho_P w_7 - (D_v + \mu_{A_h} + \mu_r) w_8 + \rho_{A_o} w_{10} &= 0 \\ D_v w_8 - (\rho_{A_r} + \mu_{A_r}) w_9 &= 0 \\ \rho_{A_r} w_9 - (\rho_{A_o} + \mu_{A_o} + \mu_r) w_{10} &= 0 \\ \frac{\beta_2 \epsilon \kappa \mu_h \theta_1}{\phi_h \theta_2} w_8 - (\rho_{E_v} + \mu_{E_v}) w_{11} &= 0 \\ \rho_{E_v} w_{11} - \mu_{I_v} w_{12} &= 0 \end{aligned} \tag{6.24}$$

we have the following system

$$\begin{aligned}
-\mu_h v_1 &= 0 \\
-(\rho_{E_h} + \mu_h)v_2 + \rho_{E_h} v_3 &= 0 \\
-(\rho_{I_h} + \mu_h + \alpha)v_3 + \rho_{I_h} v_4 - \frac{\beta_2 \epsilon \kappa \mu_h \theta_1}{\phi_h \theta_2} v_8 &= 0 \\
\rho_{R_h} v_1 - (\rho_{R_h} + \mu_h)v_4 &= 0 \\
-(\rho_e + \mu_e)v_5 + \rho_e v_6 &= 0 \\
-(\rho_L + \mu_{L_1} + \mu_{L_2})v_6 + \rho_L v_7 &= 0 \\
-(\rho_P + \mu_P)v_7 + \rho_P v_8 &= 0 \\
-(D_v + \mu_{A_h} + \mu_r)v_8 + D_v v_9 + \frac{\beta_2 \epsilon \kappa \mu_h \theta_1}{\phi_h \theta_2} v_{11} &= 0 \\
-(\rho_{A_r} + \mu_{A_r})v_9 + \rho_{A_o} v_{10} &= 0 \\
n\rho_{A_o} v_5 + \rho_{A_o} v_8 - (\rho_{A_o} + \mu_{A_o} + \mu_r)v_{10} &= 0 \\
-(\rho_{E_v} + \mu_{E_v})v_{11} + \rho_{E_v} v_{12} &= 0 \\
-\epsilon \kappa \Psi v_1 + \epsilon \kappa \Psi v_2 + n\rho_{A_o} v_5 - \mu_{I_v} v_{12} &= 0
\end{aligned} \tag{6.26}$$

From the left eigenvector we have the following results

$$v_1 = 0, \quad v_2 = v_2 > 0, \quad v_3 = \frac{\beta_2 \epsilon \kappa \mu_h \theta_1 v_8 - \phi_h v_4 \theta_2 \rho_{I_h}}{\phi_h \theta_2 (\rho_{I_h} + \mu_h + \alpha)}, \quad v_4 = \frac{\rho_{R_h} v_1}{(\rho_{R_h} + \mu_h)} = 0,$$

$$v_5 = \frac{\rho_e v_6}{(\rho_e + \mu_e)}, v_6 = \frac{\rho_L v_7}{(\rho_L + \mu_{L_1} + \mu_{L_2})}, v_7 = \frac{\rho_P v_8}{(\rho_P + \mu_P)}, v_8 = \frac{D_v \phi_h \theta_2 v_9 + \beta_2 \epsilon \kappa \mu_h \theta_1 v_{11}}{\phi_h \theta_2 (D_v + \mu_{A_h} + \mu_r)},$$

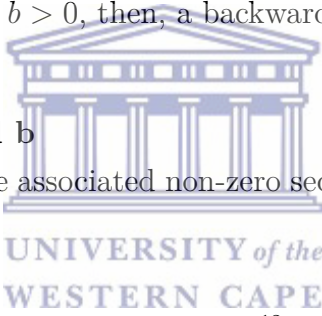
$$v_9 = \frac{\rho_{A_o} v_{10}}{(\rho_{A_r} + \mu_{A_r})}, v_{10} = \frac{n \rho_{A_o} v_5 + \rho_{A_o} v_8}{(\rho_{A_o} + \mu_{A_o} + \mu_r)}, v_{11} = \frac{\rho_{E_v} v_{12}}{(\rho_{E_v} + \mu_{E_v})},$$

$$v_{12} = -\frac{\epsilon \kappa \Psi v_1 + \epsilon \kappa \Psi v_2 + n \rho_{A_o} v_5}{\mu_{I_v}} = \frac{\epsilon \kappa \Psi v_2 + n \rho_{A_o} v_5}{\mu_{I_v}}.$$

Particularly, if $a > 0$ and $b > 0$, then, a backward bifurcation occurs at $\Psi = 0$

Computation of a and b

For the system (6.21), the associated non-zero second order partial derivatives (at DFE) are given by



$$a = \sum_{k,i,j=2}^3 v_k w_i w_j \frac{\partial^2 h_k}{\partial x_i \partial x_j}(0,0) + \sum_{k,i,j=5}^{12} v_k w_i w_j \frac{\partial^2 h_k}{\partial x_i \partial x_j}(0,0)$$

$$b = \sum_{k,i=2}^3 v_k w_i \frac{\partial^2 h_k}{\partial x_i \partial \Psi}(0,0) + \sum_{k,i=5}^{12} v_k w_i \frac{\partial^2 h_k}{\partial x_i \partial \Psi}(0,0).$$

Since $v_1 = v_4 = 0$ for $k = 1, 4$; then $k = 2, 3, 5, 6, 7, 8, 9, 10, 11, 12$ should be considered. It implies that the following functions will be used to compute a and b from the system (6.21).

$$h_2 = \frac{\Psi \epsilon \kappa \mu_h x_{12} x_1}{\phi_h} - (\rho_{E_h} + \mu_h) x_2 = \frac{\Psi \epsilon \kappa \mu_h x_{12}}{\phi_h} (N_h - x_2 - x_3) - (\rho_{E_h} + \mu_h) x_2$$

$$\begin{aligned}
&= \frac{\Psi\epsilon\kappa\mu_h x_{12} N_h}{\phi_h} - \frac{\Psi\epsilon\kappa\mu_h x_{12} x_2}{\phi_h} - \frac{\Psi\epsilon\kappa\mu_h x_{12} x_3}{\phi_h} - (\rho_{E_h} + \mu_h) x_2 \\
h_{11} &= \frac{\beta_2\epsilon\kappa\mu_h x_3 N_v^s}{\phi_h} - (\rho_{E_v} + \mu_{E_v}) x_{11} = \frac{\beta_2\epsilon\kappa\mu_h x_3}{\phi_h} (N_v - x_{11} - x_{12}) - (\rho_{E_v} + \mu_{E_v}) x_{11} \\
&= \frac{\beta_2\epsilon\kappa\mu_h x_3 N_v}{\phi_h} - \frac{\beta_2\epsilon\kappa\mu_h x_3 x_{11}}{\phi_h} - \frac{\beta_2\epsilon\kappa\mu_h x_3 x_{12}}{\phi_h} - (\rho_{E_v} + \mu_{E_v}) x_{11}
\end{aligned}$$

we let N_v^s represents uninfected mosquito population, such that $N_v^s = x_5 + x_6 + x_7 + x_8 + x_9 + x_{11}$. Hence the partial derivatives that are not zero at the disease-free equilibrium are

$$\frac{\partial^2 h_2}{\partial x_2 \partial x_{12}} = -\frac{\epsilon\kappa\mu_h}{\phi_h}, \quad \frac{\partial^2 h_2}{\partial x_3 \partial x_{12}} = -\frac{\epsilon\kappa\mu_h}{\phi_h}, \quad \frac{\partial^2 h_2}{\partial x_3 \partial x_{11}} = -\frac{\beta_2\epsilon\kappa\mu_h}{\phi_h}, \quad \frac{\partial^2 h_2}{\partial x_3 \partial x_{12}} = -\frac{\beta_2\epsilon\kappa\mu_h}{\phi_h}.$$

Hence

$$\begin{aligned}
a &= v_2 w_2 w_{12} \frac{\partial^2 h_2}{\partial x_2 \partial x_{12}} + v_2 w_3 w_{12} \frac{\partial^2 h_2}{\partial x_3 \partial x_{12}} + v_{11} w_3 w_{11} \frac{\partial^2 h_2}{\partial x_3 \partial x_{11}} + v_{11} w_3 w_{12} \frac{\partial^2 h_2}{\partial x_3 \partial x_{12}} \\
&= -\frac{\epsilon\kappa\mu_h}{\phi_h} [v_2 w_{12} \Psi(w_2 + w_3) + v_6 w_3 \beta_2 (w_{11} + w_{12})]
\end{aligned}$$

$$a = -\frac{\epsilon\kappa\mu_h}{\phi_h} \left[v_2 w_{12}^2 \Psi_{12}^2 \epsilon\kappa \left(\frac{\rho_{I_h} + \mu_h + \alpha \rho_{E_h}}{(\rho_{E_h} + \mu_h)(\rho_{I_h} + \mu_h + \alpha)} \right) + \right.$$

$$\left. v_6 w_3 \beta_2 \left(1 + \frac{\mu_h \rho_{E_h} \rho_{R_h} \Psi \beta_2 (\epsilon\kappa)^2}{\phi_h \theta_2 \mu_{I_v} (\rho_{E_v} + \theta_2 \mu_{I_v}) (\rho_{I_h} + \mu_h \alpha) (\rho_{E_h} + \mu_h)} \right) \right] < 0. \quad (6.27)$$

Similarly, the partial derivatives that are not zero for b are

$$\frac{\partial h_2}{\partial \Psi} = \frac{\epsilon \kappa \mu_h x_{12} x_1}{\phi_h}, \quad \frac{\partial^2 h_2}{\partial x_{12} \partial \Psi} = \frac{\epsilon \kappa \mu_h x_1}{\phi_h} = \epsilon \kappa$$

Therefore,

$$b = v_2 w_{12} \frac{\partial^2 h_2}{\partial x_{12} \partial \Psi} = v_2 w_{12} \epsilon \kappa > 0. \tag{6.28}$$

Hence $a < 0$ and $b > 0$. Therefore the following holds.

Theorem 6.4.7. *The malaria model has a unique endemic equilibrium which is locally asymptotically stable when $\mathcal{R}_0 < 1$ and unstable when $\mathcal{R}_0 > 1$.*

Our analyses reveal the existence of the phenomenon of backward bifurcation (See Fig. 6.2). This implies that the stable disease-free equilibrium of the model co-exists with a stable endemic equilibrium when the reproduction number of the disease is less than unity. The epidemiological consequence of backward bifurcation is that the typical requirement of having the reproduction number less than unity, while necessary, is no longer sufficient for malaria elimination from the population [15].

6.5 Sensitivity analysis of model parameters

We carried out the sensitivity analysis to determine the model robustness to parameter values, also to know the parameters that have a high impact on the disease transmission. The analysis also determines the effects of parameters on model outcomes [26]. To carry out local sensitivity analysis, we use a simple approach to compute the sensitivity index, which is a partial derivative of the output variable with respect to the input parameters [26, 35].

Definition.

The normalized forward sensitivity index of a variable, d_1 , that depends on a

differentiable parameter, d_2 , is defined as:

$$\Upsilon_{d_2}^{d_1} := \frac{\partial d_1}{\partial d_2} \times \frac{d_2}{d_1}.$$

Sensitivity analysis of reproduction number

Hence, we derive the sensitivity of \mathcal{R}_0 to each of the parameters described in Table 6.1. The sensitivity index of \mathcal{R}_0 with respect to ρ_{E_v} , for example is,

$$\Upsilon_{\rho_{E_v}}^{\mathcal{R}_0} := \frac{\partial \mathcal{R}_0}{\partial \rho_{E_v}} \times \frac{\rho_{E_v}}{\mathcal{R}_0} := \frac{-\mathcal{R}_0}{2(\mu_{E_v} + \rho_{E_v})} = -0.5$$

The detail sensitivity indices of \mathcal{R}_0 resulting from the evaluation to some other parameters of the model are shown in Fig. 6.3. Since $\Upsilon_{\rho_{E_v}}^{\mathcal{R}_0} = -0.5$, increasing (or decreasing) the biting rate ϵ by 10%, increases (or decreases) the \mathcal{R}_0 by 5%. In the same way, increasing (or decreasing) the mosquito biting rate rate, ϵ by 10%, increases (or decreases) the \mathcal{R}_0 by 10%. This suggests that strategies that can be applied in combating malaria are to focus on the mosquito biting rate and death rate.

6.6 Results and discussion

Numerical analysis without climate variables

Ignoring climatic influence on our model, we carry out numerical simulations using a fourth order Runge-Kutta scheme in Matlab to verify some of the analytical results on the stability of the system (6.1). We also aim to illustrate the dynamics of each epidemiological class of our model with time using the constant parameter values presented in Table 6.1 with the following initial conditions; $S_h = 2000, E_h = 15000, I_h = 1000, R_h = 300, E = 10000, L = 700, P = 500, A_h = 100, A_r = 80, A_o = 60, E_v = 40, I_v = 30$. we examine the time series plot of both mosquito and human population with constant parameter values as shown in Fig. 6.4 and Fig. 6.5 respectively. With low

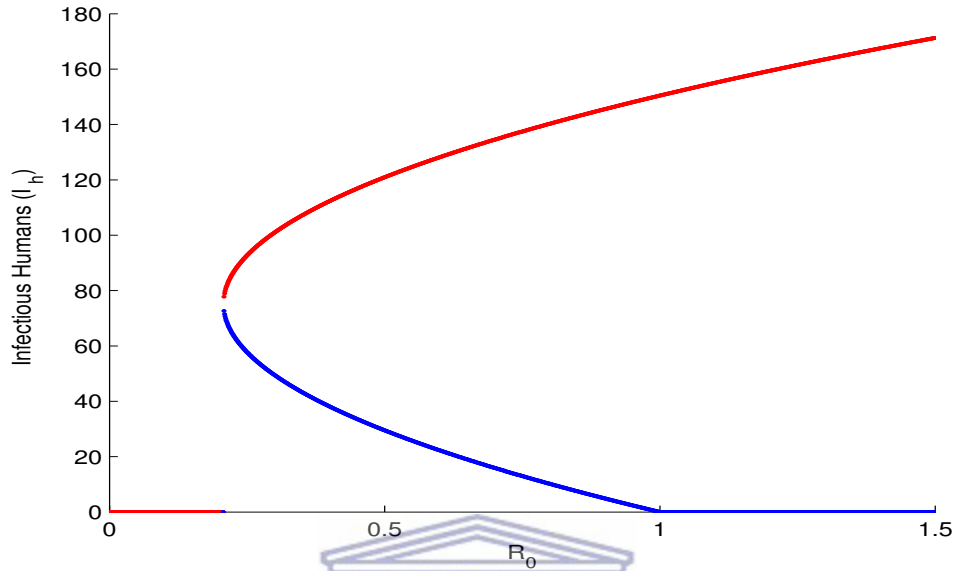


Figure 6.2: Bifurcation diagram for model 6.1 showing the endemic equilibrium values for the proportion of infectious, using parameters in Table 6.1

biting rate (ϵ), we observe in Fig. 6.4(a - c) that each population tends to zero with time and $\mathcal{R}_0 = 0.3$. This is evidence to Theorem 6.4.3, that at disease-free equilibrium, the system converges and is globally stable whenever $\mathcal{R}_0 < 1$, which implies that the population is eradicated. On the other hand, in Fig. 6.5(a - c), the disease-free equilibrium of the system becomes unstable as $\mathcal{R}_0 > 1$. To achieve this, we increase the mosquito biting rate (ϵ) from 0.2 to 0.5. This increment gives rise to the previous value of \mathcal{R}_0 from 0.3 to 1.1, thus makes disease-persistence equilibrium to be stable as stated in Theorem 6.4.3.

6.7 Conclusion

We developed a compartmental model for malaria transmission involving the human host and mosquito populations. The mosquito population was divided

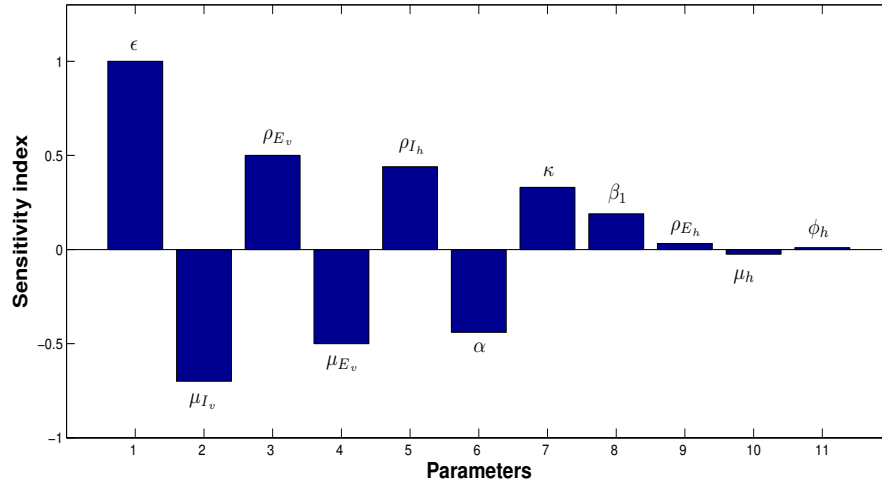


Figure 6.3: Sensitivity index of \mathcal{R}_0 to parameters evaluated at the baseline parameter values given in Table 6.1

into six classes: egg, larva, pupa, susceptible adult searching for host, resting adult and adult searching for breeding site. We established that the model is epidemiologically feasible and well-posed and we also showed the existence of the disease-free equilibrium.

Furthermore, we employed the next generation matrix technique to derive the reproduction number \mathcal{R}_0 . We proved that the model has two equilibrium points; the disease-free equilibrium which is locally asymptotically stable whenever $\mathcal{R}_0 < 1$, unstable otherwise giving rise to the existence of the endemic equilibrium for $\mathcal{R}_0 > 1$.

We found that the system exhibits backward bifurcation, meaning that the stability of the disease-free equilibrium of the model co-existed with a stable endemic equilibrium even when $\mathcal{R}_0 < 1$.

We performed the sensitivity analysis on the reproductive number, \mathcal{R}_0 . Our analyses revealed that mosquito biting rate is highly sensitive over the reproduction number. This implies that biting rate plays a crucial part in transmitting malaria. Since *Anopheles* need blood-meals to complete their gonotrophic and sporogonic cycle, activities (such as bed netting, use of insecticides) to

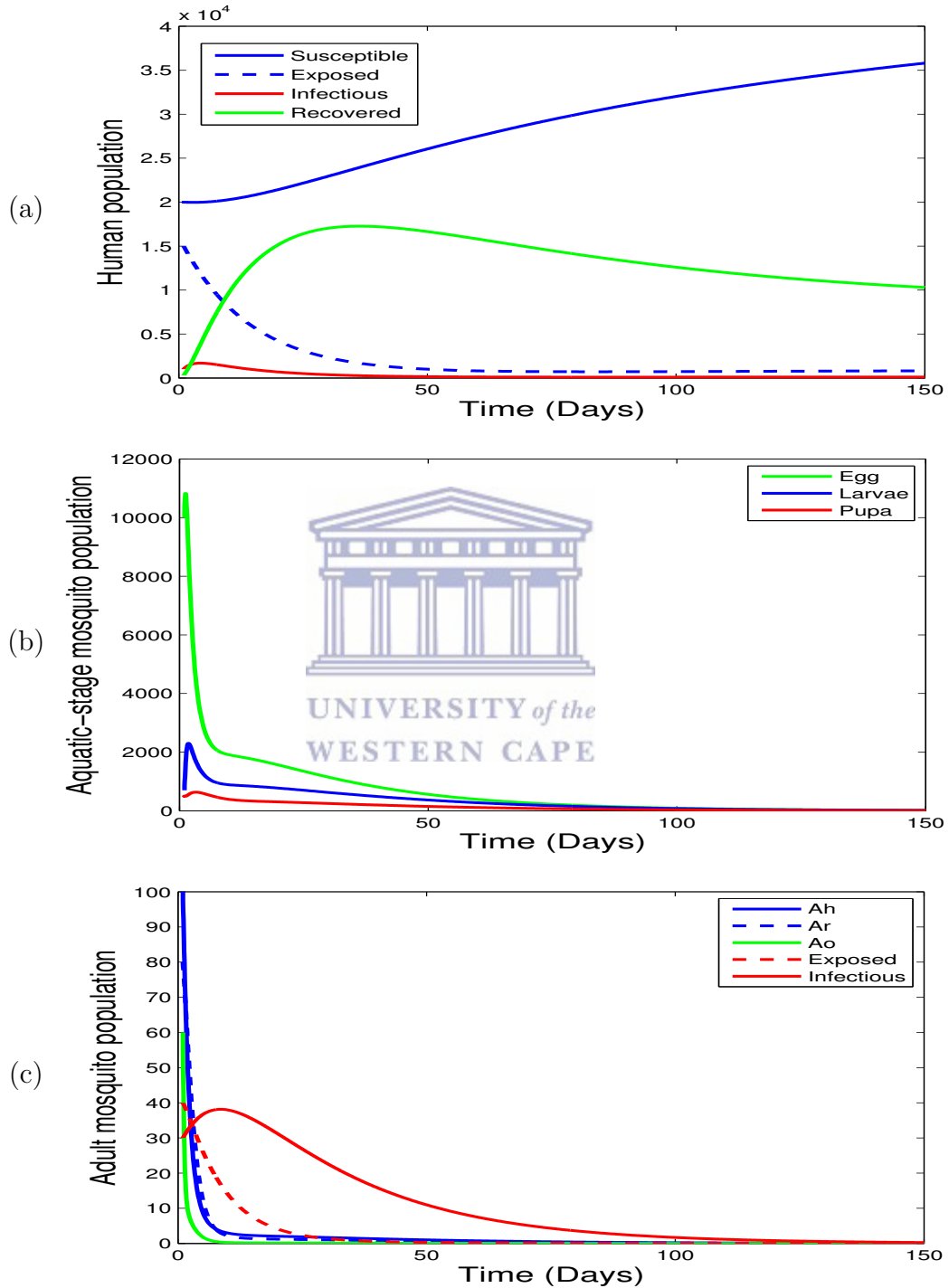


Figure 6.4: Simulations of human and mosquito population with low biting rate, $\epsilon = 0.2$, $\mathcal{R}_0 = 0.3$

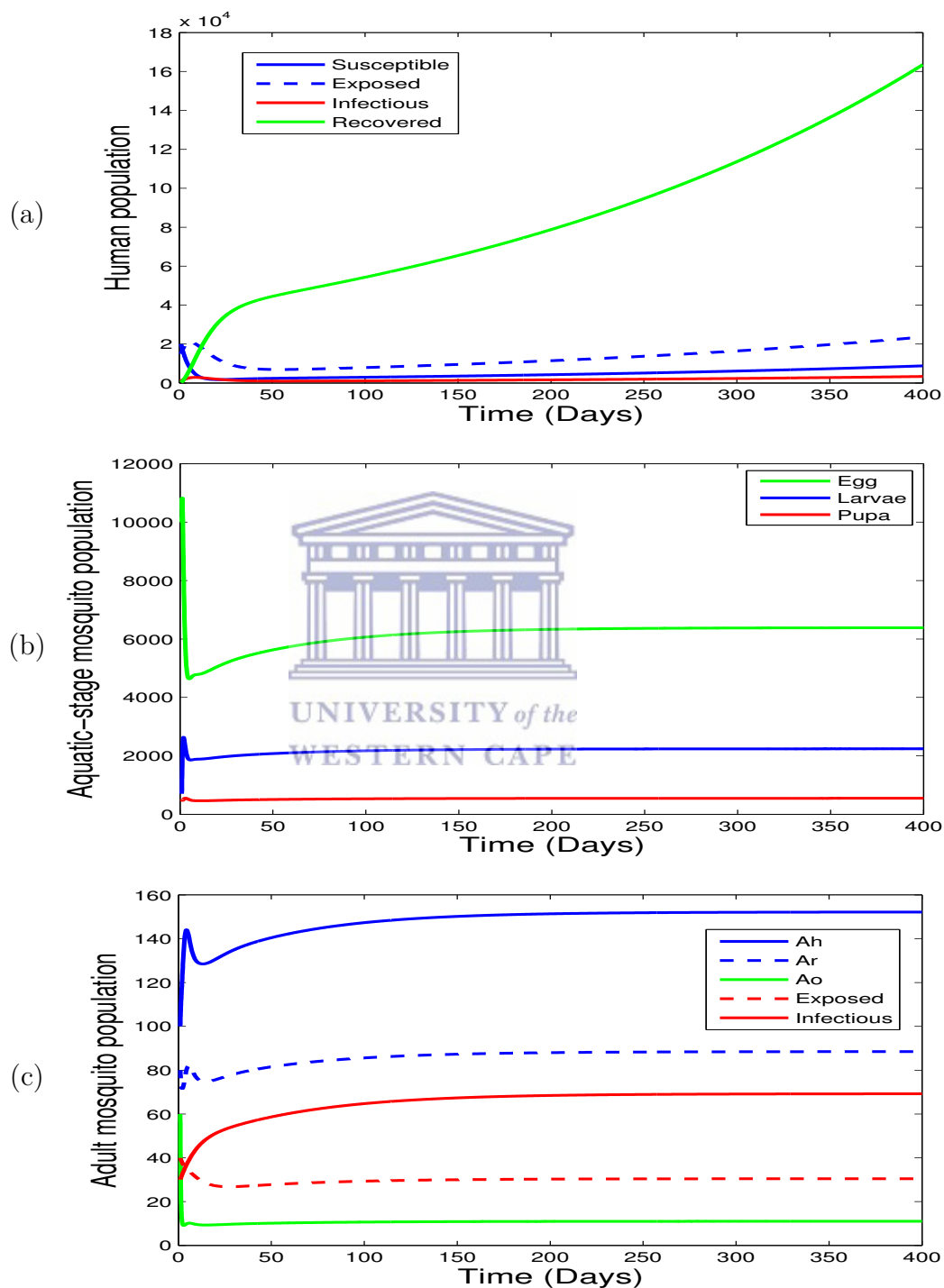


Figure 6.5: Simulations of human and mosquito population with high biting rate, $\epsilon = 0.5$, $\mathcal{R}_0 = 1.1$

Table 6.1: Parameters of the malaria model 6.1

Description	Parameter	Value	Source
Number of eggs laid per oviposition	n	100	[103, 104, 172]
Egg hatching rate into larvae	ρ_E	0.5 day ⁻¹	[42, 103, 104, 172]
Development rate of L to P	ρ_L	0.14 day ⁻¹	[103, 104, 172]
Development rate of pupae to adult	ρ_P	0.5 day ⁻¹	[103, 104, 172]
Egg mortality rate	μ_E	0.56 day ⁻¹	[103, 104, 140]
Density-independent larvae mortality rate	μ_L	0.44 day ⁻¹	[103, 104, 140]
Pupa mortality rate	μ_P	0.37 day ⁻¹	[103, 104, 140]
Rate at which A_h move to A_r	ρ_{Ah}	0.46 day ⁻¹	[35, 103, 104]
Rate at which A_r move to A_o	ρ_{Ar}	0.43 day ⁻¹	[35, 103, 104]
Oviposition rate	ρ_{Ao}	3.0 day ⁻¹	[35, 103, 104]
Mortality rate of A_h	μ_{Ah}	0.18 day ⁻¹	[35, 103, 104]
Mortality rate of A_r	μ_{Ar}	0.0043 day ⁻¹	[35, 103, 104]
Mortality rate of A_o	μ_{Ao}	0.41 day ⁻¹	[35, 103, 104]
Carrying capacity	K	100000	Assumed
Probability of human getting infected	β_1	0.533	Assumed
Probability of mosquito getting infected	β_2	0.09	[14, 106, 142]
Natural death rate in human	μ_h	0.00004 day ⁻¹	[34, 142]
Natural death rate in mosquitoes	μ_r	0.1429 day ⁻¹	[14, 106, 142]
Human recruitment rate	ϕ_h	100 day ⁻¹	[14, 106, 142]
Contact rate of mosquito per human	κ	0.6 day ⁻¹	[34, 142]
Mosquito biting rate	ϵ	0.2	[14, 106, 142]
Disease induced death rate	α	0.05 day ⁻¹	[106, 142]
Progression from E_h to I_h	ρ_{E_h}	1/17day ⁻¹	[14, 106, 142]
Progression from E_v to I_v	ρ_{E_v}	1/18day ⁻¹	[14, 106, 142]
Recovered individuals' loss of immunity	ρ_{R_h}	1/730	[14, 106, 142]

prevent biting rate should be constantly practiced in a malaria-epidemic region. We implemented and carried out the numerical simulations to confirm the theoretical analysis and explored more patterns of dynamical behaviors of our model.

Chapter 7

Exploring the impact of climate variability on malaria transmission using a dynamic mosquito-human malaria model



Submitted for publication.

Authors: G.J. Abiodun, P. Witbooi, K.O. Okosun, R. Maharaj

Here in this chapter, we incorporate climate parameters into the model in Chapter 6. We use the model outputs to investigate the impact of climate variability on malaria transmission over KwaZulu-Natal province using some statistical analyses.

7.1 Abstract

The reasons for malaria resurgence mostly in Africa are yet to be well understood. Although the causes are often linked to regional climate change, it is important to understand the impact of climate variability on the dynamics of the disease. However, this is difficult due to the unavailability of long-term malaria data over the study areas. In this study, we develop a climate-based mosquito-human malaria model to study malaria dynamics in the human population over KwaZulu-Natal, one of the epidemic provinces in South Africa, from 1970-2005. We compare the model output with available observed monthly malaria cases over the province from 2002-2004. We further use the model outputs to explore the relationship between the climate variables (rainfall and temperature) and malaria incidence over the province using Principal Component Analysis (PCA), Wavelet Power Spectrum (WPS) and Wavelet Coherence Analysis (WCA). The model produces a reasonable fit with the observed data and in particular, it captures all the spikes in malaria prevalence. Our results highlight the importance of climate factors on malaria transmission and show the seasonality of malaria epidemics over the province. Results from the PCA on the model outputs suggest that there are two major processes in the model simulation. One of the processes indicate high loadings on Susceptible, Exposed and Infected humans, while the other is more correlated with Susceptible and Recovered humans. However, both factors reveal an inverse correlation between Susceptible-Infected and Susceptible-Recovered humans respectively. Through the spectrum analysis, we notice a strong annual cycle of malaria incidence over the province and ascertain a dominant periodicity of one year. Consequently, our findings indicate that an average of 0 to 120-day lag is generally noted over the study period, but the 120-day lag is more associated with temperature than rainfall. This is consistent with other results obtained from our analyses that malaria transmission is more tightly coupled with temperature than with rainfall in KwaZulu-Natal province.

7.2 Introduction

Malaria continues to be a serious concern as it causes almost one million deaths globally every year [208]. It is also estimated that approximately half of the world's population is at risk of contracting malaria [208]. The disease is closely associated with Africa, which is classified as a region carrying the largest share of the global malaria burden [208]. For instance, in 2015, 90% of recorded malaria cases led to death in Africa [208]. Malaria is sensitive to atmospheric conditions and the occurrence is strongly influenced by climate variability [55]. For this reason, the recent concerns about global warming have triggered several studies on the impact of climate variability and climate change on inter-annual patterns of the disease [29, 118, 120, 154].

Previous studies have examined year-to-year variation of seasonal epidemics over the African highlands [152]. For example, using the time-series modelling approach, Zhou *et al* [212] recently ascertained that rainfall and temperature play a significant role in the interannual variability of malaria across multiple East African highlands. Their results in contrast to Hay *et al* [75] suggested that malaria epidemics in the highlands are initiated by climate variability. More recently, Pascual *et al* [152] combined both a time-series epidemiological model and a statistical approach to analyse monthly cases of malaria from 1970 to 2003 over a highland in Western Kenya. The findings from their study revealed the existence of multiyear cycles of malaria incidence over the study period. Their findings also demonstrated the impact of rainfall over malaria resurgence in 1990. It is concluded in line with the study of Zhou *et al* [212] that climate variables play significant roles at different temporal scales and should be considered when building predictive malaria models.

However, assessing the impact of climate variability on malaria transmission over a region is difficult without long-term data series of malaria cases of the region [212]. For this reason, several studies have considered using dynamical malaria models to generate reported cases of epidemic regions over a long period. For instance, in the study of Laneri *et al* [95], dynamical mod-

els are used to understudy the impact of immunity and climate variability on malaria transmission in Senegal over two decades. Their results highlighted the possibility of forecasting malaria from climate in endemic regions but only after accounting for the interaction between climate and immunity. Following the same trend, Roy *et al* [167] examined the impact of climate variability and the predictability of epidemic malaria over different districts in India using dynamical models. It is established in their study that process-based models and climate variables, are informative and useful under non-stationary conditions. More recently, in the study of Abiodun *et al* [2], a climate-based mosquito model was presented to examine the impact of climate variables on mosquito population dynamics over Dondotha village, KwaZulu-Natal province in South Africa. The model demonstrates and quantifies the influence of temperature and rainfall on the abundance of *Anopheles arabiensis* over time and presents a strong seasonal variability over the region.

The current study aims to further develop the mosquito model presented in [2] to investigate the impact of climate variability on malaria transmission over KwaZulu-Natal province during the period 1970-2005. The newly developed mosquito-human malaria model will be used to analyse the temporal dynamics of the diseases over the province.

7.3 Material and methods

7.3.1 Study area

The study area focuses on KwaZulu-Natal province in South Africa. The province is situated in the northeast of the country, and share borders with three other provinces (Mpumalanga, Free State and Eastern Cape) and countries (Mozambique, Swaziland and Lesotho) as shown in Fig. 7.1.

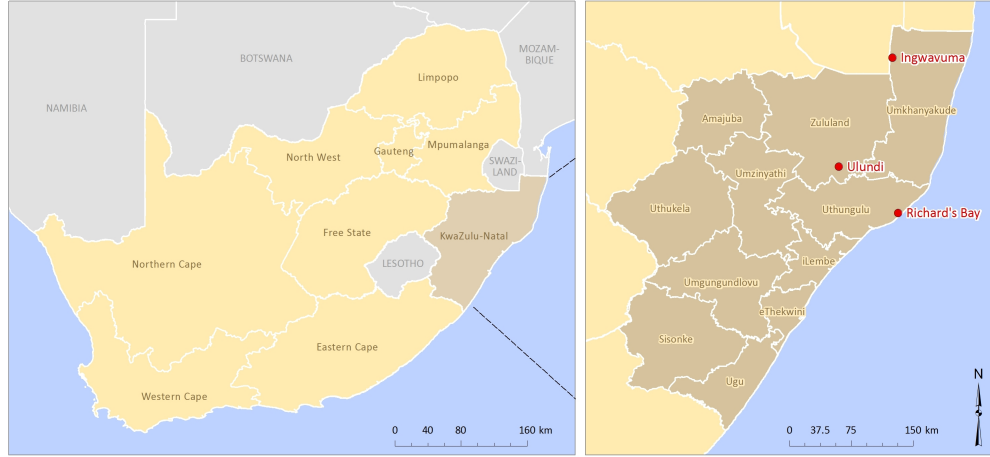
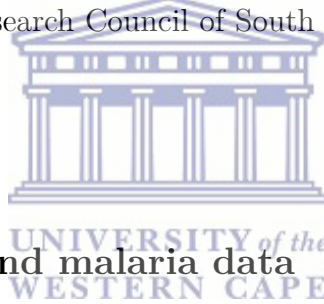


Figure 7.1: The map of KwaZulu-Natal province, South Africa. Source: GIS unit of the Medical Research Council of South Africa.



7.3.2 Climate and malaria data

Two different datasets were considered for the purpose of this study. To estimate the climate data of KwaZulu-Natal province, we averaged the climate data of three towns within malaria risk areas in the province. The towns namely; Ingwavuma (27.1322°S , 31.9942°E), Richards Bay (28.7807°S , 32.0383°E) and Ulundi (28.2997°S , 31.4342°E) are selected from Umkhanyakude, Uthungulu, and Zululand districts respectively. The Observational-Reanalysis hybrid datasets of each town is obtained from the Princeton University Global Meteorological Forcing Datasets ((PUGMFD), see [174] for details), and consist of the daily precipitation, minimum and maximum temperatures between 1970-2005. The averaged climate data of the three towns for the daily mean temperature and rainfall over the study period is shown in Fig. 7.4a and 7.4b respectively. The monthly provincial malaria cases data of KwaZulu-Natal between 2002-2004 were obtained from the South African Department of Health.

7.3.3 Mosquito-malaria model formulation

In this study, we develop a climate-based mosquito-human malaria model to examine malaria transmission over KwaZulu-Natal province. We incorporate into the mosquito model of [2], additional mosquito classes and human compartments. The total mosquito population N_v , is sub-divided into: Eggs (E), Larvae (L), Pupae (P), Susceptible adult searching for host (A_h), Adult at resting state (A_r), Adult searching for oviposition site (A_o), Adult exposed to malaria parasite (E_v) and infectious mosquitoes (I_v), and then $N_v = E + L + P + A_h + A_r + A_o + E_v + I_v$. After feeding, we assume that some proportion ($D_v A_h$) of susceptible mosquito move to resting class for gonotrophic process without being infected while others ($\beta_v A_h$) move to exposed class for sporogonic process. They acquire malaria through contact with infected humans at rate β_v , and later progress to the infected class at a rate ρ_{E_v} . It is noted that $\beta_h = \frac{\beta_1 \epsilon \kappa I_v}{N_h}$, $\beta_v = \frac{\beta_2 \epsilon \kappa I_h}{N_h}$ and $D_v = \frac{\epsilon \kappa A_h}{N_h}$, where β_1 and β_2 represent the transmission probability of human and mosquito respectively with contact rate (κ) and biting rate (ϵ) of mosquito per human per unit time. We refer readers to the study of [2] for details on the formulation of the mosquito model.

The total human population, denoted by N_h is sub-divided into susceptible individuals (S_h), those exposed to malaria parasite (E_h), individuals with malaria symptoms (I_h) and recovered humans (R_h) such that $N_h = S_h + E_h + I_h + R_h$. Since (a) not all individuals in KwaZulu-Natal are living in malaria transmission area, (b) there is significant migration away from rural areas where malaria mostly occur, (c) some people might take malaria medication or live in regions where nets are used or dichlorodiphenyltrichloroethane (DDT) is sprayed to reduce mosquito populations and (d) susceptible humans also die of other causes, we assume susceptible individuals are recruited into the community at a rate ϕ_h and acquire malaria through contact with infectious mosquitoes at a rate β_h . Exposed individuals move to infectious class at a rate ρ_{E_h} . Infectious individuals move to the recovered class at a rate ρ_{I_h} , while infected individuals die at a rate α . Recovered individuals lose immu-

nity at a rate ρ_{R_h} , and become susceptible again and the natural death rate is denoted by μ_h . The dynamics of the mosquito-human malaria model are described by the following system of differential equations (7.1) with the flow diagram illustrated in Fig. 7.2.

$$\begin{aligned}
 \frac{dS_h}{dt} &= \phi_h + \rho_{R_h}R_h - (\beta_h + \mu_h)S_h \\
 \frac{dE_h}{dt} &= \beta_h S_h - (\rho_{E_h} + \mu_h)E_h \\
 \frac{dI_h}{dt} &= \rho_{E_h}E_h - (\rho_{I_h} + \mu_h + \alpha)I_h \\
 \frac{dR_h}{dt} &= \rho_{I_h}I_h - (\rho_{R_h} + \mu_h)R_h \\
 \frac{dE}{dt} &= n(\rho_{A_o}A_o + \rho_{I_v}I_v) - (\rho_e + \mu_e)E \\
 \frac{dL}{dt} &= \rho_e E - (\rho_L + \mu_L(1 + L/K))L \\
 \frac{dP}{dt} &= \rho_L L - (\rho_P + \mu_P)P \\
 \frac{dA_h}{dt} &= \rho_P P + \rho_{A_o}A_o - (\beta_v + D_v + \mu_{A_h})A_h \\
 \frac{dA_r}{dt} &= D_v A_h - (\rho_{A_r} + \mu_{A_r})A_r \\
 \frac{dA_o}{dt} &= \rho_{A_r}A_r - (\rho_{A_o} + \mu_{A_o})A_o \\
 \frac{dE_v}{dt} &= \beta_v A_h - (\rho_{E_v} + \mu_{E_v})E_v \\
 \frac{dI_v}{dt} &= \rho_{E_v}E_v - \mu_{I_v}I_v
 \end{aligned} \tag{7.1}$$

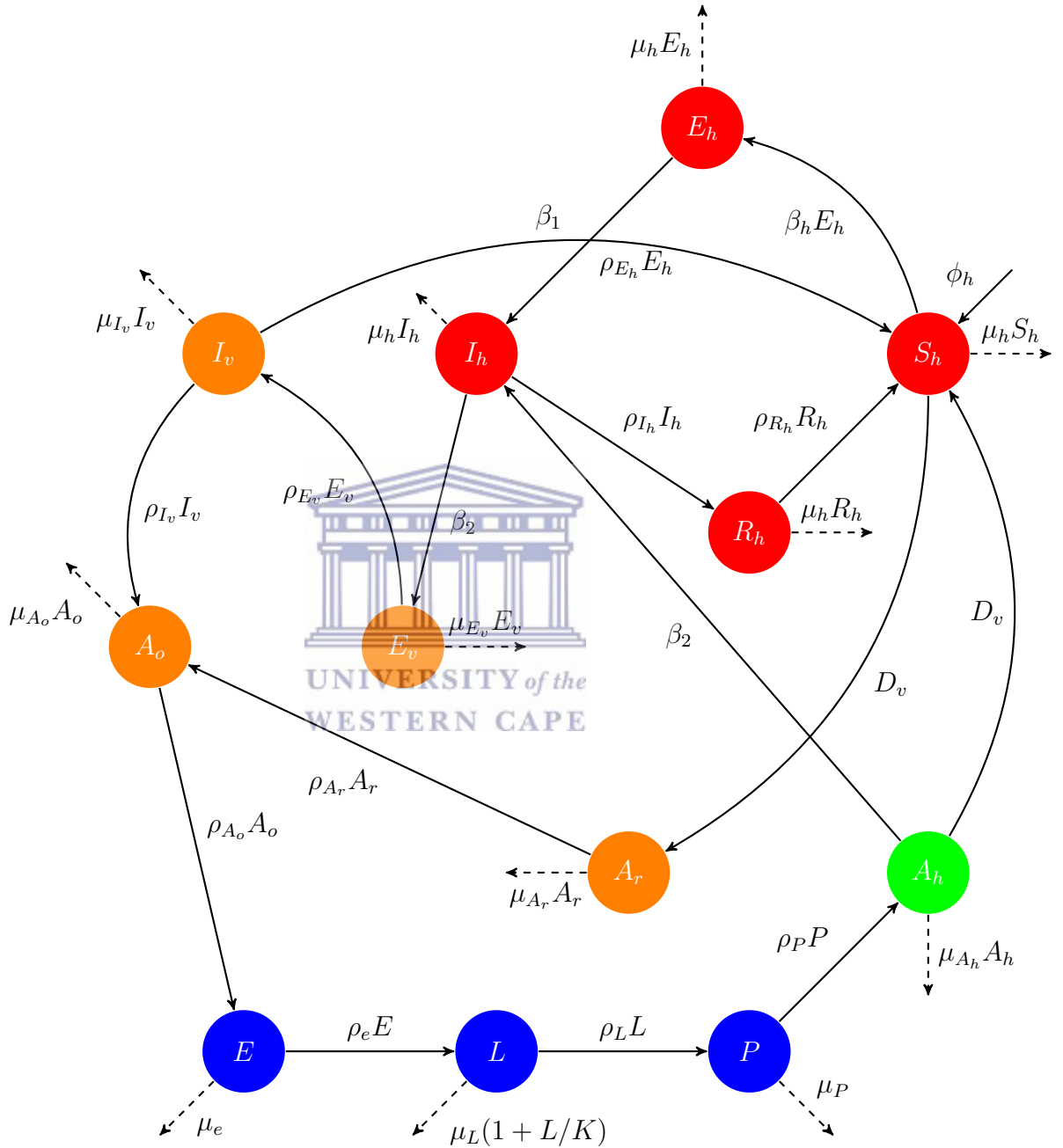
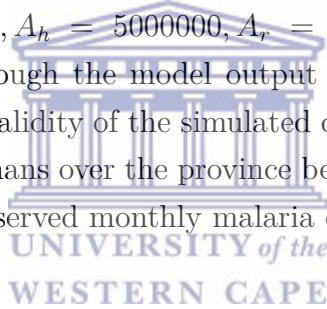


Figure 7.2: The flow diagram of the mosquito-human malaria model

The mosquito climate-dependent parameters used for this model are adopted from the data generated from the laboratory experiments of Maharaj [114]. For details on this, we refer readers to [2]. Parameters are estimated and adopted from other studies as shown in Table 7.2.

Since mosquitoes and malaria parasites respond to weather conditions in days [55], the impact of climate variables on malaria transmission will be underestimated when using a monthly dataset. For this reason, we run our model with daily climate data to simulate the daily human population dynamics over the study region. Considering the assumptions a-d above and the parameters in Table 7.2, we chose the following initial conditions for the model simulations; $S_h = 1000000$, $E_h = 600$, $I_h = 250$, $R_h = 120$, $E = 10000000$, $L = 8000000$, $P = 6000000$, $A_h = 5000000$, $A_r = 4000000$, $A_o = 100000$, $E_v = 8000$, $I_v = 5000$. Although the model output is obtained on daily basis, in order to ascertain the validity of the simulated data, we calculate the monthly number of infected humans over the province between 2002-2004 and compare our results with the observed monthly malaria cases over the province.



7.3.4 Analysis of the model outputs

In order to investigate the impact of climate variability on malaria transmission, we perform the following analysis on the model outputs.

7.3.4.1 Principal Component Analysis (PCA)

In this study, Principal Component Analysis (PCA) is used to analyse the data generated from the model. PCA is useful in identifying common modes of variability between variables [83, 139, 161], and can reduce numerous number of inter-related variables to a few principal components that capture much of the variance of the original dataset [139]. PCA has been widely and successfully used to help understand, interpret, and reconstruct large, multivariate datasets, both with spatial extent [197] and at single sites [160]. Here, PCA

is applied to identify the meteorological variables that are coupled with the model outputs. To achieve this, Statistica software (Statsoft Inc., 2013) using the varimax rotation option to obtain a clear pattern of loadings is used for the analysis.

7.3.4.2 Wavelet Power Spectrum (WPS)

Wavelet analysis is a method of decomposing a time series into time-frequency space. This view offers interesting insights into the dominant modes of a time series and how those modes vary over time. In contrast to Fourier analysis, wavelet analysis highlights the study of signals whose spectra change with time. In addition, the time-frequency analysis reveals further characteristics such as the periodic components with time progression [29, 152, 191]. The WPS also calculates the distribution of variance between frequency f and different time locations τ . In order to compare the WPS with classical spectral methods, the global wavelet spectrum is computed as the time average of the WPS for each frequency component [152]. For a better understanding of this method and analysis, see [30].

Here in this study, we introduce the basic approach of using wavelet analysis to extract periodic components from the climate variables and our model outputs. The wavelet analysis investigates the time-scale decomposition of the signal by estimating its spectral characteristics as a function of time [191, 202]. This approach reveals how the different scales (periodic components) of the time series change over time as the wavelet function is stretched in time by varying its scale [43, 202]. We have considered here the continuous Morlet wavelet transform as the wavelet base function since it provides a good balance between time and frequency localization, which is desirable for feature extraction purposes [67, 202]. The Morlet function is essentially a damped complex exponential, which can capture local (in time) cyclical fluctuations in the time series [202]. Although, the wavelet spectra are scale dependent and can produce distorted power spectra by underestimating short-period peaks

[98, 191], the problem can be corrected through normalising the power spectra by the corresponding scale, so that spectral peaks can be compared across scales [98, 202].

7.3.4.3 Wavelet Cross-coherence Analysis (WCA)

Time-series analyses have been used to examine the dynamics of several disease epidemics, as it seemed to be the only substitute [28, 77], they are more useful in short-term analyses [11, 50]. They are typically noisy and complex [30]. For these reasons, and in order to qualitatively explore the correspondence of the wavelet spectra of rainfall and temperature on malaria incidence, we examine their cross-coherence spectrum as shown in Fig. 7.10 and Fig. 7.11 using Wavelet Cross-coherence Analysis (WCA).

Wavelet Cross-coherence Analysis is a method for analyzing the coherence and phase lag between two time series as a function of both time and frequency [31]. As given in Fourier analysis, the univariate WPS can be extended to quantify statistical relationships between two time series $x(t)$ and $y(t)$ by computing the wavelet coherence

$$R_{x,y}(f, \tau) = \frac{|\langle W_{x,y}(f, \tau) \rangle|}{|\langle W_x(f, \tau) \rangle|^{1/2} \cdot |\langle W_y(f, \tau) \rangle|^{1/2}},$$

where $\langle \rangle$ indicates smoothing in both time and frequency; $W_x(f, \tau)$ represents the wavelet transform of series $x(t)$; $W_y(f, \tau)$ is the wavelet transform of series $y(t)$; and $W_{x,y}(f, \tau) = W_x(f, \tau) \cdot W_y^*(f, \tau)$ is the cross WPS. The wavelet coherence provides local information about the extend to which two non-stationary signals $x(t)$ and $y(t)$, are linearly correlated at a particular frequency (or period). $R_{x,y}(f, \tau)$ is equal to 1 when there is a perfect linear relationship at a particular time and frequency between the two signals [30].

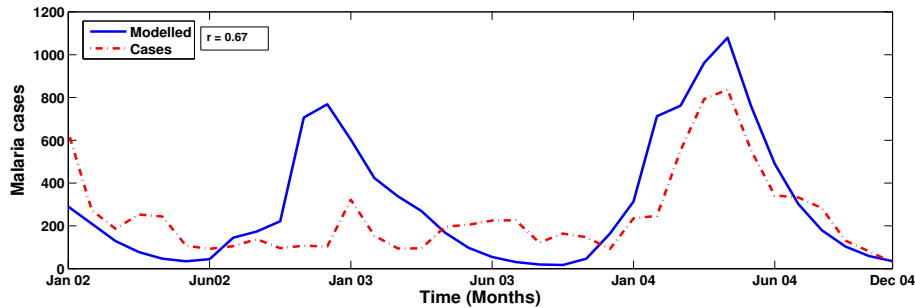


Figure 7.3: The modelled and reported cases of malaria over KwaZulu-Natal province, South Africa for 2002-2004.

7.4 Results and discussion



7.4.1 Model validation

Comparing the model output with observed data, our results produce a fairly similar curve with the observed data as shown in Fig. 7.3. However, we do notice some discrepancies between the simulated and observed data. For instance, in January 2002, our model estimates almost 600 infected humans, whereas only 300 cases were observed. This is one of the limitations of the model, it could also be as a result of some control measures implemented at that particular period which are not considered in our model. Also, our model underestimates malaria incidence as noticed in June 2003, which might be the lack of other factors affecting malaria in our model. However, the model output further indicates along with observed data that malaria transmission over the province is seasonal, and that malaria incidence in the province was higher in 2004 than in 2003. These results are consistent with the previous study of Craig *et al* [41].

7.4.2 Time series of human population dynamics

More relationships between climate variables and malaria transmission over KwaZulu-Natal province are shown in Fig. 7.4. The results (in Fig. 7.4 (a-f)) further highlight the seasonality of malaria transmission over the province. The effect of the climatic spikes are clearly reflected in the human classes as shown in Fig. 7.4 (c-f). Although the relationships are not well captured in some of the classes over the 35-year period. For example, we notice a weak similarity between the recovered human population and climate variables as shown in Fig. 7.4f. There are several factors to be considered for this particular class. For instance, infected individuals could have undergone several treatments for quick recovery. These factors are not considered in the present model. However, it is interesting to see that the model captures the fact that an increase in malaria epidemics will reduce the human population who are still vulnerable to the disease. This can be seen in Fig. 7.4c and Fig. 7.4 (d-e) that each curve decreasing in the susceptible humans results to a peak in exposed and infected humans.



7.4.3 Malaria and climate variability

7.4.3.1 Correlation between climate variables and model outputs

In order to investigate the possible correlation between malaria and climate, we perform PCA on the model outputs. Our results indicate that there are two principal factors or processes coordinating the relationship between climate variables and malaria. As indicated in Table 7.1, the first principal factor (PF_1) shows high loadings on E_h and I_h . It also increases E_h and I_h , at the same time decreases S_h . The second principal factor (PF_2) shows an increase in S_h , decreases the population of R_h . This is reasonable to the fact that recovered humans can be infected again if bitten by infected mosquito. Our findings here are also consistent with the previous studies of Okosun [141], that an increase in infected humans negatively influences the susceptible human population.

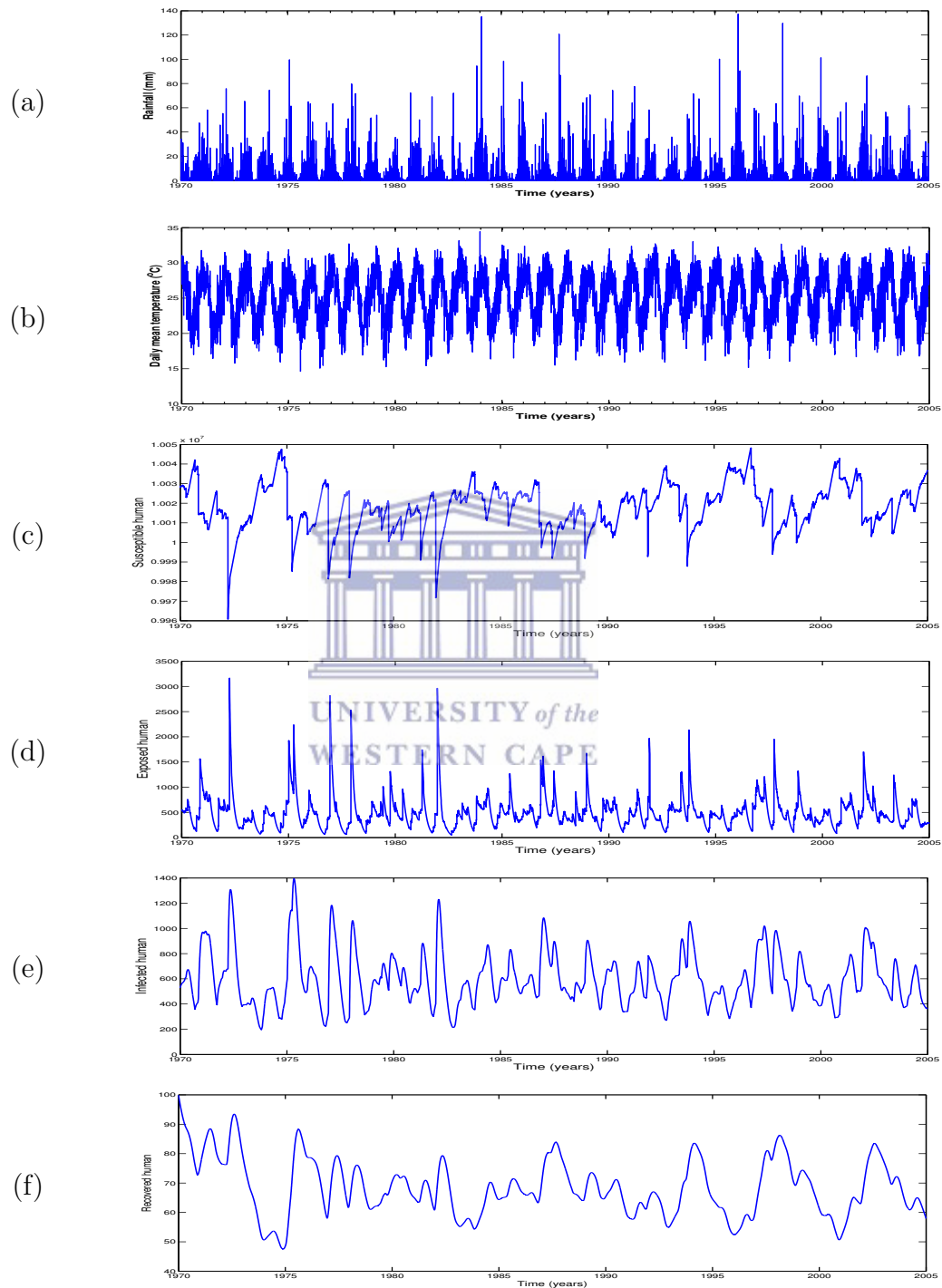


Figure 7.4: Time series of (a) daily mean temperature, (b) rainfall and simulated (c) Susceptible human, (d) Exposed human, (e) Infected human and (f) Recovered human over KwaZulu-Natal province from 1970 - 2005.

Table 7.1: The Principal Component Analyses (with varimax normalized loadings) showing the possible correlation between the model outputs.

Variable	Principal Factor 1 (PF_1)	Principal Factor 2 (PF_2)
S_h	-0.68	0.62
E_h	0.94	0.15
I_h	0.76	-0.42
R_h	0.01	-0.97
Expl. Var	1.92	1.53
Prp. Totl	0.48	0.38

7.4.3.2 Wavelet time series analysis of climate variables and malaria

In general, two dominant peaks are noticed over the province between 1970-2005 as shown in Fig. 7.5 (c & f), Fig. 7.6 (c, f, i & l) and Fig. 7.7 (c & f). The figures also reveal that 1-year periodicity is highly significant over the study period and describe the largest proportion of the time series. In addition, the monthly time-series, as shown in Fig. 7.5 (a & d), Fig. 7.6 (a, d, g & j) and Fig. 7.7 (a & d), highlight a recurrent cycle with an apparent 1-year period, and additional components of variability in some years.

The WPS, as illustrated in Fig. 7.5 (b & e), Fig. 7.6 (b, e, h & k) and Fig. 7.7 (b & e) indicate the decomposition of the series in time (along the x-axis) and period (along the y-axis) scale. The results from the analyses identify a strong annual cycle and ascertained a dominant 1-year periodicity (in red). Additional components of variability at shorter periods are also highlighted in the figures. In particular, the cycles in Fig. 7.5b over the study period are noticeable for rainfall between 1986-1996 and 2001-2003, while those of temperature are significantly noticeable between 1986-1991 as revealed in Fig. 7.5e. However, both climate variables show similar patterns in the cycles. This is an indication that on a seasonal scale, both variables increase and decrease simultaneously over the province. Other cycles for human population dynamics and connecting factors are also similarly in patterns and are noticeable between 1972-1988 as shown in Fig. 7.6 (b, e, h & k) and Fig. 7.7 (b & e). This is an indication that the climate variability affects the human population dynamics

in a similar pattern.

7.4.3.3 The lag and cross-correlation of climate variability and malaria

Also, the results in Fig. 7.8 (a-c) and Fig. 7.9 (a-c) show that malaria transmission over KwaZulu-Natal province between 1970-2005 is more influenced by temperature than rainfall. For instance, the highest correlation between rainfall and malaria incidence as shown in Fig. 7.8c is below 0.4, while that of temperature is 0.9. In addition, the red and blue bars clearly indicate the existence of both positive and negative correlation between climate variables and malaria transmission over the study period. However, the positive correlations are more noticeable in all the figures. This is an indication that both rainfall and temperature contribute positively to the transmission of malaria over the province. Furthermore, an average of 0 to 120-day lag is generally noticeable over the years. The 120-day lag is more associated with temperature than rainfall. Also, in some of the years, rainfall is negatively correlated with number of malaria cases at lags of 0 and 1 month. This is consistent with the previous study of Sena *et al* [171]. However, our result here contradicts their findings that temperature is weakly correlated at lags of 0 to 4 months. A stronger correlation in the case of temperature is obtained in this study. Other study in line with our findings here is the study of Mohammadkhani *et al* [126]. It is established in their study that the maximum positive cross-correlation was observed between malaria and climatic factors with 1 to 4 months lag [126]. Further studies associated with these findings are Bi *et al* [12], Wangdi *et al* [198] and Zhang *et al* [211].

In addition, the results in Fig. 7.10 (a-f) and Fig. 7.11 (a-f) show a strong relationship and significant cross-coherence between the climate variables and malaria incidence over the province. The results, in line with our previous findings clearly indicate that malaria incidences over the province are more and closely associated with the temperature rather than with rainfall. For instance, the annual cycle is dominated and fairly consistent, through the year

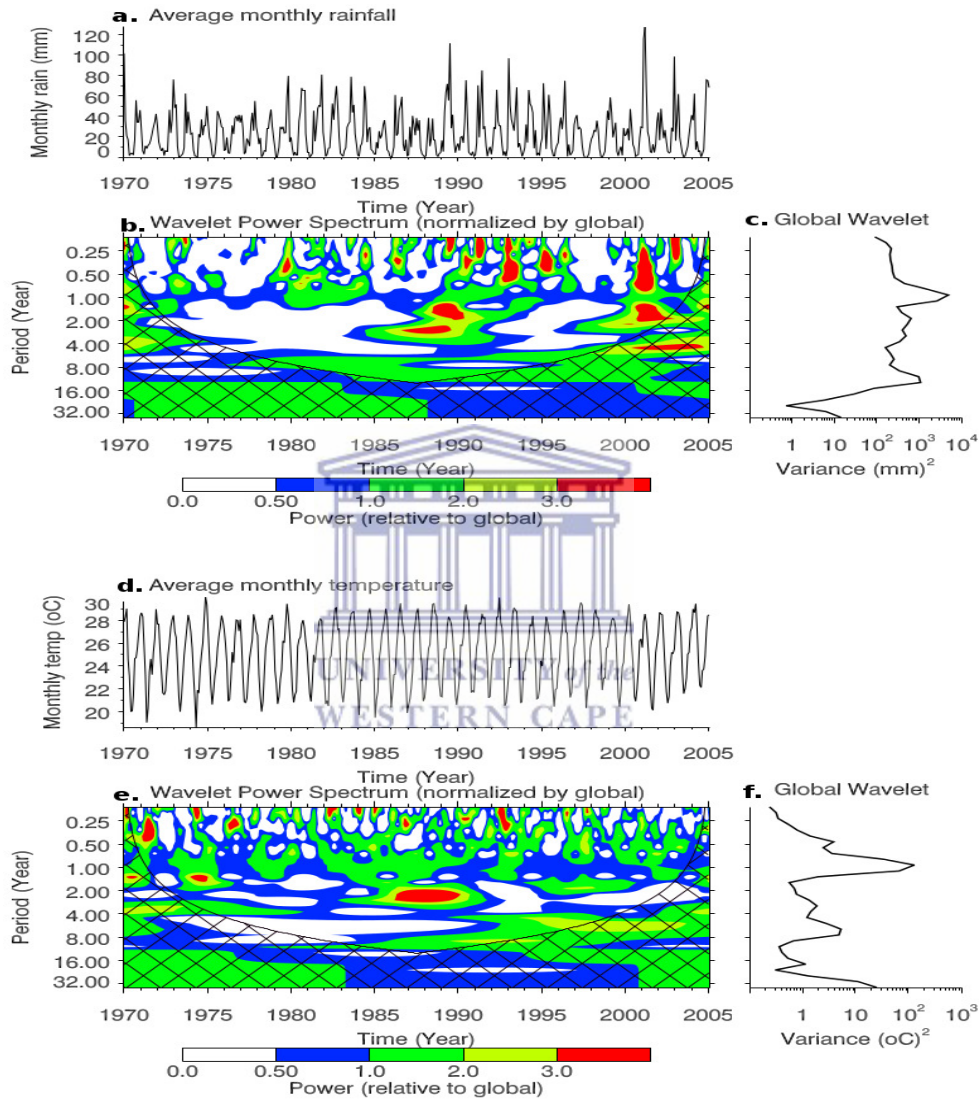


Figure 7.5: The wavelet analysis of the climate variables of KwaZulu-Natal province from 1970-2005. The time series of average monthly (a) rainfall and (d) temperature. The WPS of (b) rainfall and (e) temperature time series. The cross-hatched region is the cone of influence, where zero padding has reduced the variance and only pattern above the region are considered reliable. The colour code values from blue (low values) to red (high values). The power has been scaled by the global wavelet spectrum (at right). The global WPS of (c) rainfall and (f) temperature. The black contour line corresponds to 10% significance level, using the global wavelet as the background spectrum.

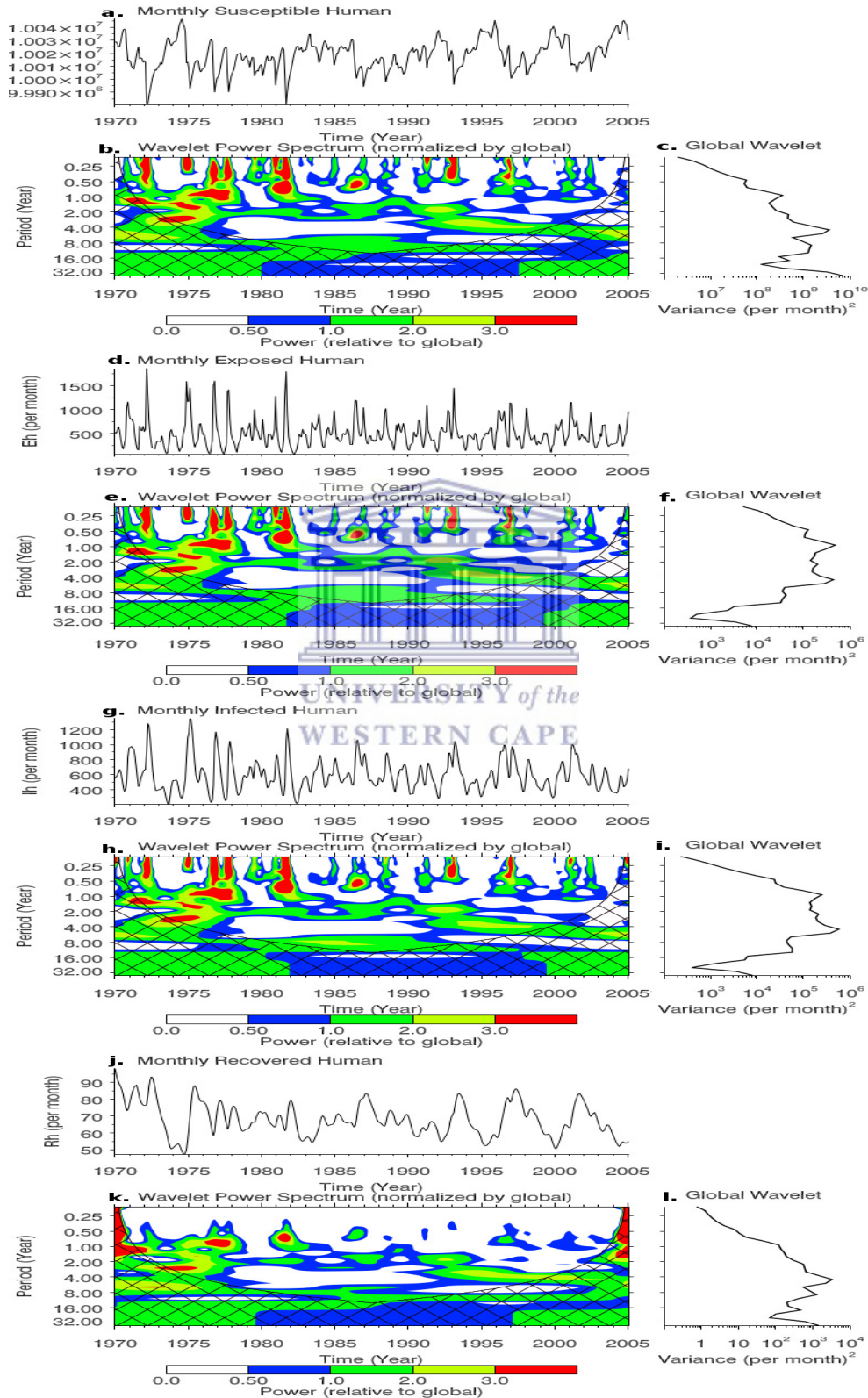


Figure 7.6: The wavelet analysis of simulated human population dynamics of KwaZulu-Natal province from 1970-2005. The time series of monthly (a) Susceptible, (d) Exposed, (g) Infected and (j) Recovered human. The WPS of (b) Susceptible, (e) Exposed, (h) Infected and (k) Recovered human monthly time series. The cross-hatched region is the cone of influence, where zero padding has reduced the variance and only pattern above the region are considered reliable. The colour code values from blue (low values) to red (high values). The power has been scaled by the global wavelet spectrum (at right). The global WPS of (c) Susceptible, (f) Exposed, (i) Infected and (l) Recovered human. The black contour line corresponds to 10% significance level, using the global wavelet as the background spectrum.

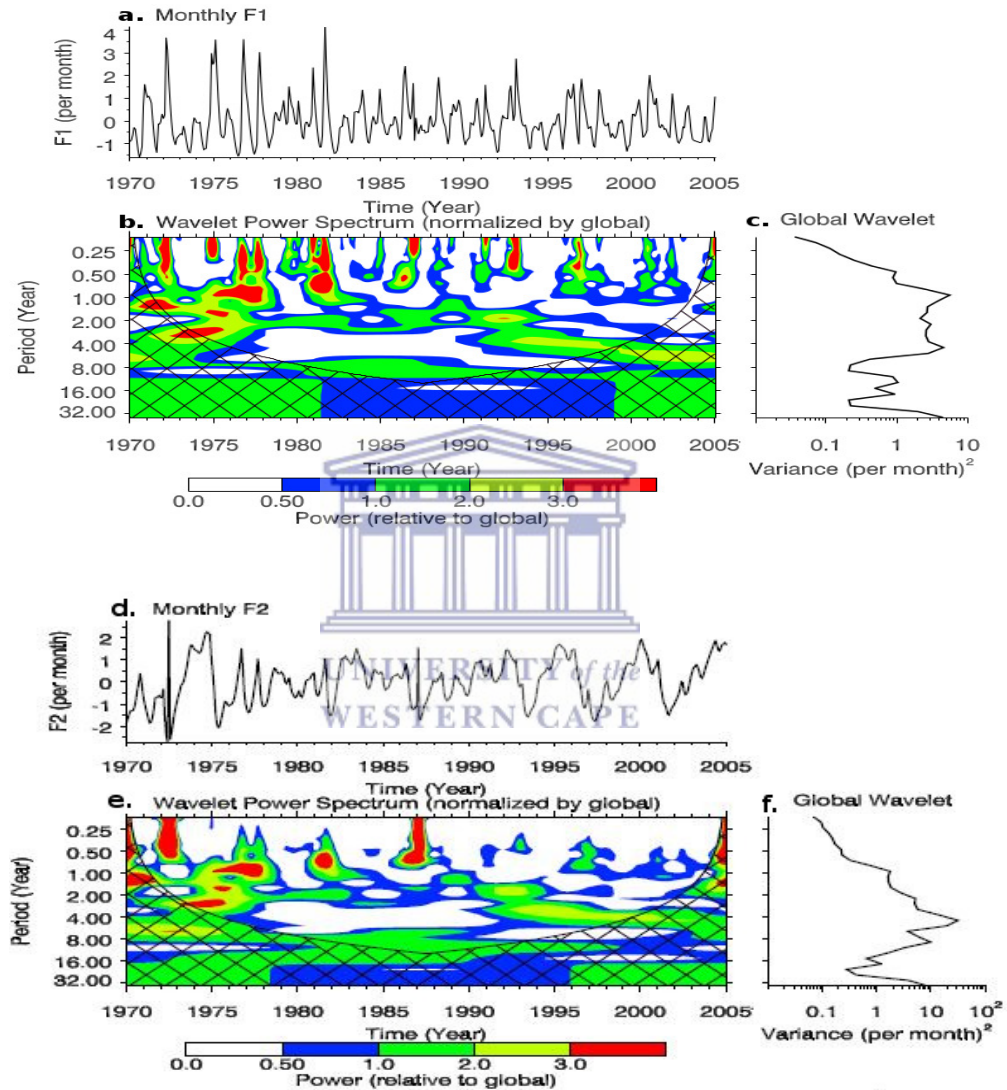


Figure 7.7: The wavelet analysis of the principal components connecting the simulated human population from 1970-2005. The time series of average monthly (a) Factor 1 and (d) Factor 2. The WPS of (b) Factor 1 and (e) Factor 2 time series. The cross-hatched region is the cone of influence, where zero padding has reduced the variance and only pattern above the region are considered reliable. The colour code values from blue (low values) to red (high values). The power has been scaled by the global wavelet spectrum (at right). The global WPS of (c) Factor 1 and (f) Factor 2. The black contour line corresponds to 10% significance level, using the global wavelet as the background spectrum.

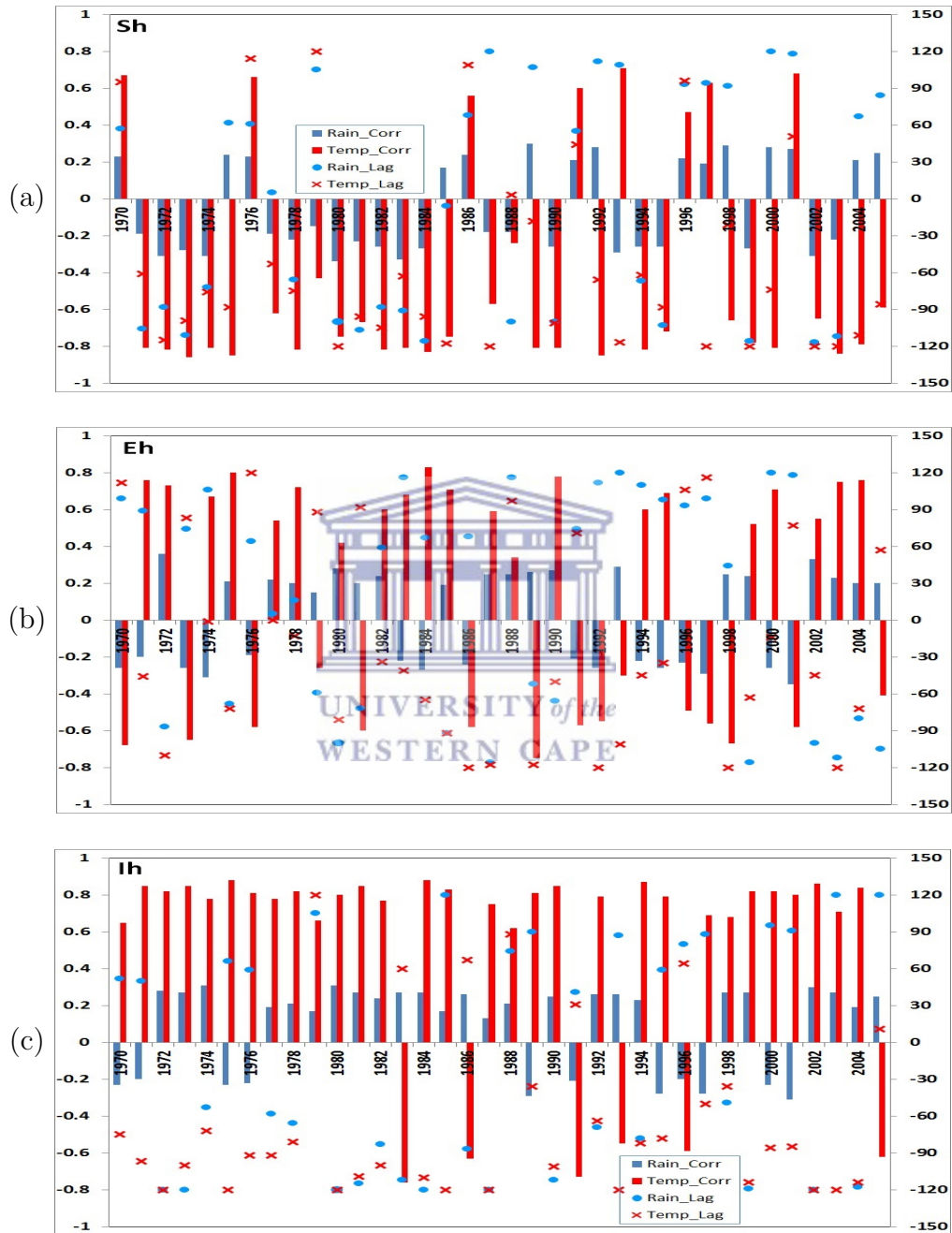


Figure 7.8: Cross-correlation coefficients of time series of daily climate variables and simulated (a) Susceptible human, (b) Exposed human, and (c) Infected human at several lags.

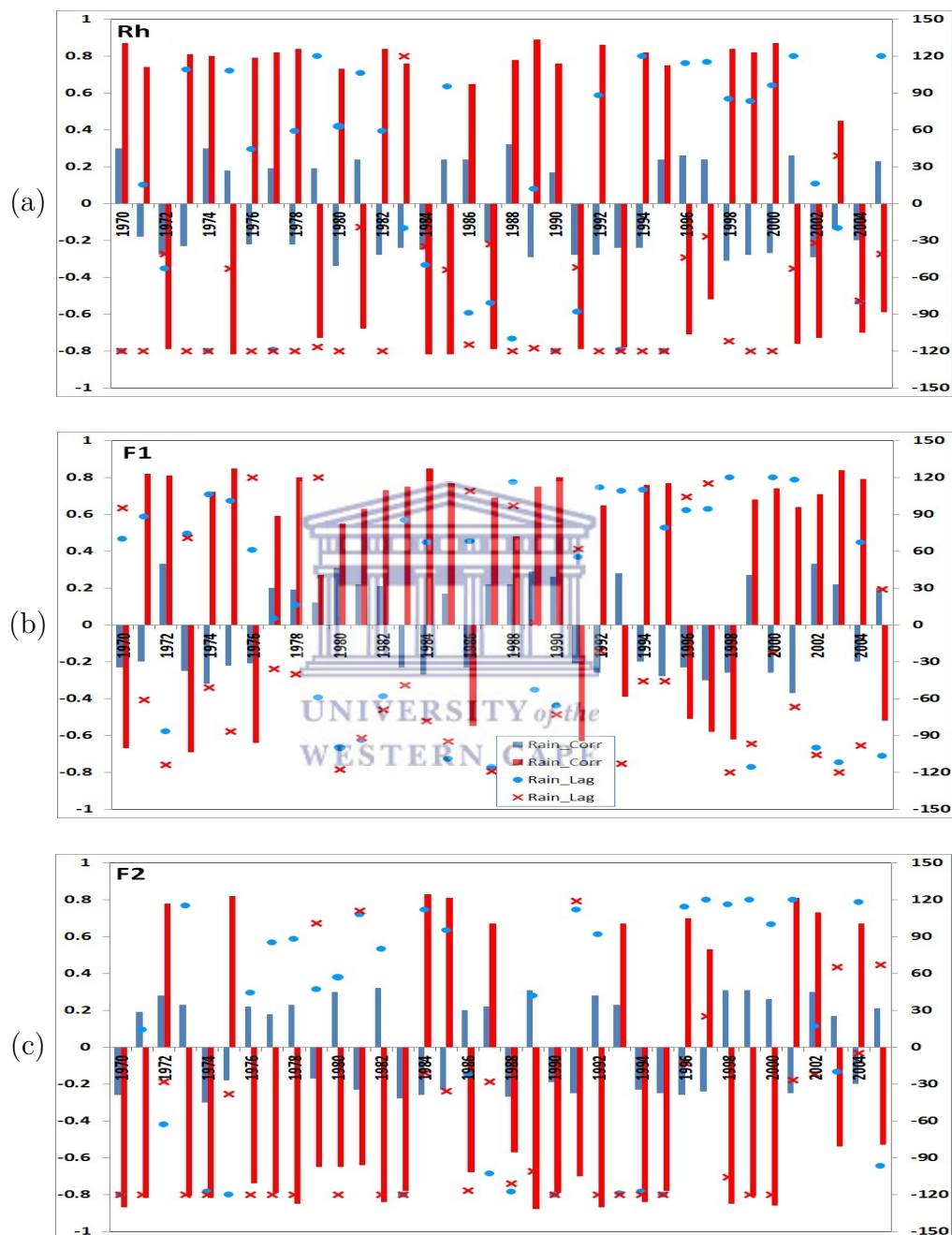
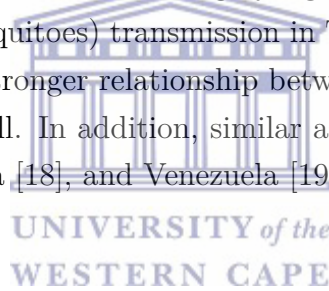


Figure 7.9: Cross-correlation coefficients of time series of daily climate variables and simulated (a) Recovered human, (b) Factor 1, and (c) Factor 2 at several lags.

for both rainfall and temperature as shown in Fig. 7.10 and Fig. 7.11. The biennial pattern are additionally noted and more pronounced for temperature than rainfall. Malaria occurrence period is also noticed to fall within 256-512 days on both figures. Focusing more on Fig. 7.10c and 7.11c, the cross-spectral analysis reveals that the correlation between malaria incidence and rainfall are noticeably stronger between 1971-1978 and 1987-2003, while that of temperature are noticeable all through the year as highlighted in both figures. Although we notice a weak in-phase relationship between temperature and malaria incidence on the biennial cycle between 1984-1987 as shown in Fig. 7.10c, no significant cycle or coherence is noted between this period for rainfall (see Fig. 7.11c). These results are consistent with the findings of Cazelles *et al* [29] that temperature and rainfall are highly significant on dengue (which are also transmitted by mosquitoes) transmission in Thailand. Their findings also made emphasis on the stronger relationship between temperature and dengue fever than that of rainfall. In addition, similar associations were documented for Colombia [155], India [18], and Venezuela [19], among others.



7.5 Conclusion

In this study, we have developed a climate-based mosquito-malaria model to examine malaria incidence over KwaZulu-Natal province between 1970-2005. The model is developed from the previous study of Abiodun *et al* [2] to investigate the human population dynamics of the province between the study period.

The model outputs are further analysed with Principal Component Analysis, Wavelet Power Spectrum and Wavelet Coherence Analysis to investigate the relationship between the climate variables and malaria incidence over the province.

Our results highlighted the importance of climate factors on malaria transmission and ascertained that malaria transmission in KwaZulu-Natal province

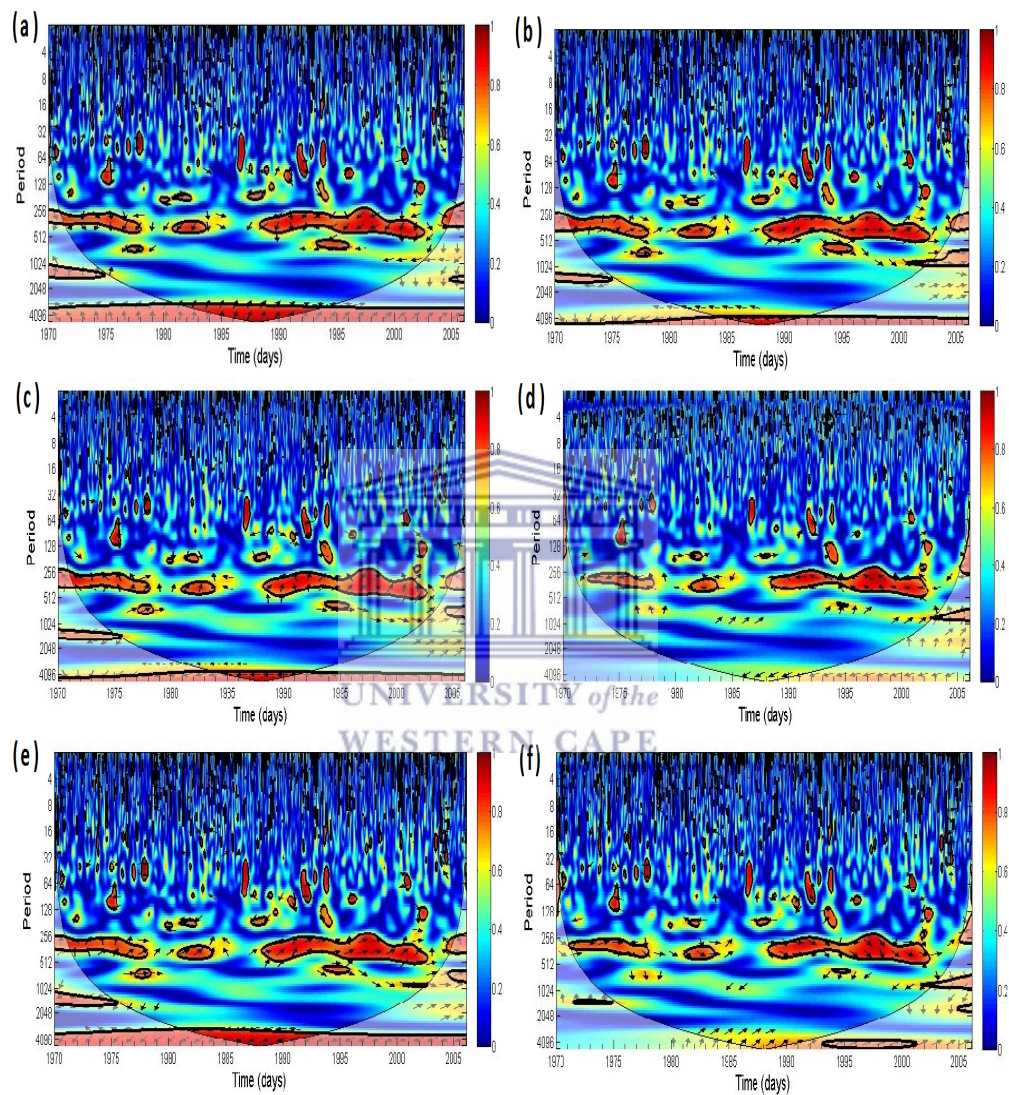


Figure 7.10: Wavelet coherence of rainfall and simulated (a) Susceptible human, (b) Exposed human, (c) Infected human, (d) Recovered human, (e) Factor 1 and (f) Factor 2 over KwaZulu-Natal province between 1970-2005. The arrows indicate the relative phasing of the variables, while the faded regions represent the cone of influence and are not considered for the analyses

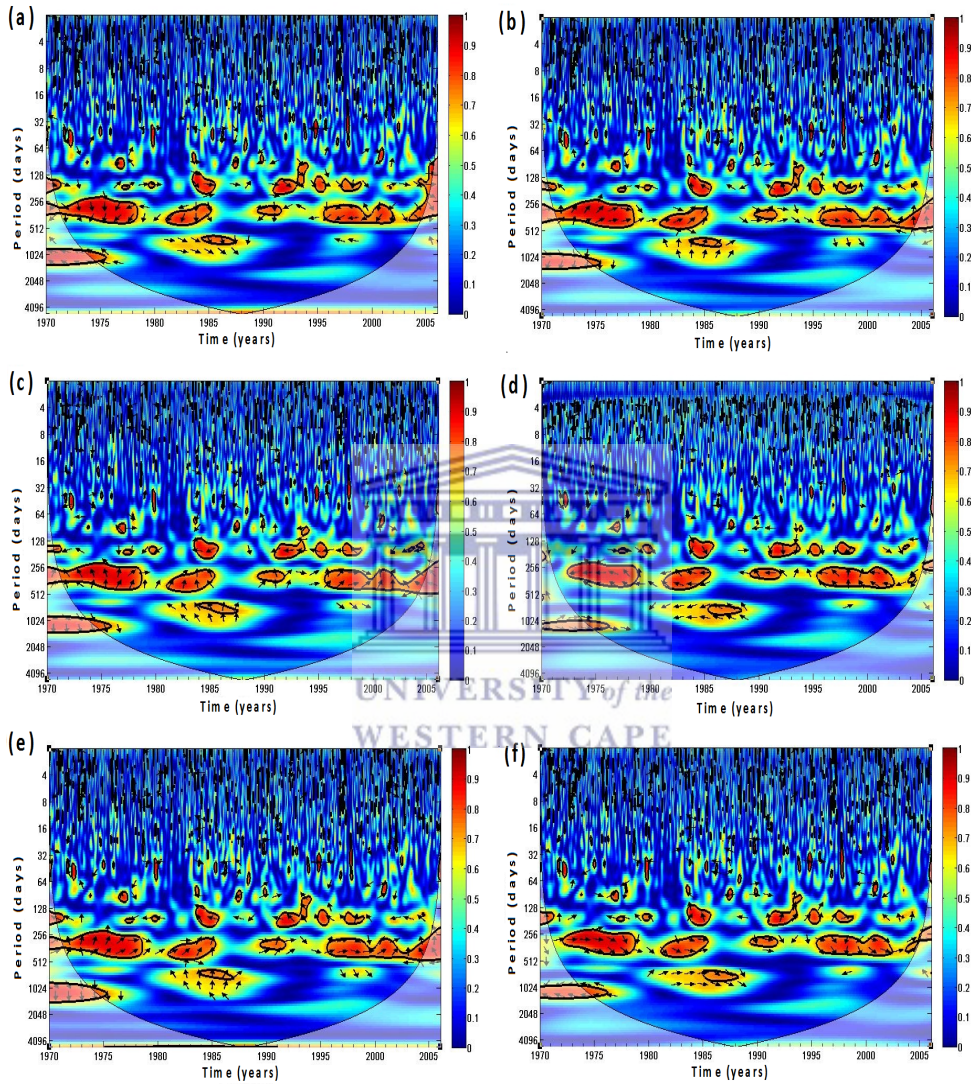


Figure 7.11: Wavelet coherence of temperature and simulated (a) Susceptible human, (b) Exposed human, (c) Infected human, (d) Recovered human, (e) Factor 1 and (f) Factor 2 over KwaZulu-Natal between 1970-2005. The arrows indicate the relative phasing of the variables, while the faded regions represent the cone of influence and are not considered for the analyses.

is seasonal. The findings from our analyses further suggested that, there are two principal factors controlling climate variables and the model outputs. The first principal factor is more correlated with Susceptible, Exposed and Infected humans, while the other is associated with Susceptible and Recovered humans. It is further established in our findings that both temperature and rainfall are responsible for the transmission of the disease, but malaria is more influenced by temperature than rainfall over the province. We also concluded that the average of 0 to 120-day lag is noticeable over the study period, but the 120-day lag is more prominent with temperature than rainfall

The findings of this study would be useful in early warning or forecasting of malaria transmission over KwaZulu-Natal province. More importantly, attention should be paid to the more expected occurrences of malaria between the period of 256-512 days.

Currently, the model ignores some other important factors influencing the dynamics of the vector population and malaria transmission over KwaZulu-Natal province. Several studies [55, 65, 102] have highlighted the importance of migration, relative humidity, land cover, irrigation and deforestation mosquito abundance and malaria incidence over a region. We therefore leave these aspects for further studies.

Table 7.2: Parameters of the mosquito-malaria model

Description	Parameters/Functional form	Ref.
Number of eggs, $n(T_a)$	$-0.61411T_a^3 + 38.93T_a^2 - 801.27T_a + 5391.4$	[2]
Egg development rate, $\rho_e(T_w)$	$0.012T_w^3 - 0.81T_w^2 + 18T_w - 135.93$	[2]
Larva development rate, $\rho_L(T_w)$	$-0.002T_w^3 + 0.14T_w^2 - 3T_w + 22$	[2]
Pupa development rate, $\rho_P(T_w)$	$-0.0018T_w^3 + 0.12T_w^2 - 2.7T_w + 20$	[2]
Egg mortality rate, $\mu_e(T_w)$	$0.0033T_w^3 - 0.23T_w^2 + 5.3T_w - 40$	[2]
Larva mortality rate, $\mu_L(T_w)$	$0.00081T_w^3 - 0.056T_w^2 + 1.3T_w - 8.6$	[2]
Pupa mortality rate, $\mu_P(T_w)$	$0.0034T_w^3 - 0.22T_w^2 - 4.9T_w - 34$	[2]
Gonotrophic rate, $\rho_{A_o}(T_a)$	$0.00054T_a^3 - 0.038T_a^2 + 0.88T_a$	[2]
Adult mortality rate $\mu_A(T_a)$	$\exp[-1/(-4.4 + 1.31T_a - 0.03T_a^2)]$	[41, 190]
Mosquito biting rate, ϵ	$0.000203T_a(T_a - 11.7)\sqrt{42.3 - T_a}$	[137, 148]
Progression from E_v to I_v , $\rho_{E_v}(T_a)$	$\frac{(T_a - T_{min})}{111}$	[137, 190]
Min. temp. for <i>P. falc.</i> survival, T_{min}	16 °C	[41, 137]
Rate adult seeks blood meal, ρ_{A_h}	0.46	[35, 103, 104]
Rate adult seeks resting site, ρ_{A_r}	0.43	[35, 103, 104]
Prob. of human getting infected, β_1	0.533	Nominal
Prob. of mosquito getting infected, β_2	0.09	[14, 106, 141]
Natural death rate in human, μ_h	$1/49.1/365 \text{ day}^{-1}$	[105, 204], Est.
Human recruitment rate, ϕ_h	51.67 day^{-1}	[105, 204], Est.
Contact rate of mosquito per human, κ	0.6 day^{-1}	[34, 141]
Disease induced death rate, α	0.05 day^{-1}	[106, 141]
Progression from E_v to I_v , ρ_{E_v}	$1/18 \text{ day}^{-1}$	[14, 106, 141]
Recovered ind. loss of immunity, ρ_{R_h}	$1/730$	[14, 106, 141]

Chapter 8

Concluding remarks and scope for future research

8.1 Concluding remarks



The main aim of this thesis was to develop, analyse and implement mosquito-human climate-based malaria model to be validated over epidemic regions in South Africa. We began with detailed background on malaria in Chapter 1. In the same chapter, we described to a certain length, the mosquito *binomics*, that is, the ecology of mosquito species and its behaviour. Malaria parasite cycles and the various malaria species were also discussed with images. Furthermore, the chapter highlighted some factors affecting malaria and offered few literature reviews on malaria models.

A basic deterministic malaria model without climate-dependent variables or control interventions was formulated and analysed in Chapter 2. The analysis of the seven compartmental model was shown to be epidemiologically meaningful and mathematically well-posed. We investigated the existence and stability of the disease-free equilibrium and endemic equilibrium points, and hence calculated the reproduction number, \mathcal{R}_0 using the next generation matrix. We

further showed that the disease-free equilibrium E_0 is locally asymptotically stable if $\mathcal{R}_0 < 1$, and become unstable, and there exists endemic equilibrium E_1 stable when $\mathcal{R}_0 > 1$.

The model was extended in Chapter 3 by incorporating the climate-dependent parameters of *Anopheles gambiae*. The model was analysed and used to investigate the impact of temperature and rainfall on malaria transmission over Limpopo province. The model was used to provide a numerical basis for further refinement towards prediction of the impact of climate variability on malaria transmission.

Focusing only on mosquito population dynamics, and ignoring climate-dependent parameters, we analysed a mosquito model in Chapter 4. The model which was motivated by the study of [103], Lutambi2013thesis comprises of three aquatic and adult stages. The six compartmental model was analytically and numerically analysed. Both analyses indicated that the mosquito-free equilibrium point is locally and globally asymptotically stable whenever $\mathcal{R}_0 < 1$, and becomes unstable when $\mathcal{R}_0 > 1$.

In an attempt to understudy the impact of climate on the dynamics of both immature and adult *An. arabiensis*, in Chapter 5 of this thesis, we further developed the mosquito model of Chapter 4 by incorporating climate factors and puddle dynamics into the model. Additional mosquito compartments, that is, mate seeking adult mosquito (A_m) was also included in the model. We derived the functions for the climate-dependent parameters from the study of [114] and validated the model over a town in eastern Sudan. The model sensitivity analysis was further carried out to investigate the sensitivity of the model to parameters. Incorporating the climate data of Dondotha village in KwaZulu-Natal province, the model was hence used to simulate the dynamics of the mosquito population over the province. The results indicated the importance of climate on *An. arabiensis* which is responsible for malaria transmission over the province.

The mosquito model in Chapter 4 was further developed in Chapter 6 by

coupling human compartments into the model. Also ignoring climate variable in the same chapter, the model was analytically and numerically analysed. It was established that the model is epidemiologically feasible and well-posed and we also showed the existence of the disease-free equilibrium. Furthermore, we also used the next generation matrix technique to derive the reproduction number \mathcal{R}_0 and proved the disease-free equilibrium which is locally asymptotically stable whenever $\mathcal{R}_0 < 1$, unstable otherwise giving rise to the existence of the endemic equilibrium for $\mathcal{R}_0 > 1$. We also verified that the system exhibits backward bifurcation, which implies that the stability of the disease-free equilibrium of the model co-exists with a stable endemic equilibrium even when $\mathcal{R}_0 < 1$. We carried out the sensitivity analysis on the reproductive number, \mathcal{R}_0 and noticed that mosquito biting rate is highly sensitive over the reproduction number. This is an indication that the biting rate plays a significant role in transmitting malaria. Our findings suggested that activities (such as bed netting, use of insecticides) to prevent biting rate should be constantly practiced in a malaria-epidemic region since *Anopheles* need blood-meals to complete their gonotrophic and sporogonic cycle.

In Chapter 7, we further developed the model of Abiodun *et al* [2] as in Chapter 4 by introducing human compartments into the model. We hence used the climate-based mosquito-malaria model to examine malaria incidence over KwaZulu-Natal province between 1970-2005. The model produced a reasonable fit with the observed data over the province which ascertained that malaria transmission over the province is seasonal. Also, in order to understand the population dynamics of humans, and to investigate the impact of climate variability on malaria transmission over the province between the study period, we performed Principal Component Analysis (PCA), Wavelet Power Spectrum (WPS) and Wavelet Cross-coherence Analyses (WCA) on the model outputs. Results from the PCA highlighted two principal factors associated with climate variables and the model outputs. One of the factors is more correlated with Susceptible, Exposed and Infected humans, while the other is traceable to Susceptible and Recovered humans. However, both factors revealed the inverse correlation between Susceptible-Infected and Susceptible-

Recovered humans respectively. Consequently, our findings showed that an average of 0 to 120-day lag is generally noted over the study period, but the 120-day lag is more associated with temperature than rainfall. This is in line with other findings from previous sections that malaria transmission is more tightly coupled with temperature than with rainfall in KwaZulu-Natal province. Furthermore, our findings suggest that more attention should be given to the expected malaria occurrences period. The findings of this study would be useful in early warning or forecasting of malaria transmission over the province.

8.2 Scope for future research

Currently, the models presented in this study lack some other important factors influencing the dynamics of the vector population and malaria transmission. Several studies [55, 65, 102] have highlighted the importance of migration, relative humidity, land cover, irrigation and deforestation on mosquito population dynamics over epidemic regions. We aim to consider these factors in our subsequent studies.

In our mosquito model, we have used cylindrical shape for the puddle dynamics. In future, we would like to consider other shapes such as cone to understudy the population dynamics of mosquito and validate the model on adult mosquito population over malaria epidemic regions in South Africa as soon as we have access to such data.

We would also like to consider the impact of more climate variability phenomena such as oscillations (including El Nino/La Nina, MJO, North Atlantic Oscillation) and Indian Ocean Dipole (IOD) on malaria transmission in our future studies. We also aim to extend this work in future by examining the impact of climate change on malaria transmission of the epidemic-prone regions over South Africa.



Model parameterization

The following figures (Fig. 1) show the curve fits for other temperature-dependent parameter in Chapter 5.

Spatial distribution

The following figures (Fig. 2 and Fig. 3) illustrate the spatial distribution of *An. arabiensis* biting rate and larvae development over South Africa for 2002.



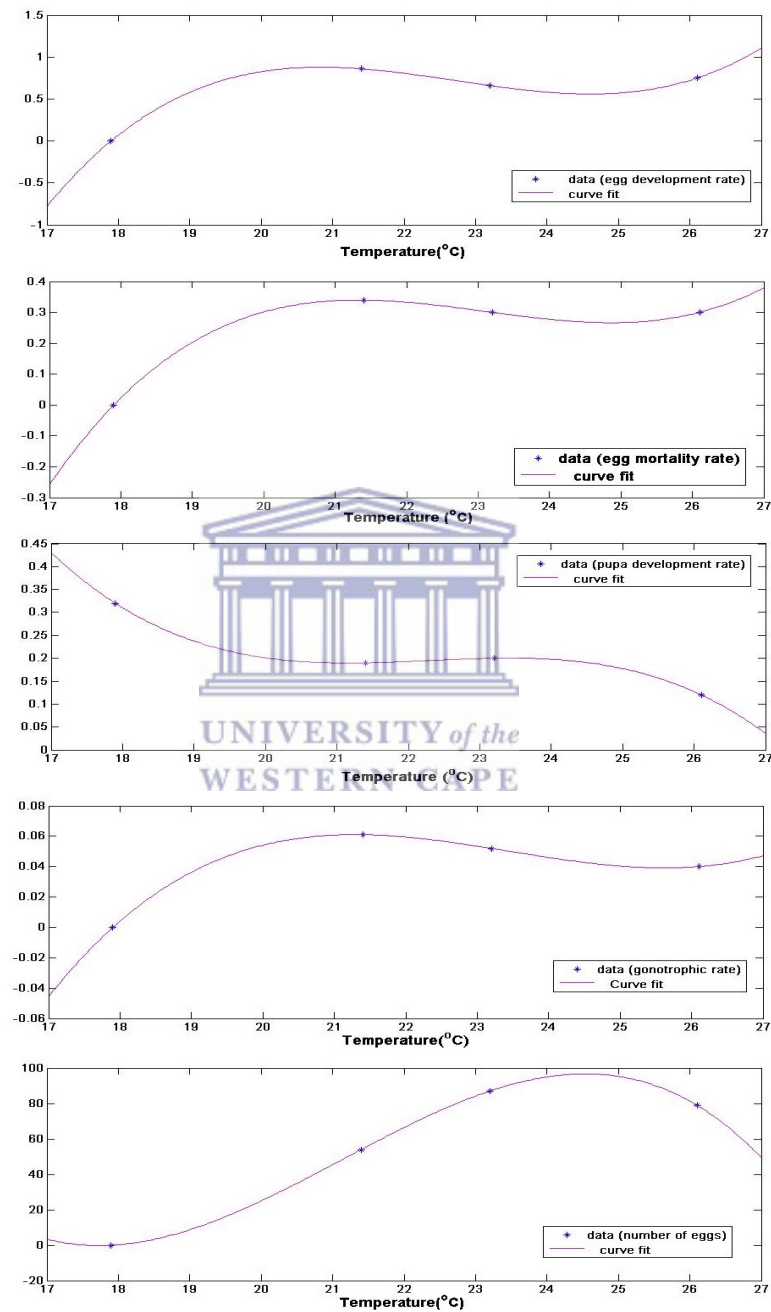


Figure 1: Additional File 1: Curves fit for gonotrophic rate, development and mortality rate of immature *An. arabiensis*.

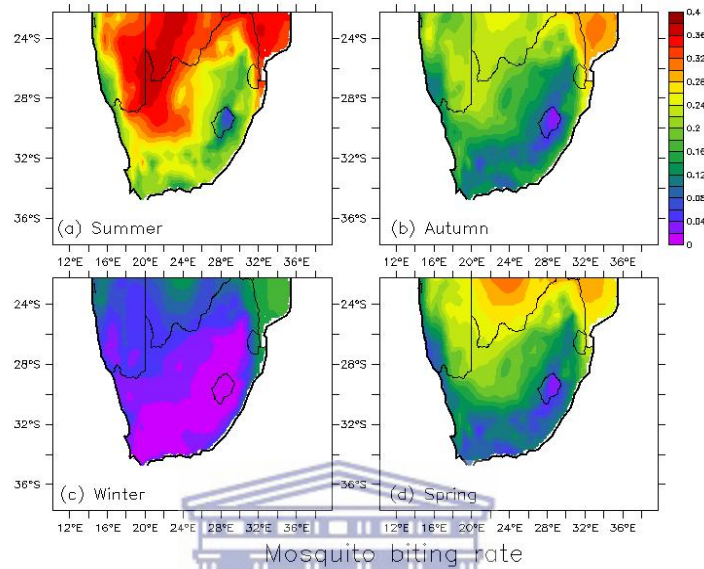


Figure 2: Additional File 2: Simulated biting rate of *An. arabiensis* for 2002.

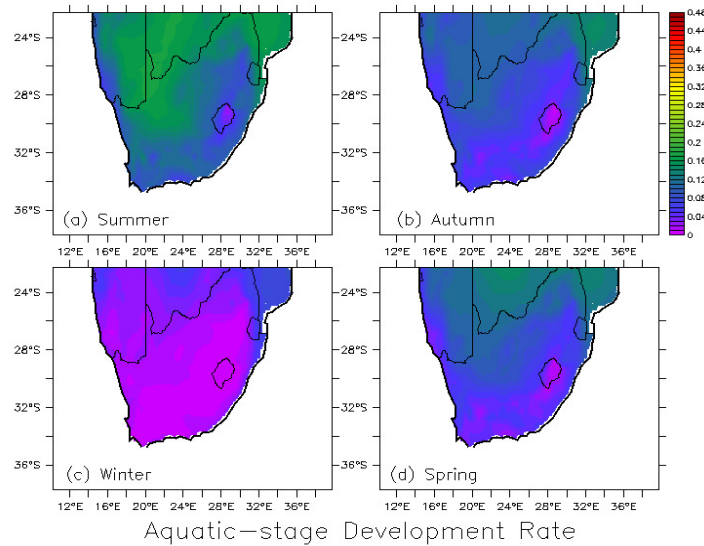


Figure 3: Additional File 3: Simulated larvae development rate of *An. arabiensis* for 2002.

$$\begin{aligned}
eq1 &:= -P \cdot S[h] + \Phi[h] + q \cdot R[h]; & -P S_h + \Phi_h + q R_h \\
eq2 &:= Q \cdot S[h] - V \cdot E[h]; & Q S_h - V E_h \\
eq3 &:= \eta[h] \cdot E[h] - W \cdot I[h]; & \eta_h E_h - W I_h \\
eq4 &:= \alpha \cdot I[h] - K \cdot R[h]; & \alpha I_h - K R_h \\
eq5 &:= \Gamma[v] - G \cdot S[v]; & \Gamma_v - G S_v \\
eq6 &:= \xi[v] \cdot S[v] - H \cdot E[v]; & \xi_v S_v - H E_v \\
eq7 &:= \eta[v] \cdot E[v] - \mu[v] \cdot I[v]; & \eta_v E_v - \mu_v I_v
\end{aligned}$$

`E[1] := solvefor[S[h], E[h], I[h], R[h], S[v], E[v], I[v]](eq1, eq2, eq3, eq4, eq5, eq6, eq7);`

$$\left\{ E_h = \frac{W \Phi_h K Q}{P V W K - q \alpha \eta_h Q}, E_v = \frac{\xi_v \Gamma_v}{H G}, R_h = \frac{\alpha \Phi_h Q \eta_h}{P V W K - q \alpha \eta_h Q}, S_h = \frac{V W \Phi_h K}{P V W K - q \alpha \eta_h Q}, S_v = \frac{\Gamma_v}{G}, I_h = \frac{\Phi_h K Q \eta_h}{P V W K - q \alpha \eta_h Q}, I_v = \frac{\xi_v \Gamma_v \eta_v}{H \mu_v G} \right\}$$

`subs(P = (\beta[h] + \mu[h]), Q = (\beta[h]), V = (\eta[h] + \mu[h]), W = (\alpha + \gamma + \mu[h]), K = (q + \mu[h]), G = (\xi[v] + \mu[v]), H = (\eta[v] + \mu[v]), %);`

$$\left\{ E_h = \frac{(\alpha + \gamma + \mu_h) \Phi_h (q + \mu_h) \beta_h}{(\beta_h + \mu_h) (\eta_h + \mu_h) (\alpha + \gamma + \mu_h) (q + \mu_h) - q \alpha \eta_h \beta_h}, E_v = \frac{\xi_v \Gamma_v}{(\eta_v + \mu_v) (\xi_v + \mu_v)}, R_h = \frac{\alpha \Phi_h \beta_h \eta_h}{(\beta_h + \mu_h) (\eta_h + \mu_h) (\alpha + \gamma + \mu_h) (q + \mu_h) - q \alpha \eta_h \beta_h}, S_h = \frac{(\eta_h + \mu_h) (\alpha + \gamma + \mu_h) \Phi_h (q + \mu_h)}{(\beta_h + \mu_h) (\eta_h + \mu_h) (\alpha + \gamma + \mu_h) (q + \mu_h) - q \alpha \eta_h \beta_h}, S_v = \frac{\Gamma_v}{\xi_v + \mu_v}, I_h = \frac{\Phi_h (q + \mu_h) \beta_h \eta_h}{(\beta_h + \mu_h) (\eta_h + \mu_h) (\alpha + \gamma + \mu_h) (q + \mu_h) - q \alpha \eta_h \beta_h}, I_v = \frac{\xi_v \Gamma_v \eta_v}{(\eta_v + \mu_v) \mu_v (\xi_v + \mu_v)} \right\}$$

`latex(%)`

```

\left\{ E_{\{h\}} = \frac{\left( \alpha + \gamma + \mu_{\{h\}} \right) \Phi_{\{h\}} \left( q + \mu_{\{h\}} \right) \beta_{\{h\}}}{\left( \beta_{\{h\}} + \mu_{\{h\}} \right) \left( \eta_{\{h\}} + \mu_{\{h\}} \right) \left( \alpha + \gamma + \mu_{\{h\}} \right) \left( q + \mu_{\{h\}} \right) - q \alpha \eta_{\{h\}} \beta_{\{h\}}}, E_{\{v\}} = \frac{\xi_{\{v\}} \Gamma_{\{v\}}}{\left( \eta_{\{v\}} + \mu_{\{v\}} \right) \left( \xi_{\{v\}} + \mu_{\{v\}} \right)}, R_{\{h\}} = \frac{\alpha \Phi_{\{h\}} \beta_{\{h\}} \eta_{\{h\}}}{\left( \beta_{\{h\}} + \mu_{\{h\}} \right) \left( \eta_{\{h\}} + \mu_{\{h\}} \right) \left( \alpha + \gamma + \mu_{\{h\}} \right) \left( q + \mu_{\{h\}} \right) - q \alpha \eta_{\{h\}} \beta_{\{h\}}}, S_{\{h\}} = \frac{\left( \eta_{\{h\}} + \mu_{\{h\}} \right) \left( \alpha + \gamma + \mu_{\{h\}} \right) \Phi_{\{h\}} \left( q + \mu_{\{h\}} \right)}{\left( \beta_{\{h\}} + \mu_{\{h\}} \right) \left( \eta_{\{h\}} + \mu_{\{h\}} \right) \left( \alpha + \gamma + \mu_{\{h\}} \right) \left( q + \mu_{\{h\}} \right) - q \alpha \eta_{\{h\}} \beta_{\{h\}}}, S_{\{v\}} = \frac{\Gamma_{\{v\}}}{\xi_{\{v\}} + \mu_{\{v\}}}, I_{\{h\}} = \frac{\Phi_{\{h\}} \left( q + \mu_{\{h\}} \right) \beta_{\{h\}} \eta_{\{h\}}}{\left( \beta_{\{h\}} + \mu_{\{h\}} \right) \left( \eta_{\{h\}} + \mu_{\{h\}} \right) \left( \alpha + \gamma + \mu_{\{h\}} \right) \left( q + \mu_{\{h\}} \right) - q \alpha \eta_{\{h\}} \beta_{\{h\}}}, I_{\{v\}} = \frac{\xi_{\{v\}} \Gamma_{\{v\}} \eta_{\{v\}}}{\left( \eta_{\{v\}} + \mu_{\{v\}} \right) \mu_{\{v\}} \left( \xi_{\{v\}} + \mu_{\{v\}} \right)} \right\}

```

Figure 4: Maple code for endemic equilibrium

Bibliography

- [1] Abdullah, M.A. and Merdan, A.I., 1995. Distribution and ecology of the mosquito fauna in the southwestern Saudi Arabia. *Journal of the Egyptian Society of Parasitology*, 25(3), pp.815-837.
- [2] Abiodun, G.J., Maharaj, R., Witbooi, P. and Okosun, K.O., 2016. Modelling the influence of temperature and rainfall on the population dynamics of *Anopheles arabiensis*. *Malaria Journal*, 15(1),p.1.
- [3] Allen, R.G., Pereira, L.S., Raes, D. and Smith, M., 1998. Crop evapotranspiration-Guidelines for computing crop water requirements-FAO Irrigation and drainage paper 56. *FAO, Rome*, 300(9), p.D05109.
- [4] Alonso, D., Bouma, M.J. and Pascual, M., 2011. Epidemic malaria and warmer temperatures in recent decades in an East African highland. *Proceedings of the Royal Society of London B: Biological Sciences*, 278(1712), pp.1661-1669.
- [5] Anderson, R.M., May, R.M. and Anderson, B., 1992. Infectious diseases of humans: dynamics and control (Vol. 28). Oxford University Press.
- [6] Aron, J.L., 1988. Mathematical modelling of immunity to malaria. *Mathematical Biosciences*, 90(1), pp.385-396.
- [7] Bayoh, M.N., 2001. Studies on the development and survival of *Anopheles gambiae sensu stricto* at various temperatures and relative humidities (Doctoral dissertation, Durham University).

- [8] Bayoh, M.N. and Lindsay, S.W., 2003. Effect of temperature on the development of the aquatic stages of *Anopheles gambiae sensu stricto* (Diptera: Culicidae). *Bulletin of Entomological Research*, 93(05), pp.375-381.
- [9] Beck-Johnson, L.M., Nelson, W.A., Paaijmans, K.P., Read, A.F., Thomas, M.B. and Bjørnstad, O.N., 2013. The effect of temperature on *Anopheles* mosquito population dynamics and the potential for malaria transmission. *PLOS one*, 8(11), p.e79276.
- [10] Beier, J.C., 1996. Frequent blood-feeding and restrictive sugar-feeding behavior enhance the malaria vector potential of *Anopheles gambiae sl* and *An. funestus* (Diptera: Culicidae) in western Kenya. *Journal of Medical Entomology*, 33(4), pp.613-618.
- [11] Bell, M.L., Samet, J.M. and Dominici, F., 2004. Time-series studies of particulate matter. *Annu. Rev. Public Health*, 25, pp.247-280.
- [12] Bi, P., Tong, S., Donald, K., Parton, K.A. and Ni, J., 2003. Climatic variables and transmission of malaria: a 12-year data analysis in Shuchen County, China. *Public Health Reports*, 118(1), p.65.
- [13] Birkhoff, G. and Rota, G.C., Ordinary Differential Equations (1978). *Ginn, Boston*.
- [14] Blayneh, K., Cao, Y. and Kwon, H.D., 2009. Optimal control of vector-borne diseases: treatment and prevention. *Discrete and Continuous Dynamical Systems B*, 11(3), pp.587-611.
- [15] Blayneh, K.W., Gumel, A.B., Lenhart, S. and Clayton, T., 2010. Backward bifurcation and optimal control in transmission dynamics of West Nile virus. *Bulletin of Mathematical Biology*, 72(4), pp.1006-1028.
- [16] Blumberg, L. and Frean, J., 2007. Malaria control in South Africa-challenges and successes. *South African Medical Journal*, 92(3).

- [17] Bomblies, A., Duchemin, J.B. and Eltahir, E.A., 2008. Hydrology of malaria: Model development and application to a Sahelian village. *Water Resources Research*, 44(12).
- [18] Bouma, M.J. and Van der Kaay, H.J., 1994. Epidemic malaria in India and the El Nino southern oscillation. *The Lancet*, 344(8937), pp.1638-1639.
- [19] Bouma, M.J. and Dye, C., 1997. Cycles of malaria associated with El Niño in Venezuela. *Jama*, 278(21), pp.1772-1774.
- [20] Bouma, M.J. and Pascual, M., 2001. Seasonal and interannual cycles of endemic cholera in Bengal 1891-1940 in relation to climate and geography. *In The Ecology and Etiology of Newly Emerging Marine Diseases*, pp.147-156. Springer Netherlands.
- [21] Briere, J.F., Pracros, P., Le Roux, A.Y. and Pierre, J.S., 1999. A novel rate model of temperature-dependent development for arthropods. *Environmental Entomology*, 28(1), pp.22-29.
- [22] Briët, O.J., Dossou-Yovo, J., Akodo, E., Van De Giesen, N. and Teuscher, T.M., 2003. The relationship between Anopheles gambiae density and rice cultivation in the savannah zone and forest zone of Cote d'Ivoire. *Tropical Medicine & International Health*, 8(5), pp.439-448.
- [23] Burton, T.A., 2005. Volterra integral and differential equations (Vol. 202). Elsevier.
- [24] Cailly, P., Tran, A., Balenghien, T., Lambert, G., Toty, C. and Ezanno, P., 2012. A climate-driven abundance model to assess mosquito control strategies. *Ecological Modelling*, 227, pp.7-17.
- [25] Cancre, N., Tall, A., Rogier, C., Faye, J., Sarr, O., Trape, J.F., Spiegel, A. and Bois, F., 2000. Bayesian analysis of an epidemiologic model of *Plasmodium falciparum* malaria infection in Ndiop, Senegal. *American Journal of Epidemiology*, 152(8), pp.760-770.

- [26] Cariboni, J., Gatelli, D., Liska, R. and Saltelli, A., 2007. The role of sensitivity analysis in ecological modelling. *Ecological Modelling*, 203(1), pp.167-182.
- [27] Castillo-Chavez, C. and Song, B., 2004. Dynamical models of tuberculosis and their applications. *Mathematical Biosciences and Engineering*, 1(2), pp.361-404.
- [28] Catalano, R. and Serxner, S., 1987. Time series designs of potential interest to epidemiologists. *American Journal of Epidemiology*, 126(4), pp.724-731.
- [29] Cazelles, B., Chavez, M., McMichael, A.J. and Hales, S., 2005. Non-stationary influence of El Nino on the synchronous dengue epidemics in Thailand. *PLoS Med*, 2(4), p.e106.
- [30] Cazelles, B., Chavez, M., de Magny, G.C., Guégan, J.F. and Hales, S., 2007. Time-dependent spectral analysis of epidemiological time-series with wavelets. *Journal of the Royal Society Interface*, 4(15), pp.625-636.
- [31] Chang, C. and Glover, G.H., 2010. Time-frequency dynamics of resting-state brain connectivity measured with fMRI. *Neuroimage*, 50(1), pp.81-98.
- [32] Charlwood, J.D., Thompson, R. and Madsen, H., 2003. Observations on the swarming and mating behaviour of *Anopheles funestus* from southern Mozambique. *Malaria Journal*, 2(1), p.1.
- [33] Chebotarev, N.G.E. and Meiman, N.N., 1949. The Routh-Hurwitz problem for polynomials and entire functions. *Trudy Matematicheskogo Instituta imeni VA Steklova*, 26, pp.3-331.
- [34] Chitnis, N., Cushing, J.M. and Hyman, J.M., 2006. Bifurcation analysis of a mathematical model for malaria transmission. *SIAM Journal on Applied Mathematics*, 67(1), pp.24-45.

- [35] Chitnis, N., Smith, T. and Steketee, R., 2008. A mathematical model for the dynamics of malaria in mosquitoes feeding on a heterogeneous host population. *Journal of Biological Dynamics*, 2(3), pp.259-285.
- [36] Chiyaka, C., Tchuente, J.M., Garira, W. and Dube, S., 2008. A mathematical analysis of the effects of control strategies on the transmission dynamics of malaria. *Applied Mathematics and Computation*, 195(2), pp.641-662.
- [37] Chiyaka, C., Garira, W. and Dube, S., 2009. Effects of treatment and drug resistance on the transmission dynamics of malaria in endemic areas. *Theoretical Population Biology*, 75(1), pp.14-29.
- [38] Coetzee, M., 2004. Distribution of the African malaria vectors of the *Anopheles gambiae* complex. *The American Journal of Tropical Medicine and Hygiene*, 70(2), pp.103-104.
- [39] Coluzzi, M., Sabatini, A., Petrarca, V. and Di Deco, M.A., 1979. Chromosomal differentiation and adaptation to human environments in the *Anopheles gambiae* complex. *Transactions of the Royal Society of Tropical Medicine and Hygiene*, 73(5), pp.483-497.
- [40] Colwell, R.R. and Patz, J., 1998. Climate, Infectious Disease, and Health: An Interdisciplinary Perspective: a Report from the American Academy of Microbiology. *American Academy of Microbiology*.
- [41] Craig, M.H., Snow, R.W. and Le Sueur, D., 1999. A climate-based distribution model of malaria transmission in sub-Saharan Africa. *Parasitology today*, 15(3), pp.105-111.
- [42] Dao, A., Adamou, A., Crawford, J.E., Ribeiro, J.M., Gwadz, R., Traoré, S.F. and Lehmann, T., 2006. The distribution of hatching time in *Anopheles gambiae*. *Malaria Journal*, 5(1), p.1.
- [43] Daubechies, I., 1992. Ten lectures on wavelets. *Society for Industrial and Applied Mathematics*, Vol. 61, pp. 198-202.

- [44] Defries, R.S., Bounoua, L. and Collatz, G.J., 2002. Human modification of the landscape and surface climate in the next fifty years. *Global Change Biology*, 8(5), pp.438-458.
- [45] Depinay, J.M.O., Mbogo, C.M., Killeen, G., Knols, B., Beier, J., Carlson, J., Dushoff, J., Billingsley, P., Mwambi, H., Githure, J. and Toure, A.M., 2004. A simulation model of African *Anopheles* ecology and population dynamics for the analysis of malaria transmission. *Malaria journal*, 3(1), p.1.
- [46] Detinova, T.S., 1962. Age grouping methods in Diptera of medical importance: With special reference to some vectors of malaria. *California medicine*, 98(3), p.185.
- [47] Diekmann, O., Heesterbeek, J.A.P. and Metz, J.A., 1990. On the definition and the computation of the basic reproduction ratio R_0 in models for infectious diseases in heterogeneous populations. *Journal of Mathematical Biology*, 28(4), pp.365-382.
- [48] Diekmann, O., Heesterbeek, J.A.P. and Roberts, M.G., 2009. The construction of next-generation matrices for compartmental epidemic models. *Journal of the Royal Society Interface*, p.rsif20090386.
- [49] Dietz, K., Molineaux, L. and Thomas, A., 1974. A malaria model tested in the African savannah. *Bulletin of the World Health Organization*, 50(3-4), p.347.
- [50] Dominici, F., McDermott, A., Zeger, S.L. and Samet, J.M., 2002. On the use of generalized additive models in time-series studies of air pollution and health. *American Journal of Epidemiology*, 156(3), pp.193-203.
- [51] Drakeley, C.J., Carneiro, I., Reyburn, H., Malima, R., Lusingu, J.P., Cox, J., Theander, T.G., Nkya, W.M., Lemnge, M.M. and Riley, E.M., 2005. Altitude-dependent and-independent variations in *Plasmodium falciparum* prevalence in northeastern Tanzania. *Journal of Infectious Diseases*, 191(10), pp.1589-1598.

- [52] Eckhoff, P.A., 2011. A malaria transmission-directed model of mosquito life cycle and ecology. *Malaria Journal*, 10(1), p.1.
- [53] Edillo, F.E., Touré, Y.T., Lanzaro, G.C., Dolo, G. and Taylor, C.E., 2002. Spatial and habitat distribution of *Anopheles gambiae* and *Anopheles arabiensis* (Diptera: Culicidae) in Banambani village, Mali. *Journal of Medical Entomology*, 39(1), pp.70-77.
- [54] eMEDtv, 2000. <http://copd.emedtv.com/>
- [55] Ermert, V., 2010. Risk assessment with regard to the occurrence of malaria in Africa under the influence of observed and projected climate change (Doctoral dissertation, Universität zu Köln).
- [56] Fontenille, D., Lochouart, L., Diagne, N., Sokhna, C., Lemasson, J.J., Diatta, M., Konate, L., Faye, F., Rogier, C. and Trape, J.F., 1997. High annual and seasonal variations in malaria transmission by anophelines and vector species composition in Dielmo, a holoendemic area in Senegal. *American Journal of Tropical Medicine and Hygiene*, 56(3), pp.247-253.
- [57] Fontenille, D., Meunier, J.Y., Nkondjio, C.A. and Tchuinkam, T., 2001. Use of circumsporozoite protein enzyme-linked immunosorbent assay compared with microscopic examination of salivary glands for calculation of malaria infectivity rates in mosquitoes (Diptera: Culicidae) from Cameroon. *Journal of Medical Entomology*, 38(3), pp.451-454.
- [58] Garros, C., Koekemoer, L.L., Coetzee, M., Coosemans, M. and Manguin, S., 2004. A single multiplex assay to identify major malaria vectors within the African *Anopheles funestus* and the Oriental *An. minimus* groups. *The American Journal of Tropical Medicine and Hygiene*, 70(6), pp.583-590.
- [59] Gear, J.H.S., 1989. Malaria in South Africa: Its history and present problems. *S Afr J Epidemiol Infect*, 4, pp.63-66.
- [60] Gerritsen, A.A., Kruger, P., van der Loeff, M.F.S. and Grobusch, M.P., 2008. Malaria incidence in Limpopo Province, South Africa, 1998–2007. *Malaria Journal*, 7(1), p.1.

- [61] Gillies, M.T. and De Meillon, B., 1968. The anophelinae of Africa south of the Sahara (Ethiopian zoogeographical region). The *Anophelinae* of Africa south of the Sahara (Ethiopian Zoogeographical Region)
- [62] Gillies, M.T. and Coetzee, M., 1987. A Supplement to the *Anophelinae* of Africa South of the Sahara. *Publ S Afr Inst Med Res*, 55, pp.1-143.
- [63] Gimnig, J.E., Ombok, M., Kamau, L. and Hawley, W.A., 2001. Characteristics of larval *anopheline* (*Diptera: Culicidae*) habitats in Western Kenya. *Journal of Medical Entomology*, 38(2), pp.282-288.
- [64] Githeko, A.K., Adungo, N.I., Karanja, D.M., Hawley, W.A., Vulule, J.M., Seroney, I.K., Ofulla, A.V., Atieli, F.K., Ondijo, S.O., Genga, I.O. and Odada, P.K., 1996. Some Observations on the Biting Behavior of *Anopheles gambiae* ss, *Anopheles arabiensis*, and *Anopheles funestus* and Their Implications for Malaria Control. *Experimental parasitology*, 82(3), pp.306-315.
- [65] Githeko, A.K., Lindsay, S.W., Confalonieri, U.E. and Patz, J.A., 2000. Climate change and vector-borne diseases: a regional analysis. *Bulletin of the World Health Organization*, 78(9), pp.1136-1147.
- [66] Greenwood, B.M., Bojang, K., Whitty, C.J.M. and Targett, G.A.T., 2005. Malaria. *The Lancet*, 365: 1487-1498. Publisher Full Text OpenURL.
- [67] Grinsted, A., Moore, J.C. and Jevrejeva, S., 2004. Application of the cross wavelet transform and wavelet coherence to geophysical time series. *Nonlinear Processes in Geophysics*, 11(5/6), pp.561-566.
- [68] Guerra, C.A., Snow, R.W. and Hay, S.I., 2006. A global assessment of closed forests, deforestation and malaria risk. *Annals of Tropical Medicine and Parasitology*, 100(3), p.189.
- [69] Guerra, C.A., Gikandi, P.W., Tatem, A.J., Noor, A.M., Smith, D.L., Hay, S.I. and Snow, R.W., 2008. The limits and intensity of *Plasmodium falciparum* transmission: implications for malaria control and elimination worldwide. *PLoS Med*, 5(2), p.e38.

- [70] Gupta, S., Snow, R.W., Donnelly, C.A., Marsh, K. and Newbold, C., 1999. Immunity to non-cerebral severe malaria is acquired after one or two infections. *Nature Medicine*, 5(3), pp.340-343.
- [71] Haines, A. and Fuchs, C., 1991. Potential impacts on health of atmospheric change. *Journal of Public Health*, 13(2), pp.69-80.
- [72] Haith, D.A. and Shoenaker, L.L., 1987. Generalized watershed loading functions for stream flow nutrients. *JAWRA Journal of the American Water Resources Association*, 23(3), pp.471-478.
- [73] Hamon, W.R., 1960. Estimating potential evapotranspiration (Doctoral dissertation, Massachusetts Institute of Technology).
- [74] Hay, S.I., Rogers, D.J., Shanks, G.D., Myers, M.F. and Snow, R.W., 2001. Malaria early warning in Kenya. *Trends in Parasitology*, 17(2), pp.95-99.
- [75] Hay, S.I., Cox, J., Rogers, D.J., Randolph, S.E., Stern, D.I., Shanks, G.D., Myers, M.F. and Snow, R.W., 2002. Climate change and the resurgence of malaria in the East African highlands. *Nature*, 415(6874), pp.905-909.
- [76] Hay, S.I. and Snow, R.W., 2006. The Malaria Atlas Project: developing global maps of malaria risk. *PLoS Med*, 3(12), p.e473.
- [77] Helfenstein, U., 1986. Box-enkins modelling of some viral infectious diseases. *Statistics in medicine*, 5(1), pp.37-47.
- [78] Hethcote, H.W., 2000. The mathematics of infectious diseases. *SIAM review*, 42(4), pp.599-653.
- [79] Himeidan, Y.E. and Rayah, E.E.A., 2008. Role of some environmental factors on the breeding activity of *Anopheles arabiensis* in New Halfa town, eastern Sudan. *East Mediterr Health J.*, 14:2529.
- [80] Hoshen, M.B. and Morse, A.P., 2004. A weather-driven model of malaria transmission. *Malaria Journal*, 3(1), p.1.

- [81] Jetten, T.H. and Takken, W., 1994. *Anophelism* without malaria in Europe. A review of the ecology and distribution of the genus *Anopheles* in Europe (No. 94-5). Landbouwwuniversiteit Wageningen (Wageningen Agricultural University).
- [82] Jetten, T.H., Martens, W.J.M. and Takken, W., 1996. Model simulations to estimate malaria risk under climate change. *Journal of Medical Entomology*, 33(3), pp.361-371.
- [83] Jolliffe, I.T., 1990. Principal component analysis: a beginner's guide I. Introduction and application. *Weather*, 45(10), pp.375-382.
- [84] Jones, A.E. and Morse, A.P., 2010. Application and validation of a seasonal ensemble prediction system using a dynamic malaria model. *Journal of Climate*, 23(15), pp.4202-4215.
- [85] Kirby, M.J. and Lindsay, S.W., 2004. Responses of adult mosquitoes of two sibling species, *Anopheles arabiensis* and *A. gambiae* ss (Diptera: Culicidae), to high temperatures. *Bulletin of Entomological Research*, 94(05), pp.441-448.
- [86] Killeen, G.F., McKenzie, F.E., Foy, B.D., Bøgh, C. and Beier, J.C., 2001. The availability of potential hosts as a determinant of feeding behaviours and malaria transmission by African mosquito populations. *Transactions of the Royal Society of Tropical Medicine and Hygiene*, 95(5), pp.469-476.
- [87] Kleinschmidt, I., Bagayoko, M., Clarke, G.P.Y., Craig, M. and Le Sueur, D., 2000. A spatial statistical approach to malaria mapping. *International Journal of Epidemiology*, 29(2), pp.355-361.
- [88] Kleinschmidt, I., Omumbo, J., Briet, O., Van De Giesen, N., Sogoba, N., Mensah, N.K., Windmeijer, P., Moussa, M. and Teuscher, T., 2001. An empirical malaria distribution map for West Africa. *Tropical Medicine & International Health*, 6(10), pp.779-786.
- [89] Koella, J.C., 1991. On the use of mathematical models of malaria transmission. *Acta Tropica*, 49(1), pp.1-25.

- [90] Kovats, R.S., Campbell-Lendrum, D.H., McMichel, A.J., Woodward, A. and Cox, J.S.H., 2001. Early effects of climate change: do they include changes in vector-borne disease?. *Philosophical Transactions of the Royal Society of London B: Biological Sciences*, 356(1411), pp.1057-1068.
- [91] Kribs-Zaleta, C.M. and Velasco-Hernandez, J.X., 2000. A simple vaccination model with multiple endemic states. *Mathematical Biosciences*, 164(2), pp.183-201.
- [92] Labadin, J., Kon, C.M.L. and Juan, S.F.S., 2009, October. Deterministic malaria transmission model with acquired immunity. *Proceedings of the World Congress on Engineering and Computer Science* (Vol. 2, pp. 20-22).
- [93] Lafferty, K.D., 2009. The ecology of climate change and infectious diseases. *Ecology*, 90(4), pp.888-900.
- [94] Lakshmikantham, V., Leela, S. and Martynyuk, A.A. (1989). Stability analysis of nonlinear systems. Marcel Dekker, Inc., New York and Basel.
- [95] Laneri, K., Paul, R.E., Tall, A., Faye, J., Diene-Sarr, F., Sokhna, C., Trape, J.F. and Rodó, X., 2015. Dynamical malaria models reveal how immunity buffers effect of climate variability. *Proceedings of the National Academy of Sciences*, 112(28), pp.8786-8791.
- [96] Lenhart, S., Workman, J.T., Optimal Control Applied to Biological Models. *Chapman and Hall*, (2007).
- [97] Levine, R.S., Peterson, A.T. and Benedict, M.Q., 2004. Distribution of members of *Anopheles quadrimaculatus* Say *sl* (Diptera: Culicidae) and implications for their roles in malaria transmission in the United States. *Journal of Medical Entomology*, 41(4), pp.607-613.
- [98] Liu, Y., San Liang, X. and Weisberg, R.H., 2007. Rectification of the bias in the wavelet power spectrum. *Journal of Atmospheric and Oceanic Technology*, 24(12), pp.2093-2102.

- [99] Li, J., 2011. Malaria model with stage-structured mosquitoes. *Mathematical Biosciences and Engineering: MBE*, 8(3), pp.753-768.
- [100] Lindsay, S.W. and Birley, M.H., 1996. Climate change and malaria transmission. *Annals of Tropical Medicine and Parasitology*, 90(6), pp.573-588.
- [101] Lindsay, S.W. and Martens, W.J., 1998. Malaria in the African highlands: past, present and future. *Bulletin of the World Health Organization*, 76(1), p.33.
- [102] Lunde, T.M., Korecha, D., Loha, E., Sorteberg, A. and Lindtjørn, B., 2013. A dynamic model of some malaria-transmitting anopheline mosquitoes of the Afrotropical region. I. Model description and sensitivity analysis. *Malaria Journal*, 12(1), p.1.
- [103] Lutambi, A.M., Penny, M.A., Smith, T. and Chitnis, N., 2013. Mathematical modelling of mosquito dispersal in a heterogeneous environment. *Mathematical Biosciences*, 241(2), pp.198-216.
- [104] Lutambi, A.M., 2013. Mathematical modelling of Mosquito Dispersal for Malaria Vector Control (Doctoral dissertation, University of Basel).
- [105] Lou, Y. and Zhao, X.Q., 2010. A climate-based malaria transmission model with structured vector population. *SIAM Journal on Applied Mathematics*, 70(6), pp.2023-2044.
- [106] Makinde, O.D. and Okosun, K.O., 2011. Impact of chemo-therapy on optimal control of malaria disease with infected immigrants. *BioSystems*, 104(1), pp.32-41.
- [107] Martens, W.J.M., Jetten, T.H., Rotmans, J. and Niessen, L.W., 1995a. Climate change and vector-borne diseases: a global modelling perspective. *Global Environmental Change*, 5(3), pp.195-209.
- [108] Martens, W.J., Niessen, L.W., Rotmans, J., Jetten, T.H. and McMichael, A.J., 1995. Potential impact of global climate change on malaria risk. *Environmental Health Perspectives*, 103(5), p.458.

- [109] Martens, W.J., Jetten, T.H. and Focks, D.A., 1997. Sensitivity of malaria, *schistosomiasis* and dengue to global warming. *Climatic Change*, 35(2), pp.145-156.
- [110] Martens, P., Kovats, R.S., Nijhof, S., De Vries, P., Livermore, M.T.J., Bradley, D.J., Cox, J. and McMichael, A.J., 1999. Climate change and future populations at risk of malaria. *Global Environmental Change*, 9, pp.S89-S107.
- [111] Macdonald, G., 1955. The measurement of malaria transmission. *Proceedings of the Royal Society of Medicine*, 48, 295-301.
- [112] Macdonald, G., 1956. Epidemiological basis of malaria control. *Bulletin of the World Health Organisation*, 15, 613-626.
- [113] Macdonald, G., 1957. The epidemiology and control of malaria. Oxford University Press, London, United Kingdom.
- [114] Maharaj, R., 2003. Life table characteristics of *Anopheles arabiensis* (Diptera: Culicidae) under simulated seasonal conditions. *Journal of Medical Entomology*, 40(6), pp.737-742.
- [115] Maharaj, R., Mthembu, D.J. and Sharp, B.L., 2008. Impact of DDT re-introduction on malaria transmission in KwaZulu-Natal. *South African Medical Journal*, 95(11), p.871.
- [116] Mali, S., Steele, S., Slutsker, L., Arguin, P.M. and Centers for Disease Control and Prevention (CDC), 2010. Malaria surveillance-United States, 2008. *Department of Health and Human Services, Centers for Disease Control and Prevention*.
- [117] MARA, 1998: Towards an Atlas of Malaria Risk in Africa: First Technical Report of the MARA/ARMA Collaboration. Tech. rep., MARA/ARMA, 32 pp., Durban, South Africa.

- [118] McCarthy, J.J., Canziani, O.F., Leary, N.A., Dokken, D.J. and White, K.S., 2001. Climate change 2001: Impacts, adaptation, and vulnerability, United Nations Intergovernmental Panel on Climate Change.
- [119] McKenzie, F.E., 2000. Why model malaria?. *Parasitology Today*, 16(12), pp.511-516.
- [120] McMichael, A.J., Woodruff, R.E. and Hales, S., 2006. Climate change and human health: present and future risks. *The Lancet*, 367(9513), pp.859-869.
- [121] Meinsma, G., 1995. Elementary proof of the Routh-Hurwitz test. *Systems & Control Letters*, 25(4), pp.237-242.
- [122] Menendez, C., 1999. Priority areas for current research on malaria during pregnancy. *Annals of Tropical Medicine and Parasitology*, 93, pp.S71-4.
- [123] Minakawa, N., Sonye, G., Mogi, M. and Yan, G., 2004. Habitat characteristics of *Anopheles gambiae* ss larvae in a Kenyan highland. *Medical and Veterinary Entomology*, 18(3), pp.301-305.
- [124] Minakawa, N., Munga, S., Atieli, F., Mushinzimana, E., Zhou, G., Githeko, A.K. and Yan, G., 2005. Spatial distribution of anopheline larval habitats in Western Kenyan highlands: effects of land cover types and topography. *The American Journal of Tropical Medicine and Hygiene*, 73(1), pp.157-165.
- [125] Moghadas, S.M. and Gumel, A.B., 2002. Global stability of a two-stage epidemic model with generalized non-linear incidence. *Mathematics and Computers in Simulation*, 60(1), pp.107-118.
- [126] Mohammadkhani, M., Khanjani, N., Bakhtiari, B. and Sheikhzadeh, K., 2016. The relation between climatic factors and malaria incidence in Kerman, South East of Iran. *Parasite Epidemiology and Control*, 1(3), pp.205-210.

- [127] Moonasar, D., Nuthulaganti, T., Kruger, P.S., Mabuza, A., Rasiswi, E.S., Benson, F.G. and Maharaj, R., 2012. Malaria control in South Africa 2000-2010: beyond MDG6. *Malaria Journal*, 11(1), p.1.
- [128] Mordecai, E.A., Paaijmans, K.P., Johnson, L.R., Balzer, C., Ben-Horin, T., Moor, E., McNally, A., Pawar, S., Ryan, S.J., Smith, T.C. and Lafferty, K.D., 2013. Optimal temperature for malaria transmission is dramatically lower than previously predicted. *Ecology Letters*, 16(1), pp.22-30.
- [129] Morris, N., Freen, J., Baker, L., Ukpe, I.S., Barnes, K.I., Kruger, P., Mabuza, A., Raswiswi, E., Maharaj, R., Blumberg, L. and Moonasar, D., 2013. Re-defining the extent of malaria transmission in South Africa: Implications for chemoprophylaxis. *SAMJ: South African Medical Journal*, 103(11), pp.858-860.
- [130] Morse, A.P., DOBLAS-REYES, F.J., Hoshen, M.B., Hagedorn, R. and Palmer, T.N., 2005. A forecast quality assessment of an end-to-end probabilistic multi-model seasonal forecast system using a malaria model. *Tellus A*, 57(3), pp.464-475.
- [131] Mouchet, J.E.A.N., Manguin, S., Sircoulon, J., Laventure, S.T.E.P.H.A.N.E., Faye, O.U.S.M.A.N.E., Onapa, A.W., Carnevale, P., Julvez, J. and Fontenille, D., 1998. Evolution of malaria in Africa for the past 40 years: impact of climatic and human factors. *Journal of the American Mosquito Control Association*, 14(2), pp.121-130.
- [132] Mtisi, E., Rwezaura, H. and Tchuente, J.M., 2009. A mathematical analysis of malaria and tuberculosis co-dynamics. *Discrete Cont. Dyn. Syst. B*, 12(4), pp.827-864.
- [133] Munga, S., Minakawa, N., Zhou, G., Mushinzimana, E., Barrack, O.O.J., Githeko, A.K. and Yan, G., 2006. Association between land cover and habitat productivity of malaria vectors in western Kenyan highlands. *The American Journal of Tropical Medicine and Hygiene*, 74(1), pp.69-75.

- [134] Nabarro, D.N. and Tayler, E.M., 1998. The "roll back malaria" Campaign. *Science*, 280(5372), pp.2067-2068.
- [135] Nakazawa, M., Ohmae, H., Ishii, A. and Leafasia, J., 1998. Malaria infection and human behavioral factors: A stochastic model analysis for direct observation data in the Solomon Islands. *American Journal of Human Biology*, 10(6), pp.781-789.
- [136] Nedelman, J., 1985. Estimation for a model of multiple malaria infections. *Biometrics*, pp.447-453.
- [137] Ngarakana-Gwasira, E.T., Bhunu, C.P. and Mashonjowa, E., 2014. Assessing the impact of temperature on malaria transmission dynamics. *Afrika Matematika*, 25(4), pp.1095-1112.
- [138] Ngwa, G.A. and Shu, W.S., 2000. A mathematical model for endemic malaria with variable human and mosquito populations. *Mathematical and Computer Modelling*, 32(7-8), pp.747-763.
- [139] Oguntunde, P.G., Abiodun, B.J., Olukunle, O.J. and Olufayo, A.A., 2012. Trends and variability in pan evaporation and other climatic variables at Ibadan, Nigeria, 1973-2008. *Meteorological Applications*, 19(4), pp.464-472.
- [140] Okogun, G.R.A., 2005. Life-table analysis of Anopheles malaria vectors: generational mortality as tool in mosquito vector abundance and control studies. *Journal of Vector Borne Diseases*, 42(2), p.45.
- [141] Okosun, K., 2010. Mathematical epidemiology of Malaria disease transmission and its optimal control analyses (*Doctoral dissertation, PhD thesis, University of the Western Cape, South Africa*).
- [142] Okosun, K.O. and Makinde, O.D., 2011. Modelling the impact of drug resistance in malaria transmission and its optimal control analysis. *International Journal of Physical Sciences*, 6(28), pp.6479-6487.

- [143] Olayemi, I.K. and Ande, A.T., 2008. Survivorship of *Anopheles gambiae* in relation to malaria transmission in Ilorin, Nigeria. *Online Journal of Health and Allied Sciences*, 7(3).
- [144] Omer, S.M. and Cloudsley-Thompson, J.L., 1970. Survival of female *Anopheles gambiae* Giles through a 9-month dry season in Sudan. *Bulletin of the World Health Organization*, 42(2), p.319.
- [145] Paaijmans, K.P., Wandago, M.O., Githeko, A.K. and Takken, W., 2007. Unexpected high losses of *Anopheles gambiae* larvae due to rainfall. *PLoS One*, 2(11), p.e1146.
- [146] Paaijmans, K.P., Heusinkveld, B.G. and Jacobs, A.F., 2008. A simplified model to predict diurnal water temperature dynamics in a shallow tropical water pool. *International Journal of Biometeorology*, 52(8), pp.797-803.
- [147] Paaijmans, K.P., Blanford, S., Bell, A.S., Blanford, J.I., Read, A.F. and Thomas, M.B., 2010. Influence of climate on malaria transmission depends on daily temperature variation. *Proceedings of the National Academy of Sciences*, 107(34), pp.15135-15139.
- [148] Paaijmans, K.P., Cator, L.J. and Thomas, M.B., 2013. Temperature-dependent pre-bloodmeal period and temperature-driven asynchrony between parasite development and mosquito biting rate reduce malaria transmission intensity. *PLOS one*, 8(1), p.e55777.
- [149] Palmer, T.N., Alessandri, A., Andersen, U. and Cantelaube, P., 2004. Development of a European multimodel ensemble system for seasonal-to-interannual prediction (DEMETER). *Bulletin of the American Meteorological Society*, 85(6), p.853.
- [150] Parham, P.E. and Michael, E., 2010. Modelling climate change and malaria transmission. In *Modelling Parasite Transmission and Control*. Springer New York, pp. 184-199.

- [151] Pascual, M., Ahumada, J.A., Chaves, L.F., Rodo, X. and Bouma, M., 2006. Malaria resurgence in the East African highlands: temperature trends revisited. *Proceedings of the National Academy of Sciences*, 103(15), pp.5829-5834.
- [152] Pascual, M., Cazelles, B., Bouma, M.J., Chaves, L.F. and Koelle, K., 2008. Shifting patterns: malaria dynamics and rainfall variability in an African highland. *Proceedings of the Royal Society of London B: Biological Sciences*, 275(1631), pp.123-132.
- [153] Paskewitz, S.M. and Collins, F.H., 1990. Use of the polymerase chain reaction to identify mosquito species of the *Anopheles gambiae* complex. *Medical and Veterinary Entomology*, 4(4), pp.367-373.
- [154] Patz, J.A., Campbell-Lendrum, D., Holloway, T. and Foley, J.A., 2005. Impact of regional climate change on human health. *Nature*, 438(7066), pp.310-317.
- [155] Poveda, G., Rojas, W., Quiñones, M.L., Vélez, I.D., Mantilla, R.I., Ruiz, D., Zuluaga, J.S. and Rua, G.L., 2001. Coupling between annual and ENSO timescales in the malaria-climate association in Colombia. *Environmental Health Perspectives*, 109(5), p.489.
- [156] Rao, L.Y., Sun, G., Ford, C.R. and Vose, J.M., 2011. Modeling potential evapotranspiration of two forested watersheds in the southern Appalachians. *Transactions of the ASABE*, 54(6), pp.2067-2078.
- [157] Rastogi, M., Pal, N.L. and Sen, A.B., 1986. Effect of variation in temperature on development of *Plasmodium berghei* (NK 65 strain) in *Anopheles stephensi*. *Folia Parasitologica*, 34(4), pp.289-297.
- [158] Reisen, W.K., 1995. Effect of temperature on *Culex tarsalis* (Diptera: Culicidae) from the Coachella and San Joaquin valleys of California. *Journal of Medical Entomology*, 32(5), pp.636-645.
- [159] Reiter, R., 2001. Knowledge in action: logical foundations for specifying and implementing dynamical systems. MIT press.

- [160] Reusch, D.B., Mayewski, P.A., Whitlow, S.I., Pittalwala, I.I. and Twickler, M.S., 1999. Spatial variability of climate and past atmospheric circulation patterns from central West Antarctic glaciochemistry. *Journal of Geophysical Research: Atmospheres*, 104(D6), pp.5985-6001.
- [161] Richman, M.B., 1986. Rotation of principal components. *Journal of Climatology*, 6(3), pp.293-335.
- [162] Rizzo, C., Ronca, R., Fiorentino, G., Mangano, V.D., Sirima, S.B., Nèbiè, I., Petrarca, V., Modiano, D. and Arcà, B., 2011. Wide cross-reactivity between *Anopheles gambiae* and *Anopheles funestus* SG6 salivary proteins supports exploitation of gSG6 as a marker of human exposure to major malaria vectors in tropical Africa. *Malaria Journal*, 10(1), p.1.
- [163] Rogers, D.J. and Randolph, S.E., 2000. The global spread of malaria in a future, warmer world. *Science*, 289(5485), pp.1763-1766.
- [164] Roiz, D., Rosa, R., Arnoldi, D. and Rizzoli, A., 2010. Effects of temperature and rainfall on the activity and dynamics of host-seeking *Aedes albopictus* females in northern Italy. *Vector-Borne and Zoonotic Diseases*, 10(8), pp.811-816.
- [165] Ross, R., 1911. The prevention of malaria. 2d ed., John Murray, London, United Kingdom, 669 pp.
- [166] Ross, R., 1928. Studies on malaria. John Murray, London, United Kingdom, 196 pp.
- [167] Roy, M., Bouma, M., Dhiman, R.C. and Pascual, M., 2015. Predictability of epidemic malaria under non-stationary conditions with process-based models combining epidemiological updates and climate variability. *Malaria Journal*, 14(1), p.1.
- [168] Rubel, F. and Brugger, K., 2011. Dynamics of infectious diseases according to climate change: the Usutu virus epidemics in Vienna. *Game Meat Hygiene in Focus*, pp. 173-198.

- [169] Sachs, J. and Malaney, P., 2002. The economic and social burden of malaria. *Nature*, 415(6872), pp.680-685.
- [170] Saji, N.H., Goswami, B.N., Vinayachandran, P.N. and Yamagata, T., 1999. A dipole mode in the tropical Indian Ocean. *Nature*, 401(6751), pp.360-363.
- [171] Sena, L., Deressa, W. and Ali, A., 2015. Correlation of climate variability and malaria: a retrospective comparative study, southwest Ethiopia. *Ethiopian Journal of Health Sciences*, 25(2), pp.129-138.
- [172] MW Service, 2008. Medical entomology for students. Cambridge University Press.
- [173] Shaman, J. and Day, J.F., 2007. Reproductive phase locking of mosquito populations in response to rainfall frequency. *PLoS One*, 2(3), p.e331.
- [174] Sheffield, J., Goteti, G. and Wood, E.F., 2006. Development of a 50-year high-resolution global dataset of meteorological forcings for land surface modeling. *Journal of Climate*, 19(13), pp.3088-3111.
- [175] Smith, T.A., 2008. Estimation of heterogeneity in malaria transmission by stochastic modelling of apparent deviations from mass action kinetics. *Malaria Journal*, 7(1), p.1.
- [176] Snow, R.W., Omumbo, J.A., Lowe, B., Molyneux, C.S., Obiero, J.O., Palmer, A., Weber, M.W., Pinder, M., Nahlen, B., Obonyo, C. and Newbold, C., 1997. Relation between severe malaria morbidity in children and level of *Plasmodium falciparum* transmission in Africa. *The Lancet*, 349(9066), pp.1650-1654.
- [177] Silal, S.P., Barnes, K.I., Kok, G., Mabuza, A. and Little, F., 2013. Exploring the seasonality of reported treated malaria cases in Mpumalanga, South Africa. *PloS one*, 8(10), p.e76640.
- [178] Sinka, M.E., Bangs, M.J., Manguin, S., Coetzee, M., Mbogo, C.M., Hemingway, J., Patil, A.P., Temperley, W.H., Gething, P.W., Kabaria,

- C.W. and Okara, R.M., 2010. The dominant *Anopheles* vectors of human malaria in Africa, Europe and the Middle East: occurrence data, distribution maps and bionomic précis. *Parasites & Vectors*, 3(1), p.1.
- [179] South African National Census of 2001. <http://www.statssa.gov.za/census01/html/>.
- [180] Steketee, R.W. and Mutabingwa, T.K., 1999. Malaria in pregnant women: research, epidemiology, policy and practice. *Annals of Tropical Medicine and Parasitology*, 93, pp.S7-9.
- [181] Struchiner, C.J., Halloran, M.E. and Spielman, A., 1989. Modeling malaria vaccines I: new uses for old ideas. *Mathematical Biosciences*, 94(1), pp.87-113.
- [182] le Sueur, D. and Sharp, B.L., 1988. The breeding requirements of three members of the *Anopheles gambiae* Giles complex (*Diptera: Culicidae*) in the endemic malaria area of Natal, South Africa. *Bulletin of Entomological Research*, 78(04), pp.549-560.
- [183] Sutherst, R.W., 2004. Global change and human vulnerability to vector-borne diseases. *Clinical Microbiology Reviews*, 17(1), pp.136-173.
- [184] Tanser, F.C., Sharp, B. and Le Sueur, D., 2003. Potential effect of climate change on malaria transmission in Africa. *The Lancet*, 362(9398), pp.1792-1798.
- [185] Thomson, M.C., Connor, S.J., Milligan, P. and Flasse, S.P., 1997. Mapping malaria risk in Africa: What can satellite data contribute?. *Parasitology Today*, 13(8), pp.313-318.
- [186] Thomson, M.C., Doblas-Reyes, F.J., Mason, S.J., Hagedorn, R., Connor, S.J., Phindela, T., Morse, A.P. and Palmer, T.N., 2006. Malaria early warnings based on seasonal climate forecasts from multi-model ensembles. *Nature*, 439(7076), pp.576-579.

- [187] Thomson, M.C., Palmer, T., Morse, A.P., Cresswell, M. and Connor, S.J., 2000. Forecasting disease risk with seasonal climate predictions. *The Lancet*, 355(9214), pp.1559-1560.
- [188] Thomson, M.C., Mason, S.J., Phindela, T. and Connor, S.J., 2005. Use of rainfall and sea surface temperature monitoring for malaria early warning in Botswana. *The American Journal of Tropical Medicine and Hygiene*, 73(1), pp.214–221.
- [189] Tirados, I., Costantini, C., Gibson, G. and Torr, S.J., 2006. Blood-feeding behaviour of the malarial mosquito *Anopheles arabiensis*: implications for vector control. *Medical and Veterinary Entomology*, 20(4), pp.425-437.
- [190] Tompkins, A.M. and Ermert, V., 2013. A regional-scale, high resolution dynamical malaria model that accounts for population density, climate and surface hydrology. *Malaria Journal*, 12(1), p.1.
- [191] Torrence, C. and Compo, G.P., 1998. A practical guide to wavelet analysis. *Bulletin of the American Meteorological Society*, 79(1), pp.61-78.
- [192] Touré, Y.T. and Oduola, A., 2004. Focus: malaria. *Nature Reviews Microbiology*, 2(4), pp.276-277
- [193] Tran, A., L'Ambert, G., Lacour, G., Benoît, R., Demarchi, M., Cros, M., Cailly, P., Aubry-Kientz, M., Balenghien, T. and Ezanno, P., 2013. A rainfall-and temperature-driven abundance model for *Aedes albopictus* populations. *International Journal of Environmental Research and Public Health*, 10(5), pp.1698-1719.
- [194] Tumwiine, J., Mugisha, J.Y.T. and Luboobi, L.S., 2007. A mathematical model for the dynamics of malaria in a human host and mosquito vector with temporary immunity. *Applied Mathematics and Computation*, 189(2), pp.1953-1965.
- [195] World Health Organization and UNICEF., 2013. Progress on sanitation and drinking-water. World Health Organization.

- [196] Van den Driessche, P. and Watmough, J., 2002. Reproduction numbers and sub-threshold endemic equilibria for compartmental models of disease transmission. *Mathematical Biosciences*, 180(1), pp.29-48.
- [197] Walsh, J.E., 1978. Temporal and spatial scales of the Arctic circulation. *Monthly Weather Review*, 106(11), pp.1532-1544.
- [198] Wangdi, K., Singhasivanon, P., Silawan, T., Lawpoolsri, S., White, N.J. and Kaewkungwal, J., 2010. Development of temporal modelling for forecasting and prediction of malaria infections using time-series and ARIMA analyses: a case study in endemic districts of Bhutan. *Malaria Journal*, 9(1), p.1.
- [199] Warrell, D.A. and Gilles, H.M., 2002. *Essential Malariology* (No. Ed. 4). Arnold.
- [200] Wernsdorfer, W.H. and McGregor, I., 1988. *Malaria: Principles and Practice of Malariology*, Vols 1 and 2 Churchill Livingstone.
- [201] White, G.B., 1974. *Anopheles gambiae* complex and disease transmission in Africa. *Transactions of the Royal Society of Tropical Medicine and Hygiene*, 68(4), pp.278-298.
- [202] Winder, M. and Cloern, J.E., 2010. The annual cycles of phytoplankton biomass. *Philosophical Transactions of the Royal Society B: Biological Sciences*, 365(1555), pp.3215-3226.
- [203] WHO, 1997. World malaria situation in 1994. Weekly epidemiological record, 72, 269-276.
- [204] WHO, 2003. World Malaria Report: World Health Organization
<http://www.who.int/malaria/publications/atoz/whocdsmal20031093/en/>
- [205] WHO, 2008. World Malaria Report: World Health Organization
<http://www.who.int/malaria/publications/atoz/9789241563697/en/>

- [206] WHO, 2012. World Malaria Report: World Health Organization
http://www.who.int/malaria/publications/world_malaria_report2012/en/
- [207] WHO, 2014. World Malaria Report: World Health Organization
http://www.who.int/malaria/publications/world_malaria_report_2014/report/en/
- [208] WHO, 2015. World Malaria Report: World Health Organization
<http://www.who.int/malaria/publications/world-malaria-report-2015/report/en/>
- [209] Yamana, T.K. and Eltahir, E.A., 2013. Incorporating the effects of humidity in a mechanistic model of *Anopheles gambiae* mosquito population dynamics in the Sahel region of Africa. *Parasites & Vectors*, 6(1), p.1.
- [210] Yazoume, Y., Hoshen, M., Kyobutungi, C., Louis, V.R. and Sauerborn, R., 2009. Local scale prediction of *Plasmodium falciparum* malaria transmission in an endemic region using temperature and rainfall. *Global Health Action*, 2.
- [211] Zhang, Y., Bi, P. and Hiller, J.E., 2010. Meteorological variables and malaria in a Chinese temperate city: A twenty-year time-series data analysis. *Environment International*, 36(5), pp.439-445.
- [212] Zhou, G., Minakawa, N., Githeko, A.K. and Yan, G., 2004. Association between climate variability and malaria epidemics in the East African highlands. *Proceedings of the National Academy of Sciences of the United States of America*, 101(8), pp.2375-2380.